THE UNIVERSITY OF HULL

Electro-generated chemiluminescence with conducting sol-gels

being a Thesis submitted for the Degree of Ph.D.

in the University of Hull

by

Alan Greenwood B.Sc. (Hons)

March 2006

ACKNOWLEDGEMENTS

I would like to thank my supervisors, Dr Gillian Greenway and Dr Jonathan Aylott for giving me this opportunity, and providing continued guidance and endless encouragement.

In addition I would also like to thank the staff and students at Hull who have kindly gave me their time and knowledge; it was and is much appreciated. However special thanks must go to Dr Geir-Rune Flatten, Dr Charlotte Wiles and Dr Abigail Webster; their knowledge, friendship and supply of coffee kept me going through the gritty bits.

My final love and thanks go to my family and friends, without whom this would never have happened.

Alan Greenwood (March 2006)

Abstract

This thesis describes the development of novel sol-gel materials to be used as reagents for electro-generated chemiluminescence. Chapter one presents an overview of sol-gel materials and discusses the background theory covering aspect such as reagents choice, catalysis, and drying and curing protocols. Discussing the effect these properties have on sol-gel formations including possible applications. This chapter also discusses the electro-conduction theory for indium tin oxide and introduces some current applications. The chapter finishes through the introduction of chemiluminescence (CL) and electro-generated chemiluminescence (ECL) theory, describing the advantages with each type and providing current examples of reagents and their uses.

Chapter two describes a novel method for the fabrication of an electro-conducting tetramethoxysilane (TMOS) based sol-gel. The novelty of this work is based on the development of a transparent conducting material that can be used for electro-generated chemiluminescence measurements. The sol-gels were initially fabricated into a monolithic cuboid design by encapsulating indium tin oxide (ITO) (the conducting medium) within the sol-gel. An optimum electrical resistivity of 167.4 Ω/Sq was observed for these sol-gels monoliths which also demonstrated acceptable optical transparency given their structural dimensions (15x6x6 mm). Sol-gels encapsulating PEDOT (Poly-3,4-ethylenedioxythiophene) were also evaluated, however these exhibited no electro-conducting properties.

In chapter three the ITO doped sol-gel material was further developed in the form of thin films applied to glassy carbon electrodes *via* a dip coating procedure. These coatings were evaluated using electro-generated chemiluminescence (ECL) in a static electrochemical cell. The reaction between tris(2,2'-bipyridine)ruthenium(II) dichloride hexahydrate ($Ru(bpy)_3^{2+}$) and tertiary amine containing drugs (atropine and codeine) was investigated using the dip coated electrodes. The blank sol-gel and the ITO doped sol-gel coatings gave increases in ECL signal of 132 % and 179 % respectively in comparison to the non coated electrodes. This increase in ECL signal was thought to occur due to the formation of an advantageous conducting micro-environment within the sol-gel.

Chapter four describes the immobilisation of the $Ru(bpy)_3^{2+}$ within the conducting sol-gel matrix to produce an integrated sensing system. Initially this was attempted through the introduction of $Ru(bpy)_3^{2+}$ to the sol-gel during its solution phase, however due to $Ru(bpy)_3^{2+}$ being water soluble the ECL reagent leached out of the sol-gel into the bulk aqueous based analyte solution, thus reducing any ECL signals. Initial attempts to overcome this involved the use of Nafion ion exchange resin within the sol-gel. This was found to reduce $Ru(bpy)_3^{2+}$ leaching, but the ECL signal still decreased.

Finally in chapter four a different approach was investigated in which a $Ru(bpy)_3^{2+}$ derivative capable of covalently bonding to silica substrates such as glass coils, micro channels and optical fibres was investigated. This derivative, 4,4'-bis[(3-triethoxysilylpropyl)amide]-2,2'-bipyridine] bis-(2,2'-bipyridine) ruthenium (II) dichloride, was analysed through both CL and ECL techniques *via* its attachment to

controlled pore glass (CPG) and a sol-gel coating respectively. The successful immobilisation of the derivative to CPG, and its CL application for the detection of codeine, produced an average CL signal of 35.5 mV (RSD = 2.98 %). With regards to the ECL analysis of codeine, reproducible ECL signals of 7.7 mV (% RSD = 1.07, n = 24) were achieved. In addition no leaching was observed in a range of commonly used solvents over a one year period.

In conclusion it has been demonstrated that it is possible to design and develop an ECL sensing systems in which the reagents are produced electrochemical or are immobilised. This type of approach is invaluable for *in situ* sensing.

Glossary of terms

CA: Chrono-Amperometry

CL: Chemiluminescence

CV: Cyclic Voltammetry

CPG: Controlled pore glass

ECL: Electro-generated chemiluminescence

EtOH: Ethanol

HPLC: High Performance Liquid Chromatography

ITO: Indium Tin Oxide

LC-MS: Liquid Chromatography-Mass Spectrometry

LED: Light Emitting Diode

MeOH: Methanol

MS: Mass Spectrometry

MP-ITO: Micro Particle size Indium Tin Oxide

NP-ITO: Nano Particle size Indium Tin Oxide

OLED: Organic Light Emitting Diode

PAH: Polynuclear Aromatic Hydrocarbon

PEDOT: Poly-3,4-ethylenedioxythiophene

PLED: Polymer Light Emitting Diode

PMT: Photo Multiplier Tube

PTFE: Polytetrafluoroethylene

$Ru(bpy)_3^{2+}$: Tris(2,2'-bipyridyl)ruthenium(II) dichloride hexahydrate

SERS/SERRS: Surface Enhanced Raman Spectroscopy

TEOS: Tetraethoxysilane

TMOS: Tetramethoxysilane

UV/VIS: Ultraviolet/Visible (spectrometry/spectrometer)

Table of contents

Chapter 1 – Introduction

1.0 Aims of chapter

The aims of this chapter are to describe and discuss the techniques and theory that underpin this work and to provide the reader with a general understanding of the how this project developed. This will be achieved by describing the theory, where possible in the same order in which it was used although some of this theory will be left until the relevant chapters if it can be better described using relevant examples from the work.

1.1 Overview of project aims

This project aimed to develop an optically transparent, electro-conducting sol-gel through the immobilisation of indium tin oxide or another suitable moiety within the sol-gel matrix. Then to further develop this material for use in a sensor system for the analysis of tertiary amine containing drugs of abuse.

1.2 Sol-gels

1.2.1 Sol-gels: History and current uses

A sol-gel is a porous, optically transparent homogeneous glass that exhibits good chemical inertness and has low processing temperatures. They were discovered by chance in 1846 by Ebelman [1] who found that solutions of $SiCl_4$ and alcohol gelled with exposure to air. He wrote that it was his wish that sol-gels could be employed in the construction of optical instruments, a wish that only now is coming to fruition through the introduction of sol-gel lenses [2, 3]. This work was of little interest outside the chemistry community until 1930's when the Schott Glaswerke Company

of Germany attempted to devise a method to cover industrial glass with a thin oxide layer. This work provided the basis for the dip coating techniques that are use today, but was later abandoned by Schott due to economic reasons brought upon by World War II. Other groups have also studied sol-gels, for example Roy and Roy [4, 5] in the 1950's attempted to fabricate sol-gel nano-spheres as a means of containing radioactive powders produced in the manufacture of fuel cells used in nuclear reactors. It was not until the 1970's when Yoldas [6] and Yamane [7] demonstrated that it was possible to produce sol-gel monoliths at room temperature through careful drying that the current interest in sol-gel fabrication was triggered. Ironically the area of sol-gel research that seems to have produced the most promising applications has been in thin films and spheres, the very areas of research undertook by the Schott company in the 30's and Roy and Roy in the 50's; work which was largely ignored.

Yoldas and Yamane's research instigated a new awareness in sol-gel chemistry that has led to a multitude of new applications for the technique including solid-state electrochemical sensors [8-10], antistatic/reflective coatings [11, 12], chemical processing [13] and novel glasses [14, 15]. An example of this would be the work undertaken by Avnir *et al.* [16] who demonstrated that it was possible to entrap organic molecules in a sol-gel matrix. The importance of this discovery was that it overcame the inherent difficulty of incorporating organic molecules within glass or ceramics due to the differences in working temperature. Typically the manipulation of glass or ceramics occurs above 1000 °C; whereas organic compounds rarely survive past 200 °C. This work demonstrated that it was possible to encapsulate heat sensitive molecules into the sol-gel matrix at room temperature without a severe loss of activity. This led to a global expansion of related research into molecule

encapsulation inside sol-gel matrices that included examples such as proteins [17], enzymes [18-20], redox probes [8, 21, 22] and dyes [23-27]. This work has allowed the development of methodologically novel sensors, including pH [23, 24, 26, 28], glucose [18, 20, 29], oxygen [17, 27, 30] and lactate oxidase [19] amongst others.

As mentioned, thin films and nano-spheres have provided the basis for the more successful application in sol-gel research, particularly in the area of sensor fabrication and optical coatings. As such, much of the current interest in sol-gel has its origins in these areas [31-34].

1.2.2 Non-silicate sol-gels

This section provides an overview of non-silicate based sol-gels including aluminium, borate and transition metal alkoxide precursors. However much of the related discussion on hydrolysis and condensation will be delayed until the discussion of the silicate sol-gels used in this work (See section 1.2.3.).

The first type of sol-gels to be examined are the transition metal alkoxide based sol-gels which are typically formed when metal alkoxides undergo hydrolysis and condensation reactions to produce the bulk sol-gel glasses, films or fibres required. The rates of these reactions and the properties of the sol-gels are subject to, amongst other things, the initial transition metal precursor, pH, water concentration and temperature. These are the same parameters that govern the formation and properties of silicate sol-gels as discussed in section 1.2.3.

However there are several differences between the transition metal alkoxides and the silicon alkoxides. Firstly the lower electro-negativity of the transition metals make them more electrophilic and thus less stable towards hydrolysis and condensation reactions than the silicon alkoxide counterparts [2]. In addition transition metal alkoxides often exhibit the ability to form several stable coordination forms. Also due to the high reactivity of the transition metal alkoxides great care must be taken with regards to moisture and hydrolysis conditions in order to prepare homogeneous sol-gels as opposed to precipitates.

The most commonly used transition metals in sol-gel chemistry include titanium, zirconium, and vanadium and these produce some of the most industrially successful sol-gels products [16]. An example of which is IROX™ [15] , a palladium containing TiO_2 coating produced by Schott in Germany which is used extensively on architectural glass to prevent heat loss in buildings. However the transition metal sol-gels are often chemically modified with alcohols, halides, chelating ligands and other types of sol-gel precursor, either *via* mixing or through covalent bonding. This is often performed in order to retard or stop the rapid hydrolysis reactions found with this type of sol-gel, in order to allow for a more controlled sol-gel forming condensation reaction. In general, less electronegative ligands are removed first during hydrolysis therefore by modifying existing ligands with more electronegative ligands it is possible to delay (or stop) this reaction. This can be utilised in a number of ways, for example, delaying the onset of the condensation reaction provides more time in which to perform spin-coating (a technique used to fabricate thin films, discussed in 2.3.4.1), therefore making this procedure easier. In addition it is possible to modify the sol-gel precursor ligands with a secondary active component such as

fluorescent or pH active dyes in order to provide the basis for a sensor, again many of these dyes are structurally bulky which will also reduce the hydrolysis reaction due to steric hindrance [35].

As well as the transition metal sol-gels there are two other common types of non-silicate sol-gels; those formed by aluminium and borate systems. Yoldas [6] discovered in the 1970's that is was possible to fabricate aluminium based sol-gels from aluminium alkoxide precursors. This is typically performed using tributoxyaluminium, shown in Figure 1.1, in a large excess of water at 80-100 °C. This produces a fibrillar boehmite (γ-AlO(OH), an ore mineral of aluminium found in bauxite [36]) which through the reaction shown in Figure 1.2 forms a stable particulate sol-gel [2]. Gelation, the condensation part of this reaction, is typically reached through the concentration of the sol solution through boiling or evaporation; with changes to any of the aforementioned parameters resulting in structural changes in the sol-gel matrix.

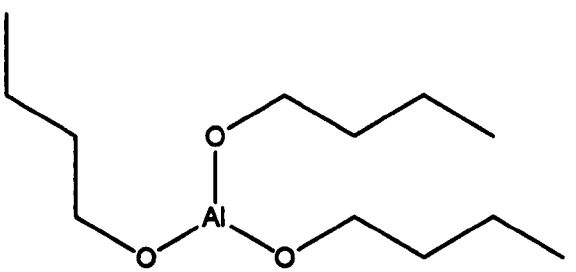

Figure 1.1: Tributoxyaluminium, the typical alkoxide precursor used in aluminium sol-gel fabrication.

Figure 1.2, adapted from Brinker and Scherer [2], demonstrates the aluminium based sol-gel reaction discussed previously. This process, developed by Yoldas [6] greatly contributed to the current interest in sol-gel science. This system differs slightly from

the silicon and the transition metal alkoxide sol-gels discussed, because a different condensation reaction is observed due to the excess of water in this reaction.

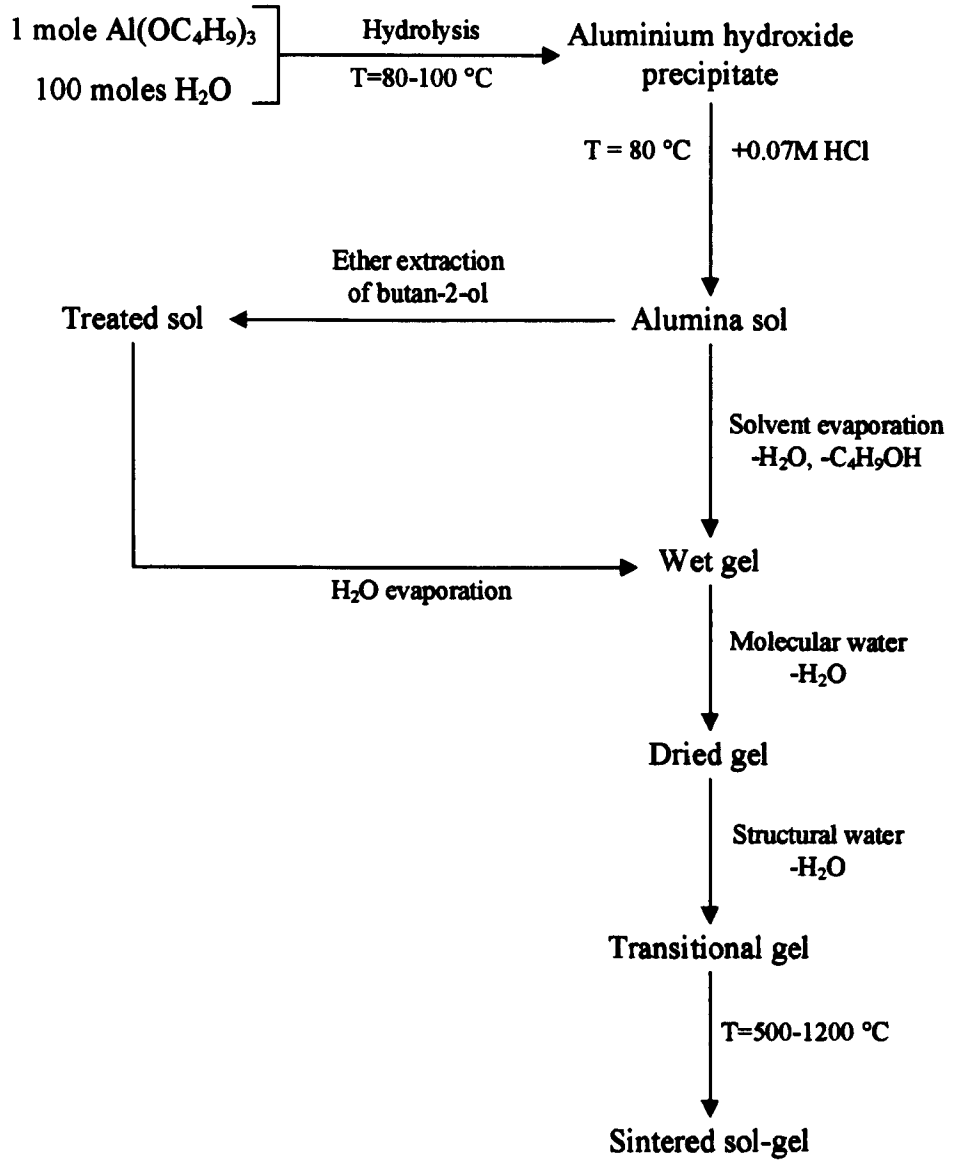

Figure 1.2: Graphical representation of the Yoldas method for aluminium alkoxide based sol-gel preparation.

Borate sol-gels were first synthesised by Toghe *et al* [37] in 1984 with ensuing work by Brinker, discussed in his book "Sol-gel science" [2] concentrating on reactions involving a lithium borate system. Commonly borate gels are formed *via* the Brinker

method using a tributoxyboron (Figure 1.3), lithium methoxide and water synthesis technique, as shown in Figure 1.4.

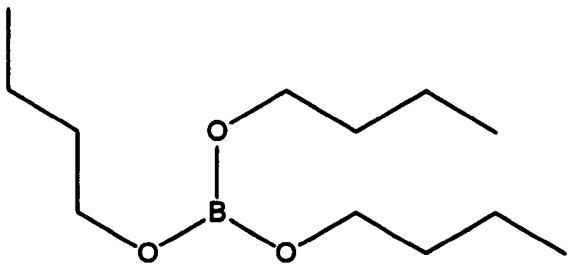

Figure 1.3: The chemical structure of Tributoxyboron.

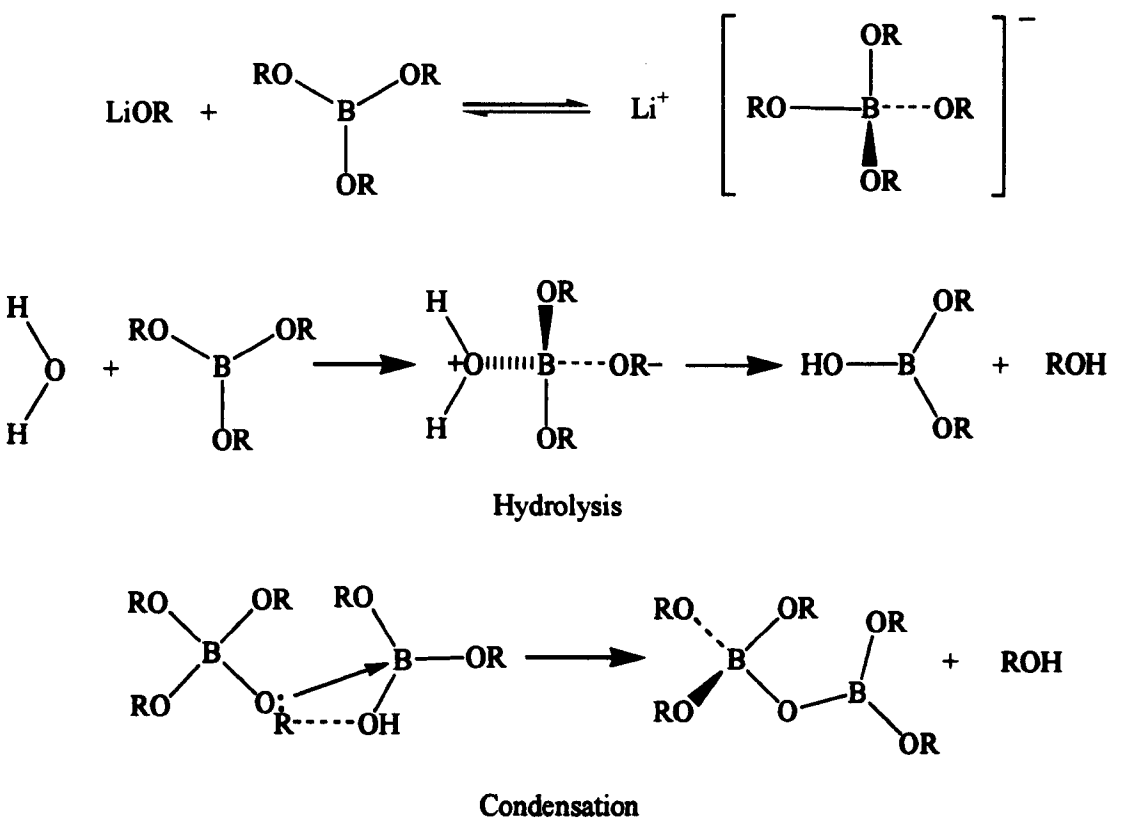

Figure 1.4: Chemical reaction of a typical lithium borate sol-gel system.

Both hydrolysis and condensation can occur with mechanisms involving nucleophilic attack of the OH or OR ligands on a trigonal boron, generating alcohol or water as

reaction by-product, as demonstrated in Figure 1.4. Brinker *et al.* state that due to the lack of sp^3d hybridisation requirement for the intermediates in Figure 1.4, nucleophilic reaction between tetrahedral boron is unlikely. However, as is also shown in Figure 1.4 a reaction between a trigonal and tetrahedral boron is permitted, and according to Brinker essential for the formation of sol-gel structures. Brinker's group discovered using Small Angle X-ray Scattering (SAXS) that there was a minimum fraction of tetrahedral coordinated boron (N_4) needed to instigate gelation. When N_4 was below 0.14 no gel growth was observed, between N_4 = 0.14 and 0.19 weak sol-gels were formed whist value ranging from 0.22 & 0.28 produced rigid sol-gels. This is due to the stability of B-O-B bonds towards dissociative reaction of the type shown in Figure 1.5.

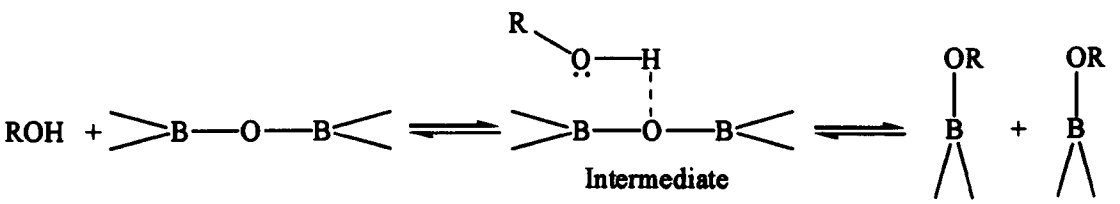

Figure 1.5: Demonstrating the dissociative reaction of B-O-B bonds found in borate based sol-gels.

This nucleophilic reaction is not possible for tetrahedral coordinated boron as boron cannot utilise sp^3d hybridisation. Therefore according to Brinker the kinetic stability of B-O-B bonds is expected to decrease as shown in Figure 1.6.

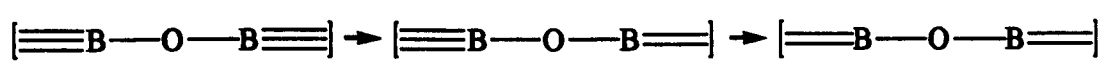

Figure 1.6: According to Brinker the kinetic stability of B-O-B bonds is expected to decrease in the above manor.

1.2.3 Silicate sol-gel

This section aims to discuss the different types of silicate sol-gels including examples of silicon alkoxides, hybrids and organically modified silicate (ORMOSILs); and will discuss their chemistry, fabrication techniques and uses.

As mentioned in section 1.1.1, silicon alkoxide based sol-gels are the most widely studied and used sol-gel type [2]. In their simplest form silicon alkoxides have a $Si(OR)_4$ tetrafunctional structure with the R group being an identical alkoxide ligand, with commonly used ligands include methoxy, ethoxy, n-propoxy, n-butoxy. In some studies one or more ligands have been substituted to form organotrialkoxysilane or a diorganodialkoxysilane, with the substituted ligand imparting a property desirable for the study, for example being non-hydrolysable However the most common types of silicon alkoxide are tetramethoxysilane (TMOS) and tetraethoxysilane (TEOS), shown in Figure 1.7

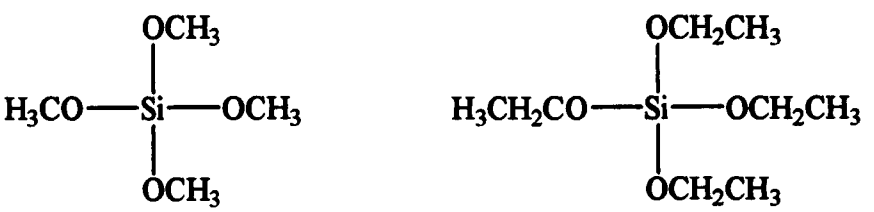

TMOS
$C_4H_{12}O_4Si$

TEOS
$C_8H_{20}O_4Si$

Figure 1.7: Chemical structures of tetramethoxysilane (TMOS) and tetraethoxysilane (TEOS).

TMOS is the main sol-gel precursor in this work although some experiments have been performed using TEOS for comparison. Since TMOS is the primary precursor

all data and reaction mechanisms will be with reference to it unless otherwise stated, however most of the reaction mechanisms can be safely extrapolated between the different $Si(OR)_4$ sol-gel types.

The sol-gel process can be broken down into three main reaction mechanisms as shown in Figure 1.8, each of which will be described in details in the following order.

Hydrolysis: Where alkoxide groups are replace with hydroxyl groups (Figure 1.8a).

Water condensation: Where siloxane groups are formed from a reaction between silanol groups (Figure 1.8b).

Alcohol condensation: Where siloxane groups are formed through a silanol/silanate reaction (Figure 1.8c).

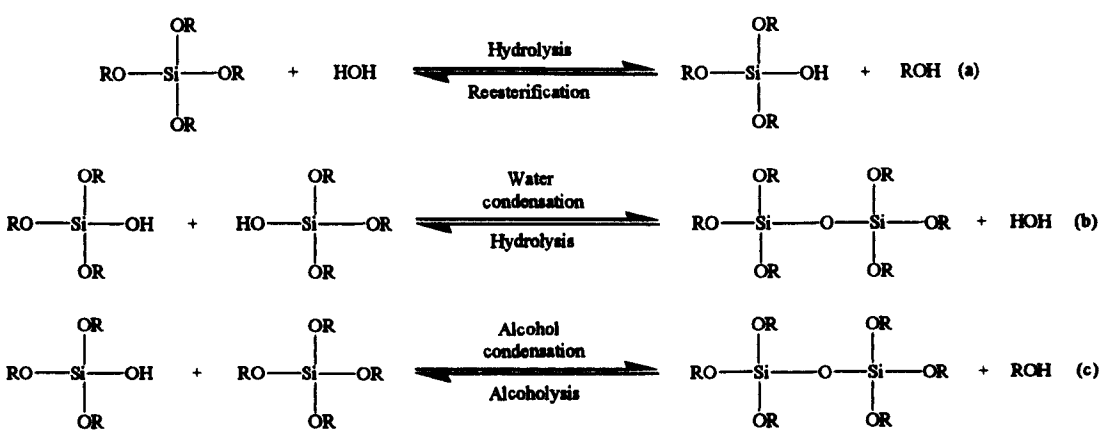

Figure 1.8: Simplified sol-gel reaction.

1.2.3.1 Hydrolysis

The first step in the sol-gel process is the hydrolysis reaction which is believed to follow an S_n2 type transition state initiated through the addition of water to the silicon alkoxide precursor with the aid of a specific acid (hydronium ion) or specific base (hydroxyl ion) catalyst; were the alkoxide group (OR) is replaced by a hydroxyl group (OH). As silicon alkoxides and water are immiscible a co-solvent such as methanol is often used to initiate the reaction. Although it is not essential as alcohol is produced in sufficient amounts initially to instigate this reaction; indeed during this work no co-solvent was employed for this purpose

It is possible for the hydrolysis reaction to go to completion, converting each of the ligands from an alkoxide to a hydroxyl group. However this depends on a number of factors including water : Si ratio (R-value), type and volume of catalyst, temperature and pH, therefore a more accurate reaction mechanism is shown in Figure 1.9.

$$Si(OCH_3)_4 + nH_2O \rightarrow Si(OCH_3)_{4-n}(OH)_n + 4_{-n}CH_3OH$$

Figure 1.9: A more accurate representation of the hydrolysis reaction given that not all the alkoxide groups have to be substituted for hydroxy groups in the reaction.

Figure 1.9 demonstrates that hydrolysis may go to partial completion helping to provide an explanation for the two condensation reactions "silanol to silanol" and "silanol to silanate" as shown in Figure 1.8.

Hydrolysis occurs from the nucleophilic attack of the oxygen atom of water on the silicon atom. In acid catalysed hydrolysis, with the catalyst typically being a mineral acid, the alkoxide group is protonated; which withdraws electron density away from the silicon atom making it more electrophilic. The water molecule then attacks from the rear of the silicon atom and acquires a partial positive charge. This in turn reduces the positive charge of the protonated alkoxide group, making the alcohol a superior leaving group as shown in Figure 1.10. Factors such as steric interference and R-values can affect this mechanism and will be discussed later in this section.

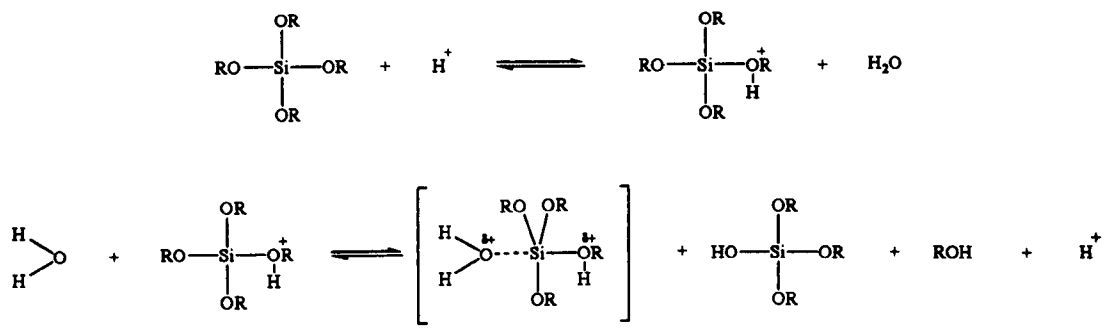

Figure 1.10: Acid catalysed hydrolysis reaction.

Under base catalysis, with the catalyst typically being ammonia, it is thought that water dissociates to produce a nucleophilic hydroxyl anion that initiates hydrolysis by attacking the silicon atom via an S_n2 reaction mechanism, as shown in Figure 1.11 [38]. However under these conditions the hydrolysis reaction proceeds at a slower rate than that observed in acid catalysed reactions due to the silicon atom acquiring a formal negative charge that repels the attacking anion. However as each alkoxide group is replaced by more electron withdrawing substituent, such as the hydroxide and siloxane groups', the negative charge on the silicon stabilises increasing the rate of hydrolysis.

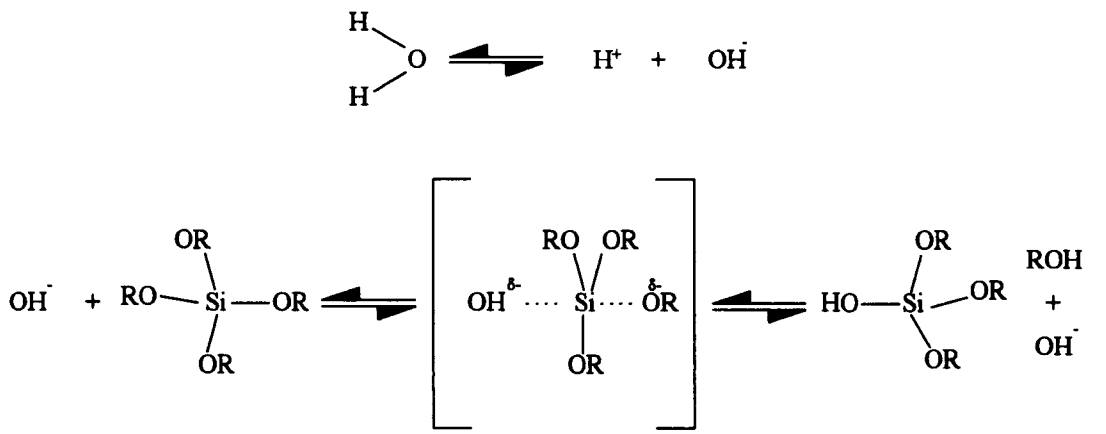

Figure 1.11: Base catalysed hydrolysis reaction.

As noted steric effects can also change the hydrolysis rate of reaction in sol-gels. Steric crowding caused by long chain-length or branched alkoxides can reduce the rate by which the attacking nucleophilic molecules react with the central silicon atom and leads to an increase in hydrolysis times. Aelion *et al.* [39] compared the effect of different alkyl chain lengths and branching on the rate constant (*k*) for the hydrolysis under acid catalysis, as shown in Table 1.1.

R	*k* 10^2 (l mol^{-1} s^{-1} $[h^+]^{-1}$)
C_2H_5	5.1
C_4H_9	1.9
C_6H_{13}	0.83
$(CH_3)_2CH(CH_2)_3CH(CH_3)CH_2$	0.3

Table 1.1: Rate constant *k* for acid hydrolysis of tetraalkoxysilanes $Si(OR)_4$ at 20°C

Source for Table 1.1: Aelion *et al.* [39].

The subsequent substitution of alkoxy groups for hydroxyl groups also affects the rate of the hydrolysis reaction, this effect is different for acid and base catalysis. Work undertaken by Schmidt *et al.* [40] found that under acid catalysis conditions each subsequent substitution of alkoxy group to that of a hydroxy group reduced the

rate of reaction of the hydrolysis reaction. This is due to the stabilisation of the positively charged transition state brought about through the superior electron withdrawing properties of the hydroxy group compared to the alkoxy group. This increase in electron withdrawing demonstrated by the hydroxy ligand leads to a reduced electron density on the silicon and a gradual stabilisation of the molecule. With each subsequent substitution reducing the rate of reaction of the hydrolysis step and increasing the stability of the molecule, as shown in Figure 1.10. By comparison the increased stability of the molecule resulting from the increased electron withdrawing properties of the hydroxy group favours the base catalysis reaction. Therefore with each subsequent hydroxy substitution the rate of reaction for the hydrolysis step increases. Both reactions however benefit equally from the reduced steric effects given through the reduction of lengthy or branched alkoxy groups with hydroxy groups.

Along with solvent and catalyst effect, another compositional variation that can affect the hydrolysis reaction is the H_2O:Si ratio, know as the R-value and which has considerable effect on the physical characteristics of the resulting sol-gel. R-values are calculated by dividing the molar concentration of the water content in the sol-gel solution with the silicon content. It is generally considered that increased R-values result in a decrease in gelation times. Schmitt *et al.* [40] studied the acid catalysed hydrolysis reactions of three different R-value types, R = 0.3 (low water), R = 4 (medium water) and R = 10 (high water). This study confirmed the increase in R-value decreased gelation time; additionally it was found that lower R-values left residual unhydrolysed monomer. This may be expected at R = 0.3 given the scarcity of water in the reaction, but it was found that after four hours unhydrolysed

monomers remained in the R = 4 solutions. In addition, completely hydrolysed monomers (*i.e.* $Si(OH)_{4-n}(OR)_n$) were formed at higher R-values, slightly contradicting Schmitt with regards to the retarding effect of water on acid catalysed hydrolysis discussed previously. Though it is believed that from $R \geq 2$ water condensation is favoured but below this figure alcohol condensation is favoured.

Changes in R-values have also been found to effect sol-gels physical properties and have been specifically tailored to suit a specific task such as spin coating, monolith fabrication or SiO_2 nano-particle production. For example by using high R-values in the range of 30 with concentration of ammonia ranging from 1 to 7 M it is possible to fabricate monodispersed spherical particles.

1.2.3.2 Sol-gel condensation reactions

As noted in section 1.1.3, the sol-gel structure forms through a polymerisation step consisting of two different reactions, water condensation and alcohol condensation, shown in Figure 1.12. Here the partly or fully hydrolysed sol-gel monomers ($Si(OH)_{4-x}(OR)_x$) polymerise into larger particles in a stepwise fashion governed by the pH of the hydrolysed sol. Although it should be noted that under most conditions the hydrolysis step continues whilst the condensation reactions proliferates, in fact hydrolysis and alcoholysis are essential in forming sol-gels as will be discussed later.

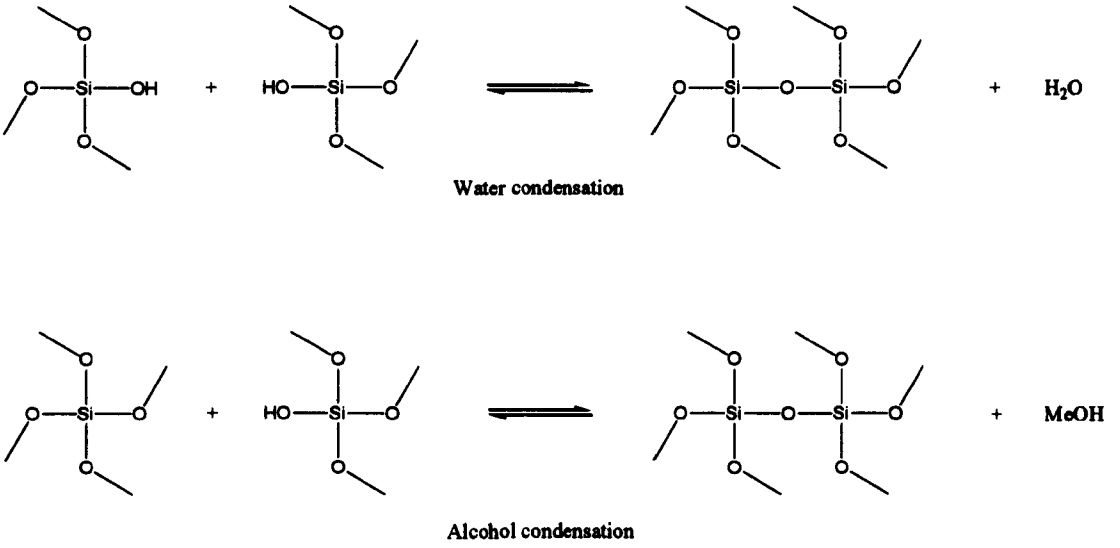

Figure 1.12: Water and alcohol condensation reactions.

As with hydrolysis, the condensation reactions can be both acid and base catalysed (shown in Figures 1.13 and 1.14), although in this instance the name is ambiguous as it is considered that base catalysis occurs at pHs greater the pH 2. pH 2 corresponds to the isoelectric point of silica, were the lack of surface charge results in the minimum condensation rate. As shown in Figure 1.13, acid condensation involves a protonated silanol species.

The reaction mechanism proposed by Pohl and Osterholtz [41] and discussed by Brinker *et al.* [2] hypothesised that the protonation of the silicon makes it more electrophilic, and hence more susceptible to nucleophilic attack. With the more simple silanol species, *i.e.* monomers or weakly branched oligomers, being most likely to be protonated. Resulting in acid condensation reactions occurring preferentially between neutral species and protonated silanols situated on monomers, end groups and the end groups of chains. Below pH 2 the condensation rate is proportional to the H^+ concentration. However as solubility of silica is very low at these pHs (see Figure 1.15) the structural evolution of the sol-gel occurs simultaneously with the growth of the primary particles, the dimers and trimers and

other polysilicates. This drastically reduces particle growth and ultimately leads to the formation of highly fractal structure composed of small primary particles of generally no more than 2nm in diameter.

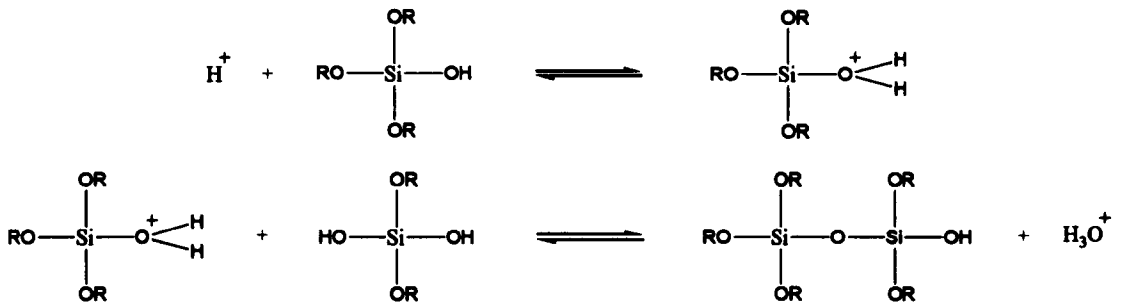

Figure 1.13: Proposed mechanism for acid condensation of silica sol-gels.

By comparison, Iler [38] provides the most widely accepted mechanism for base catalysed condensation reactions for silica alkoxide based sol-gels (Figure 1.14), although other groups have suggested changes to this mechanism. As stated previously, base catalysed condensation reactions actually relate to reactions above the isoelectric point of silica at approximately pH 2, and are the most common method for fabricating sol-gels. Iler [38] stated that replacing OH or OR groups with OSi resulted in a reduced electron density around the silicon atom which in turn increased the acidity of the remaining silanols [2].

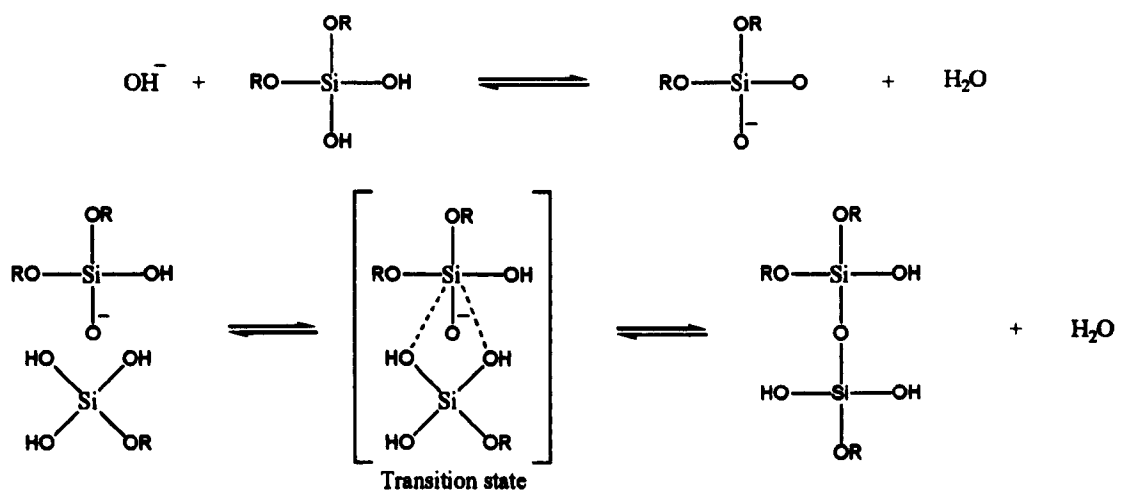

Figure 1.14: Proposed mechanism for base condensation of silica sol-gels.

According to Brinker [2], Iler's mechanism favours reactions between larger, more highly condensed species that contain acidic silanols and smaller less weakly branched species. With a maximum condensation rate occurring around neutral pH's where significant concentrations of both protonated and deprotonated silanols exist [2].

Further subdivisions can be made between pH 2-8 and pH 8-12 with regards to base catalysed condensation. With both pH ranges the condensation rates are proportional to –OH concentration, with the sol-gel developing from monomers to dimers, and then with subsequent monomer addition to form trimers, tetramers and finally cyclic structures. Between pH 2-8 sol-gel particles grow through the addition of lower molecular weight species to more condensed species to form larger sol-gel particles. However a lack of solubility at this pH (see Figure 1.15) prevents these larger particles depolymerising which restricts particle size to approximately 2-4nm in diameter; these particles subsequently aggregate to form fractal networks.

Above pH 8 the solubility of silica is greater, and therefore smaller particles and aggregates may dissolve and repolymerise into larger aggregates, a process called Ostwald ripening, with average particle size being between 5-10 nm [2]. This process produces a final sol-gel structure of highly branched clusters of these large particles.

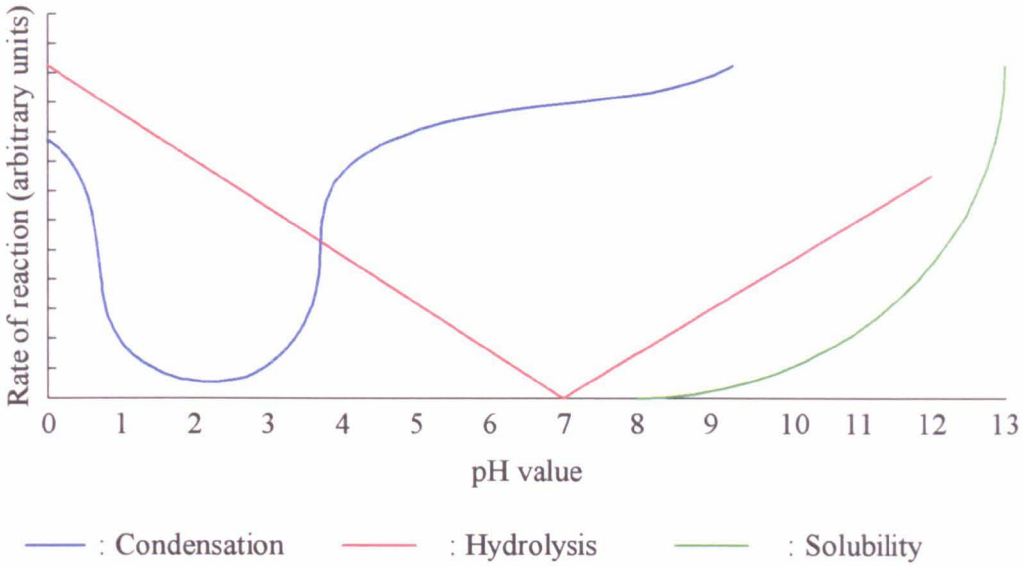

Figure 1.15: pH dependence on the solubility of silica and the reaction rates for hydrolysis and condensation.

To conclude this section it is worth reiterating that both acid and base hydrolysis and condensation occur *via* S_N2 routes and that the formation and subsequent structural characteristics of sol-gel glasses is dependent on a number of parameters, including pH, R-value and starting materials. An understanding of these parameters will help enable the user to specifically develop a sol-gel fit for purpose, *i.e.* thin films, monoliths or spheres.

1.2.3.3 Ageing

Once a sol-gel polymerises, for example into a sol-gel monolith, it undergoes the transition stage of ageing. In fact, ageing is nothing more than a continuation of the condensation reactions, and to a lesser extent to hydrolysis reaction that formed the sol-gel structure. However ageing provides a pivotal role in determining the structure of the sol-gel and may introduce a number of fabrication problems with regards to satisfactory sol-gel fabrication. The additional condensation reactions that occur

during the aging process promotes greater cross linking in the structure, which leads to an increase in structural strength and a reduction in pore size. This can also lead to the sol-gel shrinking and also in certain conditions cracking; these properties are discussed further in 1.2.3.4 and Chapter 2. However if the sol-gel is maintained in an aqueous solution during the aging process, shrinkage can be reduced and the resulting gel is termed a hydrogel as the pores contain the aqueous solution [42].

1.2.3.4 Drying

In essence drying is removing the liquid from the porous structure of the sol-gel resulting in the fabrication of either a zerogel (a minimal or non porous sol-gel) or an aerogel (a sol-gel that maintains a substantial porous structure). Drying is usually accomplished through evaporation, where the pore based water and alcohol are driven off. This process often leads to cracking and warping if it proceeds too rapidly or unevenly; and with cost of fabrication is one of the main reasons why sol-gel monoliths have been relatively unsuccessful industrially [43].

Evaporation during the drying process leads to the exposure of the sol-gel network to air; when this occurs capillary forces between the liquid and solid phases of the sol-gel withdraw liquid from the interior of the sol-gel to replace that which has been lost. Since the liquid volume in the sol-gel has been reduced, the liquid forms a concave meniscus in the surface pores of the gel, which produces a contracting tension. This tension is taken up by the solid structure of the pore walls and is defined by the following equation, where P = tension in liquid; γ_{LV} = liquid-vapour interfacial energy and r = radius of curvature of the meniscus.

$$P = \frac{-2\gamma_{LV}}{r}$$

During the early stages of drying, the solid structures being formed are pliant enough to allow them to be pulled back toward the liquid surface, therefore reducing the volume and the tension in the gel. As the sol-gel develops through formation of new siloxane bonds it becomes stronger, less porous and more rigid. Eventually, the structure is able to withstand the liquid tension and the meniscus line is forced into the body of sol-gel. Evaporation subsequently occurs within the body of the sol-gel and the liquid is transported to the surface of the gel as vapour, decreasing the rate of evaporation.

However as previously mentioned cracking and warping are major problems in the development of sol-gels, particularly monoliths. The higher tension found between the liquid and the sol-gel network near to the outer surface, which results from uneven drying, causes this section to shrink faster than the internal body of the sol-gel, which can lead to the sol-gel cracking. However if the drying surface is pliable, the shrinking differential between the drying and internal/covered part of the sol-gel can result in the monolith warping, although this usually happens in plate type monoliths (as shown in Figure 1.16).

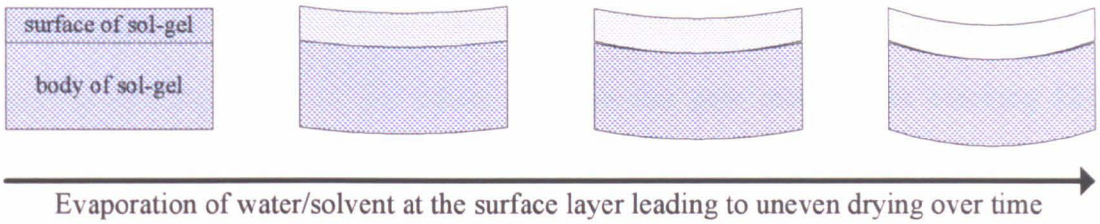

Figure 1.16: Demonstrating the warping effects produced by uneven drying on sol-gel monoliths. Here the outer surface of the sol-gel dries and shrinks more rapidly than the core which results in this effect.

Many ways have been examined in an attempt to overcome cracking and warping, by changing the rate of drying either through the use of Drying Control Chemical Additives (DCCAs) [2, 23], or changing the fabrication conditions in which the sol-gel dries [44]. Some examples of changes to the fabrication techniques are discussed in section 1.2.3.1 and 1.2.3.2, and examine alkoxide type, pH, R-value and form of catalysis. These changes in fabrication technique have been used to successfully produce different sol-gel types including spin coated and dip coated thin films, monoliths and spheres as discussed in section 1.2.1. However other techniques include supercritical drying [45], and freeze drying [46] have also been used successfully to promote crack free sol-gels. Both techniques work by preventing the formation of a liquid-vapour interface in the sol-gel pores that would normally produce the capillary stresses that cause shrinkage and cracking. In supercritical drying the pore liquid is removed by raising the temperature and pressure of the liquid in such a way that the liquid-vapour phase boundary is not crossed. Once the critical temperature/pressure point is reached the liquid and vapour densities become equal which removes the capillary stresses on the sol-gel and allows the solvent to be vented. With freeze drying the pore liquid is frozen and then sublimed off under

vacuum. However this technique cannot be used for the production of monolithic sol-gels as the expansion of the liquid stretches the gels resulting in cracking [2]. However if a silica sol is frozen, it is possible to produce flakes of silica, referred to as lepidoidal silica, if the freezing is unidirectional it is also possible to produce fibres. Although these techniques are valuable the extreme temperatures and pressure required to use them prevents their use with many organic or protein based encapsulation systems due to degradation.

Drying Control Chemical Additives (DCCAs), as already mentioned, may also be used to reduce the interfacial energy at the liquid-vapour interface and are normally introduced to the sol-gel prior to gelation. Examples of these compounds include surfactants (such as Triton X-100), glycerol formamide and oxalic acid, for instance formamide can be used to replace half the solvent ordinarily used when making silica sol-gels; and results in sol-gels with larger and more uniform pores, features that can help the sol-gel to be fabricated crack free [2, 47].

According to Zarzycki *et al.* [48] in their study of monolithic sol-gels, supercritical drying provided the best means by which to fabricate monolithic sol-gel, although as discussed previously this technique also has inherent problems.

1.2.3.5 Sol-gel fabrication types

The previous sections in this chapter have discussed the ways in which sol-gels may be fabricated using various techniques and reagents or levels of reagents. The following will briefly discuss some of the applications for the different types of sol-gels, such as thin films and monoliths and discuss some industrial applications. Out

of necessity some of this information will overlap some of the technical information already provided, however it is felt necessary in order to provide a coherent explanation of the different types of sol-gels.

Sol-gel monoliths: -

According to Brinker *et al.* [2] a sol-gel monolith is a block of sol-gel material with dimensions greater than a few millimetres. This definition is a little imprecise but in essence correct, as it does not account for fibres which are generally greater than this dimension in one aspect but not normally classed as monoliths. As mentioned in section 1.2.1, the work in the 1970's by Yoldas [6] and Yamane [7] initiated the current interest in sol-gels through their work into the fabrication of monoliths. Although this work started the current interest into sol-gels it is the least used of the sol-gel types due to a number of different aspects. Firstly, as discussed in the previous sections it is difficult to make large crack and warp free sol-gel monoliths. Of which those produced suffer from shrinkage, even when techniques such as supercritical drying are used; results shown in section 2.1.2 demonstrates the variance in this shrinking helping to explain its lack of use in industrial processes. Finally for most situations where large glass monoliths are required such as glazing and lenses it is simply cheaper and simpler to manufacture them *via* conventional methods.

However there are uses for sol-gels monoliths, for example Collinson *et al.* [49] have used monolithic gels as an encapsulating material for tris (2,2-'bypyridyl) ruthenium (II) dichloride hexahydrate ($Ru(bpy)_3^{2+}$) for use in solid state electro-generated

chemiluminescence work. Avnir [16] used sol-gel monoliths to entrap enzymes within a sol-gel matrix; whilst Lan [17] amongst others has encapsulated heme proteins, both were accomplished whilst maintaining activity and minimising denaturing. Schottner [50], in a review on hybrid sol-gels discusses research using acrylate modified alkoxide sol-gels as a replacement for dental amalgam. However it is apparent that the allure and dream that first instigated this work in producing room temperature bricks of sol-gel is nonsense and that a more realistic aim is in the realm of smaller monoliths. For example taking advantage of the encapsulation properties to produce filters or solid state sensors like Collinson's group [49], or in the development of smaller windows such as the sample window in UV/Vis spectrometers that may benefit from the excellent UV transparency provided by a sol-gel.

Sol-gel thin films: -

Thin films are unquestionably the most successful sol-gel technique with regards to industrial applications. There are three main techniques employed with regards to the application of thin films, spin coating, dip coating and spray coating. Both spin coating and dip coating are employed in the work conducted in this thesis and the principles are discussed in 2.3.4.1 and 3.2.3 respectively. All these techniques however share a basic premise in providing a thin sol-gel layer on the substrate of choice with a thickness of approximately 1μm. Each technique does this differently, in spin coating an aliquot of sol-gel solution is applied to the substrate of choice which is subsequently spun rapidly, thus forcing the solution outwards due to inertia and providing a thin film. Obviously a flat surface is required for this and therefore this technique is commonly employed with glass slides, and metal/ceramic sheets

and has been used to encapsulate dyes [24, 25, 51], proteins [17] or enzymes [52] in order to quantify properties such a pH [23-25] and oxygen [17].

In comparison dip coating, as the name suggests involves dipping the substrate of interest in to the sol-gel solution that has previously undergone hydrolysis and slowly removing it to leave a thin sol-gel coating. This technique is used in this work to provide an encapsulation matrix on carbon electrodes as discussed in Chapters 3 and 4. Industrially, it has also been used to fabricate a dye encapsulating sol-gel coating on fibre optic cables for fluorescent based oxygen sensor such as the Ocean Optics INC FOXY probe, where the sol-gel acts as an encapsulating matrix for the dye. This technique is most notably used with fibres and thin rods, such as the FOXY probe and the electrodes as discussed in Chapters 3 & 4, were using spray or spin coating would be difficult. Although it has been used successfully with glass plates to produce scratch resistant [53] and antireflective coatings [54]. Other applications of dip coating include the fabrication of sol-gel composite electrodes, where a sol-gel is doped with a conducting material, typically carbon black or a metal [55, 56]. In addition this procedure is used to provide an encapsulating matrix for secondary moieties such as dyes [22, 30] and enzymes [18, 57] which have been coated on to optical fibres or electrodes for the analysis of pH [58] glucose [18] and oxygen [22, 30].

The final technique to be discussed is spray coating, which again as the names suggests involves the application of a thin sol-gel coating onto a substrate *via* a sprayed aerosol, much like spray painting. This technique is popular when large or

complexly shaped samples have to be treated, such as glazing and crystal glassware (As shown in Figure 1.17).

Figure 1.17: Demonstrating the use of coloured sol-gels to coat crystal glassware for decorative purposes.

This allows the preparation of sol-gel coatings that may provide a number of different properties including scratch resistance, solar protection and as decorative colour coatings on a variety of products ranging from windows, spectacles to crystal glassware as shown. Industrially, the Japanese car manufacturers, Honda, Mazda, Toyota and Nissan use fluoroalkoxysilane based sol-gel coatings on the windscreens of a number of their models to provide a water repelling coating [59]. This coating reduces the surface energy of the glass reducing the interaction between the water and the windscreen resulting in the water forming beads that easily run off the surface. This coating also allows the easy removal of ice, snow and even insect matter from the windscreen; however due to its industrial importance there is little information with regards to the coatings durability.

Sol-gel fibres: -

Sol-gel fibres are of interest due to their potential use as catalyst supports, high temperature filters and as reinforcing supports in metal/ceramic composites [60]. As with other types of sol-gel, specific compositional requirements have to be met in order for the fibre to be produced. An example given by Muralidharan and Agrawal [60] uses a mixture of tetraethylorthosilicate (TEOS), titanium tetrabutoxide (TTB), isopropanol, water and hydrochloric acid in a molar ratio of 1:0.09:10:0.5:0.1 , mixed and kept at 60 °C for 24 hours. Where upon fibres can be manufactured by rapidly dipping and extracting a steel wire within the sol-gel solution. However this technique does not appear to be as developed as sol-gel thin films are with regards to industrial applications and some of the potential applications are also applicable to sol-gel powders that appear to be easier to fabricate (catalyst support).

Sol-gel powders and PEBBLEs: -

Sol-gel powders and PEBBLEs (probes encapsulated by biological localised embedding) are the last fabrication types to be discussed and one that along with thin films seems to show promise with regards to industrial applications. Sol-gel PEBBLEs, nano to micro-sized silica particles, are commonly produced using the Stöber process [61] or related variations. In this process tetraalkylsilicates are typically mixed with an alcohol/water solution through which ammonia gas is bubbled. Stöber *et al.* found that a high pH and R-value were needed to form the micro-sized monodispersed silica spheres; in addition the absence of ammonia caused the silica to flocculate into irregular shaped particles, suggesting that ammonia influenced the morphology of the sphere fabrication. In modern research this process is typically performed in the presence of sensing components, such as

fluorescent dyes and enzymes [27, 62, 63], and has allowed the use of PEBBLE systems within live cells [27, 62] for the analysis of oxygen [27, 64], H^+ [62] and numerous cell signalling metal ions [62, 63]. The small size of the PEBBLEs makes them ideal for this work as they can be introduced to cells *via* injection, gene gun delivery, liposomal fusing or phagocytosis; with their small size reducing the risk of cell death. In conjunction with their ability to encapsulate situation specific dyes and enzymes, PEBBLEs make an excellent analytical platform for use in the analysis of cell mechanisms and toxic/environmental effects and may obviously be used for similar analysis in other medias such as waste water.

It is also possible to produce similar powders through conventional crushing and milling of sol-gel monoliths, which again may have encapsulated reagents; however it would be difficult to obtain such small and regular particles using this method.

1.3 Indium tin oxide

1.3.1 Indium tin oxide: History and current uses

Indium tin oxide (In_2O_3:Sn) more commonly referred to as ITO is an n-type semi conductor that demonstrates a high transmission in visible and near infrared light and has a low electrical resistivity.

Uses for ITO are numerous but usually involve its applications as a coating; normally taking advantage of its commercially desirable properties, *i.e.* being transparent and electrically conducting. Examples of these including its use as a charge carrier in electrochromic devices and computer screens [65], transparent electrodes [66, 67], organic light emitting diodes (OLEDs) and also as coating on aircraft and car

windows that allows them to be electrically heated for de-icing purposes [65]. In addition ITO is used on the canopy and windscreens of stealth aircraft and boats were it renders them radar silent [65]. This is achieved by absorbing the radar signals, preventing them from returning to the source emitter where detection would occur. ITO has also been used as an electro-conducting coating on glass in order to fabricate transparent electrodes. This offers obvious advantages for reactions such as electro-generated chemiluminescence (ECL) where a CCD could be co-attached to the electrode to allow photon collection near the emission site.

1.3.2 Chemical and physical characteristics of ITO

Pure indium oxide (In_2O_3) crystallises in a cubic bixbyite structure, with a space group of Ia3, meaning that it has a body centred cell (Figure 1.18) [68]. The indium cations are contained within two different six-fold-coordinated sites. A quarter of the indium cations occupy trigonally compressed octahedral units (Site b in figure 1.18) whilst the remaining ¾ occupy highly distorted octahedral units (Site d in Figure 1.18).

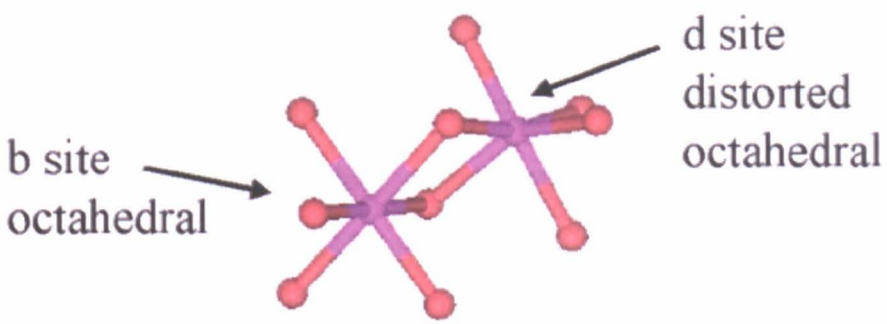

Figure 1.18: Indium cationic sites in the cubic bixbyite structure for In_2O_3 [68].

With regards to ITO (In_2O_3:Sn) structure it is generally recognised that the tin (Sn) atoms substitute for the indium in the structure with preference given to the less distorted site b. The difference in valance between In^{3+} and Sn^{4+} permits the donation of a free electron to the lattice, which allows for electrical conductance.

Before discussing conduction and orbital band properties of ITO, those of metals will be considered first in order to provide a point of reference for comparison. Band theory states that the electrical properties exhibited by a metallic solid result from the interactions between the atomic orbitals with the formation of atomic bands. Therefore bands are groups of molecular orbitals whose energy difference are so small that the system behaves as a continuous, non-quantised unit [65]. Under the influence of an electric field electrons are able to migrate within vacant orbitals within these bands, resulting in electrical conductance.

Although so far only one orbital has been examined, this theory also applies to migration between different atomic orbitals. Using sodium as an example, it is found that its atomic orbital structure is [Ne] $3s^1$. With the core atomic levels of this element (1s2 2s2 2p6) being held closely to the nucleus, and therefore being unable to react with neighbouring atoms, which of course will exhibit the same properties. However the higher energy 3s orbital extends away from the nucleus and overlaps with similar orbitals on neighbouring atoms to produce a conduction band, as previously discussed. With the application of an electric field, electrons in the 3s band are able to move to a higher energy band, which in the case of sodium allows for interaction with neighbouring 3s and 3p orbital/bands. In order to do this, two requirements need to be met, firstly the migrating electron must obey Hund's first

law [I] and the Pauli exclusion principle [II] [65] and secondly the band gap must be small enough for the electrical charge to cross. In sodium, four orbitals are available, 3s, 3px, 3py and 3pz, allowing for a maximum of eight electrons spaces in the shell.

These partially filled bands make it theoretically possible for the solid to conduct electricity; however the correct band gap is needed to conduct electricity. In non-conducting material (insulators) the orbitals of neighbouring atoms overlap very little, if at all (indicating that the electrons are held close to the nucleus), which results in a large band gap. The effect of which is that a large amount of energy is needed to promote an electron into a neighbouring orbital thus preventing electron migration throughout the material, making the compound an insulator (or at least a poor conductor). In a strongly conducting material such as sodium, the conduction bands are large and are either touching or very close, meaning that there is a small band gap and little energy is required to promote an electron between bands.

In this work indium tin oxide (ITO), an n-type semiconductor is used in order to allow electrical conduction through sol-gels monoliths and thin films. Semiconductors have band (energy) gaps much smaller than insulators but larger than that of metals such as sodium. Semi-conductors fall into two categories, intrinsic and extrinsic, with silicon, germanium and tin being examples of the former and ITO and gallium doped silicon being examples of the later.

[I] Hund's first rule: In a set of degenerate orbitals , electrons may not be spin paired in an orbital unit until each orbital in the set contains one electron; electrons singly occupying orbitals in a degenerate set of parallel spins i.e. they have the same values of m_s.

[II] Pauli exclusion principle: No two electrons in the same atom may have the same set of quantum numbers; it follows that each orbital can accommodate a maximum of two electrons with different m_s values (different spins i.e. spin paired).

The electrical conduction of the intrinsic semiconductors is a consequence of them having four valence orbitals and four valence electrons, which under bulk material conditions results in the formation of fully occupied band with an empty one at a higher energy. The band gaps for these higher energy orbitals for silicon, germanium and tin are 106, 64 and 8 $kJmol^{-1}$ respectively [65], with the conduction properties of tin (α allotrope) approaching that of metals. The conduction properties of these materials arise when electrons from the full valence orbitals migrate into the higher conducting orbitals acting as charge carriers; in addition the loss of the electrons from the valence orbitals leaves holes that can be filled by migrating electrons from neighbouring sites which also aids conduction. An important property of semiconductors is that unlike metals, conduction increases under the application of thermal energy; this is a consequence of the energy pushing electrons into the higher energy conducting orbital.

Extrinsic semiconductors can be further sub divided into two groups, n-type and p-type semiconductors. In essence extrinsic semiconductors are intrinsic semiconductors with a small amount of dopant added to aid electrical conduction; the choice of starting material and dopant decide whether the subsequent material is as n or p type semiconductor. In p type semi conductors, an electron deficient dopant (compared with bulk compound, not an ion) is added in small quantities and provides an unoccupied level in the band structure called an acceptor level. Using the example of gallium doped silicon; which have [Ar] $4s^2$ $3d^{10}$ $4p^1$ and [Ne] $3s^2$ $3p^2$ electronic configurations respectively, it is possible to describe the conductance mechanism as follows. Here the gallium is electron deficient compared to silicon and acts as the acceptor level, the band gap to this level is small and allows for electron migration

from the valence level in silicon to this acceptor level. The electrons in the acceptor levels do not contribute entirely to the conduction of the material; however the positive holes left behind in the valance band acts as charge carriers. Conduction occurs as electrons move into these positive holes leaving another hole into which a further electron can migrate and so on. (See Figure 1.19 for graphical representation)

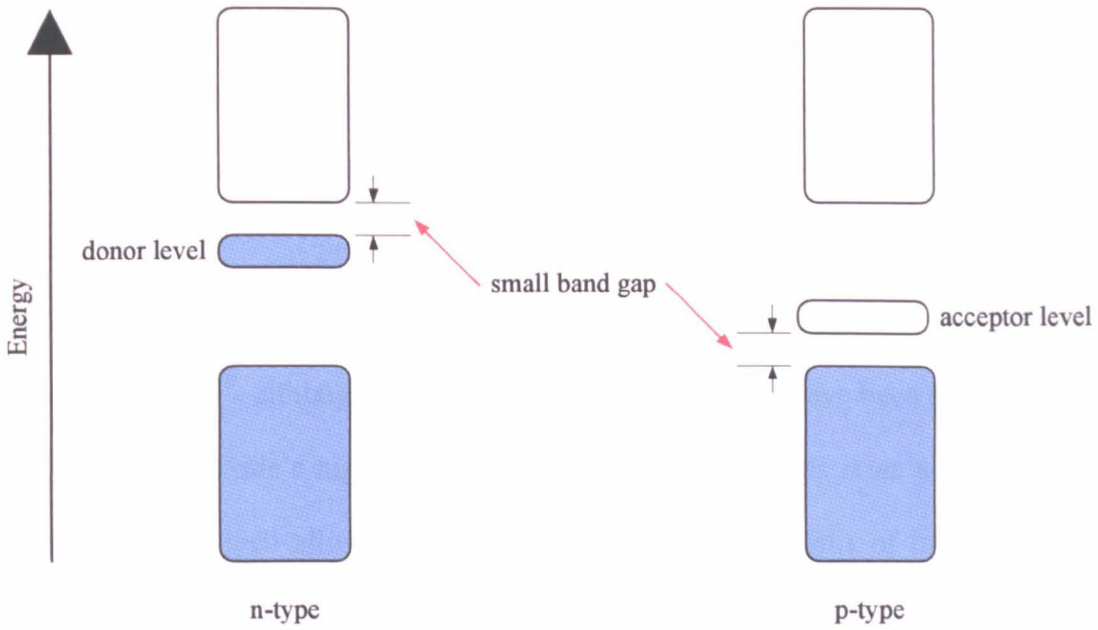

Figure 1.19: Graphical representation of different types of semi-conductor.

In comparison, n-type semiconductors, for which indium tin oxide is a variety, works in the opposite way to p-type semiconductors in that the dopant (tin in this case) provides an electron rich site. The electrons from which occupy a level below the conduction band called the donor level. (See Figure 1.19) As with the p-type, the band gap from the donor level to the conduction band is small which allows thermal migration between the bands that permits electrical conduction.

As previously mentioned both types of extrinsic semiconductor need only small amounts of dopant to improve conduction; with regards to ITO (In_2O_3:Sn) it would be expected that an increase in tin content would raise the electrical conductance. However it has been found that the peak concentration of tin is approximately 10wt% [68-71], after which the level of electro-conductance starts to drop off. Nadaud *et al.* [68] have speculated that an increase in tin concentration and/or oxygen partial pressure leads to the formation of low conducting $In_4Sn_3O_{12}$ molecules within the matrix. An increasing concentration of the non-conducting molecules has the effect of reducing the conductance efficiency.

The bandgap for indium tin oxide is generally accepted as being greater than 3.75 eV (361.81 kJ mol^{-1})[III], although values ranging from 3.3-4.2 eV have been reported [69, 70]. Indium tin oxide's high optical transparency in thin films is as a result of its wide bandgap, which allows the passage of longer wavelengths of light although factors such as surface roughness, homogeneity and unoxidised opaque tin content also influence this.

As already discussed, thin film ITO coatings have been used on a number of devices to enable the conduction of electricity whilst maintaining optical transparency or as a means of filtering unwanted light in architectural or automotive windows. The following discusses the techniques employed to deposit ITO into glass sheets or electrode surfaces.

[III] An electron volt is a non SI unit that is still commonly used in literature, 1eV = 96.4583 kJ mol^{-1}.

Sputtering: -

Sputtering encompasses a group of techniques that involve knocking atoms or molecules out of a target material by accelerated ions from an excited plasma and condensing them on the substrate. If a chemical reaction occurs between the target and the substrate the process is referred to as reactive sputtering. Reactive sputtering is commonly used when fabricating ITO thin films; with a target consisting of indium oxide (90 wt. %)) and tin oxide (10 wt. %), that react to form ITO.

As mentioned sputtering includes a group of techniques that are categorised by their method of accelerating plasma ions and include, radiofrequency (rf) sputtering [72], rf magnetron sputtering (were a magnet directs the electrons away from the substrate) [73, 74], direct current (d.c.) sputtering/magnetron sputtering [75] and ion beam sputtering [76].

Thermal evaporation: -

As the name suggests, thermal evaporation involves vaporising the required material through its heating and then recondensing onto a cooler substrate. With regards to ITO, the high temperatures are typically achieved *via* resistivity heating (heat produced through electrical resistance), by firing an electron or ion beam at the sample boat or through pulsed laser deposition [70, 77]. As with sputtering, the reaction to form ITO can be formed prior to substrate adherence using an alloy of In (90%) and Sn (10%) in the presence of oxygen [78].

Spray pyrolysis: -

With regards to ITO, spray pyrolysis is typically carried out in a furnace kept at 400 °C. Here an alcohol based solution containing indium chloride ($InCl_3$) and tin chloride ($SnCl_4.5H_2O$) in a 9:1 ratio, (see 2.2.2) is sprayed using nitrogen carrier gas onto the required substrate. The main advantage of this system is its speed of deposition and excellent optical transparency of approximately 90 % [79].

Screen printing: -

Screen printing is typically used on large-scale applications, such as anti reflective coatings on solar cells, where a relatively thick layer of ITO is needed (this varies between 10-30 μm) [80]. After the initial application of an ITO solution the substrate layer is left to crystallise at approximately 600 °C for one hour. Although the resistivity produced by this technique is similar to the others, the optical transparency is lower at approximately 80 %. Similar techniques have been used to spin and dip coat ITO solutions onto silica substrates, resulting in resistivity and optical transmissions of $1.5x10^{-2}$ Ω cm and 90 % respectively [81].

Table 1.2 represents the optical transmission and electrical resistivity for some of the techniques previously described; obviously these results are for the reference given and are merely provided to offer guidelines of the attributes of each system.

Deposition technique	Electrical resistivity (Ω cm)	Optical transmission (%)	REF
rf sputtering	1.00E-03	85 (visible)	63
rf magnetron sputtering	4.10E-03	92.83 (n/a)	65
d.c. magnetron sputtering*	8.00E-04	80 (500-600 nm)	66
Ion-beam sputtering	1.20E-03	n/a	67
Pulsed laser deposition	2.49E-04	88 (550 nm)	68
Thermal Evaporation	3.00E-03	80 (at 500 nm)	69
* *Est values from graphs*			

Table 1.2: Electrical resistivity and optical transmissions for a number of ITO deposition techniques. Note: Optical transmission data include wavelength(s) at which reading was taken.

As can be seen r.f. magnetron sputtering gives the best results for both electrical resistivity and also optical transmission. This technique also appears to be the most popular of the techniques with regards to use.

1.4 Chemiluminescence and Electro-generated chemiluminescence

The following section will examine the different mechanisms and applications of chemiluminescence (CL) and electro-chemiluminescence (ECL). Although only ECL is used in this work, both will be examined to provide a more detailed picture of the related processes.

1.4.1 Chemiluminescence (CL)

The term chemiluminescence was coined by Eilhardt Weidemann in 1888 and can be regarded as the emission of light arising from a chemical reaction without the production of heat. In this reaction one of the reactant species either emits light when it returns from an excited state to the ground state (direct CL) or transfers the energy to another molecule that emits the light (indirect CL) by a similar process, as shown in Figure 1.20.

$$a)\ A + B \rightarrow [I]^* \rightarrow \text{Products} + \text{Light}$$

$$b)\ A + B \rightarrow [I]^* + F \rightarrow F^* \rightarrow F + \text{Light}$$

Figure 1.20: Reaction mechanisms for a) Direct CL, b) Indirect CL, where A & B are reagents, I is a intermediate and F is a fluorephore

Chemiluminescence is part of a larger group of reactions termed luminescence that includes fluorescence and phosphorescence in its number. Fluorescence and phosphorescence, collectively termed photoluminescence, differ from chemiluminescence as their excited states are generated through the absorption of light as apposed to a chemical reaction. In order to understand the difference between the two photoluminescent types it is necessary to examine the mechanism by which the electron rises to and returns from the excited state. It is generally accepted that each electron orbitals may contain two electrons, each existing in one of two quantized spin states. If a molecular orbital contains two electrons, Pauli's exclusion principle states that they must be spin opposed, *i.e.* the axial spin is opposite for both electrons (clockwise and anticlockwise) the spins are then said to be paired.

When a molecule enters an electronically excited state an electron is transferred to a higher energy level (an excited state) where it typically maintains the same spin state, thus remaining paired with the electron left behind; this is know as an excited singlet state and is shown in Figure 1.21. However it is also possible for this excited state electron to change spin states, thus mimicking the electron left behind; the electrons are then said to be unpaired and the excited electron is then said to be in an excited triplet state (also shown in Figure 1.21).

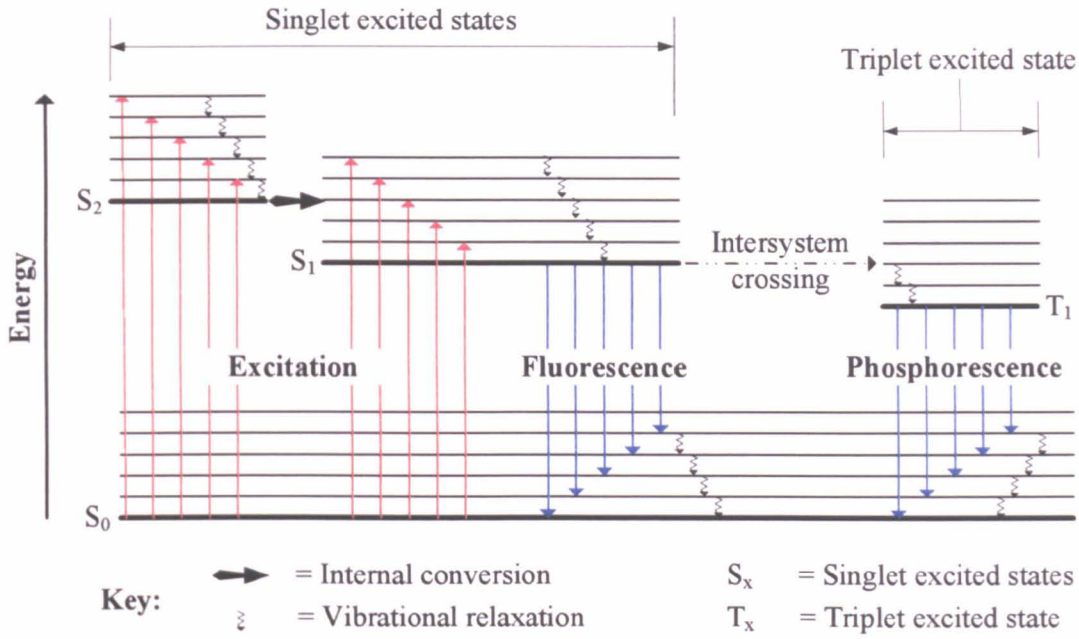

Figure 1.21: Partial energy level diagram for photoluminescent system.

Figure 1.21 represents a theoretical section of an energy level diagram for a photoluminescent system, where the thick lines represent quantized energy levels and the thin lines representing the associated vibrational energy levels. In this image S_0 corresponds to the ground state with $S_{1\,\&\,2}$ and T_1 being the excited singlet and triplet states respectively. As shown fluorescence may occur when a photon of sufficient energy is absorbed by the reactive molecules exciting it to a vibrational level of a single state. When the energy levels of a higher and lowers excited state overlap, for example S_1 and S_2, internal conversion may occur reducing the higher excited state to the lower one. Subsequent vibrational relaxation (the curly arrows) reduces the system energy to lowest vibrational energy level S_1 where upon fluorescence occurs with lifetimes ranging from $10^{-5} - 10^{-9}$ seconds, which is short lived due to the lack of electron spin change [82].

Phosphorescence occurs through a process of intersystem crossing where upon the excited electron realigns in parallel with the electron left behind forming a triplet state. This realignment occurs when there is an overlap between two vibrational states, as is shown in Figure 1.21 and results in a less energetic triplet state when compared to its singlet counterpart. However the formation of a triplet state *via* the singlet to triplet route is a less probable occurrence than the corresponding singlet-singlet transition due to the requirement of the time consuming spin change. Although a consequence of this change in spin is that phosphorescent lifetime ranges from 10^{-4} seconds to several seconds, allowing detection long after excitation has ceased [82].

It should be noted however that fluorescence and phosphorescence are just two of the ways in which a molecule can return to its ground state; as it is also possible for radiationless deactivation steps to occur. Both fluorescence and phosphorescence will occur when these processes are rapid when compared to other possible deactivation steps. When a more rapid deactivation step becomes available this will become the favoured route, reducing or eliminating any fluorescence or phosphorescence emission. Examples of radiationless deactivation processes include solution loss of vibrational energy, which is a consequence of collisions between the excited molecules and those of a solvent. This result in the rapid loss of the vibrational energy before relaxation can reduce the excited state the lowest excited electronic state. Consequently fluorescence in solutions occurs when excitation takes the molecule to the lowest excited state. Other methods of deactivation include internal conversion, a process not clearly understood where internal processes pass the molecule to the lower excited state without emission. Along with external

conversion where an energy transfer occurs between neighbouring molecules though collision; a process that can be reduced by lowering the temperature or increasing viscosity of a solution.

By comparison, in chemiluminescence a chemical reaction provides the energy that promotes an intermediate or product into an excited state as was shown in Figure 1.20. With the subsequent processes of vibrational relaxation, internal conversion and intersystem crossing occurring allowing the production of light with characteristics akin to both fluorescence and phosphorescence. However these reactions are rare as several criteria need to be met in order for the light emission to occur. Firstly the reaction must provide enough energy for the intermediate/product to enter an excited state; this is normally accomplished using strong oxidising agents such as hydrogen peroxide, cerium sulphate or ozone. Also the reaction must produce light and not transfer the energy *via* radiationless routes as previously discussed. This last requirement limits chemiluminescence reagents to just a few species some of which are shown below (Figure 1.22) and include types seen in nature and normally referred to as bioluminescent materials. Bioluminescence can be seen in nature in fireflies, glow-worms, sea pansies and some types of jellyfish. An example of this bioluminescent reaction can be seen in fireflies; where luciferin (shown in Figure 1.22), the enzyme luciferase and the cofactor ATP (adeninetriphosphate) react to producing light.

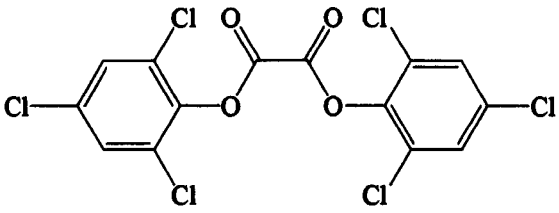

Bis-(2,4,6-trichlorophenyl) oxalate

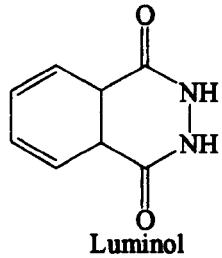

Luminol

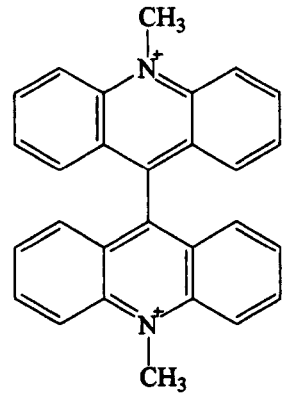

Lucigenin

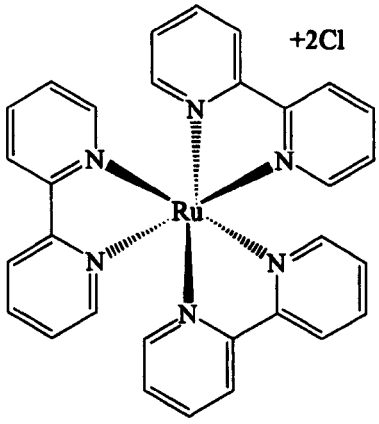

Tris(2,2'-bipyridyl) ruthenium

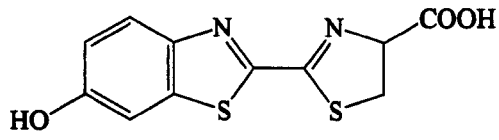

Firefly Luciferin

Figure 1.22: Examples of chemiluminescent reagents.

The molecules shown in Figure 1.22 are examples of chemiluminescence reagents and included types that use direct CL and indirect CL in the production of light. Luminol, shown in Figure 1.22 is perhaps the most widely used of all the chemiluminescence reagents has been used in many analytical analysis techniques ranging from environmental , health and crime scene analysis, as shown in Table 1.3

The oxidation of bis-(2,4,6-trichlorophenyl) oxalate in the presence of a suitable fluorescent molecule is an example of the indirect CL reaction previously discussed. Here the formation of a highly energetic dioxetane intermediate allows the transfer of energy to a fluorescer. The absorption of the dioxetane energy pushes the fluoraphor into an excited state; the fluoraphor subsequently releases the energy in the form of chemiluminescent light on returning to its ground state.

Analyte	CL reaction system	Detection limits	Ref
DDT	Luminol/H_2O_2/p-iodophenol-HRP labelled antibodies	1 nM	[83]
Glucose	O_2-glucose-glucose oxidase-luminol	7.5 nM	[84]
Adrenaline	Periodate – Luminol – Adrenaline	$7.0x10^{-9}$ g ml^{-1}	[85]
Urea	Urea – Urease – Permanganate - Luminol	2 nM	[86]
NO	H_2O_2 – Luminol – HRP – NO compound	1 nM	[87]
NH_3	O_2 – NH_3 – $LaCoO_3$ - Luminol	0.0114 ppm	[88]
Haemoglobin	Luminol - H_2O_2 – Sodium perborate tetrahydrate	N/A	[89]
Riboflavin	Periodate – Luminol - Riboflavin	0.02 ng ml^{-1}	[90]
H_2O_2	Luminol – H_2O_2 – Cobalt (III) nitrate	4.7 nmol L^{-1}	[91]

Table 1.3: Demonstrating a range of analytes that have been analysed using a luminol chemiluminescent reaction. **Note**: HRP = Horseradish peroxidase.

A more exhaustive review of chemiluminescent reactions and analysis techniques will not be performed here, although there are some excellent review articles on these subject [92, 93]. Nevertheless it is clear that the luminol reaction is a powerful technique for the analysis of both chemical and biological species and has been used successfully as both a chemiluminescent reagent and also an electro-generated chemiluminescent reagent.

1.4.2 Electro-generated chemiluminescence (ECL)

Electro-generated chemiluminescence, also known as electrochemiluminescence (ECL) can be described as chemiluminescence initiated directly or indirectly through the application of an electrical potential. ECL is normally produced though an electrochemical reaction in the vicinity of an electrode; thus providing spatial control over the emission point of the reaction. This control of emission point is considered as one of the main advantages of ECL over CL, as the reaction can be positioned for optimum signal collection. Another advantage of ECL over CL is that it can be more selective in the generation of excited states through carefully controlling the electrode potential. In addition ECL is a non-destructive technique that allows the ECL emitters to undergo post reaction regeneration, allowing for continued analysis without reagent replacement.

Due to an overlap in mechanisms and reagents it is difficult to divide ECL reactions into specific classifications; however in the following sections the ECL reactions will be separated into four groups and discussed. These groups are as follows: -

i) **Ion-annihilation reactions**: Reactions between radical cations and anions generated electrochemically by a single emitter.

ii) **Cathodic luminescence**: Light emitted during electrolysis at oxide covered aluminium electrodes.

iii) **ECL from conventional CL reagents**: The ECL reaction of common CL reagents such as luminol.

iv) **Electron transfer reaction**: Describing the electron transfer reactions of inorganic species, such as tris(2,2'-bipyridyl)(II) dichloride hexahydrate - $(Ru(bpy)_3^{2+}$.

1.4.2.1 Ion-annihilation reactions

Ion-annihilation reactions are known to occur in high energy electron transfer reactions between electro-generated radical ions of polyaromatic hydrocarbons (PAHs) in organic solutions. The radical cation and anions are typically formed in aprotic solvents through the application of a two step potential, shifting between the reduction and oxidation potentials of the reactive species (R). The subsequent reaction of the radical anion and cation, shown in Figure 1.23, generates an excited singlet state $^1R^*$ which emits light *via* a mechanism termed the singlet or s-route (Figure 1.21).

$$R - e^- \rightarrow R^{\bullet+} \qquad \text{Electro oxidation (1.23a)}$$

$$R + e^- \rightarrow R^{\bullet-} \qquad \text{Electro reduction (1.23b)}$$

$$R^{\bullet+} + R^{\bullet-} \rightarrow R + {}^1R^* \qquad \text{Electron transfer (1.23c)}$$

$$^1R^* \rightarrow R + h\nu \qquad \text{ECL (1.23d)}$$

$$-\Delta H_{ann} = E_p(R/R^{\bullet+}) - E_p(R/R^{\bullet-}) - 0.1\text{eV} \quad (1.23e)$$

Figure 1.23 (a-d): Showing the ion annihilation singlet route, for the production of ECL; **(e)** equation defining the enthalpy for ion annihilation ($-\Delta H_{ann}$ in eV).

It is also possible for the reaction to proceed along a triplet-triplet route depending on the energy from the peak electrode potential for the oxidation and reduction steps (1.23a and 1.23b). This energy can be calculated using the enthalpy of the ion annihilation equation shown in 1.23e, were E_p is the peak oxidation or reduction potential; and 0.1 eV is the entropy approximation term ($T\Delta S$) and 25 °C. If the energy estimated from equation 1.23e is greater than the energy required to generate

the lowest excited singlet state (E_s) than it would be possible to generate the $^1R^*$ excited state as shown in 1.23c and 1.23d.

However if the energy estimated from equation 1.23e is less than the energy required to generate the lowest excited singlet state (E_s) but higher than the energy required to generate the excited triplet state then it is possible to form a singlet excited state ($^1R^*$) through a triplet-triplet annihilation reaction as shown in Figure1.24

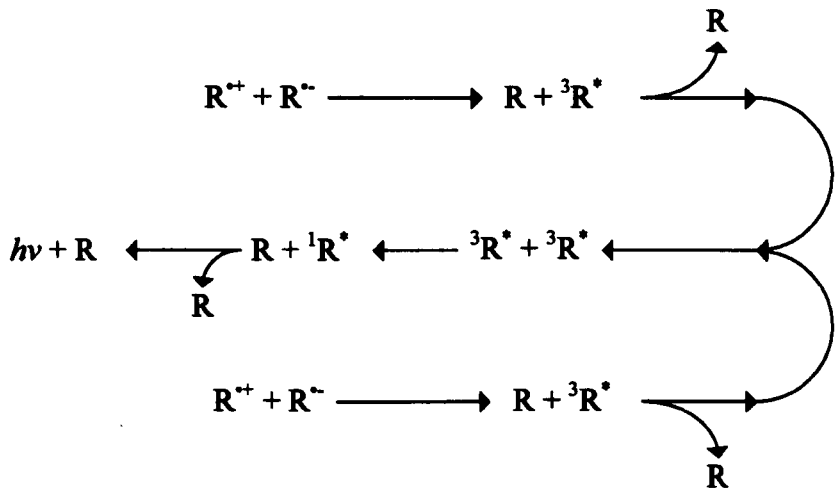

Figure 1.24: Schematic of triplet-triplet ion annihilation reaction mechanism.

So far only direct ion-annihilation ECL reactions have been discussed *i.e.* those reactions where the desired analyte is the emitting species. The problem with this system is that the number of directly luminescent compounds is limited which reduces the usefulness of this application. However an indirect method for this reaction is possible using a coreactant (C), a strong reducing or oxidising intermediate that replace the role of cation or anion in the reaction. For example a suitable electron donor such as a tertiary amine can replace the cation in the "direct" reactions to yield chemiluminescence from the luminophore *i.e.* the polyaromatic hydrocarbon. In addition because the coreactant plays an active role in the reaction

its own concentration aeffects the intensity of the light emission produced, which allows this reaction to be used for a greater number of compounds compared to the direct reaction.

Examples of direct and indirect ion annihilation ECL reactions using organic ECL compounds are shown in Table 1.4; these include examples for the analysis of rubrene, anthracene derivatives and perylene.

Organic ECL compounds used in Ion-Annihilation	References
Single reactant systems	
Tetramethoxythianthrene	[94]
Rubrene	[95]
9,10-Bis(2-naphthyl)anthracene	[96]
Perylene	[97, 98]
Mixed systems	
Perylene + 9,10-diphenylanthracene (DPA)	[99]
Rubrene + 9,10-diphenylanthracene (DPA)	[95]
Tetracene + *N,N,N',N'*-tetramethyl-p-phenylenediamine	[100]
Perylene + Thianthrene	[99]
Anthracene + Tris(2,4-dibromophenyl)amine (TDBPA)	[101]
9-Methylanthracene + Tris(2,4-dibromophenyl)amine	[101]
9-Bromoanthracene + Tris(2,4-dibromophenyl)amine	[101]
CL compounds used in Ion Annihilation ECL	
Luminol + (Ferrocene)	[102]
Luminol + (hydrazine)	[103]
N-(4-Aminobutyl)-*N*-ethylisolminol	[104]

Table 1.4: Organic ECL compounds used in Ion-Annihilation studies.

1.4.2.2 Cathodic luminescence

Cathodic luminescence also known as electroluminescence and galvoluminescence was first observed by Braun in 1898 [105]. Although often termed electro-generated chemiluminescence in the literature the mechanism for producing the luminescent light is appreciably different from the other forms of ECL discussed in this section. This type of ECL emission has been observed at an oxide covered metal electrode (such as aluminium and tantalum) under high voltages (>30 V), as discussed by Ikonopisov [106], Takima [107] and Knight [108]. This ECL emission is also observed at metal oxide and semiconductor electrodes at appreciably lower potentials (<10 V) during the reduction of persulfate, oxygen and hydrogen peroxide. With regards to persulfate the emission is a consequence of an electron transferring from the electrode to the persulfate ion, which reduces to form a sulphate radical anion. If the standard reduction potential for the radical closely matches the valance band edge, it captures an electron from the valance band, thus producing an electron hole. The transfer of an electron from the conductance band to the valence band hole produces the ECL light emission at a wavelength equivalent to the band gap energy.

In some instances however the ECL emission has a lower energy than the band gap energy; in these circumstances the ECL is produced by recombination *via* surface states. For example a number of inorganic ions and organic compounds form a stable chelates with the hydroxylated surface of the metal electrodes and act as surface states to generate a cathodic sub-band gap. This system has been used for the quantification of various analytes that are surface active and enhance the cathodic electroluminescence. Examples of these include thallium [109], glucose [110], human thyroid stimulating hormone (hTSH) [111], 1-aminonaphthalene-4-

sulphonate [112] , Yb(III) chelates [113, 114], acridinium esters [115], lucigenin [116] and hemin [116].

Due to the mechanistically different nature of this form of ECL and given that it is not used during this work, little more will be discussed with regards to cathodic luminescence. However the interested reader is encouraged to view the following excellent reviews by Richter [117], Fahnrich *et al.* [118] and Kulmala & Suomi [119].

1.4.2.3 ECL from conventional CL reagents

With regards to conventional CL reagents being used electrochemically, the best known example is that of luminol and its derivatives. The ECL reaction of luminol with hydrogen peroxide in an alkaline solution is similar to that of the CL reaction of luminol initiated through chemical oxidation [91, 120-123].

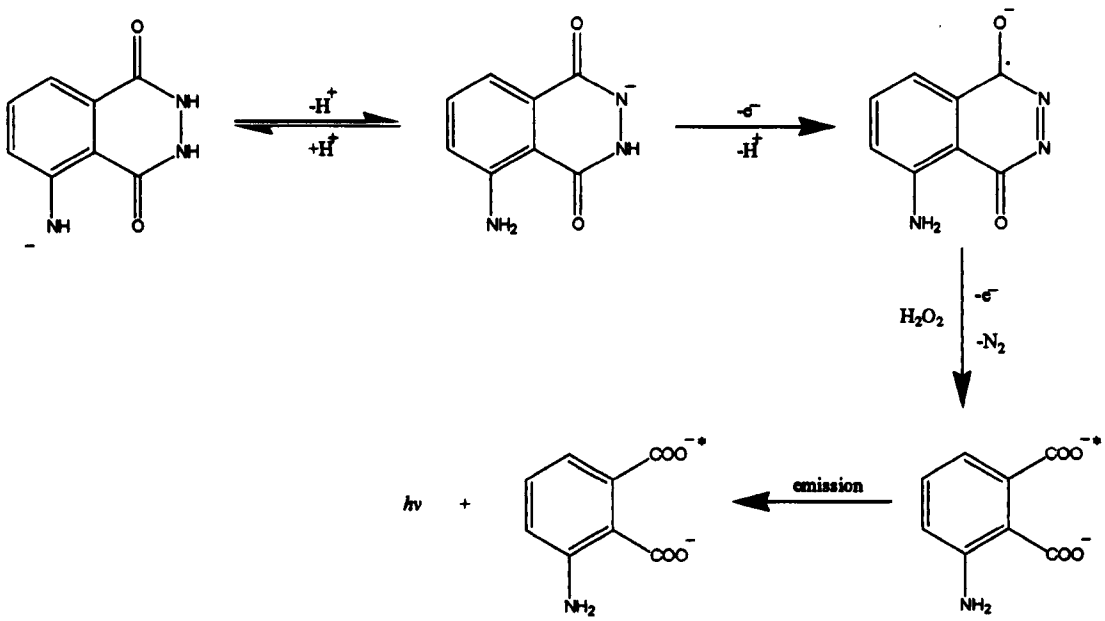

Figure 1.25: ECL reaction of luminol with hydrogen peroxide.

In an alkaline medium the luminol and hydrogen peroxide ECL reaction, as shown in Figure 1.25, progresses through the dissociation of the luminol in the alkaline solution to form a mono-anion which is electrochemically oxidised. Subsequent oxidation of the diazo compound in the presence of hydrogen peroxide produces 3-aminophtalate in an excited state, which on returning to ground state produces the ECL signal at 425 nm. In this reaction alkaline conditions are required to enable to deprotonation of the luminol with pH reductions resulting in a decrease of ECL signal. In addition the hydrogen peroxide may participate in the form of a peroxide anion HOO^- or as an electrochemically produced superoxide radical $O_2^{\cdot-}$.

This reaction has been used in the detection of a wide range of analytes, including hydrogen peroxide, both in rain water [91] and in the form of an enzymatic by-product for reactions involving glucose oxidase, lactate oxidase and horseradish peroxidase [123-126]. In addition this reaction has been used in the quantitative analysis of tryptophan [127] and as a co-reactant for immunoassay labelling [102, 128, 129]. An example being demonstrated by Wilson *et al.* [102] who used ferrocene labelled molecules (haptens) to enhance the luminol/H_2O_2 ECL prior to antibody binding. The metal ion catalyst typically used to enhance the signal in the luminol/H_2O_2 chemiluminescent reaction (for example cobalt, copper and nickel) have also been analysed using this technique [125, 130-133].

Other established CL systems that have been used electrochemically include lucigenin that has been used in the analysis of trace metals, hemin and epinephrine that act as catalysts for the lucigenin reaction [116, 134, 135].Also included in this group is the electrochemical reduction of bis-(2,4,6-trichlorophenyl) oxalate and

oxygen in the presence of a suitable fluorescer that has been used for the detection of oxygen [136]. For further examples of this type of reaction the reader is recommended to examine the excellent papers by Richter [117] and Fahnrich *et al.* [118].

1.4.2.4 ECL from Inorganic Reagents: Electron transfer reactions involving transition metal complexes

As discussed in 1.4.2.1, in typical organic systems the fluorescence emitting state is formed from an electron transfer (S-route), or in energy deficient condition *via* a triplet intermediate (T-route). However with transition metal complexes (TMC) the spin allowed excited states undergo rapid deactivation due to spin-orbital coupling. As the luminescence originates from the lowest energy excited state *via* energy sufficient routes, the lifetime of the TMC are too short to allow them to take part in subsequent annihilation reactions. Consequently the ECL emission is through a spin-forbidden excited state [137].

Many ECL active inorganic compounds have been reported including metal ligand charge transfer species such as $M(L)_3^{2+}$ complexes where M is a metal; typically ruthenium [138, 139] or osmium [140-142] and L is a chelating ligand such as 2,2'-bipyridine (bpy) or similar ligand. Other examples of this type of species include rhenium [143], iridium [144] and square planar platinum compounds [145]. Other examples of ECL active compounds include palladium and platinum porphyrins [146], $Cd(phen)_3^{2+}$ [147], $Os(phen)_2(dppene)^{2+}$ [140, 141] and multinuclear

complexes, such as $Pt_2(dpa)_3$ [148] [IV]. The most widely used, and also the first inorganic ECL complex to be discovered [117, 138] is that of the ruthenium chelate, tris(2,2'-bipyridyl)ruthenium(II) dichloride hexahydrate ($Ru(bpy)_3^{2+}$), which is also used extensively in this work.

The success of $Ru(bpy)_3^{2+}$ lies in its strong luminescence and solubility in a range of aqueous and organic solvents at room temperature. Additionally it is able to undergo a reversible one step electron transfer reaction at easily obtainable potentials in the presence of oxygen and other impurities, resulting in a suitably stable reduced or oxidised species.

An ECL emission can be obtained from a solution of $Ru(bpy)_3^{2+}$ through the application of an alternating oxidation and reducing square wave potential, (as shown in Figure 1.26); this produces a red/orange light emission with a λ_{max} at 620 nm.

$Ru(bpy)_3^{2+} - e^- \rightarrow Ru(bpy)_3^{3+}$	Electro-oxidation
$Ru(bpy)_3^{2+} + e^- \rightarrow Ru(bpy)_3^{+}$	Electro-reduction
$Ru(bpy)_3^{3+} + Ru(bpy)_3^{+} \rightarrow Ru(bpy)_3^{2+} + Ru(bpy)_3^{2+*}$	Electron transfer
$Ru(bpy)_3^{2+*} \rightarrow Ru(bpy)_3^{2+} + h\nu$	ECL

Figure 1.26: Mechanism for ECL reaction of $Ru(bpy)_3^{2+}$.

Alternatively co-reactants may be used in this reaction, these perform the role of co-oxidant or a co-reducer for the $Ru(bpy)_3^{2+}$. The first co-reactant discovered for use

[IV] (phen): 1,10-phenanthroline, (dppene): 1,2-cis-bis(diphenylphosphinoethylene), (dba): dibenzylideneacetone

with $Ru(bpy)_3^{2+}$ was the oxalate ion which is believed to produce a strong reductant upon oxidation [117, 149], as shown in Figure 1.27.

$$C_2O_4^{2-} - e^- \rightarrow [C_2O_4^{\bullet -}] \rightarrow CO_2^{\bullet -} + CO_2$$

Figure 1.27: Mechanism for the oxidation of the oxalate ion.

Oxalate is commonly termed the "oxidative-reductive" co-reactant due to its ability to form a strong reducing agent upon electrochemical oxidation. In essence the electrode oxidizers both the oxalate and the $Ru(bpy)_3^{2+}$, $CO_2^{\bullet -}$ is then generated due to bond cleavage of the oxalate ion, as shown in Figure 1.27. This allows the generation of ECL with $Ru(bpy)_3^{2+}$ to be formed in a single potential step instead of the double potential step as required with annihilation reactions.

Another important example of this system is that of the $Ru(bpy)_3^{2+}$/tri-n-propylamine (TPrA), where ECL is produced from the concurrent oxidations of both reagents as shown in Figure 1.28.

$Ru(bpy)_3^{2+} - e^- \rightarrow Ru(bpy)_3^{3+}$	Electro-oxidation
$TPrA - e^- \rightarrow [TPrA^{\bullet}]^+ \rightarrow TPrA^{\bullet} + H^+$	Electro-oxidation
$Ru(bpy)_3^{3+} + TprA^{\bullet} \rightarrow Ru(bpy)_3^{*2+} + Products$	Electron transfer
$Ru(bpy)_3^{*2+} \rightarrow Ru(bpy)_3^{2+} + h\nu$	ECL

Figure 1.28: Mechanism for $Ru(bpy)_3^{2+}$ /TPrA ECL reaction.

Studies by Leland & Powell [150] and Gross *et al.* [151] have provided a possible reaction pathway that indicate that upon oxidation, TPrA radical cations lose a proton

from an α-carbon forming the strong reducing intermediate, $TPrA^{\bullet}$. This subsequently reacts with co-oxidised $Ru(bpy)_3^{3+}$ to form the excited form of this species $Ru(bpy)_3^{*2+}$, which upon returning to the ground state produces the ECL emission.

This co-reactant system has been successfully applied to the analysis of a number of compounds containing tertiary and secondary amines; examples of compounds that have been analysed using this system include illicit drugs [152], pharmaceuticals [153-155], amino acids [156, 157], antibiotics [158, 159] and pesticides [160]. Another system, discussed previously, is that of oxalate; this system has been used to determine the levels of oxalate in vegetables (high levels of calcium oxalate can be found in vegetables and is the main component of kidney stones) and also other biological systems [149, 161]. Finally the $Ru(bpy)_3^{2+}$/ TPrA system has been used as a labelling system in immunoassays [162, 163].

It is hopefully apparent that both the CL and ECL techniques discussed here provide excellent applications for chemical analysis. Of the two systems electro-generated chemiluminescence has a number of advantages over the chemiluminescent system. These include the ability to spatially and chronologically control the luminescence; also the number of reagents required per experiment can be reduced as the reagents are oxidised electrochemically. This electrochemical oxidation also allows for an extra level of selectivity as the potential can be controlled to analyse the appropriate species. However not all compounds are suitable, indeed with regards to ECL, not all tertiary amines make effective co-reactants as shown in section 3.3.5, with the work undertaken with flunitrazepam. Nevertheless the ability of reagents regeneration and

equipment miniaturisation (*i.e.* lab on a chip and miniature photomultiplier tubes/CCD) shows promise for the future for field portable analytical ECL systems, for environmental analysis for example.

1.6 References.

1. Ebelman, J.J., Annales de Chemie et de Physique, 1846. **57**: p. 331.
2. Brinker, C.J. and Scherer G.W., *Sol-gel science - The physics and chemistry of sol-gel processing*. 1990: Academic press.
3. Biehl, S., Danzebrink R., Oliveria P., and Aegerter M.A., *Refractive microlens fabrication by ink jet process.* Journal of Sol-gel Science and Technology, 1998. **13**: p. 177-182.
4. Roy, R., Journal of the American Ceramics Society, 1956. **39**(4): p. 145-146.
5. Roy, R., Journal of the American Ceramics Society, 1969. **52**(6): p. 344.
6. Yoldas, B.E., *Alumina gels that form porous transparent Al_2O_3.* Journal of Materials Science, 1975. **10**: p. 1856 -1860.
7. Yamane, M., Shinji A., and Sakaino T., *Preparation of a gel from metal alkoxides and its properties as a precursor of oxide glass.* Journal of Materials Science, 1978. **13**: p. 865-870.
8. Collinson, M.M., Novak B., Martin S.A., and Taussig J.S., *Electrochemiluminescence of Ruthenium(II) Tris(bipyridine) encapsulated in sol-glasses.* Analytical Chemistry, 2000. **72**(13): p. 2914-2918.
9. Collinson, M.M., Taussig J.S., and Martin S.A., *Solid state electro-generated chemiluminescence from gel-entrapped Ruthenium(II) tris(bipyridine) and tripropylamine.* Chemical materials, 1999. **11**: p. 2594-2599.
10. Walcarius, A., *Electrochemical applications of silica based organic-inorganic hybrid materials.* Chemistry of Materials, 2001. **13**: p. 3351-3372.
11. Al-Dahoudi, N., Bisht H., Gobbert C., and Krajewski T., *Transparent conducting, anti-static and anti-static-anti-glare coatings on plastic substrates.* Thin solid films, 2001. **392**: p. 299-304.
12. Gaponenko, N.V., *Synthesis and optical properties of films formed by the sol-gel method in mesoporous matrices.* Journal of Applied Spectroscopy, 2002. **69**(1): p. 1.
13. Epifani, M., Carlino E., Blasi C., Giannini C., Tapfer L., and Vasanelli L., *Sol-gel processing of Au nanoparticles in bulk 10% B_2O_3 - SiO_2 glass.* Chemical materials, 2001. **13**: p. 1533-1539.
14. Mehrotra, V., Keddie J.L., Miller J.M., and Giannelis E.P., *Electrically conducting glasses: Incorporation of polypyrrole in a porous SiO_2 matrix.* Journal of Non-crystalline solids, 1991. **136**: p. 97-102.
15. Dislich, H. and Hussmann E., *Amorphous and crystalline dip coatings obtained from organometallic solutions: Procedures, chemical processes and products.* Thin solid films, 1981. **77**: p. 129-139.
16. Avnir, D., *Organic chemistry within ceramic matrices: Doped sol-gel materials.* Acc. Chemical Res., 1995. **28**: p. 328-334.
17. Lan, E.H., Dave B.C., Fukuto J.M., Dunn B., Zink J.I., and Valentine J.S., *Synthesis of sol-gel encapsulated heme proteins with chemical sensing properties.* Journal of Materials Chemistry, 1999. **9**: p. 45-53.
18. Li, J., Chia L.S., Goh N.K., Tan S.N., and Ge H., *Mediated amperometric glucose sensor modified by the sol-gel method.* Sensors and Actuators B, 1997. **40**: p. 135-141.
19. Lillis, B., Grogan C., Berney H., and Lane W.A., *Investigation into immobilisation of lactate oxidase to improve stability.* Sensors and Actuators B, 2000. **68**: p. 109-114.

20. Wolfbeis, O.S., Oehme I., Papkoskaya N., and Klimant I., *Sol-gel based glucose biosensors employing optical oxygen transducers, and a method for compensating for variable oxygen background.* Biosensors and Bioelectronics, 2000. **15**: p. 69-76.
21. Howells, A.R., Zambrano P.J., and Collinson M.M., *Diffusion of redox probes in hydrated sol-gel derived glasses.* Analytical Chemistry, 2000. **72**: p. 5265-5271.
22. McDonagh, C., MacCraith B.D., and McEvoy A.K., *Tailoring of sol-gel films for optical; sensing of oxygen in gas and aqueous phase.* Analytical Chemistry, 1998. **70**(1): p. 45-50.
23. Allain, L.R., Sorasaenee K., and Xue Z., *Doped thin-film sensors via a sol-gel process for high acidity determination.* Analytical Chemistry, 1997. **69**: p. 3076-3080.
24. Butler, T.M., MacCraith B.D., and McDonagh C., *Leaching in sol-gel derived silica films for optical pH sensing.* Journal of Non-crystalline solids, 1998. **22**: p. 249-258.
25. Grattan, K.T.V., Badini G.E., Palmer A.W., and Tseung A.C.C., *Use of sol-gel techniques for fibre-optic sensor applications.* Sensors and Actuators A, 1991. **25-27**: p. 483-487.
26. Takahashi, Y., Maeda A., Kojima K., and Uchida K., *pH Dependence of luminescence in dye-doped sol-gel coating film.* Japanese Journal of Applied Physics, 2000. **39**: p. L218-L220.
27. Xu, H., Aylott J.W., Kopelman R., Miller T.J., and Philbert M.A., *A real-time ratiometric method for the determination of molecular oxygen inside living cells using sol-gel based spherical optical nanosensors with applications to rat C6 glioma.* Analytical Chemistry, 2001. **73**(17): p. 4124-4133.
28. Thomas-Lee, S., Gin J., Nampoori V.P.N., Vallabhan C.P.G., Unnikrishnan N.V., and Radhakrishnan P., *A sensitive fibre optic pH sensor using multiple sol-gel coatings.* Journal of Optics A: Pure and Applied Optics, 2001. **3**: p. 355-359.
29. Wu, X., Choi M.M.F., and Xiao D., *A glucose biosensor with enzyme-entrapped sol-gel and an oxygen-sensitive optrode membrane.* Analyst, 2000. **125**: p. 157-162.
30. O'Keefe, G., MacCraith B.D., McEvoy A.K., McDonagh C., and McGilp J.F., *Development of a LED-based phase Fluorimetric oxygen sensor using evanescent wave excitations of a sol-gel immobilized dye.* Sensors and Actuators B, 1995. **29**: p. 226-230.
31. Atkinson, A. and Segal D.L., *Some recent developments in aqueous sol-gel processing.* Journal of Sol-gel Science and Technology, 1998. **13**: p. 133-139.
32. Pomogailo, A.D., *Polymer sol-gel synthesis of hybrid nanocomposites.* Colloid Journal, 2005. **67**(6): p. 658-677.
33. Kato, M., Sakai-Kato K., and Toyo'oka T., *Silica sol-gel monolithic materials and their use in a variety of applications.* Journal of Separation Science, 2005. **28**(15): p. 1893-1908.
34. Jin, W. and Brennan J.D., *Properties and applications of proteins encapsulated within sol-gel derived materials.* Analytica Chimica Acta, 2002. **461**(1): p. 1-36.
35. Bakul, D.C., Dunn B., Selverstone-Valentine J., and Zink J.I., *Sol-gel encapsulation methods for biosensors.* Analytical Chemistry, 1994. **66**(22): p. 1120A - 1127A.

36. Keayey, P., *The New Penguin Dictionary of Geology*. 1 ed. 1996: Penguin Books Ltd, Harmondsworth, UK. 366.
37. Tohge, N., Moore G.S., and MacKenzie J.D., *Structural developments during the gel to glass transition.* Journal of Non-crystalline solids, 1984. **63**: p. 95-103.
38. Iler, R.K., *The Chemistry of Silica*. 1979, Wiley, New York.
39. Aelion, R., Loebel A., and Eirichh F., *Hydrolysis of Ethyl silicate.* Journal of the American Chemical Society, 1950. **72**: p. 5705-5712.
40. Schmidt, H., Scholze H., and Kaiser A., *PRINCIPLES OF HYDROLYSIS AND CONDENSATION REACTION OF ALKOXYSILANES.* Journal of Non-crystalline solids, 1984. **63**(1-2): p. 1-11.
41. Pohl, E.R. and Osterholtz F.D., *Molecular characterization of composite interfaces*, ed. H. Ishida and G. Kumar. 1985: Plenum, New York. 157.
42. Klein, L.C., Annual Review of Materials Science, 1993. **23**: p. 237.
43. Zarzycki, J., *Past and present of sol-gel science and technology.* Journal of Sol-gel Science and Technology, 1997. **8**: p. 17-22.
44. Collinson, M.M., Wang H., Makote R., and Khramov A.N., *The effects of drying time and relative humidity on the stability of sol-gel derived silicate films in solution.* Journal of Electroanalytical Chemistry, 2002. **519**: p. 65-71.
45. Smirnova, I. and Arlt W., *Synthesis of silica aerogels: Influence of the supercritical CO2 on the sol-gel process.* Journal of Sol-Gel Science and Technology, 2003. **28**(2): p. 175-184.
46. Babic, B., Kaluderovic B., Vracar L., and Krstajic N., *Characterization of carbon cryogel synthesized by sol-gel polycondensation and freeze-drying.* Carbon, 2004. **42**(12-13): p. 2617-2624.
47. Orcel, G. and Hench L.L., *Better ceramics through chemistry*. Material Resources Society Symposium Proceeding, ed. C.J. Brinker, D.E. Clark, and D.R. Ulrich. Vol. 32. 1984: North-Holland, New York.
48. Zarzycki, J., Prassas M., and Phalippou J., *Synthesis of glasses from gels: The problem of monolithic gels.* Journal of Materials Science, 1982. **17**: p. 3371-3379.
49. Collinson, M.M. and Martin S.A., *Solid state electro-generated chemiluminescence in sol-gel derived monoliths.* Chemical communications, 1999: p. 899-900.
50. Schottner, G., *Hybrid sol-gel derived polymers: Applications of multifunctional materials.* Chemistry of Materials, 2001. **13**: p. 3422-3435.
51. Bardo, A.M., Collinson M.M., and Higgins D.A., *Nanoscale properties and matrix-dopant interactions in dye doped organically modified silicate thin films.* Chemical materials, 2001. **13**: p. 2713-2721.
52. Reetz, M.T., Zonta A., Simpelkamp J., and Konen W., *In-situ fixation of lipase-containing hydrophobic sol-gel materials on sintered glass - highly efficient heterogeneous biocatalysts.* Chemical communications, 1996: p. 1397.
53. Wu, G., Wang J., Shen J., Yang T., Zhang Q., Zhou B., Deng Z., Bin F., Zhou D., and Zhang F., *Properties of sol-gel derived scratch-resistant nano-porous silica films by a mixed atmosphere treatment.* Journal of Non-crystalline solids, 2000. **275**: p. 169-174.
54. Hammarberg, E. and Roos A., *Antireflection treatment of low-emitting glazings for energy efficient windows with high visable transmittance.* Thin solid films, 2003. **442**: p. 222-226.

55. Bharathi, S. and Lev O., *Sol-gel derived nanocrystalline gold-silicate composite biosensor.* Analytical Communications, 1998. **35**: p. 29-31.
56. Shankaran, D.R., Uehara N., and Kato T., *Sol-gel derived metal dispersed ceramic-graphite composite electrode for amperometric determination of dopamine.* Analytica Chimica Acta, 2003. **478**: p. 321-327.
57. Katz, E., Buckmann A.F., and Willner I., *Self-Powered enzyme-based biosensors.* Journal of the American Chemical Society, 2001. **123**: p. 10752-10753.
58. Arregui, F.J., Otano M., Fernandez-Valdivielso C., and Matias I.R., *An experimental study about the utilization of liquicoat solutions for the fabrication of pH optical fibre sensors.* Sensors and Actuators B, 2002. **87**: p. 289-295.
59. Hong, B.S., Han J.H., Kim S.T., Cho Y.J., Park M.S., Dolukhanyan T., and Sung C., *Endurable water-repellent glass for automobiles.* Thin solid films, 1999. **351**: p. 274-278.
60. Muralidharan, B.G. and Agrawal D.C., *Sol-gel derived TiO_2-SiO_2 fibres.* Journal of Sol-gel Science and Technology, 1997. **9**: p. 85-93.
61. Stober, W., Fink A., and Bohn E., *Controlled growth of monodispersed silica spheres in the micron size range.* Journal of Colloid and Interface Science, 1968. **26**: p. 62-69.
62. Buck, S.M., Xu H., Brasuel M., Philbert M., and Kopelman R., *Nanoscale probes encapsulated by biologically localized embedding (PEBBLEs) for ion sensing and imaging in live cells.* Talanta, 2004. **63**: p. 41-59.
63. Buck, S.M., Koo Y.L., Park E., Xu H., Philbert M.A., Brasuel M., and Kopelman R., *Optochemical nanosensor PEBBLEs: Photonic explorers for bioanalysis with biologically localized embedding.* Current Opinion in Chemical Biology, 2004. **8**: p. 540-546.
64. Moreno, M.J., Monson E., Reddy R.G., Rehemtulla A., Ross B.D., Philbert M.A., Schneider R.J., and Kopelman R., *Production of singlet oxygen by $Ru(dpp(SO_3)_2)_3$ incorporated in polyacrylamide PEBBLEs.* Sensors and Actuators B, 2003. **90**: p. 82-89.
65. Housecroft, C.E. and Sharpe A.G., *Inorganic Chemistry.* 2001: Pearson Education Llt, Harlow, UK. 126-127.
66. Fujikawa, H., Noda K., Tokito S., and Taga Y., *Electrical properties of Ta-Sn-O films on indium tin oxide electrode.* Applied Surface Science, 1997. **113-114**: p. 714-717.
67. Hillebrandt, H., Wiegand G., Tanaka M., and Sackmann E., *High electric resistance polymer/lipid composite films on indium tin oxide electrodes.* Langmuir, 1999. **15**(24): p. 8451-8459.
68. Nadaud, N., Lequeux N., Nanot M., Jove J., and Roisnel T., *Structural studies of tin-doped indium oxide (ITO) and $In_2Sn_3O_{12}$.* Journal of Solid State Chemistry, 1998. **135**: p. 140-148.
69. Alam, M.J. and Cameron D.C., *Optical and electrical properties of transparent conductive ITO thin films deposited by sol-gel process.* Thin solid films, 2000. **00**: p. 455-459.
70. Kim, H., Horwitz J.S., Pique A., Gilmore C.M., and Chrisey D.B., *Electrical and optical properties of indium tin oxide thin films grown by pulsed laser deposition.* Applied Physics A, 1999. **69**: p. S447-S450.
71. Frank, G. and Kostlin H., *Electrical properties and defect model of tin-doped indium oxide layers.* Applied Physics A, 1982. **27**: p. 197-206.

72. Fan, C.C. and Goodenoughm J.B., *X-Ray photoemission spectroscopy studies of Sn doped indium oxide films.* Journal of Applied Physics, 1977. **48**(8): p. 3524-3531.
73. Guillen, C. and Herrero J., *Comparison study of ITO thin films deposited by sputtering at room temerature ontp polymer and glass substrates.* Thin solid films, 2005. **480-481**: p. 129 -132.
74. Baia, I., Quintela M., Mendes L., and Martins R., *Performances exhibited by large area ITO layers produced by r.f. magnetron sputtering.* Thin solid films, 1999. **337**: p. 171-175.
75. Nishimura, E., Ohkawa H., Song P.K., and Shigesato Y., *Microstructures of ITO films deposited by DC magnetron sputtering with H_20 introduction.* Thin solid films, 2003. **445**: p. 235-240.
76. Bregman, J., Shapia Y., and Aharoni H., *Effects of oxygen partial pressure during deposition on the properties of ion-beam-sputtering indium tin oxide films.* Journal of Applied Physics, 1990. **67**(8): p. 3750-3753.
77. Kim, S.H., Park N., Kim T.Y., and Sung G.Y., *Electrical and optical characterisitcs of ITO films by pulsed laser deposition using a 10 wt.% SnO_2 doped In_2O_3 ceramic target.* Thin solid films, 2005. **475**: p. 262-266.
78. Nunes de Carvalho, C., Luis A., Conde O., Fortunato E., Leavareda G., and Amaral A., *Effect of rf power on the properties of ITO thin films deposited by plasma enhanced reactive thermal evaporation on unheated polymer substrates.* Journal of Non-crystalline solids, 2002. **229-302**: p. 1208 - 1212.
79. Vasu, V. and Subrahhmanyam A., *Phtovoltic properties of indium tin oxide (ITO)/silicon junctions prepared by spray pyrolysis- dependence on oxidation time.* Semiconductor Science and Technology, 1992. 7: p. 320-323.
80. Bessais, B., Mliki N., and Bennaceur R., *Technological, structural and morphplogical aspects of screen printing ITO used in ITO/Si type structure.* Semiconductor Science and Technology, 1993. **8**: p. 116 -121.
81. Goebbert, C., Nionninger R., Aegerter M.A., and Schmidt H., *Wet chemical deposition of ATO and ITO coatings using crystalline nanoparticles redispersable in solution.* Thin solid films, 1999. **351**: p. 79-84.
82. Skoog, D.A., *Principles of Instrumental Analysis.* 3rd ed. 1985, Philadelphia: Saunders. 174-190.
83. Botchkareva, A.E., Fini F., Eremin S., Mercader J.V., Montoya A., and Girotti S., *Development of a heterogeneous chemiluminescent flow immunoassay for DDT and related compounds.* Analytica Chimica Acta, 2002. **453**(1): p. 43-52.
84. Zhou, Y.X., Nagaoka T., Li F., and Zhu G.Y., *Evaluation of luminol-H2O2-KIO4 chemiluminescence system and its application to hydrogen peroxide, glucose and ascorbic acid assays.* Talanta, 1999. **48**(2): p. 461-467.
85. Zhou, G.J., Zhang G.F., and Chen H.Y., *Development of integrated chemiluminescence flow sensor for the determination of adrenaline and isoprenaline.* Analytica Chimica Acta, 2002. **463**(2): p. 257-263.
86. Li, J.Z. and Dasgupta P.K., *Chemiluminescence detection with a liquid core waveguide - Determination of ammonium with electro-generated hypochlorite based on the luminol-hypochlorite reaction.* Analytica Chimica Acta, 1999. **398**(1): p. 33-39.
87. Yao, D.H., Prodromidis M.I., Vlessidis A.G., Karayannis M.I., and Evmiridis N.P., *Membrane sampler for interference-free flow injection NO*

determination in biological fluids with chemiluminescence detection. Analytica Chimica Acta, 2001. **450**(1-2): p. 63-72.

88. Shi, J.J., Yan R.X., Zhu Y.F., and Zhang X.R., *Determination of NH3 gas by combination of nanosized LaCoO3 converter with chemiluminescence detector.* Talanta, 2003. **61**(2): p. 157-164.
89. King, R. and Miskelly G.M., *The inhibition by amines and amino acids of bleach-induced luminol chemiluminescence during forensic screening for blood.* Talanta, 2005. **67**(2): p. 345-353.
90. Song, Z.H. and Wang L., *Reagentless chemiluminescence flow sensor for the determination of riboflavin in pharmaceutical preparations and human urine.* Analyst, 2001. **126**(8): p. 1393-1398.
91. Marle, L. and Greenway G.M., *Determination of hydrogen peroxide in rainwater in a miniaturised analytical system.* Analytica Chimica Acta, 2005. **548**(1-2): p. 20-25.
92. Zhang, Z., Zhang S., and Zhang X., *Recent developments and applications of chemiluminescent sensors.* Analytica Chimica Acta, 2005. **541**: p. 37-47.
93. Roda, A., Guardigli M., Pasini P., Mirasoli M., Michelina E., and Musiani M., *Bio- and chemiluminescent imaging in analytical chemistry.* Analytica Chimica Acta, 2005. **541**: p. 25-36.
94. Oyama, M., Sasaki T., and Okazaki S., *Detailed analysis of reaction kinetics and mechanisms of electro-generated tetramethoxythianthrene cation radical and dication.* Journal of Electroanalytical Chemistry, 1997. **420**(1-2): p. 1-4.
95. Maness, K.M. and Wightman R.M., *Electrochemiluminescence in Low Ionic-Strength Solutions of 1,2-Dimethoxyethane.* Journal of Electroanalytical Chemistry, 1995. **396**(1-2): p. 85-95.
96. Cao, W.D., Zhang X.H., and Bard A.J., *Electro-generated chemiluminescence. 75. Electrochemistry and ECL of 9,10-bis(2-naphthyl)anthracene.* Journal of Electroanalytical Chemistry, 2004. **566**(2): p. 409-413.
97. Itagaki, M., Kobari N., and Watanabe K., *Electrochemiluminescence impedance of perylene in acetonitrile.* Journal of Electroanalytical Chemistry, 2004. **572**(2): p. 329-333.
98. Oyama, M., Mitani M., Washida M., Masuda T., and Okazaki S., *Two-dimensional CCD detection of electro-generated chemiluminescence (ECL) on an electrode surface. ECL reactions involving microcrystals of the perylene dimer cation radical salt.* Journal of Electroanalytical Chemistry, 1999. **473**(1-2): p. 166-172.
99. Oyama, M., Mitani M., and Okazaki S., *Formation of pi-excimer or pi-exciplex in electro-generated chemiluminescence involving perylene molecule revealed using a dual-electrolysis stopped-flow method.* Electrochemistry Communications, 2000. **2**(5): p. 363-366.
100. Tachikaw.H and Bard A.J., *Electro-generated Chemiluminescence .12. Magnetic-Field Effects on Ecl in Tetracene-Tmpd System - Evidence for Triplet-Triplet Annihilation of Tetracene.* Chemical Physics Letters, 1973. **19**(2): p. 287-289.
101. Matsui, J., Park H., Otsuka K., and Oyama M., *Kinetics and mechanisms of the reactions of 9-substituted anthracene cation radicals with water or methanol in acetonitrile.* Journal of Electroanalytical Chemistry, 2003. **558**: p. 49-57.

102. Wilson, R. and Schiffrin D.J., *Electrochemically oxidized ferrocenes as catalysts for the chemiluminescence oxidation of luminol.* Journal of Electroanalytical Chemistry, 1998. **448**(1): p. 125-130.
103. Zheng, X.W., Zhang Z.J., Guo Z.H., and Wang Q., *Flow-injection electro-generated chemiluminescence detection of hydrazine based on its in-situ electrochemical modification at a pre-anodized platinum electrode.* Analyst, 2002. **127**(10): p. 1375-1379.
104. Yang, M.L., Liu C.Z., Qian K.J., He P.G., and Fang Y.Z., *Study on the electrochemiluminescence behavior of ABEI and its application in DNA hybridization analysis.* Analyst, 2002. **127**(9): p. 1267-1271.
105. Braun, F., Annals of Physical Chemistry, 1898. **65**: p. 361.
106. Ikonopisov, S., Electrochimica Acta, 1975. **20**: p. 783.
107. Tajima, S., Electrochimica Acta, 1977. **22**: p. 995.
108. Knight, A.W., *A review of recent trends in analytical applications of electro-generated chemiluminescence.* Trac-Trends in Analytical Chemistry, 1999. **18**(1): p. 47-62.
109. Kulmala, S., Ala-Kleme T., Vare L., Helin M., and Lehtien T., *Hot electron-induced electro-generated luminescence of Tl(I) at disposable oxide-covered aluminum electrodes.* Analytica Chimica Acta, 1999. **398**(1): p. 41-47.
110. Zhu, L., Li Y.X., and Zhu G.Y., *A novel flow through optical fiber biosensor for glucose based on luminol electrochemiluminescence.* Sensors and Actuators B-Chemical, 2002. **86**(2-3): p. 209-214.
111. Kulmala, S., Hakansson M., Spehar A.M., Nyman A., Kankare J., Loikas K., Ala-Kleme T., and Eskola J., *Heterogeneous and homogeneous electrochemiluminoimmunoassays of hTSH at disposable oxide-covered aluminum electrodes.* Analytica Chimica Acta, 2002. **458**(2): p. 271-280.
112. Helin, M., Hakansson M., Canty P., Spehar A.M., and Kulmala S., *Hot electron-induced electro-generated chemiluminescence of 1-aminonaphthalene-4-sulphonate at oxide-covered aluminium electrodes in aqueous solution.* Analytica Chimica Acta, 2002. **454**(2): p. 193-201.
113. Ala-Kleme, T., Latva M., and Haapakka K., *Study on the radiative D-5(4) -> F-7(j) relaxation dynamics of Tb(III) in electrochemically excited self-assembled dimeric heterodinuclear Tb(III)-Ln(III)' chelates.* Analytica Chimica Acta, 2000. **403**(1-2): p. 161-171.
114. Ala-Kleme, T., Haapakka K., and Latva M., *Near-infrared electro-generated chemiluminescence of ytterbium(III) chelates in aqueous electrolytes.* Analytica Chimica Acta, 1999. **395**(1-2): p. 205-211.
115. Yang, M.L., Liu C.Z., Hu X.H., He P.G., and Fang Y.Z., *Electrochemiluminescence assay for the detection of acridinium esters.* Analytica Chimica Acta, 2002. **461**(1): p. 141-146.
116. Chen, G.N., Zhang L., Lin R.E., Yang Z.C., Duan J.P., Chen H.Q., and Hibbert D.B., *The electro-generated chemiluminescent behavior of hemin and its catalytic activity for the electro-generated chemiluminescence of lucigenin.* Talanta, 2000. **50**(6): p. 1275-1281.
117. Richter, M.M., *Electrochemiluminescence (ECL).* Chemical review, 2004. **104**: p. 3003-3036.
118. Fahnrich, K.A., Pravda M., and Guilbault G.G., *Recent applications of electro-generated chemiluminescence in chemical analysis.* Talanta, 2001. **54**(4): p. 531-559.

119. Kulmala, S. and Suomi J., *Current status of modern analytical luminescence methods.* Analytica Chimica Acta, 2003. **500**(1-2): p. 21-69.
120. Zhou, H.J., Zhang Z.J., He D.Y., and Xiong Y., *Flow through chemiluminescence sensor using molecularly imprinted polymer as recognition elements for detection of salbutamol.* Sensors and Actuators B-Chemical, 2005. **107**(2): p. 798-804.
121. Dodeigne, C., Thunus L., and Lejeune R., *Chemiluminescence as a diagnostic tool. A review.* Talanta, 2000. **51**(3): p. 415-439.
122. Zheng, X.W., Guo Z.H., and Zhang Z.J., *Flow-injection electro-generated chemiluminescence determination of epinephrine using luminol.* Analytica Chimica Acta, 2001. **441**(1): p. 81-86.
123. Corgier, B.P., Marquette C.A., and Blum L.J., *Screen-printed electrode microarray for electrochemiluminescent measurements.* Analytica Chimica Acta, 2005. **538**(1-2): p. 1-7.
124. Marquette, C.A. and Blum L.J., *Self-containing reactant biochips for the electrochemiluminescent determination of glucose, lactate and choline.* Sensors and Actuators B-Chemical, 2003. **90**(1-3): p. 112-117.
125. Ouyang, C.S. and Wang C.M., *Electrochemical characterization of the clay-enhanced luminol ecl reaction.* Journal of Electroanalytical Chemistry, 1999. **474**(1): p. 82-88.
126. Rubtsova, M.Y., Kovba G.V., and Egorov A.M., *Chemiluminescent biosensors based on porous supports with immobilized peroxidase.* Biosensors & Bioelectronics, 1998. **13**(1): p. 75-85.
127. Chen, G.N., Lin R.E., Zhao Z.F., Duan J.P., and Zhang L., *Electro-generated chemiluminescence for determination of indole and tryptophan.* Analytica Chimica Acta, 1997. **341**(2-3): p. 251-256.
128. Wilson, R., Clavering C., and Hutchinson A., *Electrochemiluminescence enzyme immunoassay for TNT.* Analyst, 2003. **128**(5): p. 480-485.
129. Wilson, R., Kremeskotter J., Schiffrin D.J., and Wilkinson J.S., *Electrochemiluminescence detection of glucose oxidase as a model for flow injection immunoassays.* Biosensors & Bioelectronics, 1996. **11**(8): p. 805-810.
130. Zhang, L., Zhou J.M., Hao Y.H., He P.G., and Fang Y.Z., *Determination of Co2+ based on the cobalt(II)-catalyzed electrochemiluminesce of luminol in acidic solution.* Electrochimica Acta, 2005. **50**(16-17): p. 3414-3419.
131. Haapakka, K.E., *The Mechanism of the Cobalt(Ii)-Catalyzed Electro-generated Chemi-Luminescence of Luminol in Aqueous Alkaline-Solution.* Analytica Chimica Acta, 1982. **141**(SEP): p. 263-268.
132. Haapakka, K.E., *Application of Electro-generated Chemi-Luminescence of Luminol to Determination of Traces of Cobalt(Ii) in Aqueous Alkaline-Solution.* Analytica Chimica Acta, 1982. **139**(JUL): p. 229-236.
133. Haapakka, K.E. and Kankare J.J., *Application of the Electrochemiluminescence of Luminol to the Determination of Copper.* Analytica Chimica Acta, 1980. **118**(2): p. 333-340.
134. Su, Y.Y., Wang J.A., and Chen G.N., *Determination of epinephrine based on its enhancement for electrochemiluminescence of lucigenin.* Talanta, 2005. **65**(2): p. 531-536.
135. Haapakka, K. and Kankare J., Analytica Chimica Acta, 1981. **130**: p. 415.
136. Brina, R. and Bard A.J., *Electro-generated Chemi-Luminescence .48. Electrochemistry and Electro-generated Chemi-Luminescence of Bis(2,4,6-*

Trichlorophenyl) Oxalate-Luminescer Systems. Journal of Electroanalytical Chemistry, 1987. **238**(1-2): p. 277-295.

137. Knight, A.W. and Greenway G.M., *Occurrence, mechanisms and analytical applications of electro-generated chemiluminescence.* Analyst, 1994. **119**: p. 879-890.
138. Tokel, N.E. and Bard A.J., *Electro-generated Chemiluminescence .9. Electrochemistry and Emission from Systems Containing Tris(2,2'-Bipyridine)Ruthenium(Ii) Dichloride.* Journal of the American Chemical Society, 1972. **94**(8): p. 2862-&.
139. Barnett, N.W., Bos R., Brand H., Jones P., Lim K.F., Purcell S.D., and Russell R.A., *Synthesis and preliminary analytical evaluation of the chemiluminescence from (4-[4-dichloromethylsilanyl)-butyl]--4'-methyl-2,2'-bipyridyl)ruthenium (II) covalently bonded to silica particles.* Analyst, 2002. **127**: p. 455-458.
140. Walworth, J., Brewer K.J., and Richter M.M., *Enhanced electrochemiluminescence from Os(phen)(2) (dppene)(2+) (phen=1,10-phenanthroline and dppene = bis (diphenylphosphino)ethene) in the presence of Triton X-100 (polyethylene glycol tert-octylphenyl ether).* Analytica Chimica Acta, 2004. **503**(2): p. 241-245.
141. Bruce, D., Richter M.M., and Brewer K.J., *Electrochemiluminescence from Os(phen)(2)(dppene)(2+) (phen=1,10-phenanthroline and dppene = bis(diphenylphosphino)ethene).* Analytical Chemistry, 2002. **74**(13): p. 3157-3159.
142. Abruna, H.D., *Electrochemiluminescence of Osmium Complexes - Spectral, Electrochemical, and Mechanistic Studies.* Journal of the Electrochemical Society, 1985. **132**(4): p. 842-849.
143. Richter, M.M., Debad J.D., Striplin D.R., Crosby G.A., and Bard A.J., *Electro-generated chemiluminescence .59. Rhenium complexes.* Analytical Chemistry, 1996. **68**(24): p. 4370-4376.
144. Cole, C., Muegge B.D., and Richter M.M., *Effects of poly(ethylene glycol) tert-octylphenyl ether on tris(2-phenylpyridine)iridium(III)tripropylamine electrochemiluminescence.* Analytical Chemistry, 2003. **75**(3): p. 601-604.
145. Bonafede, S., Ciano M., Bolletta F., Balzani V., Chassot L., and Vonzelewsky A., *Electro-generated Chemiluminescence of an Ortho-Metalated Platinum(Ii) Complex.* Journal of Physical Chemistry, 1986. **90**(16): p. 3836-3841.
146. Long, T.R. and Richter M.M., *Electro generated chemiluminescence of the platinum (II) octaethylporphyrin/tri-n-propylamine system.* Inorganica Chimica Acta, 2005. **358**(6): p. 2141-2145.
147. Whitchurch, C. and Andrews A.R.J., *Ligand and surfactant effects on a novel electrochemiluminescent reaction involving cadmium.* Analytica Chimica Acta, 2002. **454**(1): p. 45-51.
148. Kanemaguire, N.A.P., Wright L.L., Guckert J.A., and Tweet W.S., *Photoluminescence and Electro-generated Chemi-Luminescence of Palladium(0) and Platinum(0) Complexes of Dibenzylideneacetone and Tribenzylideneacetylacetone.* Inorganic Chemistry, 1988. **27**(17): p. 2905-2907.
149. Rubinstein, I. and Bard A.J., *Electro-generated Chemi-Luminescence .37. Aqueous Ecl Systems Based on Ru(2,2'-Bipyridine)32+ and Oxalate or*

Organic-Acids. Journal of the American Chemical Society, 1981. **103**(3): p. 512-516.

150. Leland, J.K. and Powell M.J., *Electro-generated Chemiluminescence - an Oxidative-Reduction Type Ecl Reaction Sequence Using Tripropyl Amine.* Journal of the Electrochemical Society, 1990. **137**(10): p. 3127-3131.
151. Gross, E.M., Anderson J.D., Slaterbeck A.F., Thayumanavan S., Barlow S., Zhang Y., Marder S.R., Hall H.K., Nabor M.F., Wang J.F., Mash E.A., Armstrong N.R., and Wightman R.M., *Electro-generated chemiluminescence from derivatives of aluminum quinolate and quinacridones: Cross-reactions with triarylamines lead to singlet emission through triplet-triplet annihilation pathways.* Journal of the American Chemical Society, 2000. **122**(20): p. 4972-4979.
152. Song, Q., Greenway G.M., and McCreedy T., *Tris(2,2'-bipyridine)ruthenium(II) electro-generated chemiluminescence of alkaloid type drugs with solid phase extraction sample preparation.* Analyst, 2001. **126**: p. 37-40.
153. Dolman, S.J.L. and Greenway G.M., *Determination of amitriptyline using electro-generated chemiluminescence.* Analytical Communications, 1996. **33**: p. 139-141.
154. Chen, X., Yi C., Li M., Lu X., Li Z., Li P., and Wang X., *Determination of sophoridine and related lupin alkaloids using tris(2,2'-bipyridine)ruthenium electro-generated chemiluminescence.* Analytica Chimica Acta, 2002. **466**: p. 79-86.
155. Greenway, G.M., Knight A.W., and Knight P.J., *Electro-generated chemiluminescent determination of codeine and related alkaloids and pharmaceuticals with tris(2,2'-bipyridine)ruthenium (II).* Analyst, 1995. **120**: p. 2549-2552.
156. Zhao, C.Z., Xu S.Y., Su Y., and Zhao G.L., *Chiral discrimination for enantiomers of amino acids using an electrochemiluminescence method.* Analyst, 2002. **127**(7): p. 889-891.
157. Chiang, M.T. and Whang C.W., *Tris(2,2 '-bipyridyl)ruthenium(III)-based electrochemiluminescence detector with indium/tin oxide working electrode for capillary electrophoresis.* Journal of Chromatography A, 2001. **934**(1-2): p. 59-66.
158. Tomita, I.N. and Bulhoes L.O.S., *Electro-generated chemiluminescence determination of cefadroxil antibiotic.* Analytica Chimica Acta, 2001. **442**(2): p. 201-206.
159. Zhao, X.C., You T.Y., Qiu H.B., Yan J.L., Yang X.R., and Wang E.K., *Electrochemiluminescence detection with integrated indium tin oxide electrode on electrophoretic microchip for direct bioanalysis of lincomycin in the urine.* Journal of Chromatography B-Analytical Technologies in the Biomedical and Life Sciences, 2004. **810**(1): p. 137-142.
160. Gonzalez, J.M., Greenway G.M., McCreedy T., and Song Q., *Determination of morpholine fungicides using the tris(2,2'-bipyridine)ruthenium (II) chemiluminescent reaction.* Analyst, 2000. **1254**: p. 765-769.
161. Egashira, N., Kumasako H., and Ohga K., Analytical Science, 1990. **6**: p. 903.
162. Fiaccabrino, G.C., de Rooij N.F., and Koudelka-Hep M., *On-chip generation and detection of electrochemiluminescence.* Analytica Chimica Acta, 1998. **359**(3): p. 263-267.

163. Namba, Y., Usami M., and Suzuki O., *Highly sensitive electrochemiluminescence immunoassay using the ruthenium chelate-labeled antibody bound on the magnetic micro beads.* Analytical Sciences, 1999. **15**(11): p. 1087-1093.

Chapter 2 – Electro-active sol-gel monoliths

2.0 Aims of chapter

The aim of this chapter is to describe the work undertaken producing electro-conducting sol-gels through the incorporation of indium tin oxide (ITO) or other electro-conductive species (PEDOT) into the sol-gel matrix. It will include sections on formulation, fabrication and analysis of both the sol-gels and ITO and provides details on the electrical and optical properties of the sol-gels and theories of conduction routes.

2.1 Introduction

As discussed in chapter 1, sol-gels are porous, optically transparent homogeneous glasses that exhibit good chemical inertness and have low processing temperatures. Historically, due to their porous network and mild manufacturing conditions they have been widely used in the fabrication of optical coatings or sensors through the encapsulation of dyes or other reactive species For a more thorough description of these systems, please refer to chapter 1 or the excellent reviews by Bakul *et al.* [1], Schottner [2], Walcarius [3] and Buck *et al.* [4].

Ordinarily sol-gels are electrically non-conducting, therefore systems utilising encapsulated moieties must be activated *via* contact, heating or photonic routes. In this work it was hoped that through the introduction of indium tin oxide (ITO) it would be possible to produce a transparent electro-conducting sol-gel that could be used for the encapsulation of light emitting, electro-active species. Electro-conducting sol-gels have already been fabricated with conducting polymers such as polypyrrole [5] and gold/graphite nanoparticles [6-8] being introduced into the sol-

gel matrix as dopants. Graphite doped sol-gels are the most common of this type of conducting sol-gel, and are frequently used as composite electrodes. The benefits of this type of electrode are that owing to the flexibility of the sol-gel process it is possible to introduce secondary dopants to add a complementary analysis. Examples of this include aquocobalamin [9] and bismuth doped lead oxide [10] used in the detection of L-cysteine and glutathione.

The disadvantage with these composite electrodes is that the graphite and gold nanoparticles greatly reduce the transparency of the sol-gel based electrodes, which is one of its main advantages, as this permits spectroscopy based analysis. As previously mentioned this work aimed to develop sol-gels doped with indium tin oxide, an n-type semiconductor with low electrical resistivity (typically 2 $x10^{-3}$ Ω-cm) and excellent transparency in visible and near infrared light [11, 12]. It was hoped that this would allow the fabrication of a transparent electro conducting sol-gel; potential applications for such a material include transparent electrodes, conducting fibres, electrochromic glass (smart windows) and light emitting electrochemical cells or sensors.

Using tris(2,2'-bipyridyl)ruthenium(II) dichloride hexahydrate ($Ru(bpy)_3^{2+}$) as an example, it is possible to demonstrate the advantage of an optically transparent electro-conductive sol-gel system. $Ru(bpy)_3^{2+}$ or its derivatives are extensively used as fluorescent dyes in oxygen sensors [13-16] where they are dip coated onto the tip of a fibre optic cable through their encapsulation in a sol-gel solution. In these systems $Ru(bpy)_3^{2+}$ is typically coated onto a bifurcated optical fibre with the excitation signal transmitted down one side of the fibre and the resulting fluorescent

signal being returned down the second fibre to a detection system. In these systems the oxygen level is determined through the analysis of the fluorescent lifetime or intensity, for which oxygen reduces or quenches respectively. However these same effects are found when employing electro-generated chemiluminescence of $Ru(bpy)_3^{2+}$, allowing for the simplification of the equipment though the removal of a light source and the bifurcated fibre-optic cable. In addition, given the low power levels needed to generate the ECL signal, approx 1.15 V, and the simplification of the equipment, it's possible to envisage a field portable oxygen measuring system. However in order to develop this system, a transparent, electro conducting, oxygen permeable matrix needs to be developed that is capable of encapsulating the $Ru(bpy)_3^{2+}$, yet will allow the transmission of the luminescent signal. Obviously, an ITO doped sol-gel would be ideal for this purpose given the sol-gels porous and transparent nature and ITO conducting yet optically transparent nature.

Before progressing to the experimental and results sections of this chapter; the related topic of conducting polymers will be discussed in order to provide comparison with the sol-gel ITO work undertaken in this study.

2.1.1 An introduction to conducting polymers, with particular attention given to PEDOT

The emergence of conducting polymers (see Figure 2.1) is a relatively recent development from conventional non-conducting saturated polymers and one which has led to the generation of a number of novel coatings and materials including thin film transistor (TFT) screens, polymer LEDs and anti static coatings [17]. Before

discussing PEDOT, a conducting polymer used in this work, a brief description of conductive polymers shall be provided that will include information pertaining to the types of polymer and their conduction properties.

The development of conducting polymers truly began in 1976 when Alan Heeger's group [18] discovered the first generation of conducting polymers, with their work on poly(sulphur-nitride) $(SN)_x$ and polyacetylene. It should however be noted that other groups discovered conducting polymers prior to this point, including Natta *et al.* [19] who first synthesised polyacetylene in 1958.

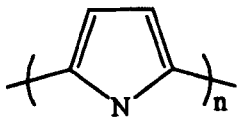

Polypyrrole

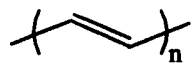

Polyacetylene

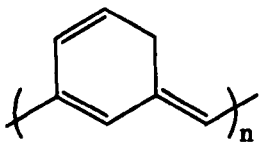

Polyheptadiyne (PHT)

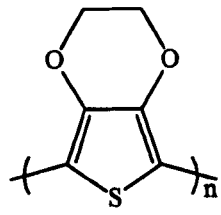

Polyethylenedioxythiophene (PEDOT)

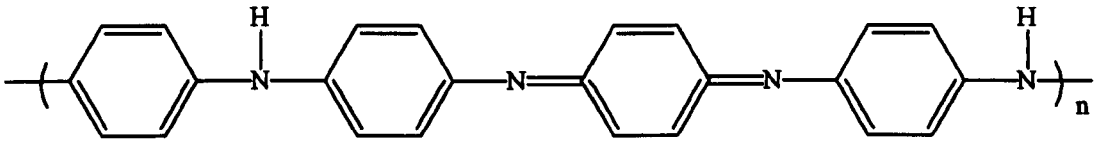

Polyaniline

Figure 2.1: Some examples of conjugated (electro-conducting) polymers.

In conventional polymers, such as polytetrafluoroethylene (PTFE/Teflon) and poly (vinyl chloride) (PVC), the carbon chains are saturated and are therefore non-conducting. Although not completely understood, in conjugated polymers the

bonding is different. It has been suggested that the electro-conductive nature of these polymers is due to a half filled valence band being formed from a continuously delocalised π system which results from a single unpaired electron (a π electron) per carbon atom.

According to Heeger, when describing conjugated polymers in his Nobel lecture based review paper, "*...π bonding, in which the carbon orbitals are in a sp^2p_z configuration and in which the orbitals of successive carbon atoms along the backbone overlap, leads to electron delocalisation along the backbone of the polymer. This electronic delocalisation provides the highway for charge mobility along the backbone of the polymer chain.*" [17].

In essence, the overlapping of the carbon orbitals in conjunction with the free electron allows the conduction of electricity to be facilitated in these structures *via* charge transfer along the polymer backbone. This suggests that the conduction characteristics of the polymer are determined by the chain symmetry, the number of uninterrupted repeat units in the polymer and the charge transfer efficiency (band gap).

Modern polymer systems however are typically chemically or electrochemically doped with an electron donator or acceptor that allows control over the system's conduction characteristics, from insulator to metal. Typical oxidising reagents include iodine, arsenic and iron (III) chloride with a classical reducing agent being sodium naphthalide. The main criteria for the dopant are to oxidise or reduce the polymer without compromising its stability or producing non-conducting side

reaction products. Through this doping the electrochemical potential (Fermi level) is moved, either through a redox or an acid base reaction into an energy region where there is a high density of electronic states.

The electro-conductivity in the doped polymer is due to the ability of the charge carriers (the dopant) to move along the π bonded "highway" [17]. According to Heeger [17], doped polymers are good conductors for two reasons. Firstly, doping introduces charge carriers into the electronic structure and since each repeat unit is a possible redox site conjugated polymers can be doped with a high density of charge carriers. In addition, the attraction of the electron in one repeat unit to the nuclei of neighbouring units leads to charge carrier mobility three dimensionally *via* interchain electron transfer. The use of doping has increased the electrical conduction in such systems considerably, early studies by Chiang *et al.* for example found increases in conductivity by a factor of 10^7 [20].

As noted in 2.1, PEDOT (poly-3,4-ethylenedioxythiophene) is used in this work as an intrinsic conductive polymer (ICP) encapsulated within a sol-gel monolith; with the intention of providing electro-conductance with excellent optical transparency. PEDOT is a member of a prominent class of ICPs called polythiophenes and is usually doped with poly(styrene sulfonate) (PSS), as shown in Figure 2.2, to form a water dispersed polymer complex. PSS is used as a dopant for two reasons, firstly as a charge balancing counter ion, and secondly it keeps the PEDOT dispersed in the aqueous medium as PEDOT is not truly soluble in its own right. The resulting PEDOT:PSS aqueous dispersion is dark blue in colour, containing approximately 5% polymer with a PEDOT:PSS ratio ranging from approximately 1:2.5 to 1:20. With

conductivity ranging from 1 to 10^{-5} S cm^{-1} and optical transmission of over 90 % (at 400 and 650 nm) for films with a thicknesses of 50 to 100 nm depending on the application [21].

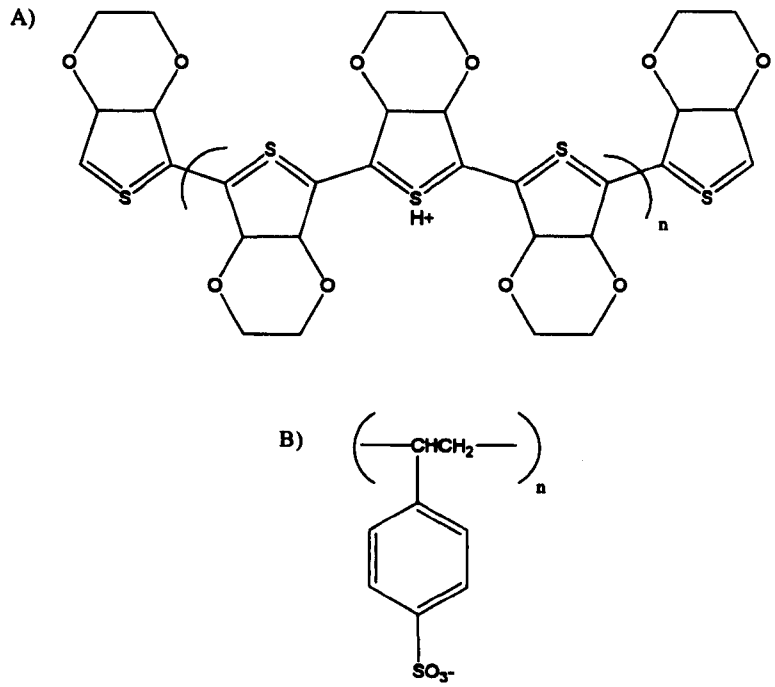

Figure 2.2: Chemical structures for A) PEDOT and B) Polystyrene sulfonate dopant.

Owing to its excellent optical transparency and electrical conductance, PEDOT is commercially used to produce transparent electronic circuitry in LED/OLED/PLED applications [21-23] and as an antistatic coating on cathode ray tubes, electronic component packaging and photographic films [21, 24]. It is also used in the manufacture of electrochromic windows [25], conducting glass [26] and in the development of biosensors [21, 27]. It can be applied to many plastics, including polycarbonate, polyethylene, polyamide and polypropylene and can be coated on glass using spin, spray and dip coating and ink jet and screen printing [21, 23, 25, 26].

2.2 Experimental

The experiments in this section can be divided into three main sections; the first section discusses the manufacture of indium tin oxide and compares this to industrially supplied material. The second section describes the work undertaken to establish a sol-gel fabrication technique that allowed the manufacture of stable non-cracking sol-gels that were strong enough to allow conductance testing. The techniques investigated included parameters such as sol-gel shrinkage, substrate adherence and cracking/warping prevention. The final section discusses the fabrication of electro-conducting sol-gels, and includes work characterising sol-gels with different combinations of indium tin oxide or PEDOT.

2.2.1 Design of instrumentation

Due to the variation in experiments discussed in this section, much of the information pertaining to experimental parameters and instrumentation will be provided during the discussion of the specific topic in an attempt to maintain clarity. Nonetheless the following discusses some of the generic instrumentation used during this work

Electro-conductance testing: -

Conduction tests on the sol-gels were performed using one of three systems, firstly an in-house designed sol-gel clamp incorporating an Iso-Tech IDM17 multimeter (R.S components, Corby, UK) as shown in Figure 2.3.

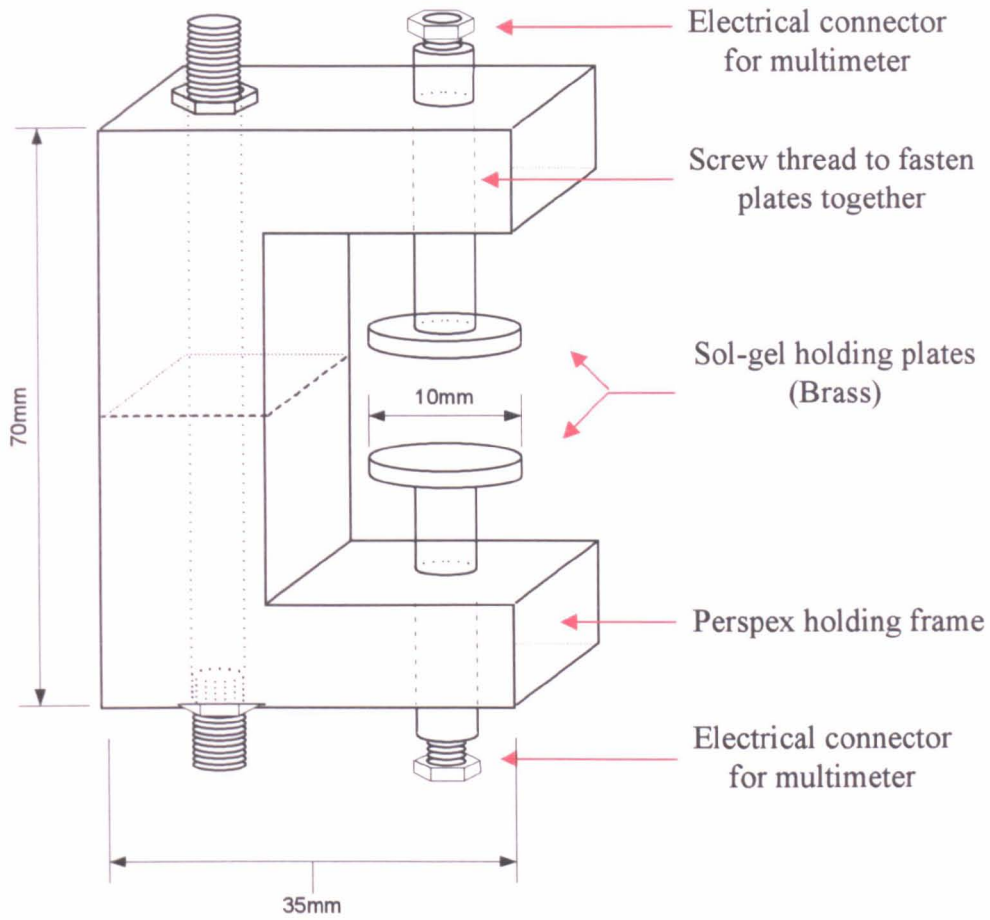

Figure 2.3: In-house designed sol-gel clamp incorporating a multimeter.

The second piece of equipment used to establish the electro-conductive properties of sol-gels was a Jandel four point conductance probe, kindly loaned by, Pilkington glass. The four point probe consisted of four spring mounted tungsten metal tips, each with a spacing of 1 mm to its adjacent tip. The outer tips were used to supply a sample current whilst a voltmeter measures the voltage across the inner two probes (See Figure 2.4).

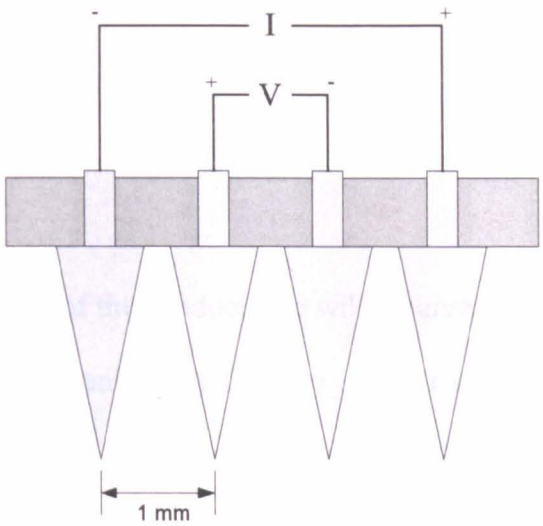

Figure 2.4: Schematic of four point probe tips.

Finally, a Nagy SRM-12 contactless sheet resistivity meter (as shown in Figure 2.5.) was used in order to establish the conductive properties of the fabricated sol-gels.

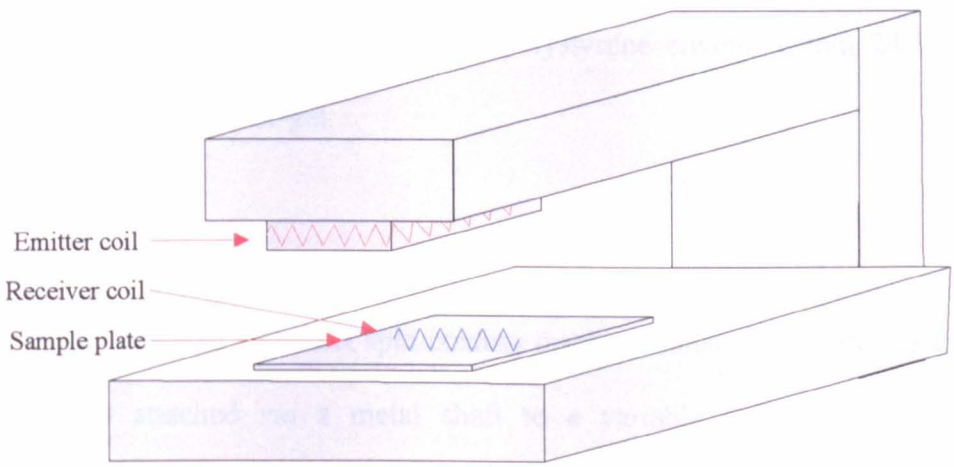

Figure 2.5: Graphical representation of Nagy SRM-12 sheet conductivity meter.

This Nagy SRM-12 works through the precise emission and detection of an electric field; which is produced and detected by electrical coils positioned above and below a sample plate respectively. The placing of a conducting material on the sample

plate results in a reduction in the field strength at the receiver, due to electro-conduction by the sample. The level of field reduction is related to the efficiency of the conductor, providing the user with information of resistivity and conduction.

Full details on the results of the conductance will be given in section 2.3.7; however the author would like to thank Mary Ormsby and her staff at the Pilkington Glass European Research Centre, Latham for the kind use of the four point probe and the Nagy SRM-12 used during this study.

Optical transmission testing: -

The optical transparency of nano particle size indium tin oxide and PEDOT encapsulated sol-gels was tested using a Perkin Elmer Lambda BIO-10 UV/Vis spectrometer; with a scan range between 350 to 800 nm. Each sol-gel sample was tested within a standard 1 cm pathlength polystyrene cuvette within 24 hours of gelation against a blank sol-gel.

Spin coating machine: -

The in-house designed and built spin coating machine consists of a housed circular rubber platter attached *via* a metal shaft to a variable speed drill. Cardboard mounting units are used to hold the glass sample plates onto the rubber platter during the spin coating, and also help remove excess sol-gel solution. The system is encased within a lockable Perspex box for safety.

2.2.2 Experimental reagents

The reagent used during these experiments were all analytical (at least 99%) grade unless otherwise stated and the water was high purity de-ionised produced by an Elga Elgastat UHQ PS (High Wycombe, UK). Tetramethoxysilane (TMOS) and tetraethoxysilane (TEOS) were both obtained from Aldrich (Gillingham, UK), hydrochloric acid from Fisher Chemicals (Loughborough, UK).

Phosphate buffer was produced using sodium dihydrogen orthophosphate (Fisher chemicals, Loughborough, UK) and disodium hydrogen orthophosphate (BDH, Poole, UK). With each buffer solutions being adjusted using a Hanna Instruments PHM2254 pH meter (Hanna Instruments, Kings Langley, UK,) pre-calibrated prior using pH 3, 7 and 9 pH reference solutions (Aldrich, Gillingham, UK).

Unless otherwise stated all sol-gels were fabricated *via* an acid catalysed reaction comprising of TMOS, water and 0.1 M hydrochloric acid in a 1:0.63:0.003 ratio; as this was found to be the optimum reaction protocol (as shown in section 2.3.2 & 2.3.3). This solution underwent sonication for 10 mins (some later studies reduced this time) before the addition of pH 6.4 (0.1 M) phosphate buffer (at a ratio of 1:1.25 to the previous reagent) which initiated the condensation reaction and will be referred to as a standard sol-gel. All other reagents used will be discussed in their relevant sections.

2.3 Results and Discussion

2.3.1 Indium tin oxide fabrication

During initial attempts to fabricate an electro-conducting sol-gel, micro-particle size indium tin oxide powder (MP-ITO) (Aldrich, Gillingham, UK), with a diameter of -325 mesh (approx 45 μm) was used for the experimentation. However for reasons that will be explained in the following sections this material proved unsuccessful and it was therefore decided to manufacture an in house alternative. It was felt that the required material should have a smaller particle size than the MP-ITO as one of the issues with the initial experiments was that the dispersed ITO sank before sol-gel gelation.

The method studied for the fabrication of the nano-particle size ITO (NP-ITO) was developed by Kim *et al.* [28], with further enhancement by Greenwood [29]. This method uses an (2-ethylhexyl sulfosuccinate)-AOT based reverse microemulsion to produce nano-size ITO particles. A reverse microemulsion is a surfactant stabilised water droplet dispersed in an oil medium. In this instance the water droplets act as nano reactors that contain the reactants and form the desired particles through collision.

In this experiment indium nitrate pentahydrate and tin chloride pentahydrate, both obtained from Aldrich (Gillingham, UK), were dissolved in water in a 9:1 ratio (by wt.). This ratio is used as it has been established that the optimum electro-conductance for ITO is achieved when the concentration of tin is 5 – 20 %wt [11, 28, 30]. To this solution, an AOT/isooctane (surfactant/oil) solution (microemulsion 1)

with a weight ratio of 45:55 was added whilst maintaining a water/AOT ratio of 22:1. The second microemulsion was prepared by adding 0.5 M ammonium hydroxide solution in to a corresponding AOT/isooctane solution (microemulsion 2) again keeping the water/AOT ratio at 22:1.

Fletcher *et al.* [31] found that microemulsions are dependent on droplet size and temperature, which allowed Greenwood [29] to calculate that the microemulsions had to be heated above 52 °C and 23 °C respectively before being mixed together for 1.5 hours under mechanical stirring. Indium tin hydroxide (ITH) particles are formed through the collision of the microemulsions containing the separate reagents (as shown in Figure 2.6). The ITH does not however precipitate out of solution as it is still bound within the surfactant structure, therefore acetone is added to break down the microemulsions and allow the ITH to precipitate out. The resultant ITH was then washed with successive washes of hexane and water to drive off residual traces of surfactant. The resultant particles were then dried and calcinated at 700 °C for two hours to produce ITO.

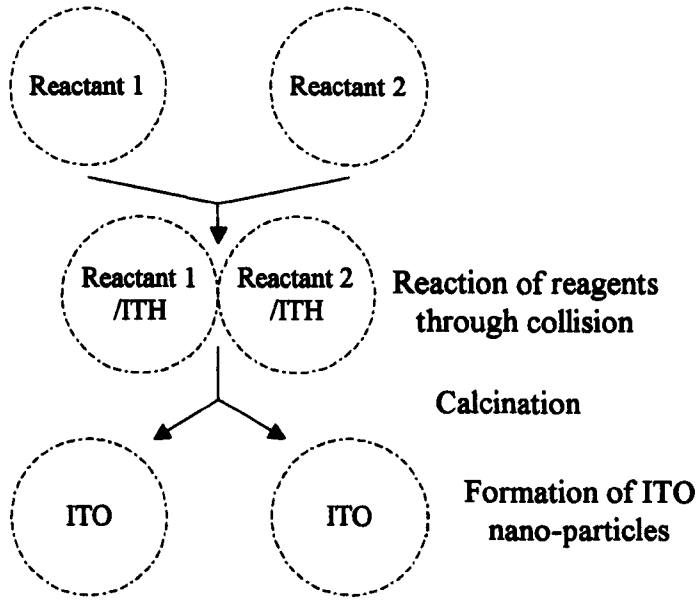

Figure 2.6: Illustration of nano-particle size ITO fabrication using method developed by Kim *et al.* [28].

With reference to Kim *et al.*[28], the mechanism for this reaction is as follows; the indium nitrate and the tin chloride react with ammonium hydroxide to produce Indium and tin hydroxides (1).

$$In(NO_3)_3 + 3NH_4OH \rightarrow In(OH)_3 + 3NH_4^+ + 3NO_3^-$$

$$SnCl_4 + 4NH_4OH \rightarrow Sn(OH)_4 + 4NH_4^+ + 4Cl^- \qquad (1)$$

A doping reaction (2) then occurs between the two metal hydroxides in proportion to their initial concentration, in this work it was attempted to establish a 9:1 ratio (wt/wt) respectively, in accordance with literature [11, 28].

$$In(OH)_3 / Sn(OH)_4 \rightarrow 7NH_4^+ + 3NO_3^- + 4Cl^- \qquad (2)$$

As previously mentioned on completion of the doping reaction (2), twice the volume of acetone is added to the microemulsion to break the surfactant emulsion structure.

This allowed the indium-tin hydroxide particles to sediment for collection and calcination at 700 °C for 2 hours (3).

$$In(OH)_3 / Sn(OH)_4 \xrightarrow{\text{Calcination at 700 °C}} In_2O_3 / SnO_2 \qquad (3)$$

At the same time that the ITO fabrication took place; it became possible to obtain nano-particle size indium tin oxide from Aldrich (Gillingham, UK). So it was decided to analyse the respective Aldrich and in-house manufacture ITO particles *via* inductively coupled plasma-atomic emission spectroscopy (ICP-AES).

2.3.1.1 ICP-AES analysis of ITO samples

The samples analysed are as follows.

Sample 1: Micro-particle sized ITO, manufactured in-house*.

Sample 2: Nano-particle sized ITO, manufactured in-house.

Sample 3: Micro-particle sized ITO, brought from Aldrich.

Sample 4: Nano-particle sized ITO, brought from Aldrich.

* This sample was kindly donated by Dr Paul Greenwood, for use in this analysis.

These samples, analysed on a Perkin Elmer Plasma 40 emission ICP, where tested for indium and tin content; the emission wavelengths being 230.606 nm for indium and 235.484 nm for tin. Initial comparison was made against a 10 ppm standard prepared from a 1000 ppm certified single element standard (Qm_x Ltd). The samples where weighed into a 7ml Teflon vessel where 1ml of nitric acid (Romil SpA grade) was added. The sample did not dissolve so HF (0.2 ml) and HCl (3 ml) where added to prepare an HF/aqua regia mixture to dissolve the sample, this was diluted to 50 ml with water.

On dilution, the samples where quantitatively analysed against a calibration of 20, 10 and 0ppm of tin and 150, 100, 50 and 0 ppm of indium, although the sample had to be diluted a further 10 times for the indium analysis. The results of this analysis are shown in Table 2.1.

	Sample 1	Sample 2	Sample 3	Sample 4
Manufacturer	In-house	In-house	Aldrich	Aldrich
Est. particle size	Micro	Nano	Micro	Nano
% Indium w/w	67.97	67.83	72.06	69.864
% Tin w/w	2.438	1.842	1.698	6.341
Ratio In:Sn	27:1	36:1	37:1	11:1

Table 2.1: Results from ICP-AES showing the levels of indium and tin in the four ITO samples.

Table 2.1 indicates that out of the four samples tested only the nano-particle size ITO purchased from Aldrich conforms to the ideal ratio as proposed by Frank and Köstlin [30]. In addition to this sample's In:Sn ratio it also had an average particle diameter of 30 nm (Aldrich, Gillingham, UK) meeting the criteria of the analysis; it was therefore decided to use the Aldrich manufactured NP-ITO for future work.

2.3.2 Sol-gel composition

Initial work focused on some of the more elementary aspects of sol-gel production including the effects of using different fabrication methods, the consequence of buffer pH and the effects of different substrates on sol-gel fabrication. This preliminary work allowed familiarisation with sol-gel fabrication. Initial experiments were aimed at evaluating the two most common types of silica alkoxide sol-gel precursor, tetramethoxysilane (TMOS) and tetraethoxysilane (TEOS) (Figure 2.7) in

order to establish which was best suited for the work to be undertaken in developing a conducting sol-gel.

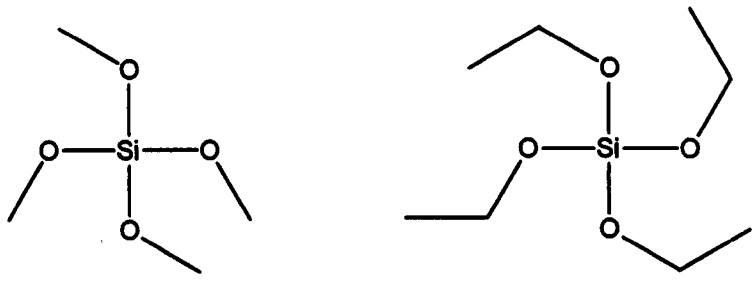

Tetramethoxysilane Tetraethoxysilane

Figure 2.7: Chemical structures for tetramethoxysilane and tetraethoxysilane.

This work demonstrated the steric effect observations made by Aelion *et al.* [32] who noted that any complication of the alkyl chains on the alkoxysilanes, such as lengthening and branching, reduces the rate of hydrolysis. This effect (discussed in more detail in the Chapter 1) is due to the longer alkyl chains reducing the effectiveness of the nucleophilic attack of water against the silicon atom in the siloxane groups.

Using an acid catalysed reaction with the same parameters for each alkoxide precursor, including buffer type and pH, R-value ($Si:H_2O$ ratio) and environment conditions the difference in gelation times for a TMOS and TEOS sol-gel were examined. An example of this using a pH 6 (0.1 M) phosphate buffer found that the sol-gel gelation time using TMOS and TEOS was approximately twelve minutes and three hours respectively. However ten minutes of this time was under sonication, which later studies with TMOS showed was unnecessary, with five minutes vigorous mixing being sufficient. This study clearly demonstrated the retarding effect of the

ethoxide groups in TEOS. This, in conjunction with the problems associated with ITO doping of the sol-gel (discussed in 2.3.4.1) were the deciding factors in choosing TMOS as the primary alkoxide precursor for the fabrication of the sol-gels in this work.

Other studies were performed with regards to sol-gel fabrication such as variation of the pH in the buffer solution, where it was shown that gelation times reduced as the pH of the buffer solution increased from pH 5 to pH 7. Changing the amount and concentration of the catalyst and altering the solution R-value was also investigated however this information only confirmed well documented information [32-34], and was merely performed for experience.

2.3.3 Sol-gel formation

This section will discuss three main topics, sol-gel shrinkage, cracking associated with substrate adherence and cracking due to environmental interaction; by their nature these topics are interrelated so will overlap.

As discussed in Chapter 1, during the drying and curing stages sol-gels undergo a shrinking process resulting from the contraction forces produced when water and solvents evaporate from the porous sol-gel matrix. This shrinking has a number of effects including making the sol-gel less porous/permeable, concentrating any dopants (discussed in more details in the next section) and physically damaging the structure, causing warping and cracking effects.

Initially experiments concentrated on the production of sol-gel monoliths, as it was felt that monoliths would be the easiest to test for conductance in subsequent work. Sol-gels are generally made into one of the following; monoliths, nano-spheres, fibres or thin films and it was felt that each of these had innate problems with regards to conductance testing. For example, thin films would be too easily damaged and scratched off by the four tungsten probes typically employed during conventional conductance testing, a theory that is backed up with experience using a multimeter in the lab. Fibres and nano-spheres it was felt, would be extremely difficult to examine using this technique due to the design of testing equipment. By comparison sol-gel monoliths, although susceptible to cracking and warping, should be able to withstand the clamping force of a conductance meters.

Initial fabrication was attempted by pipetting small amounts of a sol-gel solution (see 2.2.2) onto a glass microscope slide (Chance Proper Ltd, Whalley, UK)), which was subsequently covered in an attempt to make sol-gel monoliths. The monolith was covered for two reasons, firstly to prevent the still liquid sol from external contamination and secondly to prevent air currents from damaging the sol-gel through increasing pressure on stress lines on the surface of the sol-gels that form during drying. Stress lines are weak points on the sol-gel brought about when condensation in an area is reduced relative to the surrounding gel; these lines, if protected, often disappear as condensation continues and the sol-gel strengthens.

In these early experiments in which various concentration levels of solution were tested in this environment (0.1 → 3 ml), all of the sol-gels cracked badly on drying, regardless of being covered. Initially this was attributed to the normal cracking

process as discussed in Chapter 1.2.3.4, in which liquid rapidly evaporates from the sol-gel, thus forming stress lines due to the compressive forces of the meniscus. Various experiments using chemical additives where tried to improve the situation starting with the addition of methanol to the sol-gel solution.

Methanol (Fisher Chemicals, Loughborough, UK) was added to sol-gel solutions (4.65ml sol-gel solution, see section 2.2.2 for composition), with a volume of methanol ranging from 0.5 to 1.5 ml (0.25 ml increments) in an attempt to lower the viscosity of the sol-gels. This procedure has been used successfully by other groups when spin coating sol-gels or dip coating [35, 36]. It was hoped that this technique would allow the solution to settle into a thinner film, minimising the difference in contraction rates produced by the water in the interior and exterior sections of the sol-gel matrix. However, after a 1ml aliquot of each solution had been allowed to dry for 5 days on a covered microscope slide it was found that all the gels had cracked. Although a gradual increase in methanol concentration reduced the cracking exhibited by the sol-gels, it did not eliminate it altogether, and so this technique was abandoned.

An interesting way of visualising this cracking has been provided by Brinker and Scherer [33], when making an analogous comparison with a heated plate. In that "...one could say that a body contracts on cooling because of an effective compressive force that drives atom centres toward one another as the temperature decreases. If a temperature gradient exists in a body such that the surface is cooler, the atoms at the surface are being "compressed" more strongly, but they cannot freely move toward one another because they are bound to the warmer interior of the plate. The interior effectively stretches the surface beyond its equilibrium interatomic

spacing, and cracking may result. Then the atoms on either side of the crack can move closer together."

Still, further work was undertaken trying to produce sol-gel monoliths on glass slides with the addition of drying control chemical additive (DCCA). A number DCCAs have been investigated by other groups including surfactants [37, 38], formamide [33], which is used to produce sol-gel with a larger and more uniform pore size and oxalic acid [33] that produces large pore sizes similar to formamide. In this work Triton X-100 (Aldrich, Gillingham, UK), a non-ionic surfactant was added to a 4.65 ml sol-gel solution in an attempt to prevent cracking from occurring. In this work 1ml of Triton X-100 was added to a standard sol-gel solution, which was then pipetted onto the glass slide in a 1ml aliquot. It was hoped that the addition of the Triton X-100 would help reduce the interfacial energy of the system, a property Zarzycki *et al.* [34] have demonstrated and as a consequence reduced the capillary stress on the sol-gel. This reduction in capillary stress helps reduce the amount of gel shrinkage, which in turn increases the structural permeability of the gel. As a result the reduced capillary stress should have less compressive force on the sol-gel structure helping to reduce localised areas of tension in the sol-gel and thus reduces cracking.

Using Triton X-100 did help reduce cracking on the glass slide considerably; however it did not eliminate it; so it was decided to experiment with other substrate materials to establish if the fracturing was a characteristic of mounting substrate and not the sol-gels.

One of the factors in experimenting with different mounting substrates was that it was noted that excess sol-gel solution in the glass sample vials from previous experiments left a hard sol-gel coating on the vial. This suggested an interaction between the sol-gel solution and the mounting substrate, which needed to be investigated. Three types of mounting substrate were investigated, Teflon coated fabric sheet, Teflon coated tin plated steel sheet and cuvettes of different chemical composition and volume. The preliminary experiments were performed using the Teflon coated sheets[I] where a 1ml aliquot of standard sol-gel solution was pipetted onto the surface of each sheet. These sol-gels were covered with a glass covering plate that allowed observation during the one week drying and ageing period. As expected, during this time the sol-gels shrunk considerably (difficult to quantify due to shape), however unlike the glass based sol-gel none of the samples cracked. This experiment was repeated with multiple samples of varying volumes ranging from 1 to 2 ml of sol-gel solution onto both substrates to produce unbroken sol-gel discs; however the use of greater volumes still resulted in the sol-gels cracking, but to a much lesser extent This may have been improved further with the use of DCCAs but was not investigated here due to success of the following experiments

By pipetting 3ml of standard sol-gel solution into 45x10x10 mm polystyrene based cuvettes (Fisher, Loughborough, UK) it was possible to fabricate sol-gel blocks that perfectly mimicked the cuvette structure. This structure provided flat sides, by which it would be possible to perform conduction analysis, a property that had been lacking in previous experimental attempts. It also allowed for the first time the ability to properly quantify the level of volume change associated with shrinkage when a sol-

[I] Obtained from own supply of these products.

gel is allowed to dry and cure to completion. What was interesting was that sol-gels fabricated at the same time from the same solution provided different levels of shrinkage between gels. As shown in Table 2.2, when ten sol-gels were analysed the average volume was found to be 17 % of the initial pipetted volume; however this included a minimum of 6 % and a maximum of 24 %.

Sol-gel	Height/mm	Width/mm	Depth/mm	Volume/mm^3	% of original volume
Initial	30	10	10	3000	100
1	17	6	6	612	20
2	15	5	5	375	13
3	19	5	5	475	16
4	20	6	6	720	24
5	12	4	4	192	6
6	18	6	6	648	22
7	20	6	6	720	24
8	18	5	5	450	15
9	17	5	5	425	14
10	18	5	5	450	15
				Av % =	**17**

Table 2.2: Comparison of volume reduction in blank sol-gels due to shrinkage during drying and curing from the original dimensions of 30x10x10 mm; see section 2.2.2 for sol-gel composition.

The reason for this is not certain, but it has been observed that the sol-gels that demonstrate the greatest volume reduction sometimes fracture, unlike the larger sol-gels counterparts. This suggests that evaporation from them is more rapid producing capillary forces that the sol-gels are unable to withstand. The reason for this more vigorous evaporation is not understood as the sol-gels come from the same stock and are kept under the same environmental conditions. One possibility is that occasionally the sol-gel structure is produced with a more porous network than usual, facilitating the rapid loss of liquid from the sol-gel matrix which leads to this loss in

volume and structural integrity. However it is hard to envisage such a large change in structural development between sol-gels prepared in the same way and in the same equipment. Nevertheless other fabrication studies have resulted in equally varied final volumes for the sol-gels.

In addition to the standard size cuvettes used in the work, experiments were carried out using 2.5 mm pathlength varieties and also larger in-house designed PTFE cuvettes as shown in Figure 2.8. Both of these allowed the fabrication of sol-gel blocks; however those produced with the 2.5mm pathlength cuvette were consistently warped, though cracking was not an issue with either design.

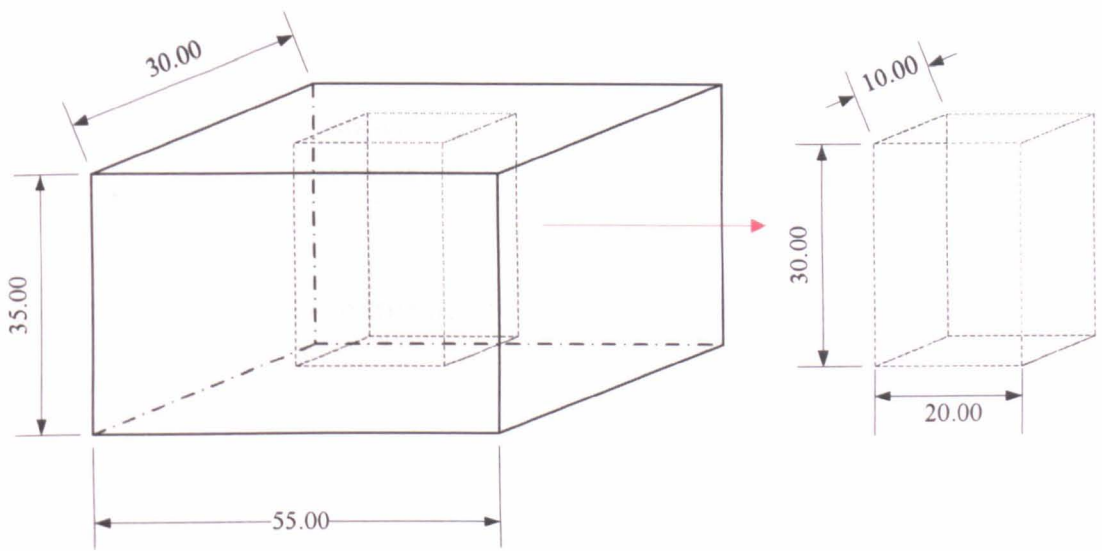

Figure 2.8: A schematic of an in-house built PTFE cuvette used for sol-gel monolith development.

It is important to consider why the monolithic sol-gels were superior to the glass slides for fabrication. To answer this, one needs to consider the sol-gel reaction and how it builds the polymeric chain that forms the sol-gel matrix. As discussed in

Chapter 1, when sol-gels undergo condensation reactions silanol and silanate groups react to form the siloxane bonds which are the backbone of the sol-gel matrix. A glass substrate, such as the microscope slides used during this work also have surface silanol groups that the sol-gel solution would be able to deprotonate and react with in a similar manner to the condensation reaction. Essentially in reacting in this way, the glass substrate becomes part of the sol-gel matrix; albeit as an unyielding anchor, thus preventing the sol-gel from shrinking in the normal way. These anchor points prevent the sol-gel from shrinking *via* the normal compressive forces produced by the capillary action of the liquid evaporating from the sol-gel, initially the sol-gel is pliant enough to withstand these forces. However as the condensation continues the sol-gel becomes more rigid and the anchor points stretch the surrounding sol-gel, putting stress on the regions around these points. These stress points eventually crack, which allows the sol-gel fragments to continue the shrinkage process.

It may be possible to overcome this problem by using silanising agents such as hexamethyldisilazane (HMDS) or chlorotrimethylsilane to endcap the silanol groups and prevent or reduce the available siloxane anchor sites. Silanising is a commonly employed technique used in biology to prevent protein adsorption onto glass; however, given the success of the other substrates it was deemed there was little need to use glass and therefore this technique.

Another problem that has been encountered whilst making standard sols-gels is that they are occasionally opaque when dried. Although no explanation has been proven so far it has been hypothesised that during the continued condensation reaction a

small water layer is occasionally trapped within the sol-gel structure. This small water layer inside the otherwise dry matrix scatters light, thus giving the sol-gel an opaque appearance. This phenomenon happens rarely, but it has been found that storing opaque sol-gels in a dessicator for a week usually returns them to a clear condition. Simpkins *et al.* [37] have postulated that the surface can become less translucent as air enters the pores during drying although given the success with the dessicator it is felt that trapped water is the more likely cause for the sol-gel opaqueness.

To conclude this section, the work undertaken suggested that the most promising method for the fabrication of conducting sol-gels was based on a rapid acid catalysed sol-gel technique using TMOS instead of other more complex silicon based alkoxide materials (such as TEOS). TMOS when allowed to dry and cure within a covered polystyrene cuvette, produced uniform sol-gel monoliths. It was also possible to fabricate sol-gel monoliths with TEOS; however the gelation time was vastly increased over that of TMOS. It was also felt that the extension of gelation time would hinder future doping experiments due to the increased possibility of the dopant falling out of the solution phase of the sol-gel. The following sections discuss the work undertaken using this technique to produce uniform, electro-conducting sol-gels.

2.3.4 Development of micro particle MP-ITO dispersed sol-gels for the production of electro-conducting sol-gel materials

As previously mentioned the initial objective of this work was to develop a transparent electro-conductive sol-gel through the incorporation of indium tin oxide (ITO) into the matrix of a sol-gel monolith. This section describes how using the experience gained from making the sol-gel described in section 2.3.3 new sol-gel materials were fabricated through the dispersion of ITO in varying amounts, so that the optimum conduction properties could be established. ITO was chosen as the electro-conducting moiety because in addition to its electro-conducting properties it demonstrates low light absorption in the visible region. This is a property important for later work when there is a need to detect light emitted from tris(2, 2-bipyridyl) ruthenium(II) dichloride hexahydrate at 610 nm. Different doping and sol-gel fabrication techniques were investigated, including the use of dispersion agents. Different grades of ITO were also used including in attempts to spin coating ITO containing sol-gel onto a glass substrate.

Initial work involved making electro-conducting sol-gel through the incorporation of micro-particle size ITO (MP-ITO) into a standard sol-gel matrix; the MP-ITO as discussed in section 2.3.1, was a fine green/yellow powder with an average diameter of 45 μm. Prior to development of the sol-gel monoliths, standard sol-gel solutions in which known amounts of MP-ITO had been added were pipetted onto microscope slides for observation. For example 0.0161 g, 0.01 g and 0.005 g of MP-ITO was added to a standard sol-gels solution with a total volume of 4.65ml, producing sol-gels with an $Si:H_2O$ ratio of 15 and ITO concentrations of $1.74x10^{-7}$, $1.1x10^{-7}$ and

$5.4x10^{-8}$ mol/l respectively. The MP-ITO was initially weighed into the sample vials followed by the introduction of the TMOS, water and HCl in a 1:0.63:0.003 ratio. These solutions were then magnetically stirred until exothermic heat from the hydrolysis reaction diminished and the ITO had become homogeneously mixed. Whilst continuing to stir, 2 ml of pH 6.4 phosphate buffer was added to each solution and 2 x 1 ml aliquots of each was pipetted onto glass microscope slides. The sol-gels took approximately two minutes to gel, by which time the ITO had sunk to the surface of the glass slide on each of the samples; as with the use of glass slides in the previous section all the sol-gels cracked on curing.

This same reaction was repeated for the addition of 0.0161 g to the ITO sol-gel solution, but this time the sol-gel was allowed to gel in the vial in order to gauge how much ITO dispersed in solution prior to gelation. In fact in this experiment so much of the ITO fell out of solution that the base of the cured sol-gel was very brittle with high ITO content and little sol-gel matrix support. Very little of the ITO stayed in solution, although this cannot be quantified; Figure 2.9 represents this graphically.

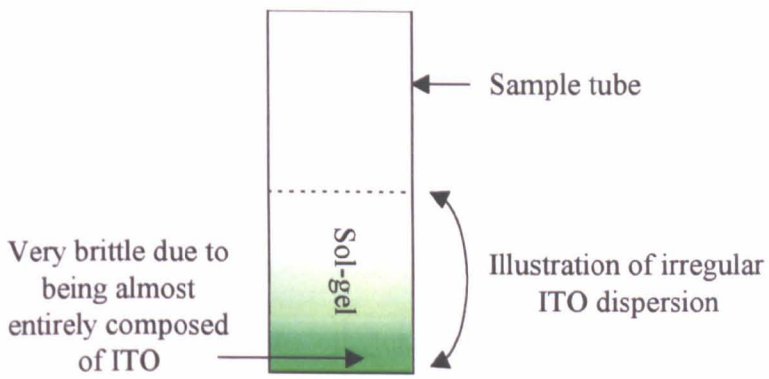

Figure 2.9: Graphical representation of irregular ITO distribution in MP-ITO encapsulating sol-gel monoliths.

Due to the problem of the ITO sinking to the base of the sol-gel prior to drying a dispersion agent was used to keep the ITO in the sol-gel solution. Previous work carried out by Goebbert *et al.* [39] used ethylene glycol and acetic acid as a dispersion agent to enable them to produce thin conducting coats on glass through spin and dip coating techniques. In Goebbert's work however nano-particle size ITO was used for the experiments.

The dispersion agent was produced from 2 ml ethylene glycol (Beercroft Anal. grade) and 20 µl acetic acid (Fischer Anal. grade) this was added to variable amounts of MP-ITO. This solution was mixed briefly (approx 10 s) with a magnetic stirrer until homogeneity was observed. A 1 ml aliquot if this solution was added to the previously produced standard sol-gel solutions, and mixed using a magnetic stirrer until homogeneity was observed. 2 ml of pH 6.4 (0.1 M) phosphate buffer was added to these solutions and the sol-gels were allowed to dry. The addition of the dispersion agent visibly increased the homogeneity of the ITO within the sol-gels, although they still showed signs of the ITO sinking prior to drying.

Additionally, the use of the dispersion agent increased the gelation time of the sol-gel. This could be due to the acetic acid lowering the pH, which subsequently reduced the efficiency of the condensation reaction (see 1.2.3 and Figure 1.15) or the effect could be attributable to the ethylene glycol. It was observed that ethylene glycol increased the viscosity of the solution which possibly lowered the mobility of the sol-gel sub units (*i.e.* the dimer and trimer sol-gel units) which in turn reduced the speed of polymerisation.

In addition to investigating the fabrication of electro-conducting sol-gel monoliths, spin coated thin films of ITO doped sol-gel were spun on 2 cm^2 glass plates. The in-house designed and built spin coating device, schematically represented in Figure 2.10, consisted of a housed circular rubber platter attached *via* a metal shaft to a variable speed drill. This system was clamped inside a lockable Perspex box for safety reasons. A cardboard mounting unit held the glass plate during the spin coating, and also helped remove excess sol-gel solution.

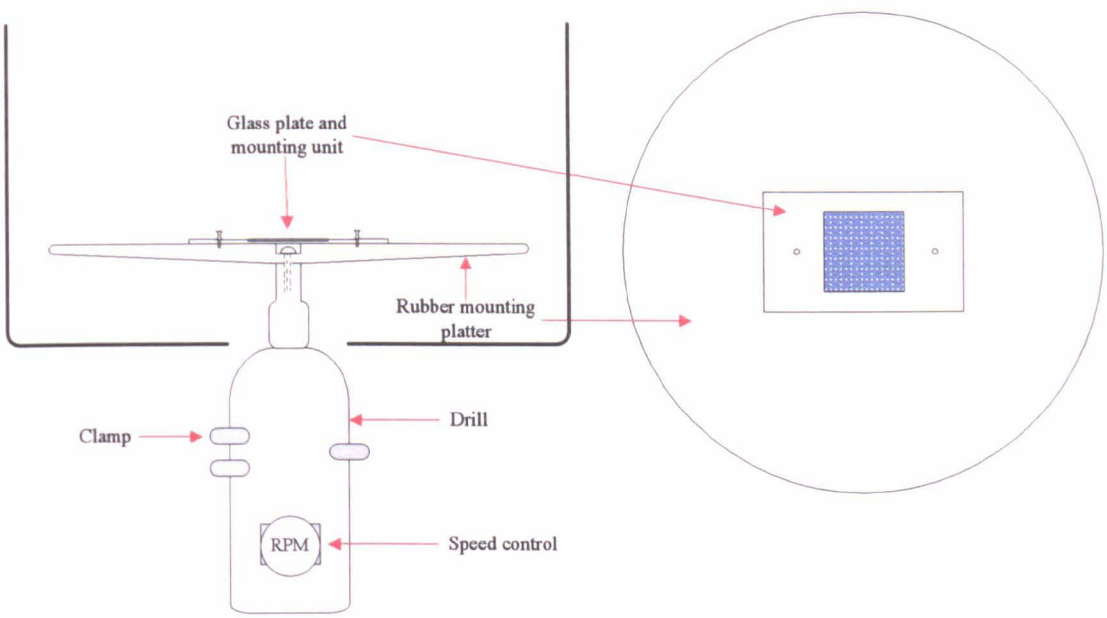

Figure 2.10: Schematic of the in-house designed spin coating device.

It was hoped that using spin coating would allow a defect free thin sol-gel coat to be applied to a glass substrate. Spin coating or the related dip coating allows rapid evaporation of the solvents from the sol-gel matrix. With monolithic sol-gels this would result in the sol-gel cracking due to capillary forces putting uneven compressive stress on the internal and external sections of the sol-gel (section 1.2.3). In thin films however gelation and evaporation occur at the same time throughout the sol-gel, which results in a dense sol-gel film being fabricated [33, 40, 41]. With thin

films, shrinkage acts in the path of least resistance which is perpendicular to the plane of the sol-gel, thus collapsing the gel producing the dense sol-gel films. This also helps reduce lateral constrictive forces (see chapter 1) which affect the larger monolithic sol-gels, improving the stability of the sol-gel film.

Two spin coating methods were investigated for this work, the first using a methanol containing standard sol-gel solution containing MP-ITO. The second method was adapted from the spin coating technique developed by Goebbert *et al.* [39]. To produce a methanol based sol-gel, TMOS, water, 0.1 M HCl and methanol in a ratio of 1:0.625:0.031:0.625, were added to 0.005 g of MP-ITO and mixed using a magnetic stirrer. A 250 µl aliquot of this solution was pipetted on the mounted glass plate and spun for 20 seconds using the spin coating device with the speed gradually increased (it was not possible to know the spin speeds using this simple device). The glass plate was then placed in a dessicator overnight to allow the solvents to evaporate and protect the coating from damaging air currents. Using this method it was found that some sol-gels still fractured, but as explained it was difficult to maintain similar fabrication environments as the rotational speed of the spin coating device could not be programmed. Some of the fabricated sol-gels though were produced undamaged but it was found the inertia during the spin coating distributed the MP-ITO on the outside edge of the sol-gel thin film in a halo profile. Obviously this is unacceptable for this work as the ITO needs to be homogeneous throughout the sol-gel. Using the method developed by Goebbert *et al.* it was not possible to produce stable sol-gels. This was thought to be as a result of the increased viscosity of the sol-gel solution making the film too thick, leading to structural fractures, as demonstrated in previous sections.

During this work it became possible to purchase nano-particle size ITO from Aldrich as discussed in section 2.3.1. This, in addition to the results obtained by the ICP analysis led to the selection of NP-ITO over MP-ITO as discussed in the next section.

Due to the fabrication problems encountered with the MP-ITO doped sol-gels, such as a lack of homogeneity and warping/cracking, it should be noted that it was not possible to carry out electro-conductance analysis on the samples.

2.3.5 Development of NP-ITO dispersed sol-gels for the production of electro-conducting sol-gel materials

To overcome the problems encountered with the MP-ITO work was undertaken to investigate the encapsulation of nano-particle size indium tin oxide (NP-ITO) within a range of sol-gels

As discussed in 2.3.1.1, the NP-ITO purchased from Aldrich met the requirements given by Frank and Köstlin [30] with regards to the concentration of tin required within the indium oxide (In_2O_3) lattice, *i.e.* that which provided the best electro conduction (see sections 2.3.11 & 1.3.2 for more details). In addition it was hoped that the smaller size of the NP-ITO would prevent it from falling out of the sol-gel solution prior to gelation, allowing the formation of an electro-conducting sol-gel monolith. The sol-gels discussed in the following section were formed within polystyrene cuvettes, unless stated otherwise; as they have proved to be ideal for this task.

The sol-gels were formed in a glass vial from a standard sol-gel solution consisting of TMOS, water, HCl (0.1 M) and phosphate buffer as discussed in section 2.2.2. NP-ITO was added to the samples prior to the addition of phosphate buffer in concentrations ranging from 5.5 $x10^{-6}$ to 5.5$x10^{-5}$ mol/l (equal to 0.5 to 5 mg of ITO in a 4.65 ml aliquot of sol-gel solution), as shown in Table 2.3. These solutions were stirred for approximately 1 min using a magnetic stirrer to provide homogeneity. The phosphate buffer was subsequently added to these solutions, still under stirring, to initiate the condensation reactions. A 3 ml aliquot of each sol-gel was then immediately pipetted into a standard 1cm pathlength polystyrene cuvette, covered in parafilm, and allowed to gel and age at room temperature; no dessicator was used for this procedure. It should be noted that the ITO concentrations given are for the sol-gel solution prior to gelation and curing.

Sample	Indium tin oxide added/g	Volume of sol-gel/ml	[ITO] $x10^{-8}$ mol/l
Blank	0	4.65	0
1	0.0005	4.65	0.54
2	0.0010	4.65	1.1
3	0.0015	4.65	1.6
4	0.0020	4.65	2.2
5	0.0025	4.65	2.7
6	0.0030	4.65	3.3
7	0.0035	4.65	3.8
8	0.0045	4.65	4.9
9	0.0050	4.65	5.4

Table 2.3: The weight (concentration) of NP-ITO used in each sol-gel monolith.

On visual inspection after gelation, the NP-ITO distribution for all of the sol-gel monoliths fabricated appeared to be homogeneous. This result allowed the continued assessment of the sol-gels with regards to optical transparency and electrical

conductance. Also as this was achieved without the use of secondary reagents, such as dispersion agents or DCCAs, the sol-gel reaction was rapid. Additionally, subsequent analysis would now be easier to interpret as these secondary reagents wouldn't have to be taken into account during any evaluation.

2.3.6 Optical transparency of NP-ITO doped sol-gel monoliths

Upon gelation each of the samples was analysed using a Perkin Elmer Lambda BIO-10 UV/Vis spectrometer, between 350 to 800 nm to assess the effect of the ITO particles on the transmission of light. (A blank sol-gel was used as the blank for each reading.)

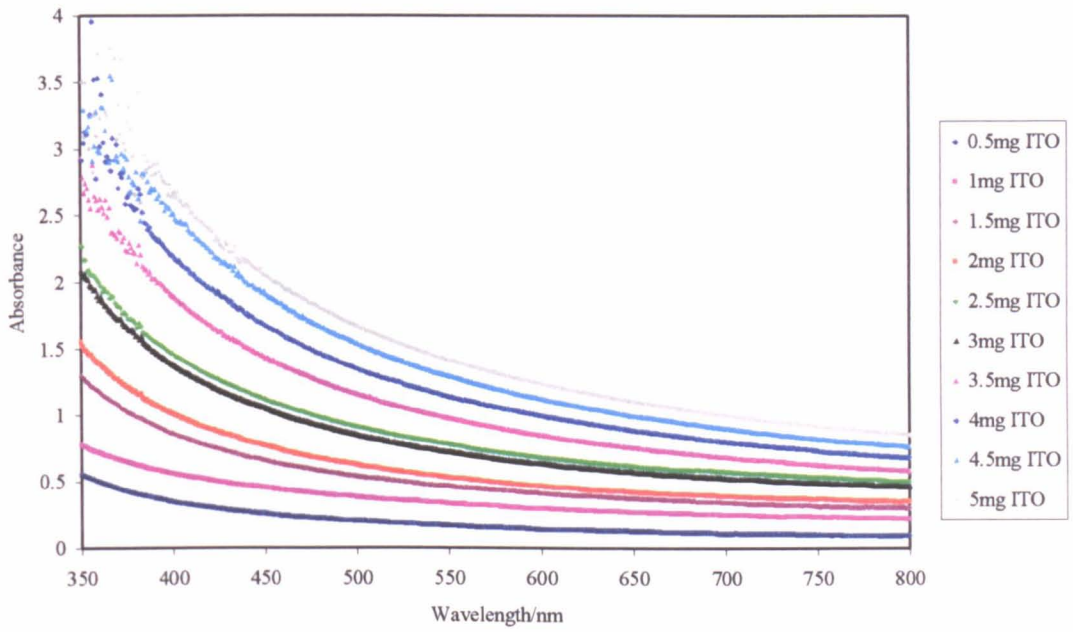

Figure 2.11: Changes in the absorbance of the sol-gel monoliths with increased NP-ITO content (see Table 2.3 also).

Although thin films of ITO, such as those on conducting glass have excellent transmission characteristics, it was not expected for these monolith type sol-gels to

be as good. In thin films, layers of ITO are coated onto the desired substrate to a depth of approximately 100nm allowing approximately 90 % optical transmission.

The absorbance for the NP-ITO doped sol-gel monoliths is shown Figure 2.11. The sol-gel encapsulated ITO does not absorb in the UV/Vis region in the truest sense of the term; it is scattering of the light (signal) away from the spectrometer detector that is being measured. This can be seen in the spectra which have no characteristic peaks, just a gradual increase in absorbance signal towards the shorter wavelengths. This noise is predicted when following the equation shown in Figure 2.12, which states that a photon's energy is inversely proportional to the wavelength and directly proportional to the frequency.

$$\varepsilon = h\nu = \frac{hc}{\lambda}$$

ε = The energy of one photon h = Planck's constant (6.62×10^{-34} J.s)

ν = Frequency (s^{-1}) λ = Wavelength (cm)

c = Speed of light (3×10^{10} cm/s)

Figure 2.12: Equation demonstration the relationship between energy, wavelength and frequency.

Figure 2.11 clearly demonstrates this effect with the increase in absorption throughout the entire range of ITO concentrations. As the concentration of ITO increases with each sol-gel the noise increases, with the effect especially noticeable at the lower wavelengths. This increase in absorbance is not entirely linear with each increase in NP-ITO concentration; as a doubling in concentration typically results in

an absorbance with a value slightly less than double. These variations could be due to complex collision pathways allowing the photon to reach the detector window.

Further work, discussed in Chapters 3 and 4, successfully uses this type of conducting sol-gel as a thin film on carbon electrodes in studies utilising electro-generated chemiluminescence. So although the absorbances are quite high in Figure 2.11, they are for sol-gel monoliths and cannot be compared with the commercial ITO thin films. Studies in which thin films were applied to a glass substrate for comparison were unsuccessful because the films developed were uneven and cracked. Commercially available ITO coated glass plates, such as those discussed in section 1.3.2, are typically annealed at approximately 400-600 °C which improves the electro-conductance and also transparency. This is not viable in this work as the sol-gel will be used to encapsulate heat sensitive reagents, which would be destroyed at these temperatures. By using elevated temperature with a sol-gel defeats one of its main advantages; in that it can be used to encapsulate heat sensitive products such as biological and organic material.

2.3.7 The Electro-conductive properties of NP-ITO doped sol-gel monoliths

With regard to the conductive properties of the sol-gels, as stated in the experimental section (2.2.1), three systems were investigated during this work. The first was an in-house design based around the clamping of the sol-gel between two brass plates (Figure 2.3) which were connected to a multimeter. It was not possible to establish steady resistivity/conductivity readings with this equipment. This is believed to be

due to a lack of, or change in contact between the brass plates and the sol-gel sample, as it was never possible to take a steady reading. This technique was further limited due to being unable to tighten the clamp heavily without causing damage to the sol-gel; therefore this technique was abandoned.

The second technique used to measure sol-gel conductance was a Jandel four point conductance probe. This is a handheld device in which four miniature tungsten tips (probes) are pushed into the sol-gel surface; which caused very little damage to the sol-gel. In this system the outer tips supply a sample current whilst a voltmeter measures the voltage *via* the inner two probes. From this the resistance and conductivity of the substrate can be analysed using the equations given in Figure 2.14.

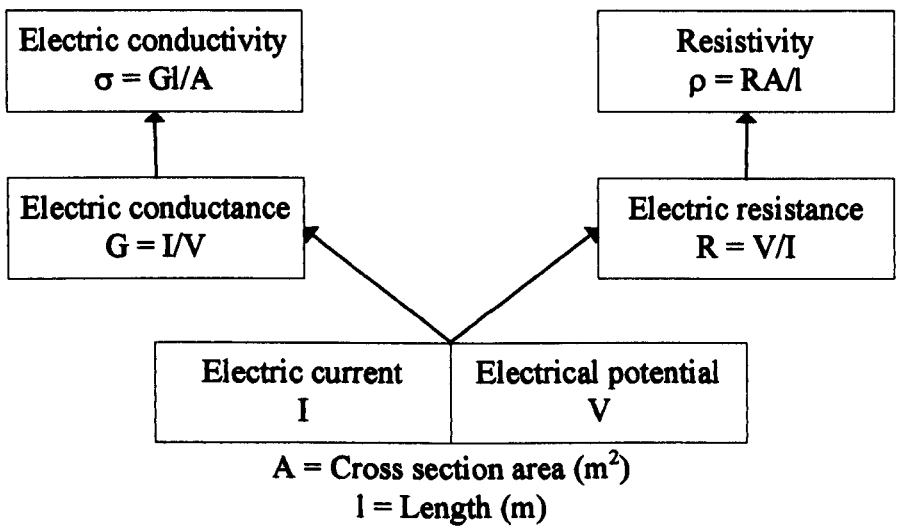

Figure 2.14: Equations used to calculate resistance and conductance properties.

However again, it was impossible to obtain a steady reading for the conductive sol-gels from this equipment. The lack of stability for both this equipment and the in-

house designed sol-gel clamp is thought to be as a result of the particles nature of the conducting ITO. For example, the four point probe was placed manually and it is believed that slight movement in the system changed the number of ITO particles the tips were in contact with in a given area of non-conducting sol-gel, and thus changed the conductivity/resistance measurements.

A way of considering these conducting sol-gels is not as one conducting block, but as a multitude of discreet conducting volumes; each in contact with neighbouring volumes, which allows conductance through the system as a whole. An analogy for this could be of human cells, each of which exist individually but work and communicate as part of a bigger system. Comparisons can be made to doped composite electrodes, in which typically a metal or graphite is added to the composite material to produce an electrode. Examples of dopants include copper [42], silver [7], graphite [6, 43], gold [44] and platinum [45] entrapped within systems including sol-gels [6, 7], Kel-F [46] and polyethylene [42]. In work involving carbon based composite electrodes, Weisshaar and Tallman [46] described the surface of these electrodes as "islands of graphite in a sea of Kel-F". They justified that each island of graphite is in effect a microelectrode separated from other microelectrodes by insulating regions of Kel-F; thus making the electrode an array of microelectrodes.

In the ITO doped sol-gel system the conducting ITO is held in a matrix of non-conducting sol-gel in the same way. As the ITO doped sol-gels were acting as an array of conducting micro-particles, a non-contact method for conductance analysis

was therefore needed. This was provided by the third technique used to measure sol-gel conductivity, the Nagy SRM-12 contactless sheet conductivity meter. Importantly, this system analyses a sample as a whole and not a random point and therefore is able to test the ITO sol-gels for conductance properties.

Table 2.4, shows the resistivity and conductivity measurements obtained for a range of sol-gels based on a standard 4.65 ml sol–gel (see 2.2.2) containing 1 – 5mg of NP-ITO. These results are graphically represented in Figures 2.16 and 2.17. The sol-gel compositions are identical to those used for shrinkage measurements in Table 2.2.

ITO in sol-gel (mg)	Conductivity (S/Sq)	Resistivity (Ω/Sq)
0	out of range	out of range
1	0.002	594
1.5	N/A	N/A
2	0.004	289.5
2.5	0.005	224.1
3	0.006	167.4
3.5	0.006	190.8
4	0.005	216.1
4.5	0.005	219.4
5	0.005	215.9

Table 2.4: Conductivity and resistance measurements for a range of NP-ITO encapsulating sol-gel monoliths using the Nagy SRM-12 contactless sheet conductivity meter, graphically represented in Figures 2.16 and 2.17 (**Note**: The sol-gel for 1.5mg of ITO was unavailable for testing due to a structural fault). [II]

[II] Siemens (symbolized S) are the Standard International (SI) unit of electrical conductance. Reduced to base SI units, 1 S is the equivalent of one second cubed ampere squared per kilogram per meter squared ($1\ s^3 \cdot A^2 \cdot kg^{-1} \cdot m^{-2}$).

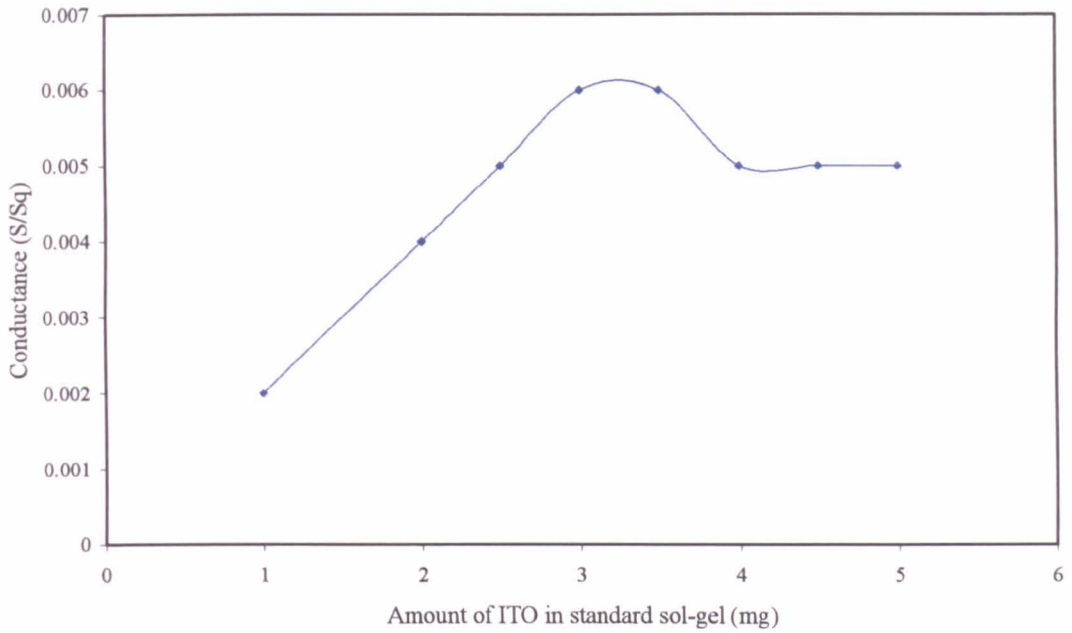

Figure 2.16: The effect of NP-ITO concentrations on the conduction properties of sol-gel monoliths fabricated using a standard 1cm pathlength polystyrene cuvette; see section 2.3.5 for compositional information.

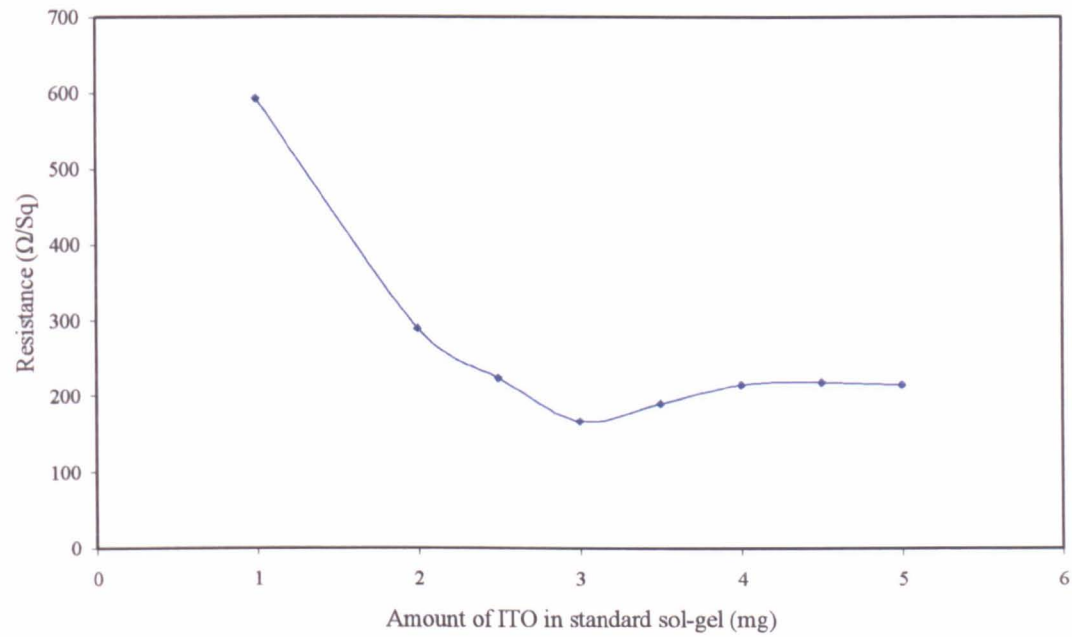

Figure 2.17: Graphical representation of the effect of NP-ITO concentration on the electrical resistance of a range of sol-gel monoliths.

As expected an increase in conduction generally occurs with a corresponding increase in ITO concentration, there is a slight dip at higher concentrations but the pattern is fairly clear. A corresponding decrease in resistivity is also understandably found with the increase in ITO concentration. To discuss the conduction properties of the sol-gels requires further examination of metal doped composite electrodes. There are a number of excellent reviews describing the conducting mechanisms of these electrodes including Tallman & Peterson [47] and Roldughin & Vysotskii [48]. As stated previously composite electrodes, like the ITO encapsulating sol-gels, are fabricated from a combination of conductor and insulator, and are classified based on the manner in which the conductor is distributed with the insulator, *i.e.* ordered or random & dispersed or consolidated.

The ITO sol-gels studied here are best described as randomly dispersed ensembles [47]; which according to Tallman and Peterson conduct in the following manner. If f represents the volume fraction of ITO in the sol-gel and σ the electrical conductance of the ITO encapsulating sol-gel; then an increase from f_0 (zero ITO) is accompanied by a gradual increase in σ. This increase is steady until $f = f_c$; f_c refers to the percolation threshold (much of this theory encompasses percolation theory) and can be considered as the minimum usable f value for a conductance. According to Roldughin and Vysotskii [48], the percolation threshold (f_c) corresponds to conducting bridges, created from either single or aggregated conducting particles, that interact to form infinite conducting clusters. From this point onwards the rise in conduction is less gradual and can be thought of as an increase in conduction bridges through the sol-gel, with the more routes resulting in better conductance and less resistance. This trend is clearly seen in Figures 2.16 and 2.17, where an increase in

ITO level results in a marked improvement in conduction properties. Percolation theory covers other factors that may influence conduction efficiency such as temperature. Temperature increases may cause the sol-gel matrix to expand effectively reducing ITO concentration in the matrix which subsequently reduces conduction.

One issue with the SRM-12 sheet resistivity meter was that it was designed to measure a 10 x 10 cm plate and not a sol-gel monolith with an area of approximately 1.5 x 0.7 cm. Comparison measurements were made using an ITO coated plate gradually reduced in size from 10 x 10cm to 2.5 x 2.5 cm to observe the effects (shown in Table 2.5). It was found that a reduction in sample size corresponded to a decrease in conduction, which is thought to be due to the system struggling to adapt to the reduced sample size.

Area of ITO coated glass plate (cm^2)	**Conductivity (S/Sq)**	**Resistivity (Ω/Sq)**
100	0.115	8.7
50	0.112	8.89
25	0.102	9.81
12.5	0.070	14.32
6.25	0.052	25.21

Table 2.5: Demonstrating the effects of decreasing sample size on conduction and resistance of a Pilkington Glass electro-conducting ITO glass sheet.

However the device was designed for sheets of conducting material and not bulk monoliths as was used in this work. Therefore the effects caused by the depth of the sol-gel monoliths should be considered when examining these results. It is felt that

although the sol-gel monolith should absorb more of the electric field due to the addition characteristic of depth, this effect is localised to the small area of the sample plate, with the remainder (approx. 95 %) being unobstructed. However if these sol-gel monoliths are thought of as pieces of copper wire; it would be expected that as the sample size increased the resistance reduce and conduction increase, as is the case with copper wires. However due to current fabrication techniques it is not possible to ascertain the level of this effect or more importantly if this hypothesis is correct. Though as shown in Table 2.5 it is possible to evaluate the effects of a reduction of surface area; although this is not a perfect solution to the problem of different sample characteristics it does give an indication to the shortcoming of this technique and provides a measure of theoretical adjustment.

As stated it is not possible to fabricate a sol-gel with the correct dimensions for analysis; and therefore this parameter must be taken into account when considering the results. The reduced ITO coated glass size resulted in a 45% decrease in conductance; if this percentage were transferred in reverse to the experimental results to obtain a theoretical conductance, the result would be as shown in Figure 2.18.

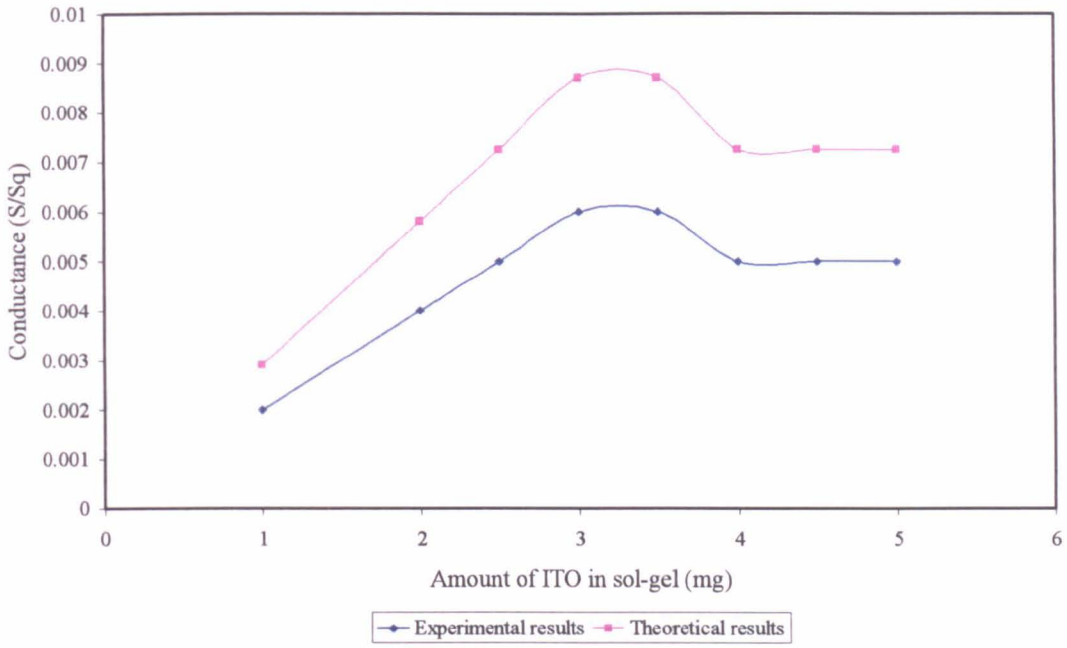

Figure 2.18: The comparison of experimental and theoretical resistance results through the extrapolation of data obtained in the study examining substrate dimension effects on observed resistance using the Nagy SRM-12 (see table 2.5).

Obviously this is all theoretical; the actual ITO encapsulating sol-gels demonstrated good electrical conductance when compared to the ITO coated glass (see table 2.5) and for the most part reasonable optical transparency, especially considering the pathlength of the sol-gel monoliths. In addition given the mild fabricating conditions of the sol-gel, this system provides the potential for secondary molecule encapsulation and excellent manufacturing freedom with regards structural configurations, as shown in Chapter 3 & 4. Furthermore, unlike the aggressive system used for coating ITO onto glass substrates, *i.e*. DC magnetron sputtering [49], thermal deposition and spray pyrolysis [50] this method does not require a 600 °C thermal annealing stage prior to use, which as already stated allows for the use of heat sensitive materials, such as proteins and enzymes.

2.3.8 Development of PEDOT dispersed sol-gels for the production of electro-conducting sol-gel materials

The following section examines the electro-conductance and optical transparency effects of PEDOT (poly(3,4-ethylenedioxythiophene)) encapsulation within sol-gel monoliths. As stated in 2.1.1, the PEDOT used for this work is doped with poly(styrene sulfonate) (PSS) in a PEDOT:PSS ratio of 1:6, allowing the formation of a water dispersed polymer complex. This complex was kindly donated by Professor Steve Kelly (University of Hull), although it was originally purchased from H.C. Starck (Leverkusen, Germany) under the trade name Baytron P.

PEDOT was added to standard sol-gel solutions (as previously fabricated, see section 2.2.2) in a range of concentrations as shown in Table 2.6, and then mixed by magnetic stirring until homogenous (approximately 10 s). This mixing could have been performed more rapidly; however it was important not to introduce air bubbles to the sol-gel solution as these would effectively become zones of non conductance. Phosphate buffer was subsequently added to these solutions to initiate the condensation reactions. A 3ml aliquot from each solution was pipetted into a standard 1cm pathlength polystyrene cuvette and covered in parafilm; and allowed to gel and age at room temperature. It is important to note that desiccators were not used for this stage as they may have promoted an increase in water evaporation that would lead to the sol-gel cracking or warping. Also note that as the PEDOT sample was donated, and that not all compositional details are known, therefore it is not possible to show definite concentrations in the sol-gel matrix. However the amounts of PEDOT solution used for the different sol-gels are shown in Table 2.6.

Sample	Total sol-gel volume in ml	PEDOT added in µl	Aliquot of sol-gel solution tested/ml
Blank	4.65	0	3
1	4.65	10	3
2	4.65	20	3
3	4.65	30	3
4	4.65	40	3
5	4.65	50	3

Table: 2.6: Showing volume of PEDOT solution added to each sol-gel sample.

As with the NP-ITO sol-gels, the optical transparency of the PEDOT sol-gel samples were establish using a Perkin Elmer Lambda BIO-10 UV/Vis spectrometer, scanning between 350 to 800 nm. Figure 2.19 compares the optical transmission results obtained when comparing the PEDOT encapsulated sol-gels as shown in Table 2.6. As with the NP-ITO, an increase in PEDOT within the sol-gel monolith decreases the optical transmission. Also, like the ITO sol-gels, PEDOT appears not to absorb in the wavelengths scanned, but to scatter the light. This can be attributed to the fact that the PEDOT solution is actually a dispersion of micro-particulate PEDOT/PSS particles. According to Kirchmeyer, a research scientist for H.C. Starck, the polymer does not exceed 1000-2500 Da, which equates to approximately 6-18 repeat units. It would appear that it is these repeat units that are causing the scatter that reduces the transmission of light through the sol-gel.

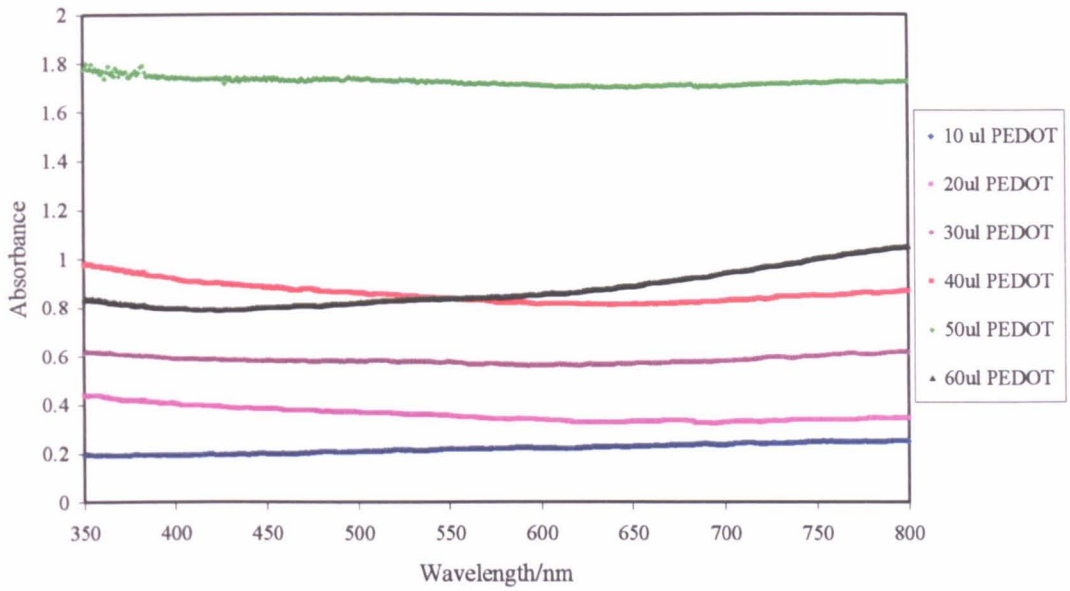

Figure 2.19: The effect of PEDOT concentration on the optical transparency of a range of sol-gel monoliths (the sol-gel monoliths are those discussed in Table 2.6).

Another observation with regard to Figure 2.19 is that the absorbance for the sol-gel encapsulating 50 µl of PEDOT appears to have a far greater absorbance than the 60 µl sol-gel. The reason for this is not clear although it is possibly that a water pocket within the sol-gel matrix has increased its opaqueness, a possible problem that has been discussed in section 2.3.3.

Following drying and curing, the electro-conductive properties of the sol-gels were tested, firstly the Jandel 4-point probe and then the NAGY SRM-12 sheet resistivity meter, as used in the previous section. As with the ITO sol-gels from the previous section a sol-gel blank was also tested for comparison.

However neither system was able to establish a level of electro-conduction on any of the PEDOT encapsulating sol-gels. The reason for this is not certain however there

are some possibilities; as discussed in section 2.1.1 one of the main issues when developing conducting polymers was their lack of stability. Although PEDOT is considered a stable conducting polymer, it is still possible that the conditions used for sol-gel fabrication, however mild, were too aggressive; leading to structural degradation or the formation of compromising side reactions. In addition if the polymer survived it is feasible that it was unable to pass the electrical charge down the polymer backbone due to sol-gel interactions; or that the PEDOT concentration was too weak. However as stated the reason for this lack of electro-conduction was not ascertained and given the success with the NP-ITO, further investigations were abandoned.

2.4. Conclusion

In this chapter novel transparent conducting sol-gels have been developed. Initial studies concentrated on ascertaining the most suitable methodology for developing the electro-conductive sol-gels. After investigations using various sol-gel types, configurations and substrate materials an acid catalysis based TMOS sol-gel system was used to prepare sol-gel monoliths within polystyrene cuvettes. This system allowed the fabrication of reproducible cuboid sol-gels without any cracking or warping that were easy to handle and analyse. It was deemed that the cuboid shape would allow for optical measurements to be taken (in the cuvette) with the flat sides also permitting easy application of conduction measurement probes

Two types of electro-active dopant were studied, poly(3,4-ethylenedioxythiophene) (PEDOT) and indium tin oxide (ITO). PEDOT was found to be unsuccessful with regards to the fabrication of electro-conductive sol-gels; although it showed good optical transparency at low levels; however due to the success with ITO, further studies were abandoned. With regard to ITO initial studies concentrated on testing four different types of ITO, two micro-particle size ITO samples and two nano-particle size ITO samples. Initial studies showed that the micro-particle sized ITO fell out of the sol-gel solution prior to gelation preventing homogeneity with in the sol-gel. In addition ICP-MS studies showed that one of the nano-particle sized ITO samples, purchased through Aldrich, also provided the optimum ratio between indium and tin and also remained in solution; so this was chosen for further studies.

With the knowledge established for developing the sol-gel monoliths coupled with the nano-particle ITO, it was possible to fabricate sol-gels containing varying

amounts of ITO dopant. Characterisation of these sol-gels showed them to be electro-conducting, whilst maintaining good optical transparency, especially when taking into account their future use as thin films electrode coatings. These results provide an opportunity to use this sol-gel system with electro-active light emitting systems as demonstrated in the following chapters

Another benefit of this system is that the conductive sol-gels are cheap to make and easy to characterise and can be fabricated into various configurations, such as thin films, powders, fibres and monoliths. In addition due to the mild conditions used for production, sensing molecules can be added to the sol-gel matrix, such as electro-active dyes and enzymes, as discussed in Chapter 1.

2.5 References

1. Bakul, D.C., Dunn B., Selverstone-Valentine J., and Zink J.I., *Sol-gel encapsulation methods for biosensors.* Analytical Chemistry, 1994. **66**(22): p. 1120A - 1127A.
2. Schottner, G., *Hybrid sol-gel derived polymers: Applications of multifunctional materials.* Chemistry of Materials, 2001. **13**: p. 3422-3435.
3. Walcarius, A., *Electrochemical applications of silica based organic-inorganic hybrid materials.* Chemistry of Materials, 2001. **13**: p. 3351-3372.
4. Buck, S.M., Koo Y.L., Park E., Xu H., Philbert M.A., Brasuel M., and Kopelman R., *Optochemical nanosensor PEBBLEs: Photonic explorers for bioanalysis with biologically localized embedding.* Current Opinion in Chemical Biology, 2004. **8**: p. 540-546.
5. Mehrotra, V., Keddie J.L., Miller J.M., and Giannelis E.P., *Electrically conducting glasses: Incorporation of polypyrrole in a porous SiO_2 matrix.* Journal of Non-crystalline solids, 1991. **136**: p. 97-102.
6. Salimi, A. and Pourbeyram A., *Renewable sol-gel carbon ceramic electrodes modified with a Ru-complex for the amperometric detection of L-cysteine and glutathione.* Talanta, 2003. **60**: p. 205-214.
7. Shankaran, D.R., Uehara N., and Kato T., *Sol-gel derived metal dispersed ceramic-graphite composite electrode for amperometric determination of dopamine.* Analytica Chimica Acta, 2003. **478**: p. 321-327.
8. Bharathi, S. and Lev O., *Sol-gel derived nanocrystalline gold-silicate composite biosensor.* Analytical Communications, 1998. **35**: p. 29-31.
9. Li, H., Li T., and Wang E., *Electrocatalytic oxidation and flow detection of cysteine at an aquocobalamin adsorbed glassy carbon electrode.* Talanta, 1995. **42**: p. 885-890.
10. Popovic, N.D., Cox J.A., and Johnson D.C., *Electrocatalytic function of Bi (V) sites in heavily doped PbO_2-film electrodes applied for the anodic detection of selected sulfur compounds.* Journal of Electroanalytical Chemistry, 1998. **455**(1-2): p. 153-160.
11. Alam, M.J. and Cameron D.C., *Optical and electrical properties of transparent conductive ITO thin films deposited by sol-gel process.* Thin solid films, 2000. **00**: p. 455-459.
12. Gao, Z., Gao Y., Li Y., and Li Y., *Effects of heat treatment on the microstructure of nanophase indium tin oxide.* NanoStructured Materials, 1999. **11**(5): p. 611-616.
13. Bergman, I., *Rapid-response atmospheric oxygen monitor based on fluorescence quenching.* Nature, 1968. **218**: p. 396.
14. Castellano, F.N. and Lakowicz J.R., *A water soluble luminescence oxygen sensor.* Photochemistry and Photobiology, 1998. **67**(2): p. 179-183.
15. McNamara, K.P. and Rosenzweig Z., *Dye-encapsulated liposomes as fluorescence-based oxygen nanosensors.* Analytical Chemistry, 1998. **70**: p. 4853-4859.
16. Xu, H., Aylott J.W., Kopelman R., Miller T.J., and Philbert M.A., *A real-time ratiometric method for the determination of molecular oxygen inside living cells using sol-gel based spherical optical nanosensors with applications to rat C6 glioma.* Analytical Chemistry, 2001. **73**(17): p. 4124-4133.

17. Heeger, A.J., *Semiconducting and metallic polymers: The fourth generation of polymeric materials (Nobel Lecture).* Angew. Chem. Int., 2001. **40**: p. 2591-2611.
18. Shirakawa, H., Louis E.J., MacDiarmid A.G., Chiang C.K., and Heeger A.J., *Synthesis of electrically conducting organic polymers - Halogen derivatives of polyacetylene, (CH)X.* Chemical communications, 1977. **16**: p. 578-580.
19. Natta, G. *From the Stereospecific Polymerization to the Asymmetric Autocatalytic Synthesis of Macromolecules.* in *Nobel lecture in chemistry.* 1963: Elsevier Publishing Company.
20. Chiang, C.K., Fincher J., C.R., Park Y.W., Heeger A.J., Shirakawa H., and Louis E.J., *Electrical-conductivity in doped polyacetylene.* Physics Review Letters, 1977. **39**(17): p. 1098-1101.
21. Kirchmeyer, S. and Reuter K., *Scientific importance, properties and growing applications of poly(3,4-ethylenedioxthiophene).* Journal of Materials Chemistry, 2005. **15**: p. 2077-2088.
22. Friend, R.H., Gymer R.W., Holmes A.B., Burroughes J.H., Marks R.N., Taliani C., Bradley D.D.C., Dos Santos D.A., Bredas J.L., Logdlund M., and Salaneck W.R., *Electroluminescence in conjugated polymers.* Nature, 1999. **397**: p. 121-128.
23. Book, K., Bassler H., Elschner A., and Kirchmeyer S., *Hole injection from an ITO/PEDT anode into the hole transporting layer of an OLED probed by bias induced absorption.* Organic Electronics, 2003. **4**: p. 227-232.
24. Pettersson, L.A.A., Carlsson F., Inganas O., and Arwin H., *Spectroscopic ellipsometry studies of the optical properties of doped poly(3,4-ethylenedioxythiophene): an anisotropic metal.* Thin solid films, 1998. **313-314**: p. 356-361.
25. Heuer, H.W., Wehrmann R., and Kirchmeyer S., *Electrochromic windows based on conducting poly(3,4-ethylenedioxythiophene)-poly(styrene sulfonate).* Advanced Functional Materials, 2002. **12**(2): p. 89-94.
26. Ballarin, B., Fraleoni-Morgera A., Frascaro D., Marazzita S., Piana C., and Setti L., *Thermal inkjet microdeposition of PEDOT:PSS on ITO ocated glass and characterization of the obtained film.* Synthetic Metals, 2004. **146**: p. 201-205.
27. Gerard, M., Chaubey A., and Malhotra B.D., *Applications of conducting polymers in biosensors.* Biosensors and Bioelectronics, 2002. **17**: p. 345-359.
28. Kim, D.W., Oh S.G., and Lee J.D., *Preparation of ultrafine monodispersed indium tin oxide particles in AOT-based reverse microemulsions as nanoreactors.* Langmuir, 1999. **15**: p. 1599-1603.
29. Greenwood, P.A., *Private communication.* 2001, University of Hull.
30. Frank, G. and Kostlin H., *Electrical properties and defect model of tin-doped indium oxide layers.* Applied Physics A, 1982. **27**: p. 197-206.
31. Fletcher, P.D.I., Howe A.M., and Robinson B.H., *The kinetics of solubilsate exchange between water droplets of a water in oil microemulsion.* Journal of Chemistry Society: Faraday Transcripts 1, 1987. **83**: p. 985-1006.
32. Aelion, R., Loebel A., and Eirichh F., *Hydrolysis of Ethyl silicate.* Journal of the American Chemical Society, 1950. **72**: p. 5705-5712.
33. Brinker, C.J. and Scherer G.W., *Sol-gel science - The physics and chemistry of sol-gel processing.* 1990: Academic press.

34. Zarzycki, J., Prassas M., and Phalippou J., *Synthesis of glasses from gels: The problem of monolithic gels.* Journal of Materials Science, 1982. **17**: p. 3371-3379.
35. Allain, L.R., Sorasaenee K., and Xue Z., *Doped thin-film sensors via a sol-gel process for high acidity determination.* Analytical Chemistry, 1997. **69**: p. 3076-3080.
36. Li, J., Chia L.S., Goh N.K., Tan S.N., and Ge H., *Mediated amperometric glucose sensor modified by the sol-gel method.* Sensors and Actuators B, 1997. **40**: p. 135-141.
37. Simpkins, P.G., *Drying behaviour of colloidal silica-gels.* Journal of the American Ceramics Society, 1989. **72**(10): p. 1816-1821.
38. Zarzycki, J., *Past and present of sol-gel science and technology.* Journal of Sol-gel Science and Technology, 1997. **8**: p. 17-22.
39. Goebbert, C., Nionninger R., Aegerter M.A., and Schmidt H., *Wet chemical deposition of ATO and ITO coatings using crystalline nanoparticles redispersable in solution.* Thin solid films, 1999. **351**: p. 79-84.
40. Collinson, M.M., Wang H., Makote R., and Khramov A.N., *The effects of drying time and relative humidity on the stability of sol-gel derived silicate films in solution.* Journal of Electroanalytical Chemistry, 2002. **519**: p. 65-71.
41. Sacks, M.D. and Sheu R.S., *Rheological properties of silica sol-gel materials.* Journal of Non-crystalline solids, 1987. **92**: p. 383-396.
42. Yorkov, G.Y., Kozinkin A.V., Nedoseikina T.I., Shuvaev A.T., Vlasenko V.G., Gubin S.P., and Kosobudskii I.D., *Copper nanoparticles in a polyethylene matrix.* Inorganic materials, 2001. **37**(10): p. 997-1001.
43. Niedziolka, J. and Opallo M., *Electrochemical redox reaction at silicate based electrode-silicate based electrolyte interface.* Electrochemistry Communications, 2003. **5**: p. 924-928.
44. Epifani, M., Carlino E., Blasi C., Giannini C., Tapfer L., and Vasanelli L., *Sol-gel processing of Au nanoparticles in bulk 10% B_2O_3 - SiO_2 glass.* Chemical materials, 2001. **13**: p. 1533-1539.
45. You, T., Niwa O., Tomita M., and Hirono S., *Characterization of platinum nanoparticle-embedded carbon film electrode and its detection of hydrogen peroxide.* Analytical Chemistry, 2003: p. A-F.
46. Weisshaar, D.E. and Tallman D.E., *Chronoamperometric response at carbon based composite electrodes.* Analytical Chemistry, 1983. **55**: p. 1141-1151.
47. Tallman, D.E. and Petersen S.L., *Composite electrodes for electroanalysis: Principles and Applications.* Electroanalysis, 1990. **2**: p. 499-510.
48. Roldughin, V.I. and Vysotskii V.V., *Percolation properties of metal-filled polymer films, structure and mechanisms of conductivity.* Progress in Organic Coatings, 2000. **39**: p. 81-100.
49. Nishimura, E., Ohkawa H., Song P.K., and Shigesato Y., *Microstructures of ITO films deposited by DC magnetron sputtering with H_20 introduction.* Thin solid films, 2003. **445**: p. 235-240.
50. Vasu, V. and Subrahhmanyam A., *Phtovoltic properties of indium tin oxide (ITO)/silicon junctions prepared by spray pyrolysis- dependence on oxidation time.* Semiconductor Science and Technology, 1992. **7**: p. 320-323.

Chapter 3 – The analysis of drugs of abuse through electro-generated chemiluminescence

3.0 Aims of chapter

The aim of this work was to investigate the application of the novel conducting sol-gels for the analysis of drugs of abuse using electro-generated chemiluminescence (ECL). Specifically to develop a reliable, selective, cheap, field portable system that could be used in a "point of attack/use" situation.

The problems encountered, particularly with regard sol-gel adhesion to the electrode surface and reproducibility are discussed. The effects and benefits of the sol-gel and sol-gel/ITO coatings on the generation of ECL are compared with the results obtained from a non-coated electrode are discussed.

3.1 Introduction

3.1.1 Novel sol-gel electrode coatings

In Chapter 2 the optical and electro-conducting properties of a novel indium tin oxide (ITO) doped sol-gel monolith were discussed. Where it was found that by doping the sol-gel with ITO it was possible to produce a porous glass-like polymer with electro-conducting properties and acceptable optical transparency. Due to a sol-gel's mild manufacturing conditions, porous nature and ability to encapsulate dopants, it was apparent that this conducting sol-gel could be used as a sensor platform.

In this following chapter, the application of this material as an electrode coating is investigated, with comparison studies being performed on bare electrodes, non doped sol-gel coated electrodes and ITO doped sol-gel coated electrodes. These studies are performed against the backdrop of drug analysis using an electro-generated chemiluminescent technique. This technique is based on the reaction between

tris(2,2'-bipyridyl)ruthenium(II) dichloride hexahydrate ($Ru(bpy)_3^{2+}$) and the tertiary amine containing drugs of abuse investigated in this work. This is a well established reaction that is discussed in greater detail in sections 1.4.2.4 and 3.1.2. This section will demonstrate the advantages of using both an undoped and doped sol-gel coating, in terms of both electrode protection and also ECL signal enhancement in addition to theorising about the conduction mechanisms within the sol-gel.

3.1.2 An introduction to the drugs of abuse analysed in this work

As previously mentioned drugs of abuse (specifically atropine and codeine) are analysed in this work through the application of an ECL technique using a novel sol-gel electrode coating. These compounds were chosen as the "drugs of abuse" as they are well researched and understood and are structurally similar to other more hazardous and difficult to obtain drugs (shown in Figure 3.1) such as morphine, cocaine and heroin due to the presence of their common tertiary amine group. However tertiary amine compounds also have other uses apart from pharmaceuticals including pesticides and surfactants, so a sensitive analytical method for their detection is obviously desirable.

The compounds shown in Figure 3.1 come from one of three separate classes of compounds, the first class, the indole alkaloids includes lysergic acid (LSD is the *N,N*-diethylamide of this compound) and serotonin. Others compounds in this group include psilocine (the psychoactive ingredient in magic mushrooms) and bufotenin (the psychoactive ingredient in cahobe beans). Serotonin is included in this group as it is an essential neurotransmitter in the central nervous system (CNS), and is the compound that the other indole alkaloids listed mimic due to their structural

similarities; thus causing the ill effects such as mental problems (schizophrenia) and hallucinations [1] associated with the compounds.

The second type of compound is the tropane alkaloids, which contain the structurally similar compounds cocaine and atropine. Cocaine is a stimulant of the central nervous system and also a local anaesthetic, it is naturally obtained from the leaves of the coco plant. In many cultures the leaves are used as used as both a pain killer and an appetite suppresser where they are smoked or chewed to release the active complex. An example of such a culture is the agricultural workers in rural Peru, who use these techniques when working to alleviate hunger, exhaustion and simple ailments such as toothache. However cocaine is toxic, addictive and may disrupt the rhythm of the heart.

Atropine, which is used extensively in this work also has a dubious history. It is derived from black henbane (*Hyoscyami folium)* and the berries of deadly nightshade (*Atropa belladonna*) and has historically been used as a poison and a pupil dilating agent. Historically Spanish and Italian aristocratic ladies used atropine in order to dilate their pupils in an attempt to make them more alluring; *belladonna* is a derivation of beautiful lady in both languages. Its medical uses include being an agent to dilute the pupils in order to perform eye examinations and to relax the smooth muscles and thereby ease intestinal and bronchial spasms. It is also very useful as an antidote to organophosphate nerve agents, examples of which include Tabun (*O*-ethyldimethylamido-phosphorylcyanide) the worlds first nerve agents developed at IG Farben, Germany in 1936; Sarin (isopropyl methylphosphonofluoridate) developed at IG Farben, Germany in 1938 and VX (*O*-

ethyl *S*-diisopropylaminomethyl methylphosphonothiolate) developed in the UK in 1952 [2].

The third type of compound is the isoquinoline alkaloids, which contain the structurally similar morphine, codeine and heroin which are derived from the unripened seed pods of the opium poppy (*Papaver somniferum*). Morphine and codeine are naturally present although codeine is only normally present in small amounts so is usually synthesised from morphine; heroin however is not found naturally and is produced by a synthetic diacetylation of morphine. Codeine, which is also used extensively in this work is a methyl ethyl ether of morphine, and like morphine is a painkiller and is also often used as a cough suppressant and as an analgesic. It is commonly used in combination with other pharmaceutical pain killers such as paracetamol, ibuprofen and aspirin where it is easily absorbed through the gastrointestinal tract. However to generate pain relief the human body must convert the codeine to morphine using the enzyme cytochrome P4502D6, which typically has a 10% conversion rate [3].

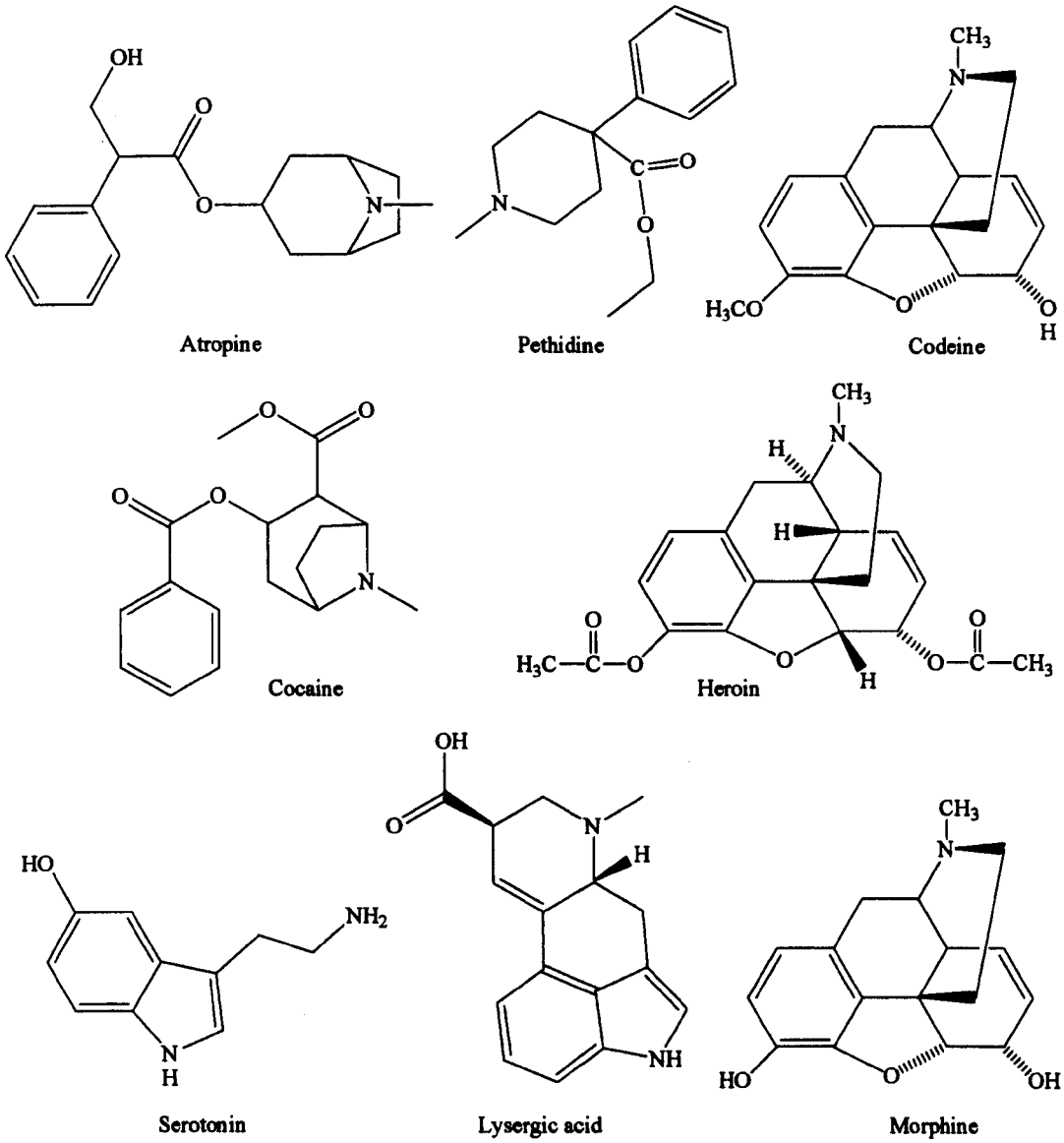

Figure 3.1: Molecular structures of a range of alkaloids, as discussed in 3.1.

These compounds are typically analysed using the following methods GCMS [4-8], HPLC-UV, HPLC-MS and SERS [9-12], both electro-generated chemiluminescence and chemiluminescence [13-17], LC-MS [18] ion pair liquid chromatography [19], spectrophotometry [20] and immunoassays [21]. Specific methods for atropine analysis also include an atropine selective electrode with a PVC membrane [22] and bulk acoustic wave sensing [23].

As part of this work the analysis of flunitrazepam was investigated; an anxiolytic and hypnotic drug better know under the trade name Rohypnol which is usually administered as a short term treatment for sleeping disorders such as insomnia [24]. In addition to its appropriate prescribed use, Rohypnol also has an illegal and immoral use, in this instance as a "date rape" drug. This illegal use typically takes place in pubs and clubs were the compound is "spiked" into the drinks of its unwary victims. This problem has become such a social issue that the manufacturers of the drug (Roche) have recently started adding a food colouring to the tablets in an attempt to stop the attacks through the dying of victim's drinks; however recent reports in the media suggest that this hasn't been entirely successful.

Currently the two main drugs used in drug facilitated sexual assault (date rape) are Rohypnol and GHB (gamma-hydroxybutyric acid) [25-27], the molecular structures of which are shown in Figure 3.2.

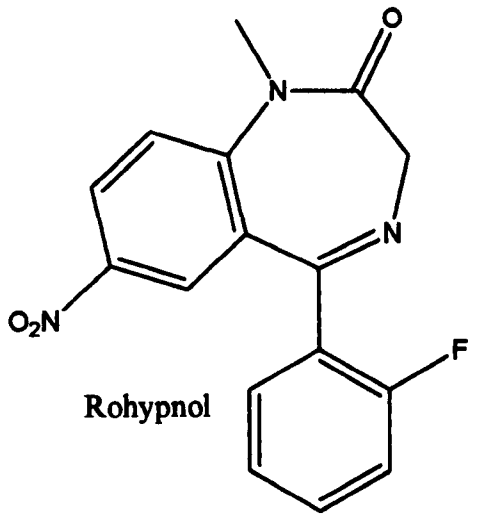

Rohypnol

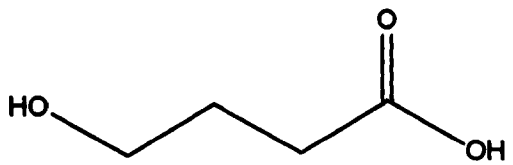

4-Hydroxy-butyric acid
(Gamma-hydoxybutyric acid (GHB))

Figure 3.2: Molecular structures for Rohypnol and GHB.

Rohypnol (flunitrazepam), is generally spiked into alcoholic drinks above the recommended pharmacological dose of 0.5-1 mg in adults [24] to produce a

prolonged and extreme intoxication. Alcohol increases the sedative effect of the drug which creates a marked psychomotor impairment and causes the victim to suffer from a "blackout", a type of short term amnesia that prevents the victim from recalling much if not all of the attack. Typically the symptoms begin approximately half an hour after ingestion and peak after approximately two hours, however the effects of the drug may be felt the following day and include drowsiness, light-headedness, confusion and ataxia (lack of muscle coordination).

Rohypnol, a benzodiazepine, is typically analysed using immunoassays or GC-MS [26, 28] methodologies involving blood/serum and urine analysis, although oral fluid analysis has also been performed [26]. Its analysis is problematic given its low dosage and high biotransformation. Wang [27] found that typical benzodiazepine immunoassays have a broad cross reactivity towards widely prescribed benzodiazepines. This results from sharing a common metabolite target, oxazepam, which is commonly biotransformed in benzodiazepine type drugs and leads to an unacceptable number of false positives. With regards to Rohypnol specific immunoassays, Wang found that due to the low dosage of the drug these systems lead to an unacceptable number of false negatives.

With regards to GC-MS analysis, a number of studies have attempted to analyse flunitrazepam or its major metabolite 7-aminoflunitrazepam in blood urine, saliva and hair [26-28]. As with immunoassays, the problem with the analysis of Rohypnol in biological samples using GC-MS is one of low dosage and high distribution. For example, Samyn *et al.* [26], using saliva samples taken over a period of seven hours from subjects who had been administered a 1 mg dose of Rohypnol had great

difficulty in obtaining analytically significant results. Samyn's initial study evaluating the level of flunitrazepam in saliva samples after 48-72 hours of storage were unsuccessful and none of the ten samples taken provided a result above the limit of detection (LOD). The subsequent analysis of the metabolite 7-aminoflunitrazepam after derivatisation, although not perfect did provide results with an LOD found to be 0.25 μg/L. According to Samyn, this would allow for the detection of the metabolite in an oral sample up to six hours after the ingestion of a 0.5-2 mg dose. The method was developed to test drivers "driving under the influence". In the case of drug facilitated sexual assault it is probable that given the confusion and disorientation associated with this type of attack, many victims would not seek medical/legal support until many hours after the attack.

As can be seen in Figure 3.2, Rohypnol has a tertiary amine containing structure and therefore may exhibit ECL like codeine and atropine (discussed in section 3.2.1). The structure of GHB made this compound unsuitable for this analysis using this technique.

3.2 Experimental

3.2.1 Design of instrumentation

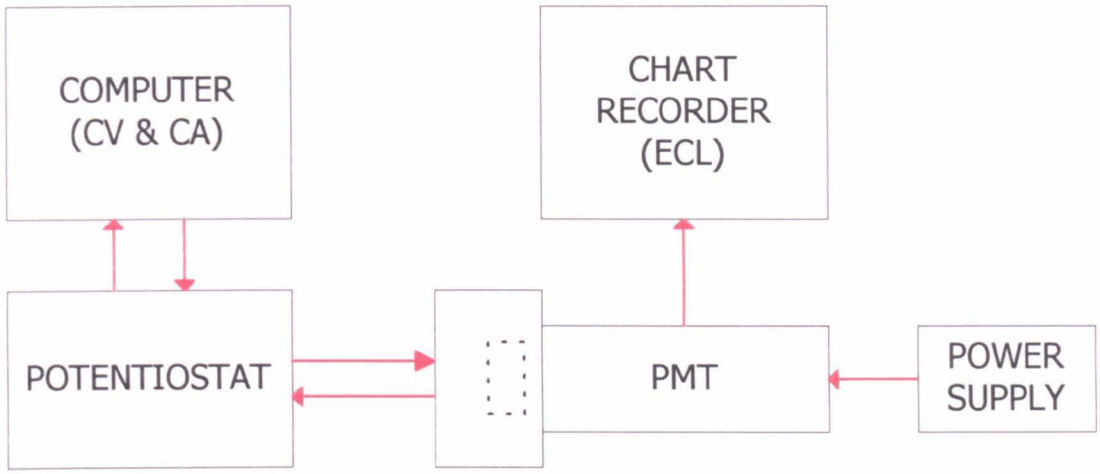

Figure 3.3: Schematic of ECL instrumentation used.

The experimental set-up for this work (shown in Figure 3.3) consisted of a photo-multiplier tube (PMT) holder that encased the PMT, electrodes and the sample vial. The PMT holder (Figure 3.4) was designed and built in-house and is essentially two separate sections, a sample chamber and the PMT holder. The sample chamber is the wider of the two sections and incorporates a zero-aperture iris diaphragm with a 57mm internal diameter (Edmund Optics Ltd, York, UK) allowing access to the sample chamber in lit environments. The diaphragm is protected from liquid spillages by a quartz glass shield that was fabricated in house.

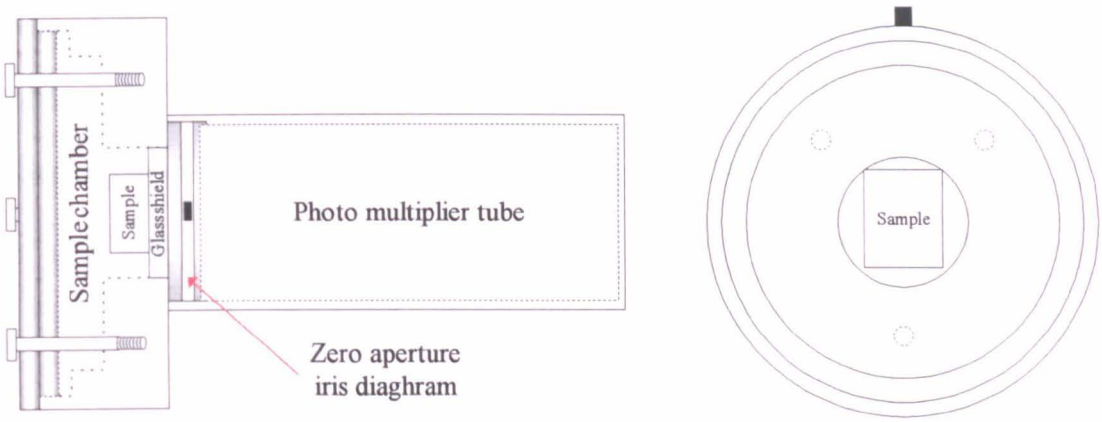

Figure 3.4: Schematic of Photo multiplier tube holder.

The sample chamber which houses the sample cuvette was designed in house and manufactured from quartz glass, as shown in Figure 3.5. The electrodes are placed within the cuvette which has dimensions of 26.5 x 50 x 15 mm.

The second section houses the photo multiplier tube (PMT), a type 9789QA (Thorn EMI, Ruislip, UK). The PMT is in turn attached to a power supply and a chart recorder *via* coaxial cables. The power supply for the PMT was a Thorn EMI model 3000R high voltage power supply (Thorn EMI, New York) running at 600 V.

The chart recorder used to quantify the PMT signal was a Chessell BD40-04, (Kipp and Zonen, The Netherlands) where the emission intensity was recorded on a mV scale.

The potentiostat used to generate the electrical potential for this work was an Eco Chemie μAutolab II system controlled by GPES software (Windsor Scientific Ltd, Slough, UK). The potential was applied to a three electrode system comprising of a 1mm diameter, type II glassy carbon rod working electrode, 0.762mm diameter platinum wire counter electrode and a 1mm diameter silver wire reference electrode; all electrodes were supplied by Alfa Aesar, Karlsruhe, Germany for some

experiments a 0.762 mm platinum working electrode was used. The electrodes were held using 5amp strip connecters which were connected to the potentiostat *via* banana plugs both supplied through RS components, Corby, UK.

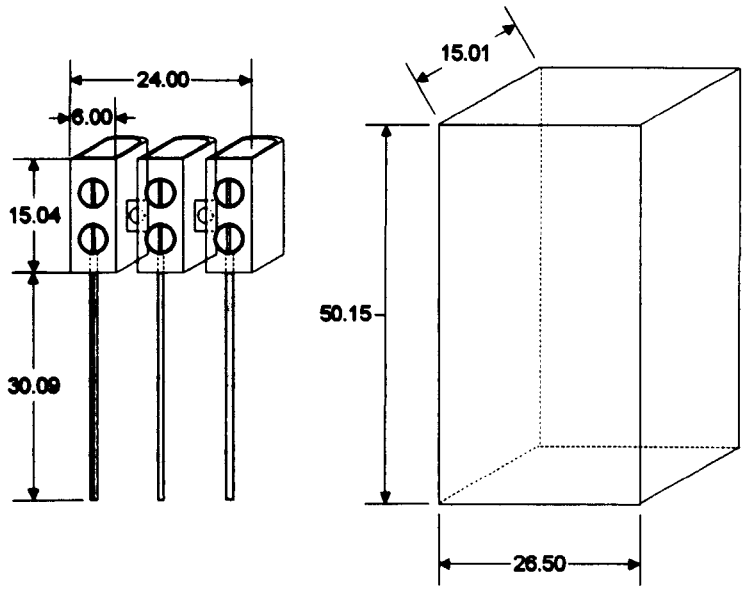

Figure 3.5: Schematic of Electrode set-up and cuvette (dimensions in mm).

3.2.2 Experiment reagents

The experiments discussed in this chapter can be separated into two main areas; the analysis of atropine and the analysis of codeine, using the electro-generated chemiluminescence reaction of tris(2,2'-bipyridyl)ruthenium(II) dichloride hexahydrate. Each of these can be further subdivided into the use of blank electrodes, sol-gel coated electrodes and sol-gel/ITO coated electrodes. A separate section involving the analysis of flunitrazepam (Rohypnol) will be discussed in greater detail later.

The reagents used during these experiments were all analytical grade unless otherwise stated and the water was high purity de-ionised (18 MΩ cm^{-1} resistivity) produced by an Elga Elgastat UHQ PS (High Wycombe, UK). Buffer solutions were adjusted using a Hanna instruments PHM2254 pH meter (Hanna Instruments, Kings Langley, UK) which was calibrated prior to use using pH 3, 7 and 9 pH buffer solutions provided by Aldrich (Gillingham, UK). The reagents used are as follows.

Sol-gel fabrication: -

The sol-gel gel solution was prepared by the acid catalysed sol-gel route (see Figure 1.10) where tetramethoxysilane (TMOS), water and 0.1 M hydrochloric acid was mixed in an 8:5:0.25 ratio. The tetraethoxysilane (99+ %) was obtained from Aldrich (Gillingham, UK), the hydrochloric acid was obtained from Fisher Chemicals (Loughborough, UK). Where appropriate, 1mg of nano-particle ITO (Aldrich, Gillingham, UK) was added to a 2.65 ml aliquot of the sol-gel solution and mixed under stirring for 10 minutes to allow both homogeneous mixing and hydrolysis of the sol-gel solution, and then left (covered) for at least a further hour.

On completion of dip coating (see section 3.2.3 for procedure) the electrodes were stored overnight in pH 6.4 (0.1 M) phosphate buffer; this buffer was produced using sodium dihydrogen orthophosphate and disodium hydrogen orthophosphate, both supplied by Fisher Chemicals, Loughborough, UK.

Atropine solution: -

The atropine solution was prepared using a method based on that proposed by Song *et al.* [29] with a pH 11 (0.1 M) borate buffer (unless otherwise stated). The atropine was obtained from Aldrich (Gillingham, UK) and the borate buffer solution was

made using boric acid (Fisher Chemicals, Loughborough, UK) and sodium hydroxide (Fisher Chemicals, Loughborough, UK).

Codeine solution: -

The codeine solution was made using a pH 4 (0.05 M) acetate buffer (unless otherwise stated) as demonstrated by Greenway *et al.* [30]. The codeine was obtained from Aldrich (Gillingham, UK) and the acetate buffer solution was made using acetic acid and sodium acetate both supplied *via* Fisher Chemicals (Loughborough, UK).

Flunitrazepam (Rohypnol) solution: -

The flunitrazepam solution was initially made using a pH 6.4 (0.1 M) phosphate buffer however this proved unsatisfactory as will be discussed in section 3.3.5. The Flunitrazepam was obtained from Aldrich (Gillingham, UK) the buffer was produced using sodium dihydrogen orthophosphate and disodium hydrogen orthophosphate (both, Fisher Chemicals, Loughborough, UK). It was also later prepared in an ethanol/buffer mix, with the ethanol obtained from Fisher Chemicals, Loughborough, UK.

3.2.3 Dip coating procedure

Glassy carbon electrodes were used for the sol-gel coating work. Two separate types of sol-gel solution were used; a blank sol-gel and one containing ITO (see section 3.2.2). After at least one hour after the preparation of the sol-gel the working electrode was dip coated in the sol-gel solution and allowed to age in a pH 6.4

phosphate buffer solution overnight. If the solution contained ITO then it was initially mixed again under stirring to allow for thorough mixing before coating

With regards to the dip coating (see Figure 3.6) the working electrode was withdrawn from the sol-gel manually with a withdrawal rate of approximately 5cm/min leaving a thin sol-gel coating on the electrode's surface. During this process small amounts of water and methanol are evaporated from the surface as the sol-gel continues to hydrolyse and condense (for more information see section 1.2.3). According to literature this process typically produces a film thickness of less than 1 μm [31].

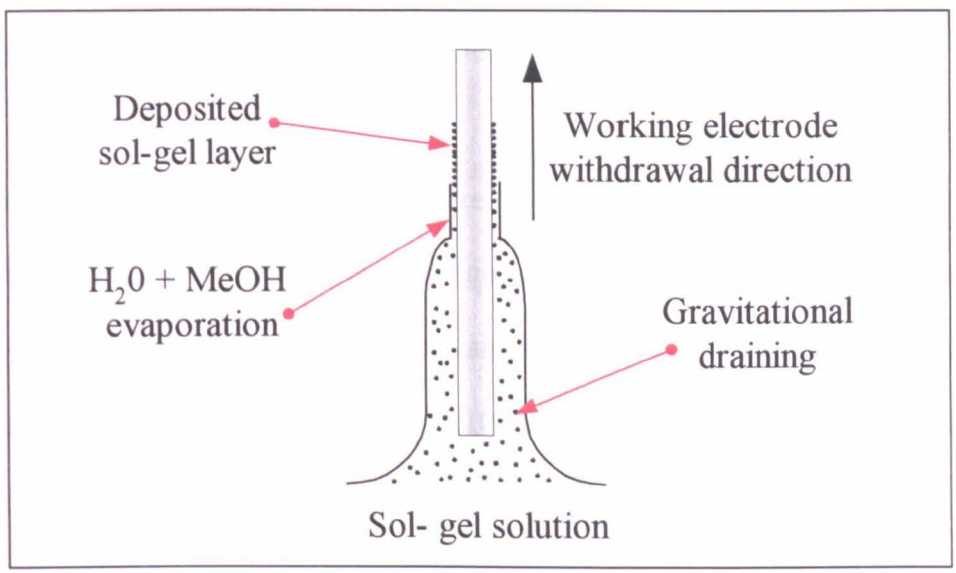

Figure 3.6: Illustration of dip coating.

3.3 Results and Discussion

In this chapter the benefits of coating the working electrode with either a sol-gel or sol-gel/ITO material for the electro-generated chemiluminescent detection of codeine and atropine are investigated.

3.3.1 Electrode control and potential levels

Throughout this work the electrode potential was controlled by the Eco Chemie μAutolab II computer controlled system as discussed in section 3.2.1. The potential levels were initially established using cyclic voltammetry from settings based on literature studies [29, 30], with subsequent calibrations being performed using pulsed chronoamperometry. Both platinum and carbon electrodes were investigated. This study of applied voltage was initially carried out on carbon electrodes.

With regards to cyclic voltammetry different scan rates were analysed and correlated against the ECL signal as shown in Figures 3.7 & 3.8. The scans were used in evaluating the correct setting for the potentiostat in order to develop the maximum sensitivity. The solutions tested were $1x10^{-3}$M $Ru(bpy)_3^{2+}$ and $1x10^{-4}$ M Codeine in pH 4 (0.05 M) acetate buffer.

As can be seen the best scan rate at this concentration of codeine was 0.25 V/s as this provided the maximum ECL signal. However it was decided to choose a lower scan rate that would allow multiple scans at lower concentrations without the signal reducing effects of analyte diffusion. This is a particular problem at lower analyte concentrations where the analyte cannot diffuse to the electrode from the bulk solution before subsequent scans, a property also found by Collinson *et al.* [32].

However, typical of such experiments the scan rate is of little importance as cyclic voltammetry is used to determine the potential at which the maximum cathodic current occurs, which as can be seen in Figure 3.7 doesn't change between scans. Pulsed chronoamperometry was used for subsequent analysis as it is less affected by the rate of diffusion of the analyte [33]. This is because unlike cyclic voltammetry that uses analyte up as the potential is ramped over a defined range (for example 0.7 – 1.3 V), chronoamperometry is pulsed at the maximum cathodic current previously established with cyclic voltammetry, this eliminates loss of analyte in build up potentials. A consequence of this technique is that higher maximum currents are generally produced which in turn leads to higher ECL signals. This effect is also demonstrated using different scan rates as shown in Figures 3.7 and 3.8. With rapid scan rates, less analyte is used up in the build up phase, which leaves more analyte which allows a higher ECL response.

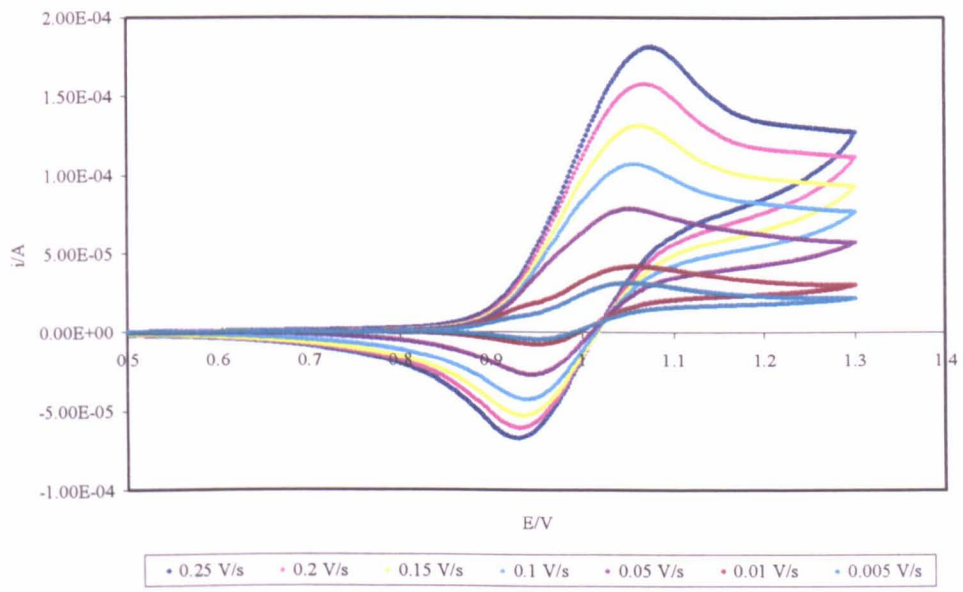

Figure 3.7: Cyclic voltammograms obtained from a scan rate analysis of 1x10-3 M Ru(bpy) and 1x10-4 M codeine in a pH4 (0.05 M) acetate buffer solution using a step potential of 0.0025 V.

A further effect of the increase in scan rate shown in Figure 3.7 is demonstrated in the form of a gradual peak shift in the applied potential; thus suggesting that at the higher scan rates some of the efficiency of this reaction is lost.

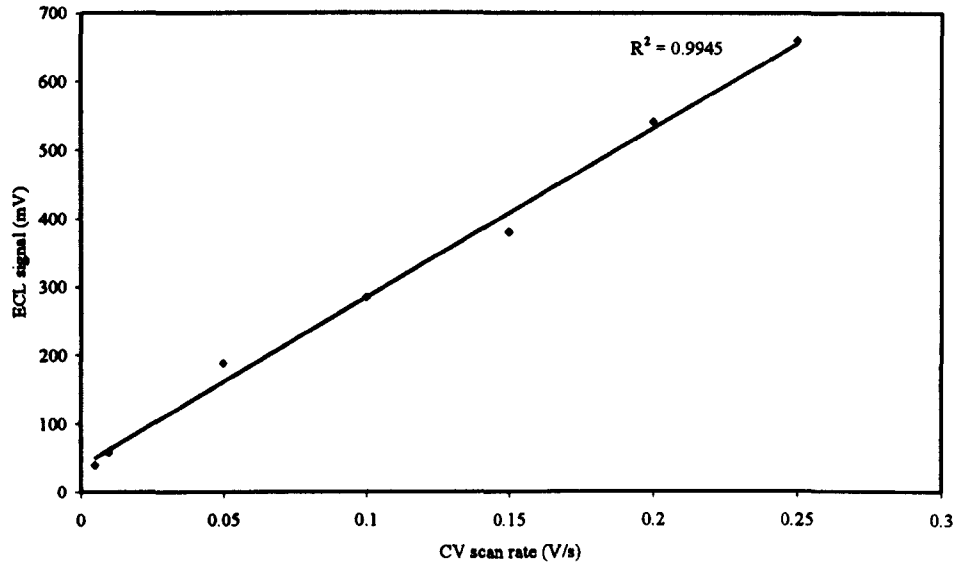

Figure 3.8: The ECL signal obtained for the codeine/$Ru(bpy)_3^{2+}$ scan rate analysis shown in Figure 3.7, with the data referring to signal peak height and not signal area).

Unless otherwise stated the voltage setting parameters for the ECL analysis of atropine, codeine and to a lesser extent Rohypnol using cyclic voltammetry and chronoamperometry are shown in Tables 3.1 and 3.2: -

	Analytes		
CV parameter	**$Ru(bpy)_3^{2+}$/Atropine**	**$Ru(bpy)_3^{2+}$/Codeine**	**$Ru(bpy)_3^{2+}$/Rohypnol**
Standby potential	0 V	0 V	0 V
First potential	0.5 V	0.7 V	0.7 V
Second potential	1.15 V	1.3 V	1.5 V
Step potential	0.0024 V	0.0024 V	0.0024 V
Scan rate	0.01 V/s	0.01 V/s	0.01 V/s

Table 3.1: Cyclic voltammetry parameters for the analysis of atropine, codeine and Rohypnol using bare carbon electrode.

	Atropine			Codeine	
Step	**Potential/V**	**Time/s**		**Potential/V**	**Time/s**
1	0	1.5		0	1.5
2	1.15	1		1.08	1
3	-1	2.5		-1	2.5
4	0	60		0	105
5	1.15	1		1.08	1
6	-1	2.5		-1	2.5
7	0	60		0	105
8	1.15	1		1.08	1
9	-1	2.5		-1	2.5
10	0	10		0	10

Table 3.2: Chronoamperometry parameters for the analysis of atropine and codeine using bare carbon electrode.

Chronoamperometry, (*Lit*: measuring electrical current over time) is a technique where a potential is applied to the compound of interest through a user defined instruction set. This instruction set is time and potential based and instructs the potentiostat to apply a given potential to the working electrode at a set time for a given length of time. Each given instruction could be regarded as step with all the steps making up the instruction set or program, Figure 3.9 demonstrates this pictorially.

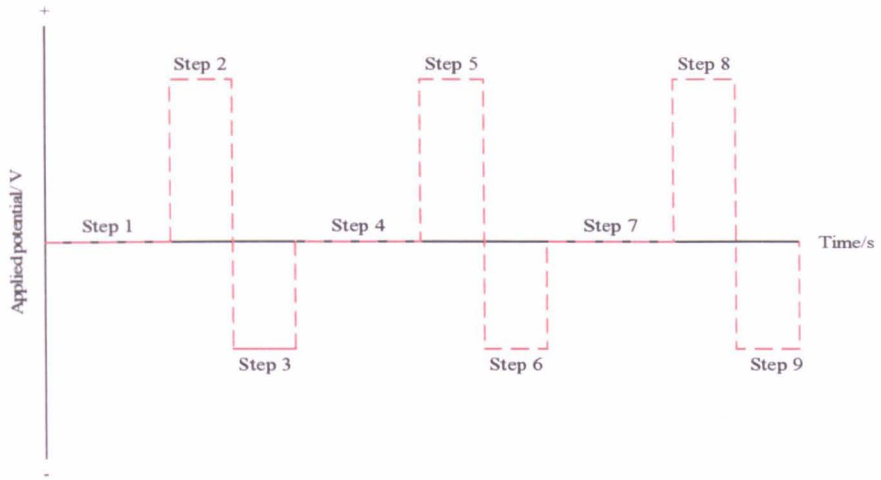

Figure 3.9: Pictorial representation of chronoamperometry instruction set.

As previously discussed each step is reached without potential ramping which removes analyte consumption prior to the application of the potential that produces the maximum cathodic peak, generally allowing for a more sensitive system. The software used for these experiments was limited to a maximum of 10 steps per instruction set; it was therefore decided to repeat each instruction set 3 times to provide more statistically viable results.

With regards to table 3.2 (instruction sets used for this work) each separate step had its own function, for example step 1 was used as a run in period allowing the user to return to the chart recorder to examine results. Steps 2, 5 and 8 were used to apply the requisite potential needed to produce the ECL signal whilst steps 3, 6 and 9 were used to clean the working electrode by applying negative potentials to remove spent analyte from the working electrode. Steps 4 and 7 were set at 0 V and were set to allow the system to return to equilibrium before applying the working potential *i.e.* allowing analyte diffusion. When observing the equilibrium time in a $Ru(bpy)_3^{2+}$/codeine system it was found that a progressive decrease in ECL signal

occurred between rapid chronoamperometric pulses when used with a sol-gel coating, as can be seen in Figure 3.10 and 3.10 (insert).

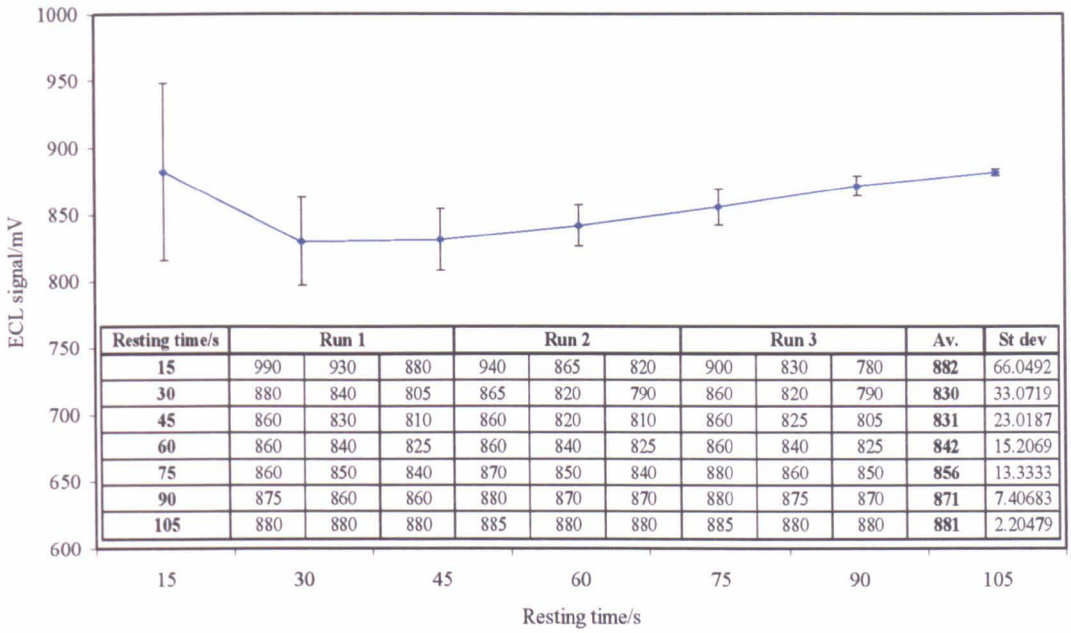

Resting time/s	Run 1			Run 2			Run 3			Av.	St dev
15	990	930	880	940	865	820	900	830	780	**882**	66.0492
30	880	840	805	865	820	790	860	820	790	**830**	33.0719
45	860	830	810	860	820	810	860	825	805	**831**	23.0187
60	860	840	825	860	840	825	860	840	825	**842**	15.2069
75	860	850	840	870	850	840	880	860	850	**856**	13.3333
90	875	860	860	880	870	870	880	875	870	**871**	7.40683
105	880	880	880	885	880	880	885	880	880	**881**	2.20479

Figure 3.10: Demonstrating the effect of the equilibrium time on the ECL signal obtained using a 1x10-3 M $Ru(bpy)_3^{2+}$ and 1x10-4 M codeine system in pH4 0.05 M acetate buffer; using a sol-gel coated glassy carbon working electrode.

Figure 3.10 (insert): Tabulated raw data from Figure 3.10.

This work was undertaken using a sol-gel coated working electrode and interestingly the resting time needed for both codeine and atropine is different, suggesting that each reacts differently with the sol-gel matrix; this will be discussed in more detail later in section 3.3.4. Figure 3.10 also shows a gradual drop in ECL signal from the first signal at 980 mV at15sec resting time to an average of 880 mV at the 105 sec resting time. A possible explanation for this is that the application of the potential is removing weakly attached elements of the sol-gel coating. This in turn is reducing the efficiency of the coating, an explanation of which is given in section 3.3.4.

Another possibility is that particles of detritus are blocking some of the sol-gel pores making the matrix less efficient. In one respect this could be considered beneficial as the sol-gel is protecting the electrode thus prevent fouling. Although after the initial runs this effect diminishes suggesting the sol-gel coating becomes homogeneous.

3.3.2 Characterisation of buffer effects on ECL response

This work was carried out using a platinum working electrode after referring to previous studies; however later work found glassy carbon working electrodes to be better for sol-gel coating, as will be discussed later. However the effects of buffer type, pH and concentration were investigated for the analysis of atropine using an uncoated 0.762 mm diameter platinum wire working electrodes (Alfa Aesar, Karlsruhe, Germany). The buffers chosen for evaluation were phosphate and borate as previous work undertaken by Song *et al.* [29] had noted that these produced the best signal with regards to sensitivity and signal to blank ratio.

As with Song [29] and Barnett [34], it was found that an increase in ECL intensity occurred with an increase in buffer pH. Song *et al.* [29] also found that the increase in signal observed when using a blank $Ru(bpy)_3^{2+}$ solution in pH 11 borate buffer negated any positive increase in signal observed in the $Ru(bpy)_3^{2+}$/atropine solution at that pH.

They stated that for these reasons the optimum pH and buffer type for the analysis of atropine was pH 10 borate buffer solution. With regards to buffer concentration Song *et al.* found that there was little difference in ECL signal observed at different concentrations and used 0.05 M buffer solutions in his work.

In this work however slightly different findings were obtained, for example when analysing the ECL emission produced from $Ru(bpy)_3^{2+}$/atropine (the concentration

of each reagent was $1x10^{-3}$ M) solutions at different pHs it was found that although the blank signal did increase at pH 11, the increase in the signal was more significant as can be seen in Figure 3.11 and 3.12.

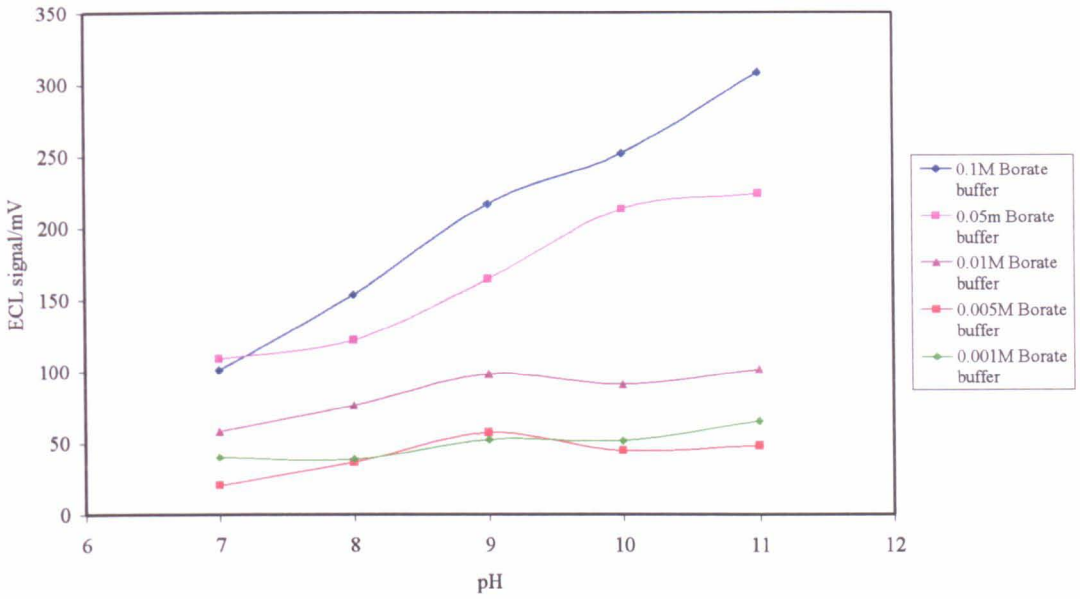

Figure 3.11: Showing a comparison of ECL signals derived from $Ru(bpy)_3^{2+}$/atropine (both reagents $1x10^{-3}$ M) solutions based on borate buffer solution ranging from pH 7 to 11 and 0.1 to 0.001 M.

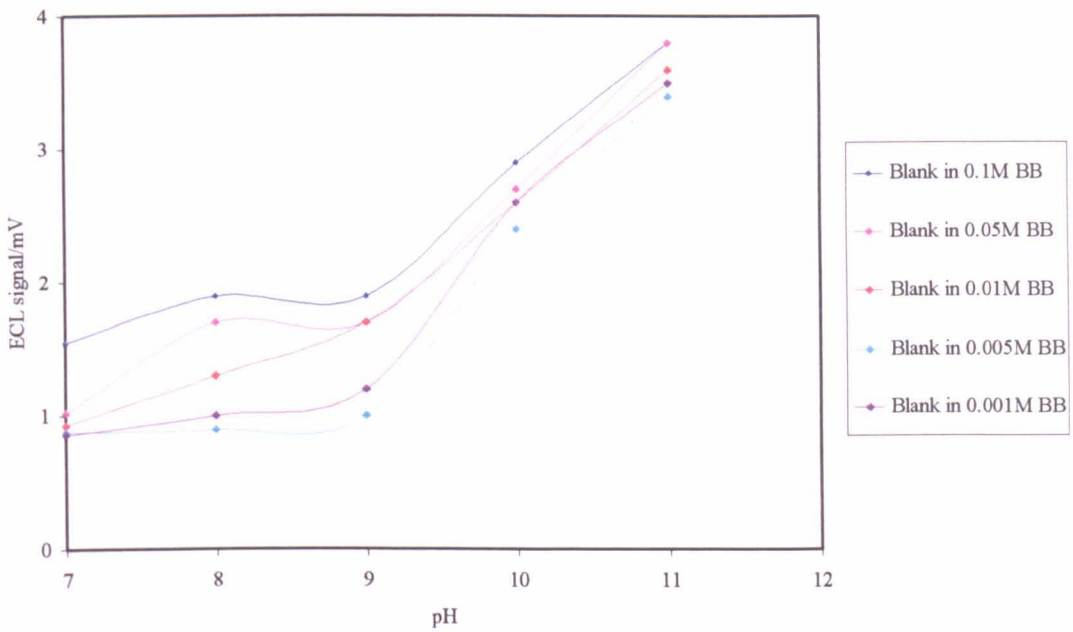

Figure 3.12: Comparison of ECL signals from (blank solutions) $1x10^{-3}$M $Ru(bpy)_3^{2+}$ borate buffer solutions (**Note**: BB denotes borate buffer).

Figure 3.11 does confirm the trend seen by Song *et al.* and Barnett *et al.* in that the ECL signal increases with the pH of the solution. However it differs with regards to the effects of concentration. Song *et al.* states that buffer concentration had little effect on ECL signal yet as can be seen in this work there was a substantial difference found between buffer concentrations as shown in Figure 3.11. The more dilute the buffer concentration the lower the ECL signal obtained, this trend is very pronounced in the range of 0.1 to 0.01 M but becomes less so after this point. The difference with the results obtained by Song *et al.* [29] could be due to difference is experimental set up as Song used a flow system.

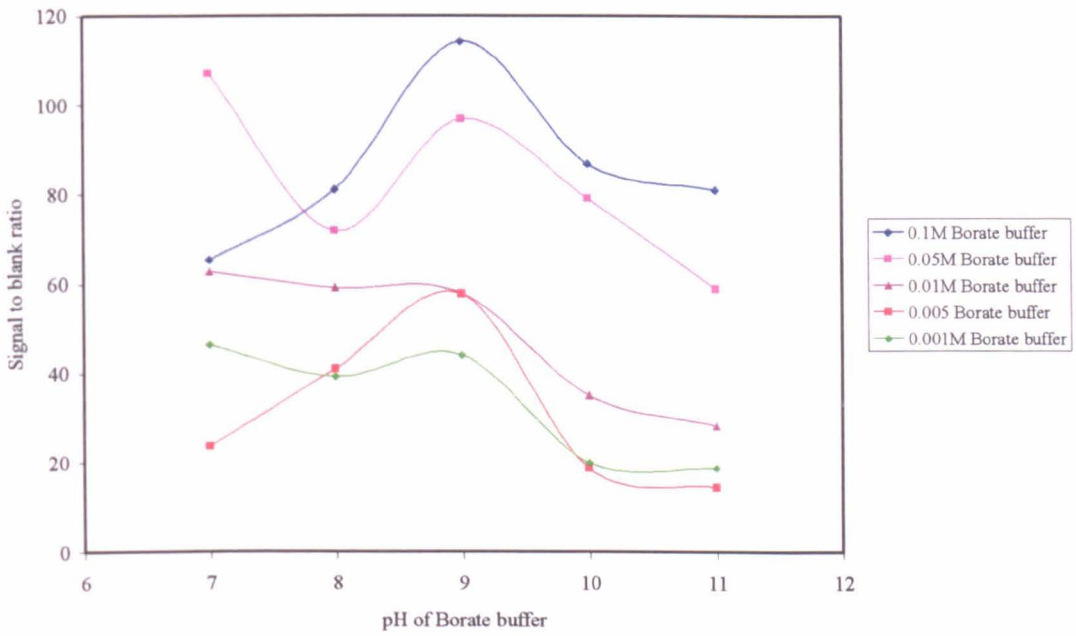

Figure 3.13: ECL) signal to blank ratio for borate buffer solutions of $Ru(bpy)_3^{2+}$/atropine, taken from Figures 3.12 & 3.11.

A similar test was performed using phosphate buffers ranging from pH 5 to 9, which also included the same concentration range as that used for the borate buffer experiments, as is shown in Figures 3.14 & 3.15. As with the borate experiments, the ECL signal increases with the buffer pH, the $Ru(bpy)_3^{2+}$ blank solutions also follow this trend although to a lesser extent.

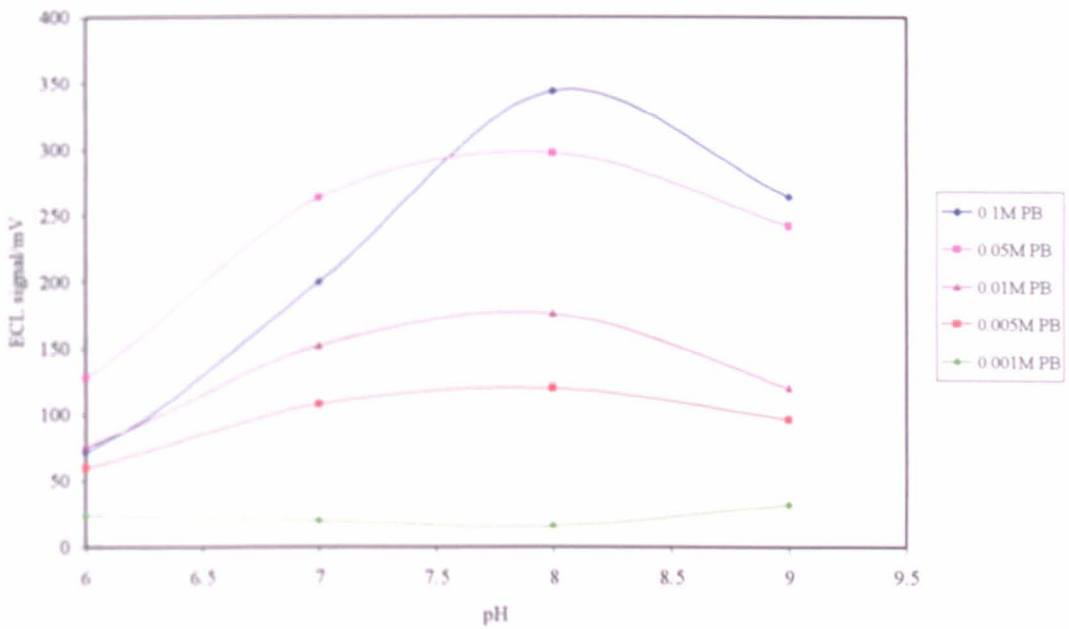

Figure 3.14 showing a comparison of ECL signals derived from $Ru(bpy)_3^{2+}$/atropine solutions based on phosphate buffer solutions ranging from pH 6 to 9 and 0.1 to 0.001 M (**Note**: PB denotes phosphate buffer).

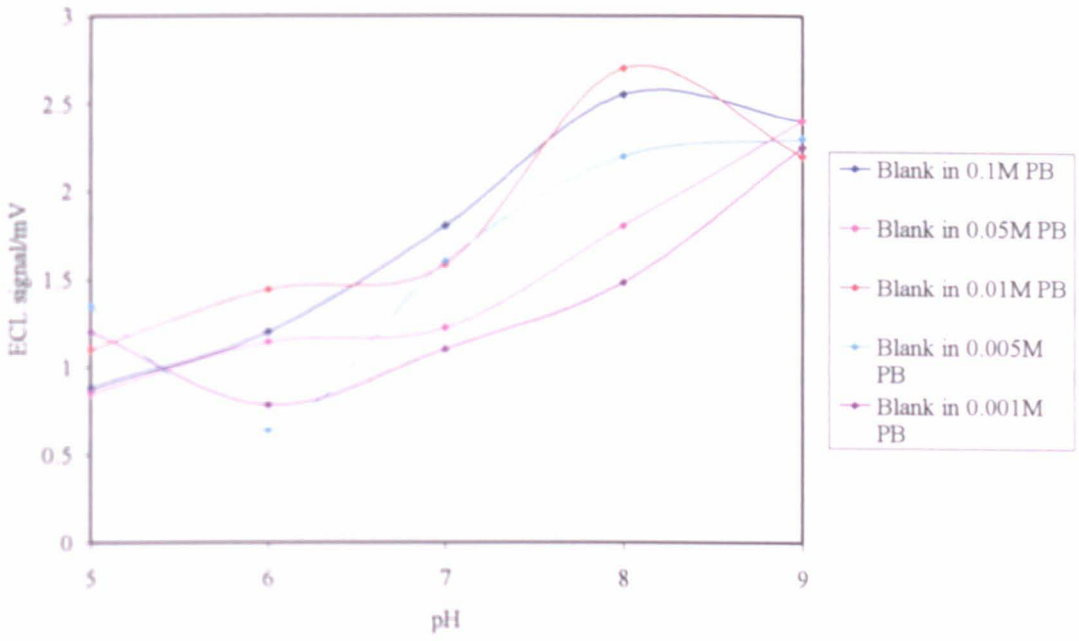

Figure 3.15: Comparison of ECL signals from (blank solutions) $1x10^{-3}$ M $Ru(bpy)_3^{2+}$ phosphate buffer solutions (**Note**: PB denotes phosphate buffer)

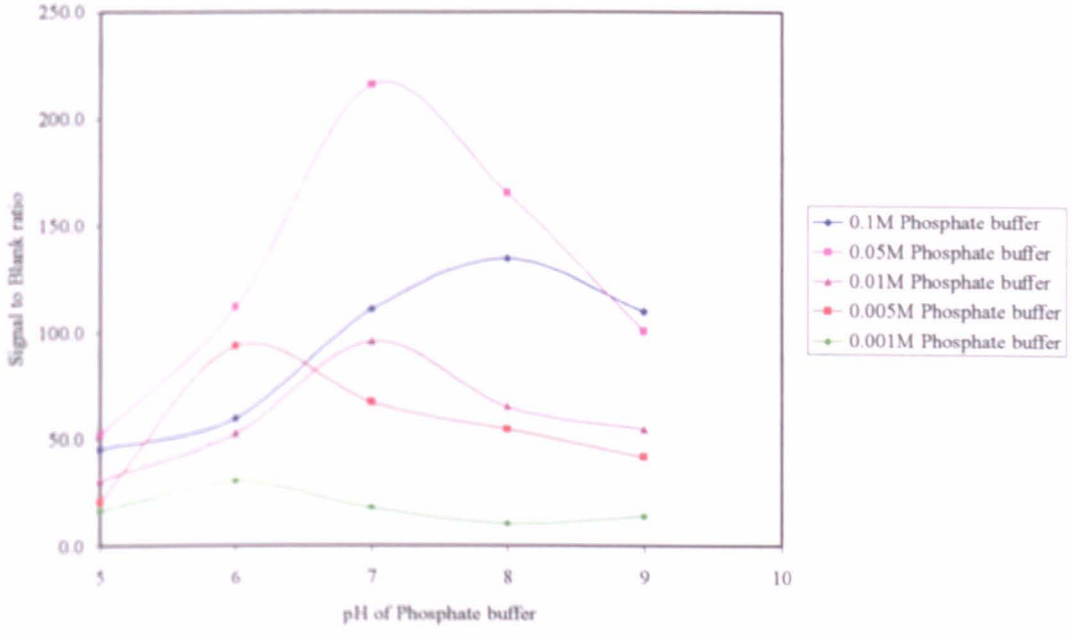

Figure 3.16: Signal to blank ratio for phosphate buffer solution of $Ru(bpy)_3^{2+}$/atropine, taken from Figures 3.14 & 3.15.

The reason for the pH effect in this reaction is uncertain, however atropine and codeine undertake the function of strong reducing intermediates [35] as a consequence of the oxidation of their tertiary amine groups. It is believed that this produces a short-lived radical cation that is proceeded by the deprotonation of the α-carbon forming the reducing agent [36]. It is this reducing agent that then reacts with the $Ru(bpy)_3^{3+}$ to generate the $Ru(bpy)_3^{2+}$ complex in a higher energy excited state that subsequently produces the light (as shown in Figure 3.17).

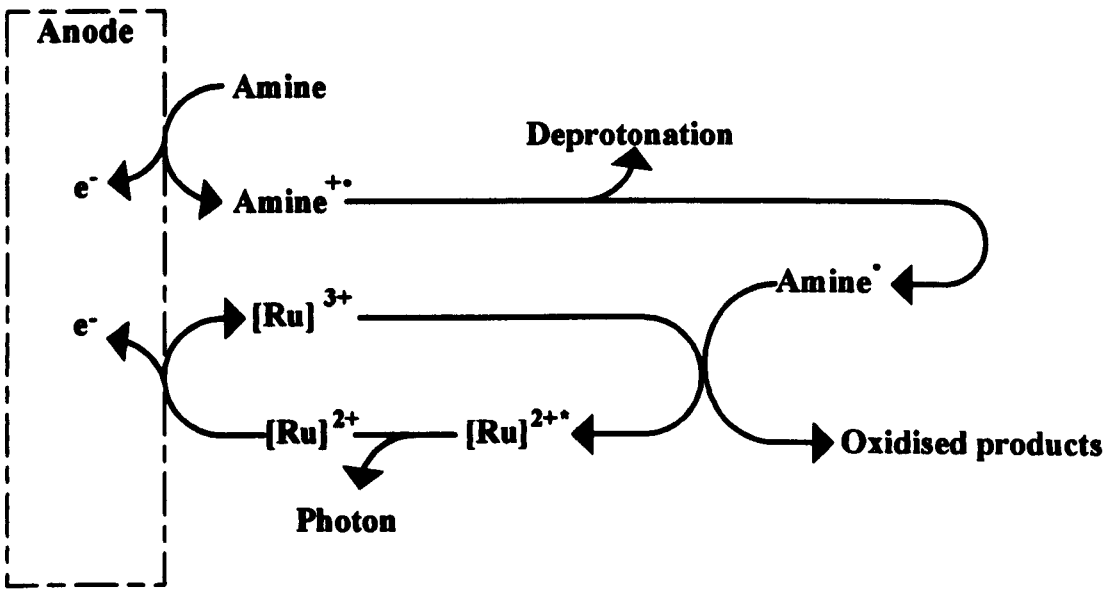

Figure 3.17: Graphical representation of reaction mechanism for a tertiary amine containing compound (codeine/atropine) and tris(2,2'-bipyridyl)ruthenium(II) dichloride hexahydrate.

It is possible that the pH of the solution affects the deprotonation of this complex and consequently prevents the $Ru(bpy)_3^{2+}$ entering the higher energy state. Investigations by Brune and Bobbitt [37] found that close proximity of carbonyl, halogen and to a lesser extent hydroxyl groups to the reactive tertiary amine could destabilize the electron deficient radical ions and reduce ECL activity. However this

in not possible in this work given the structure of these drugs, as shown in section 3.1. Although both buffers performed comparably, pH 11 (0.1 M) borate buffer was chosen as it has a greater buffering capacity at the pH of its optimum ECL signal, although it has be noted that the best signal to noise ratio was found with a pH 9 (0.1 M) borate buffer solution (Figure 3.13).

3.3.3 Characterisation of $Ru(bpy)_3^{2+}$ effect on ECL response

Being the luminescent reagent for this work the concentration of tris (2,2'-bipyridyl) ruthenium(II) dichloride hexahydrate is of paramount importance to the effectiveness of this work. When choosing the amount of $Ru(bpy)_3^{2+}$ in this experiment a number of factors were considered. Firstly the amount of $Ru(bpy)_3^{2+}$ used should be sufficient to produce a good and stable luminescent signal without excessive self quenching occurring (*i.e.* external conversion). In addition it should not be prohibitive due to excessive reagent cost.

Initial studies examining the level of $Ru(bpy)_3^{2+}$ typically used in similar studies by other groups [16, 29, 30, 38-41] found that the common concentration of $Ru(bpy)_3^{2+}$ used in these studies was $1x10^{-3}$ M. Logically a greater concentration of $Ru(bpy)_3^{2+}$ will result in a stronger ECL signal until self-quenching becomes an issue; however the rise in reagent cost must also be taken into account as must the loss of signal to quenching. With these factors in mind and with the results obtained in this work it was decided to use a $Ru(bpy)_3^{2+}$ concentration of $1x10^{-3}$ M in this work as it was deemed that beyond this levels there would be limited signal return to investment.

3.3.4 Examining the effect of the sol-gel coatings on the ECL signals

In the next part of the work the effects of sol-gel and sol-gel/ITO coated electrodes were investigated. Initially, experiments were carried out using a 0.762 mm diameter platinum wire working electrodes (Alfa Aesar, Karlsruhe, Germany) as they are relatively cheap and easy to handle and clean. In addition they are a commonly used electrode type making comparisons with related work easier [13, 15, 30, 42]. However, after initial trials, this type of electrode was abandoned after compatibility issues were discovered when attempting to dip coat the electrodes with a sol-gel solution. When attempted, the sol-gel coatings were repelled from the platinum electrode, reminiscent of a static charge effect thus preventing the electrodes from being coated. The reason for this effect is not fully understood as it was felt that the electrodes were suitably prepared using different grades of emery paper and 3 & 1 μM diameter diamond paste (Kemet International Limited, Maidenhead, UK), removing any oxide layer present.

It has not been possible to find journal references with regard to sol-gel coated platinum wire electrodes. Collinson *et al.* has used 13 μm radius platinum ultramicroelectrodes encapsulated in a tapered glass sheaf embedded in a sol-gel monolith [43-46]; although it is felt that given the small size of the electrode and the protective sheaf, any comparisons are of limited value. When not using ultramicroelectrodes, Collinson's group have applied sol-gel films to glassy carbon electrodes [47, 48]. Literature searches also suggest that other groups also use either glassy carbon electrodes, ceramic graphite composite electrodes or ITO coated glass [49-54] based electrodes when coating with sol-gel films. Given that platinum wire/disc working electrodes are commonly used, the absence of journals discussing

sol-gel coated platinum electrodes suggests that others may have tried this technique and also failed.

The following experiments were carried out using a glassy carbon working electrode, as it was found that they could be easily modified with a sol-gel coating. Initially atropine and codeine were analysed using a non-coated glassy carbon working electrode, as this provides a reference for comparison with the sol-gel coated electrodes. The drugs were initial analysed using cyclic voltammetry in order to determine the optimum potential to be used subsequently with chronoamperometry and also to further examine the effects of pH on the ECL signal.

Figure 3.18 demonstrates the effects of pH on a bare carbon electrode. As with the results obtained in section 3.3.2 for the platinum electrodes, when the pH is observed towards a more alkaline level an increase in current is seen. This of course should result in an increase in ECL signal, as will be demonstrated later in this section. One issue with these results for the bare carbon electrode is that at the higher pH values the voltammograms demonstrate an over potential. This problem is overcome in subsequent results through the reduction of the maximum applied potential.

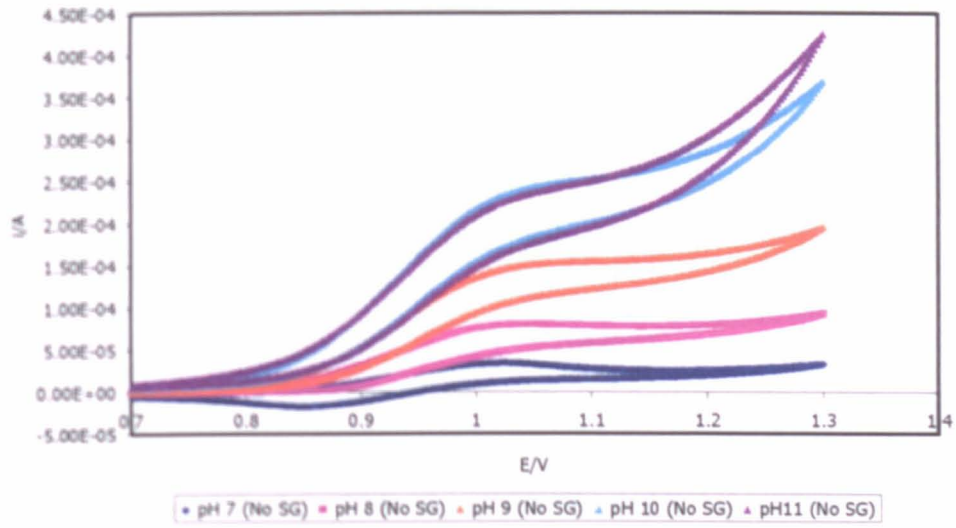

Figure 3.18: Analysis of an atropine/$Ru(bpy)_3^{2+}$ reaction in a range of borate buffers at different pHs using cyclic voltammetry (CV) at a non coated carbon working electrode; with concentrations for both reagents being $1x10^{-3}$ M and no SG referring to no sol-gel coating.

Figure 3.19 (shown on the following page) illustrates the voltammograms for the analysis of atropine over a range of pHs in the same way as Figure 3.18. In this work the glassy carbon working electrode (CWE) received a sol-gel coating and the maximum potential in the scan was reduced to 1.15 V in order to eliminate the over potential at the higher voltages seen in Figure 3.18. The effects of the sol-gel coating will be discussed in the later stages of this section. However, as with the previous work, Figure 3.19 also demonstrates the unusual property in not having a cathodic peak in the higher pH regions.

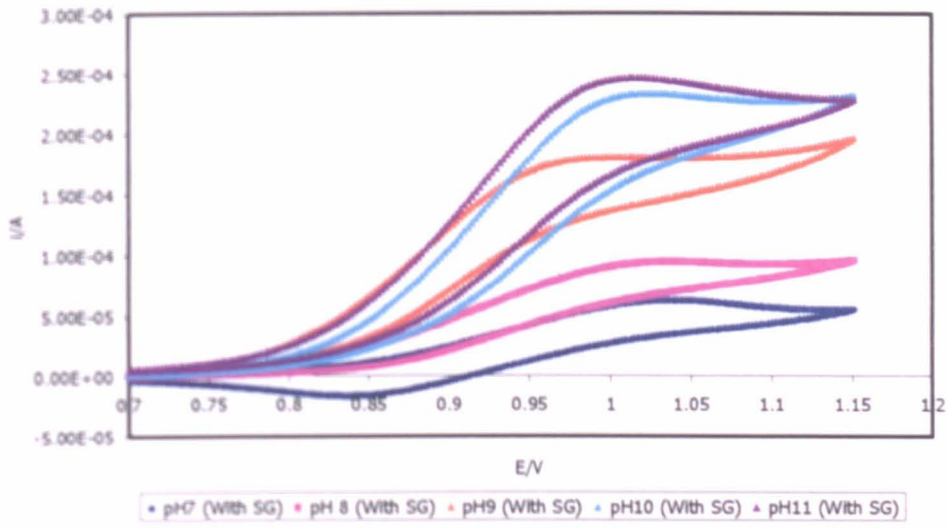

Figure 3.19: The cyclic voltammetric analysis of an atropine/$Ru(bpy)_3^{2+}$ system (both $1x10^{-3}$ M) in a range of borate buffers at different pHs (0.1 M), using a sol-gel coated glassy carbon electrode.

Figure 3.20 shows the results obtained when the working electrode was coated with a sol-gel/ITO mixture, the hybrid material that was discussed in Chapter 2.

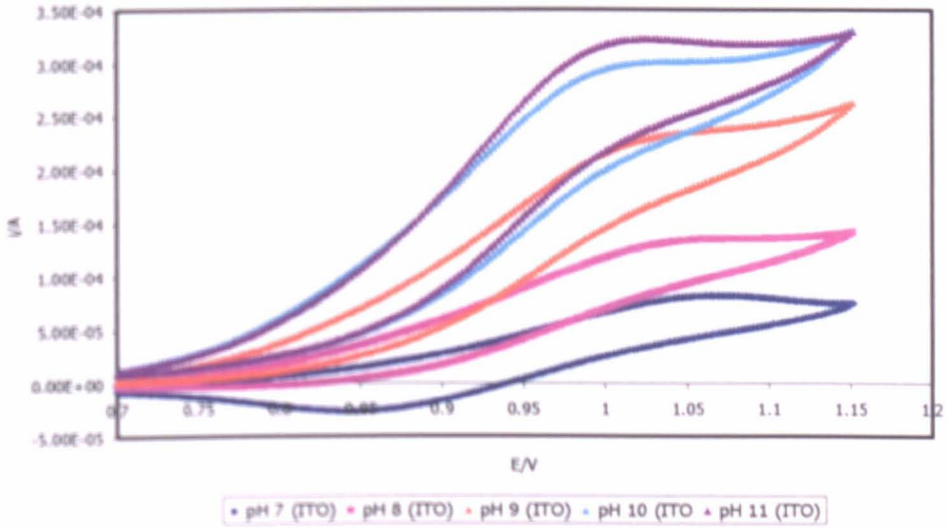

Figure 3.20: Analysis of an atropine/$Ru(bpy)_3^{2+}$ system (both $1x10^{-3}$ M) in borate buffers at a range of pHs using CV and a sol-gel/ITO coated glassy carbon electrode.

Interestingly the coatings used for this work had a desirable effect on sensitivity of the method. As shown in Figure 3.21, when comparing the voltammograms produced by the different coated electrodes an increase in maximum anodic current can be seen for the coated electrodes over the standard blank glassy carbon electrode, although the cathodic peak is less noticeable. As can be seen on Figure 3.21 the greatest improvement in anodic current could be seen for the sol-gel/ITO coating, the reason for which shall be explained shortly.

The increase in current shown in Figure 3.21 should lead to an increased level of ECL signal, Figure 3.22 and Table 3.3 demonstrate that this is the case. Although the increase in maximum anodic current is not linear between pHs, a pattern is clearly demonstrated signifying that the increase in current generated as a consequence of the coating.

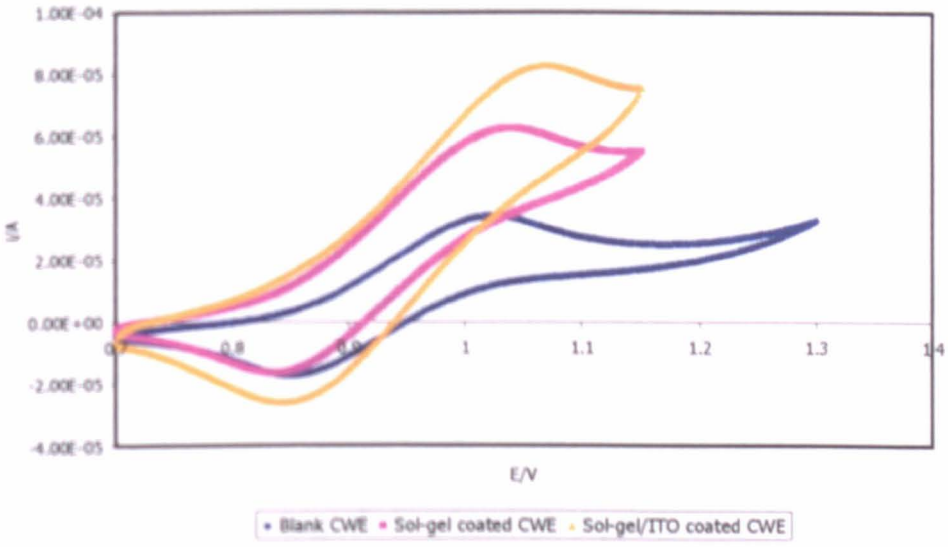

Figure 3.21: Comparing the effect of the sol-gel and sol-gel/ITO electrode coatings on the current produced in the atropine/$Ru(bpy)_3^{2+}$ reactions, as shown in Figures 3.17 to 3.20; this experiment only demonstrates the voltammograms for pH 7.

As with the scan rate analysis in Figure 3.7; Figure 3.21 also clearly illustrates a peak shift effect with regards to the respective anodic for the sol-gel and ITO/sol-gel coatings. As can be seen the anodic peak increases in potential for each subsequent electrode coating, *i.e.* bare → sol-gel → sol-gel/ITO, suggesting that the reaction is no longer demonstrating an efficient one electron transfer reaction.

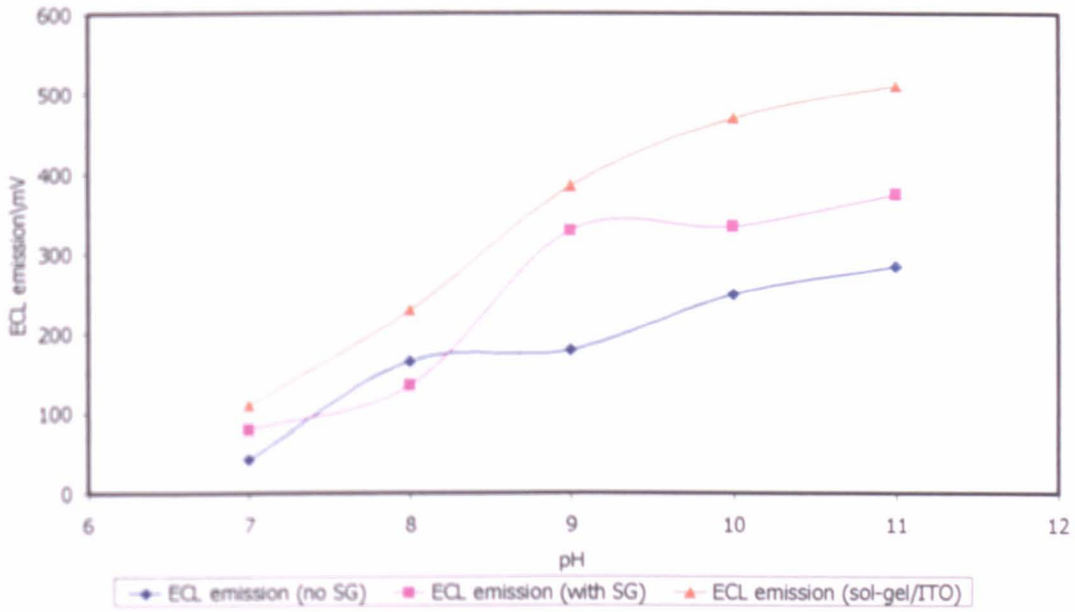

Figure 3.22. Demonstrating the effect of the sol-gel and sol-gel/ITO coatings on the ECL signal developed through the analysis of different pH atropine solutions ($1x10^{-3}$ M atropine in 0.1 M borate buffer).

Table 3.3 also helps to demonstrate the effect reagent diffusion has on the ECL emission when using rapid cyclic voltammetry. As discussed in section 3.3.1, when the cyclic voltammetry occurs more rapidly than the reagent can diffuse to the electrode a drop in signal is observed equivalent to this drop in reagent concentration. This issue is overcome in later work through the use of chrono-amperometry, a technique that allows predefined time intervals between potential pulses and which does not use potential ramping.

Cyclic voltammetry					
Carbon electrode blank					
pH	Signal 1\mV	Signal 2\mV	Signal 3\mV	Av.	St dev
7	43	30	25	33	9
8	166	118	102	129	33
9	180	125	110	138	37
10	250	100	95	148	88
11	285	110	90	162	107

Sol-gel (no ITO)					
pH	Signal 1\mV	Signal 2\mV	Signal 3\mV	Av.	St. Dev
7	80	75	75	77	3
8	135	130	125	130	5
9	330	270	250	283	42
10	335	245	215	265	62
11	375	257	235	289	75

Sol-gel/ITO					
pH	Signal 1\mV	Signal 2\mV	Signal 3\mV	Av.	St. Dev
7	110	75	57	81	27
8	230	180	150	187	40
9	385	240	200	275	97
10	470	270	230	323	129
11	510	270	210	330	159

Table 3.3: A tabulated form of the data used in Figure 3.22; clearly demonstrating the rapid reduction of ECL signal generated when using a multi run cyclic voltammetry system.

However, the reason for the increase in current and ECL signal shown as a consequence of the dip coating is probably due to the introduction of a favourable micro environment close to the electrode surface where the reaction takes place. This micro environment may produce a localized region of increased reagent concentration that leads to the increase in ECL sensitivity. However, Collinson [44] postulated that tertiary amines, present in the compounds being analysed, may hydrogen bond with the sol-gels silicate framework reducing analyte mobility. During this work it was discovered that to maintain ECL signal strength a resting time gap had to be employed between pulses and scans (see section 3.3.1), for codeine this was found to be approximately 105 seconds when using

chronoamperometry. This could be as a consequence of the sol-gel reducing analyte diffusion within the sol-gel. A number of studies have investigated what effect the sol-gel matrix has on diffusion efficiency, examining characteristics such as charge effects and permeability [55-57], however time constraints have prevented this investigation in detail. What's more given that there is possibly an increased reagent concentration inside the sol-gel due to the favourable micro environment as previously discussed, it is reasonable to surmise that this would take longer to populate by diffusion than would normal be the case using a standard non-coated electrode, and thus would also extend the time needed to maintain signal unity.

In addition, some of the sol-gels were doped with indium tin oxide; producing the same electro-conducting sol-gel material that was reported in sections 2.3.6 and 2.3.7. As reported in these sections, silicon based sol-gels such as those used in this work normally demonstrate poor electro-conductive properties. However as was shown in Chapter 2, through the introduction of the optically transparent nano particle size indium tin oxide it was possible to increase the electro conductance of the sol-gels whilst maintaining a good optical transparency.

As discussed in sections 2.3.6 and 2.3.7, entrapping ITO within a sol-gel matrix assists in electron transfer between the normally non-conductive walls of the porous network. In this way the already advantageous micro-environment produced through the application of the sol-gel is further improved by turning the sol-gel into a porous electrode. Technically this last statement is incorrect as the introduction of the ITO into the sol-gel results in the formation of a collection of microelectrodes. However it is convenient to consider the electro-conducting sol-gel coating as a single unit.

The advantage of both the sol-gel coatings used in this chapter is that the surface area of the electrode is effectively increased due to the porous nature of the sol-gel; which in turn results in a higher ECL signal than the bare electrode as shown in Figure 3.22. The further encapsulation of ITO within the sol-gel results in an increase in ECL signal compared to both the bare electrode and the non-doped sol-gel coated electrode. This is believed to be a result of an increased conduction efficiency of the sol-gel which allows an electrical potential to be applied efficiently throughout the entire sol-gel coating; which as discussed previously improves the ECL signal in its own right due to increasing the surface area of the working electrode.

As discussed in Chapter 2 the introduction of ITO into the sol-gel matrix may cause some light scattering, but given the level of ITO in the sol-gel and also the sol-gel thickness it is felt that this would be limited in this work. In addition the emission wavelength of $Ru(bpy)_3^{2+}$ is 640nm and as is illustrated in section 2.3.6 (Figure 2.10) there is little light scattering that occurs at the wavelength.

The increase in signal caused by the sol-gel coating is demonstrated again in Figures 3.23 & 3.24, calibration graphs of ECL signal over concentration of atropine and codeine respectively using chronoamperometry. This clearly demonstrates that the introduction of the sol-gel and sol-gel/ITO coatings has a desirable effect on the ECL emission. However the signal is not linear for each concentration/compound, but this is possibly due to slight changes in cuvette and electrode positioning. Although attempts were made to reduce this, due to the slightly unrefined quality of the pre-existing holder it was not always possible.

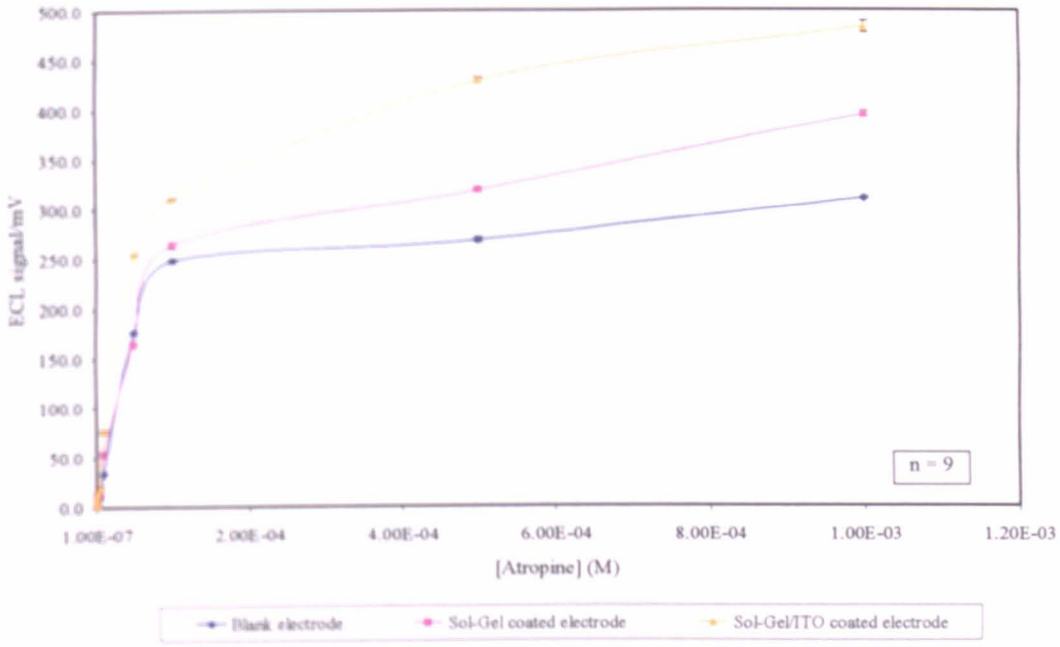

Figure 3.23: Atropine concentration calibration graph demonstrating the effect of the different sol-gel coatings on the ECL signal produced.

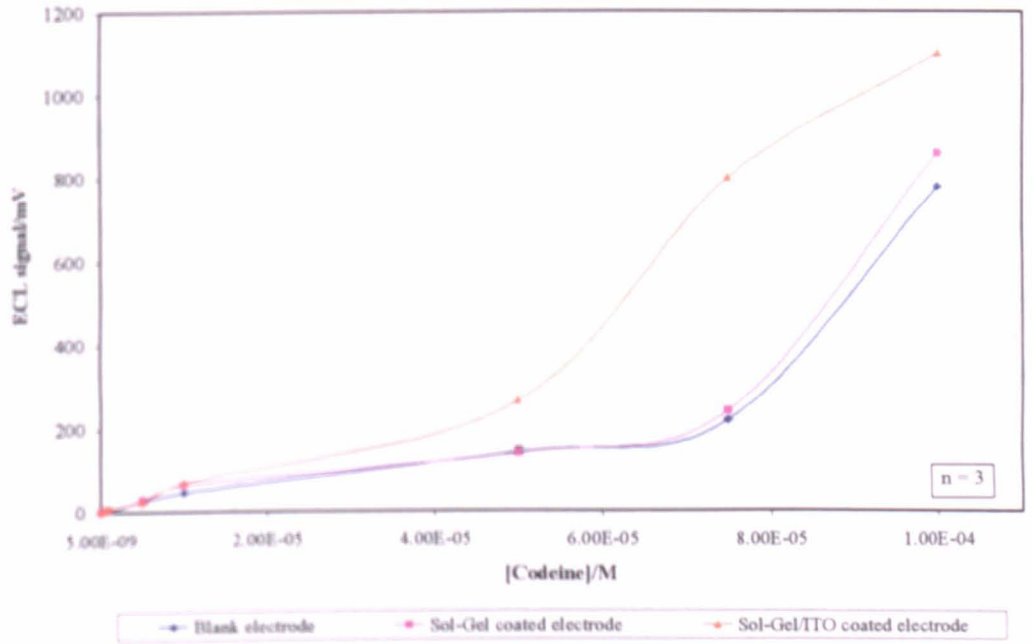

Figure 3.24: Codeine concentration calibration graph demonstrating the effect of the different sol-gel coatings on the ECL signal produced.

The limit of detection (calculated using 3x standard deviation of the noise signal) for the two analytes when using a sol-gel/ITO coated glassy carbon working electrode was found to be $1x10^{-8}$ M for atropine and $5x10^{-8}$ M for codeine (as shown in Figures 3.23 and 3.24). With regards to studies undertaken by other groups the author believes that the LOD determined in Figure 3.23 are comparable with the flow-injection work undertaken by Barnett *et al* [13] and also work done by Downey and Nieman [58] and Song *et al.* [29] ($5x10^{-9}$ to $1x10^{-6}$ mol) In addition, due to its porous nature the sol-gel coating also provides a means of protection against electrode fouling. What's more, the sol-gel proved relatively easy to remove with an initial soak in 1 M NaOH and polishing with a fine emery cloth. Allowing deteriorated/fouled electrodes to be regenerated through the removal and reapplication of the sol-gel coating, helping to establish this as a cost effective technique.

3.3.5 The analysis of Flunitrazepam (Rohypnol)

As mentioned in section 3.2.2, it was originally intended to make the Rohypnol solution in phosphate buffer, however it was determined that this could not be achieved. Many attempts were made in order to dissolve the drug in an aqueous solution, ranging from continued vigorous stirring, heating, changing buffer type, pH and concentration. However none of these had the slightest effect and the Rohypnol remained mostly insoluble in these solutions and what did go into solution was practically impossible to calibrate or reproduce. However it was possible to establish poor quality cyclic voltammograms of this Rohypnol/$Ru(bpy)_3^{2+}$ system, as shown in Figure 3.25; although as stated it is not practical to ascertain the concentration of Rohypnol is n .

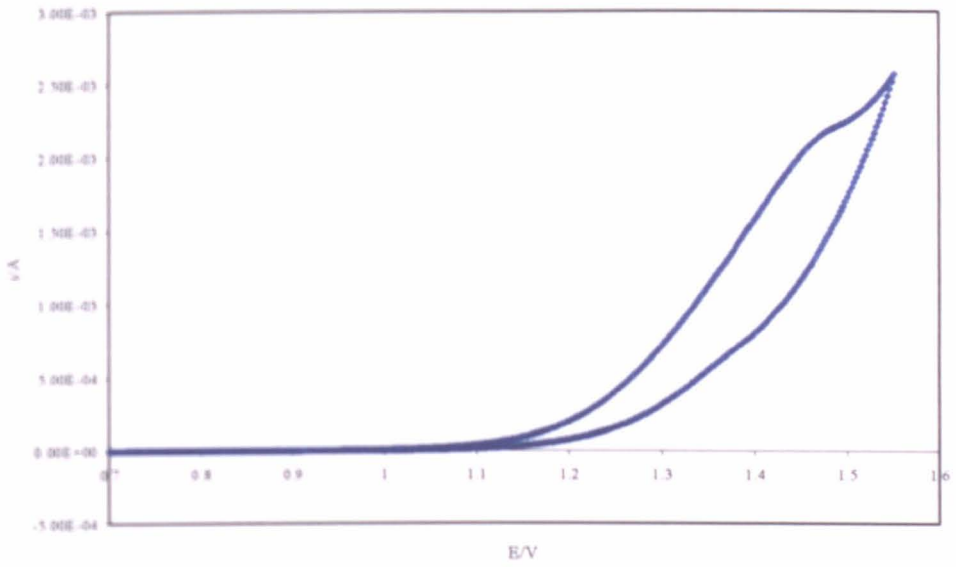

Figure 3.25: A cyclic voltammogram of the Rohypnol ($1x10^{-4}$ M) and $Ru(bpy)_3^{2+}$ ($1x10^{-3}$ M) system analysed in a pH 6.4 (0.1 M) phosphate buffer (see Table 3.1 for CV parameters). **Note**: although the Rohypnol concentration is given as $1x10^{-4}$ M, not all of this sample was soluble in the phosphate buffer.

It was known that the compound had been used in aqueous based systems due to it use in drug facilitated sexual assault in bars and clubs. Therefore the effect of ethanol on the solubility of Rohypnol in aqueous solutions was investigated and it was found that approximately 2 % ethanol was required to facilitate total solubility. Using a stock solution of $1x10^{-3}$ M Rohypnol in ethanol (Fisher chemicals, Loughborough, UK), aliquots of this solution were subsequently mixed with a solution of $1x10^{-3}$ M $Ru(bpy)_3^{2+}$ in pH 6.4 (0.1 M) phosphate buffer to form Rohypnol solutions ranging from $2x10^{-4}$ M to $2.5x10^{-7}$ M, as shown in Figure 3.26 and Figure 3.27. Acetonitrile was also investigated but found to be unsuitable.

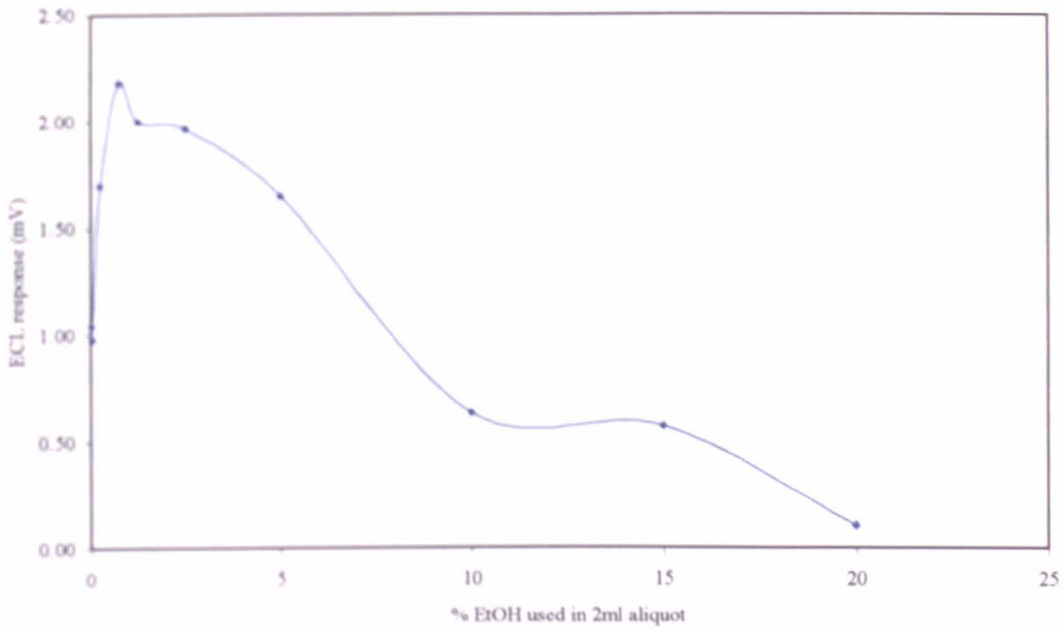

Figure 3.26: CV derived ECL signal for the Rohypnol/$Ru(bpy)_3^{2+}$ system discussed, demonstrating the effect of %volume of ethanol in phosphate buffer against ECL signal (see table 3.1 for CV parameters).

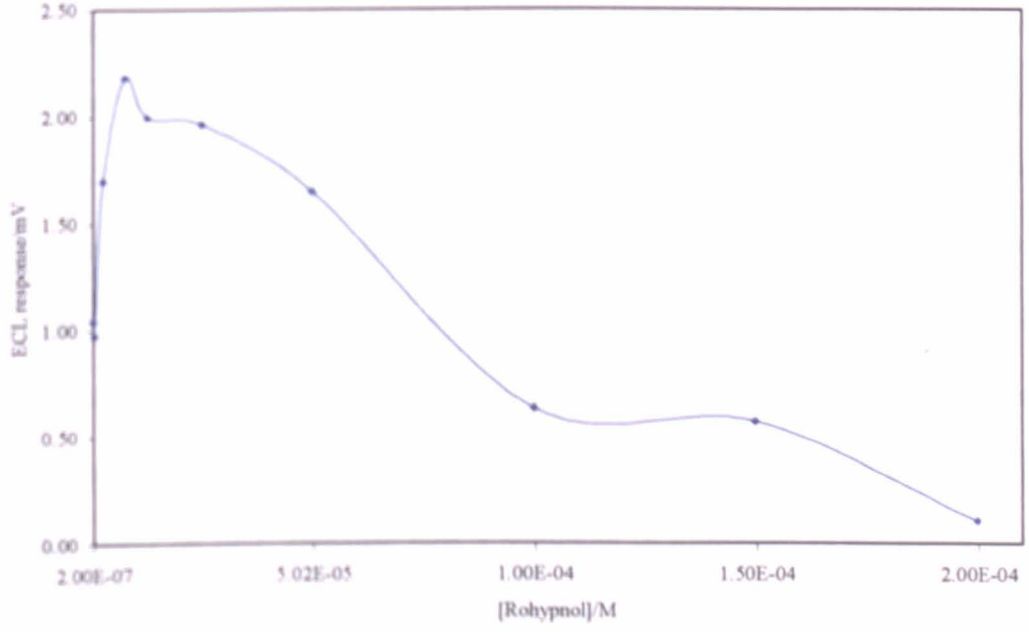

Figure 3.27: Calibration of Rohypnol concentration against ECL signal generated by CV in the Rohypnol/$Ru(bpy)_3^{2+}$ system, as discussed previously in this section..

Figures 3.26 & 3.27 demonstrate that it was possible to generate an ECL signal using the Rohypnol/$Ru(bpy)_3^{2+}$ system, this was expected given that Rohypnol contains a amide group within its structure (See Figure 3.2). However the ECL signals generated are weak compared to the other compounds analysed in this work. There are two reasons for this weak signal; a quenching effect caused by the necessary inclusion of ethanol within the analyte solution which permitted Rohypnol solubility, as discussed shortly. The second reason relates to the structure of Rohypnol; it is possible that the electron withdrawing properties of the carbonyl group situated adjacent to the amide has an effect of the co reactant properties of the compound. As stated in section 3.2.2, work by Brune and Bobbitt [37] found that close proximity of a carbonyl to the reactive tertiary amine could destabilize the electron deficient radical ions reducing ECL activity. Given the close proximity of the carbonyl group to the tertiary amine it is possible that this effect would be seen with this reaction.

With regards to the introduction of ethanol, Figure 3.26 demonstrates the response of %volume of ethanol against ECL signal and Figure 3.27 demonstrates Rohypnol calibration against ECL signal. It was known that the inclusion of ethanol would have some quenching effect on the ECL signal but the magnitude of the effect was surprising. Initially it was deemed that the difference in ethanol content of the solutions would be tolerated in order to gain a working knowledge of the system. However as can be seen in Figure 3.26 a reduction in the %volume of ethanol has a greater effect on ECL response than a reduction in Rohypnol as the signal strength increase with a reduction of analyte. However supply of Rohypnol was limited so studies of the effect of ethanol on ECL were carried out using atropine as a replacement.

In this section the atropine solution mirrored those used in Chapters 4 in that the atropine was prepared in pH 11 (0.1 M) borate buffer. In addition, as with Chapter 4, the electrode system consisted of a glassy carbon working electrode with an ITO encapsulating sol-gel/Nafion electrode coating which immobilised $1x10^{-3}$ M $Ru(bpy)_3^{2+}$ within its matrix; platinum counter and silver reference electrodes were used as described in Chapter 4.

As shown in Figures 3.28 and 3.29 a clear correlation can be seen when comparing %volume of ethanol in the $Ru(bpy)_3^{2+}$/atropine solution and the i/A to E/V response in the accompanying cyclic voltammograms. In both cases the signal reduced with a percentage increase in ethanol. The reason for the reduction in ECL response is due to collisional quenching, the same mechanism that is utilised in many (electro) chemiluminescent oxygen sensors [59-64] and excellently discussed in reviews by Wolfbeis [65] and Leiner [66].

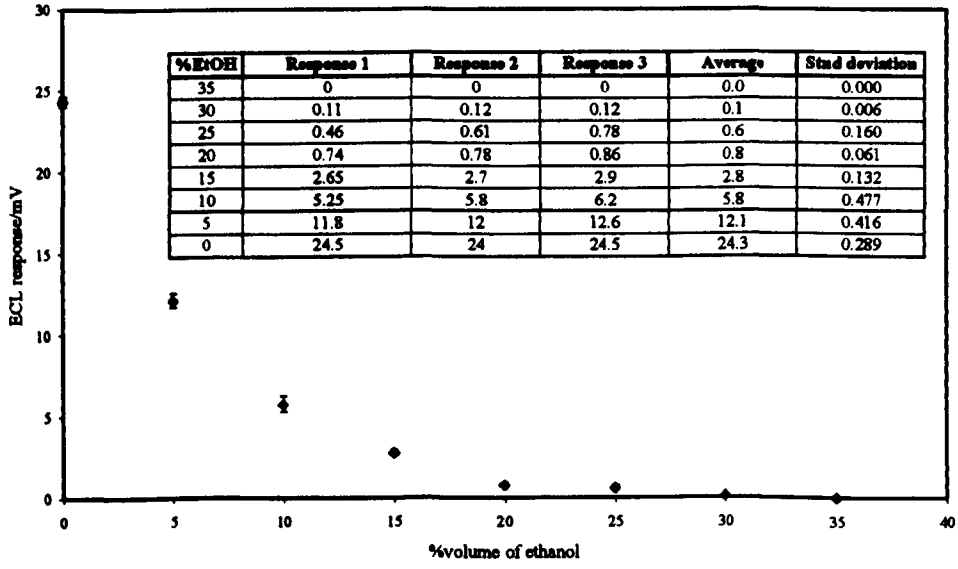

%EtOH	Response 1	Response 2	Response 3	Average	Stnd deviation
35	0	0	0	0.0	0.000
30	0.11	0.12	0.12	0.1	0.006
25	0.46	0.61	0.78	0.6	0.160
20	0.74	0.78	0.86	0.8	0.061
15	2.65	2.7	2.9	2.8	0.132
10	5.25	5.8	6.2	5.8	0.477
5	11.8	12	12.6	12.1	0.416
0	24.5	24	24.5	24.3	0.289

Figure 3.28: Examining the effect of %ethanol in borate buffer (by volume) on the ECL signal generated for a atropine/$Ru(bpy)_3^{2+}$ reaction (both $1x10^{-3}$ M.).

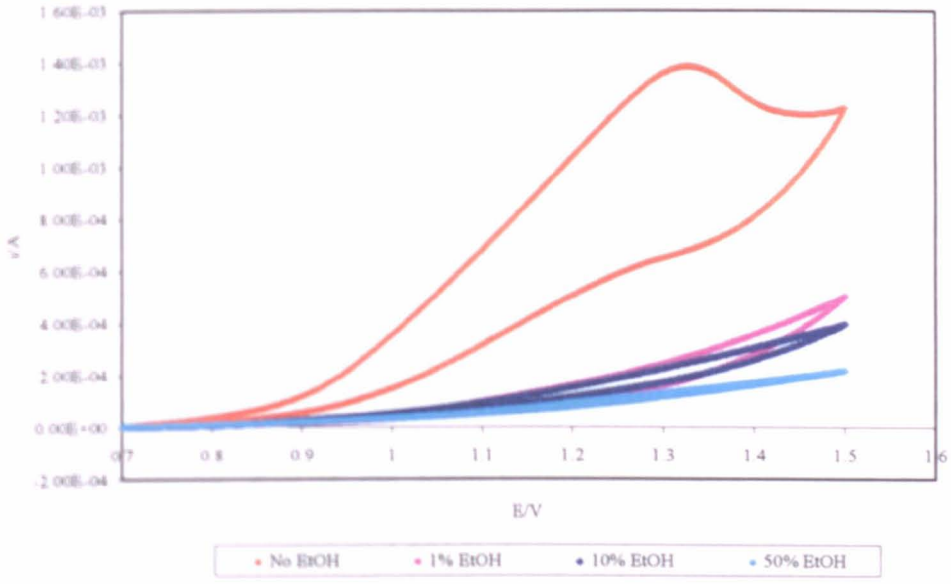

Figure 3.29: Illustrating the effect of %ethanol in the borate buffer on the cyclic voltammograms obtained for the atropine/$Ru(bpy)_3^{2+}$ reaction. **Note:** In Figure 3.28 and 3.29 both reagents have a concentration of $1x10^{-3}$ M, however the $Ru(bpy)_3^{2+}$ is entrapped within a sol-gel/Nafion electrode coating (see section 4.3.2) and the atropine has been dissolved into the borate buffer/ethanol solution.

The mechanism for this quenching is thought to be as a result of energy transfer between the quencher and the luminescent emitter. $Ru(bpy)_3^{2+}$ is a metal to ligand charge transfer species in which one of the three 2,2'-bipyridine (bpy) ligands is reduced and the ruthenium is oxidised . Here an electron is excited from a ruthenium orbital to a ligand based π^* orbital, this then undergoes intersystem crossing to the lowest triplet states of $Ru(bpy)_3^{2+\bullet}$ where ECL emission occurs on the molecules return to ground state [67, 68].

Collisional quenching results in a decrease of intensity and lifetime of the ECL emission that can be described using the Stern-Volmer equation as follows.

$$\frac{\tau_0}{\tau} = 1 + K_{SV}[Q]$$

$$\frac{I_0}{I} = 1 + K_{SV}[Q]$$

$$K_{SV} = k_2 \tau_0$$

Were I and τ are the intensities and lifetimes respectively and "0" represents the absence of quenching. K_{SV} is the Stern-Volmer quenching constant, k_2 is the bimolecular quenching constant and [Q] is the quencher concentration; Plots of I_0/I or τ_0/τ against [Q] should be linear [59].

The effect of ethanol on the $Ru(bpy)_3^{2+}$ /atropine reaction coupled with Rohypnol's lack of solubility in aqueous solutions demonstrated that another technique would be needed for the analysis of Rohypnol.

3.5 Conclusions

This chapter has shown that the introduction of a sol-gel coating to the working electrode has provided a positive increase on the ECL signal produced in the reactions investigated. This is thought to be due to the formation of a favourable micro-environment on the electrode surface. The subsequent doping of the sol-gels with indium tin oxide has demonstrated improvements in electro conduction of the sol-gel matrix that has further improved the ECL response. Although the improvements in signal were not linear it is believed that much of this is due to slight deficiencies in the equipment. Further work undertaken following this project would benefit from a redesign of the mounting system used for the electrodes and cuvette.

This work helped to show the benefits of the application of an electro-active sol-gel coating to a working electrode and provided the starting ground for the more comprehensive sensor system discussed in the following chapters. It is felt that this system could be applied to a multitude of others systems due to the favourable micro-environment of sol-gel, including the analysis of other tertiary amine containing compounds such a cocaine and heroin and other electro-active compounds.

3.6 Reference

1. Ege, S., *Organic Chemistry - Structure and Reactivity*. 3 ed. 1994: D.C. Heath and Company. 1355.
2. Health, P.D.o. *Organophosphates/Nerve Agents as a Chemical Terrorist Agent*. 2003 [cited 2005 19th January]; Available from: www.webserver.health.state.pa.us/ health/.
3. Greenwood, P.A., *PhD Thesis*. 2004, Hull.
4. Liu, F., Hu X.Y., and Luo J., Journal of Chromatography B, 1994. **658**.
5. Song, F.R., Cue M., and Liu S.Y., Rapid Communication in Mass Spectrometry, 1999. **13**: p. 478-480.
6. Staerk, U. and Kulpmann W.R., *High-temperature solid-phase microextraction procedure for the detection of drugs by gas chormatography-mass spectrometry*. Journal of Chromatography B, 2000. **745**: p. 399-411.
7. Panganiban, K., Jacob III P., Everhart E.T., Tisdale E.C., Batki S.L., Mendelson J.E., and Jones R.T., *Sulfonium slats as derivatizing agents. 3. Quantitation of the cocaine metabolite benzoylegonine in urine using gas chromatography with ion pair extraction/on column alkylation*. Journal of Analytical Toxicology, 1999. **23**: p. 581-584.
8. Rook, E.J., Hillebrand M.J.X., Rosing H., van Ree J.M., and Beijnen J.H., *The quantitative analysis of heroin, methadone and their metabolites and the simultaneous detection of cocaine, acetylcodeine and their metabolites in human plasma by high-performance liquid chromatography coupled with tandem mass spectrometry*. Journal of Chromatography B-Analytical Technologies in the Biomedical and Life Sciences, 2005. **824**(1-2): p. 213-221.
9. Clauwaert, K.M., van Bocxlear J.F., Lambert W.E., and de Leenhher A.P., *Analysis of cocaine, benzoylecgonine, and cocaethylene in urine by HPLC with diode array detection*. Analytical Chemistry, 1996. **68**(17): p. 3021-3028.
10. Steenkamp, P.A., Harding N.M., van Heerden F.R., and van Wyk B.E., *Fatal Datura poisoning: identification of atropine and scopolamine by high performance liquid chromatography/photodiode array/mass spectrometry*. Forensic Science International, 2004. **145**(1): p. 31-39.
11. Kirchhoff, C., Bitar Y., Ebel S., and Holzgrabe U., *Analysis of atropine, its degradation products and related substances of natural origin by means of reversed-phase high-performance liquid chromatography*. Journal of Chromatography A, 2004. **1046**(1-2): p. 115-120.
12. Trachta, G., Schwarze B., Sagmuller B., Brehm G., and Schneider S., *Combination of high-performance liquid chromatography and SERS detection applied to the analysis of drugs in human blood and urine*. Journal of Molecular Structure, 2004. **693**(1-3): p. 175-185.
13. Barnett, N.W., Gerardi R.D., Hampson D.L., and Russell R.A., *Determination of codeine in process streams using flow injection analysis with chemiluminescence detection*. Analytica Chimica Acta, 1996. **318**: p. 309-317.
14. Barnett, N.W., Gerardi R.D., Hampson S.L., and Russell R.A., *Some observations on the chemiluminescent reactions of tris(2,2'-*

bipyridyl)ruthenium(II) with certain Papaver somniferum alkaloids and their derivatives. Analytical Communications, 1996. **33**: p. 255-260.

15. Chen, X., Yi C., Li M., Lu X., Li Z., Li P., and Wang X., *Determination of sophoridine and related lupin alkaloids using tris(2,2'-bipyridine)ruthenium electro-generated chemiluminescence.* Analytica Chimica Acta, 2002. **466**: p. 79-86.
16. Gonzalez, J.M., Greenway G.M., McCreedy T., and Song Q., *Determination of morpholine fungicides using the tris(2,2'-bipyridine)ruthenium(II) chemiluminescent reaction.* Analyst, 2000. **1254**: p. 765-769.
17. Gorman, B.A., Barnett N.W., and Bos R., *Detection of pyrrolizidine alkaloids using flow analysis with both acidic potassium permanganate and tris(2,2 '-bipyridyl)ruthenium(II) chemiluminescence.* Analytica Chimica Acta, 2005. **541**(1-2): p. 119-124.
18. Kronstrand, R., Nystrom I., Strandberg J., and Druid H., *Screening for drugs of abuse in hair with ion spray LC-MS-MS.* Forensic Science International, 2004. **145**(2-3): p. 183-190.
19. Barnett, N.W., Rolfe D.G., Bowser T.A., and Paton T.W., Analytica Chimica Acta, 1993. **283**: p. 551.
20. Aman, T., Hassan A., Khokhar I., and Rashid A., *Spectrophotometric determination of Atropine.* Analytical Letters, 1994. **27**: p. 1833-1845.
21. Cooper, G., Wilson L., Reid C., Baldwin D., Hand C., and Spiehler V., *Validation of the Cozart (R) microplate EIA for analysis of opiates in oral fluid.* Forensic Science International, 2005. **154**(2-3): p. 240-246.
22. Alcada, M.N.M.P., Lima J.L.F.C., and Montenegro M.C.B.S.M., Analytical Science, 1995. **11**: p. 781-785.
23. Peng, H., Liang C.D., Zhou A.H., Zhang Y.Y., Xie Q.J., and Yao S.F., *Development of a new atropine sulfate bulk acoustic wave sensor based on a moleculary imprinted electrosynthesized copolymer of aniline with o-phenylenediamine.* Analytica Chimica Acta, 2000. **423**: p. 221-228.
24. *British National Formulary.* Vol. 47. 2004: British medical association & Royal pharmaceutical society of Great Britain. 868.
25. Meyers, J.E., Almirall J.R., and Almirall M.S., *Analysis of Gamma-hydroxybutyric acid (GHB) in spiked water and beverages samples using solid phase microextraction (SPME) on fiber derivatization/gas chromatography-mass spectrometry (GC/MS).* Journal of Forensic Science, 2005. **50**(1): p. 1-6.
26. Samyn, N., De Boeck G., Crimele V., Verstraete A., and Kintz P., *Detection of flunitrazepam and 7-aminoflunitrazepam in oral fluid after controlled administration of Rohypnol.* Journal of Analytical Toxicology, 2002. **26**: p. 211-215.
27. Wang, P.H., Liu C., Tsay W.I., Li J.H., Liu R.H., Wu T.G., Cheng W.J., Lin D.L., Huang T.Y., and Chen C.H., *Improved screen and confirmation test of 7-aminoflunitrazepam in urine specimens for monitoring flunitrazepam (Rohypnol) exposure.* Journal of Analytical Toxicology.
28. Elsohly, M.A., Feng S., Salamone S.J., and Brenneisen R., *GC-MS determination of flunitrazepam and its major metabolite 7-aminoflunitrazepam in whole blood and plasma.* Journal of Analytical Toxicology, 1999. **23**: p. 486-489.
29. Song, Q., Greenway G.M., and McCreedy T., *Tris(2,2'-bipyridine)ruthenium(II) electro-generated chemiluminescence of alkaloid*

type drugs with solid phase extraction sample preparation. Analyst, 2001. **126**: p. 37-40.

30. Greenway, G.M., Knight A.W., and Knight P.J., *Electro-generated chemiluminescent determination of codeine and related alkaloids and pharmaceuticals with tris(2,2'-bipyridine)ruthenium (II).* Analyst, 1995. **120**: p. 2549-2552.
31. Brinker, C.J. and Scherer G.W., *Sol-gel science - The physics and chemistry of sol-gel processing.* 1990: Academic press.
32. Collinson, M.M., Wang H., Makote R., and Khramov A.N., *The effects of drying time and relative humidity on the stability of sol-gel derived silicate films in solution.* Journal of Electroanalytical Chemistry, 2002. **519**: p. 65-71.
33. Niedziolka, J. and Opallo M., *Electrochemical redox reaction at silicate based electrode-silicate based electrolyte interface.* Electrochemistry Communications, 2003. **5**: p. 924-928.
34. Barnett, N.W., Gerardi R.D., Hampson D.L., and Russell R.A., Analytical Communications, 1996. **33**: p. 255.
35. Gerardi, R.D., Barnett N.W., and Lewis S.W., *Analytical applications of tris(2,2'-bipyridyl)ruthenium (II) as a chemiluminescent reagent.* Analytica Chimica Acta, 1999. **378**: p. 1-41.
36. Noffsinger, J.B. and Danielson N.D., *Generation of chemiluminescence upon reaction of aliphatic amines with tris(2,2'-bipyridine)ruthenium (III).* Analytical Chemistry, 1987. **59**: p. 865.
37. Brune, S.N. and Bobbitt D.R., *Role of electron-donating/withdrawing character, pH and stoichiometry on the chemiluminescent reaction of tris(2,2'-bipyridyl)ruthenium(III) with amino acids.* Analytical Chemistry, 1992. **64**: p. 166.
38. Dolman, S.J.L. and Greenway G.M., *Determination of amitriptyline using electro-generated chemiluminescence.* Analytical Communications, 1996. **33**: p. 139-141.
39. Engstrom, R.C., Johnson K.W., and DesJarlais S., *Characterization of electrode heterogeneity with electro-generated chemiluminescence.* Analytical Chemistry, 1987. **59**: p. 670-673.
40. Greenway, G.M., Nelstrop L.J., and Port S.N., *Tris(2,2'-bipyridine)ruthenium (II) chemiluminescence in a microflow injection system for codeine determination.* Analytica Chimica Acta, 2000. **405**: p. 43-50.
41. Knight, A.W. and Greenway G.M., *Electro-generated chemiluminescent determination of pyruvate using tris(2,2'-bipyridine ruthenium(II).* Analyst, 1995. **120**: p. 2543-2547.
42. Greenwood, P.A., Merrin C., McCreedy T., and Greenway G.M., *Chemiluminescence μTAS for the determination of atropine and pethidine.* Talanta, 2002. **56**: p. 539-545.
43. Collinson, M.M. and Martin S.A., *Solid state electro-generated chemiluminescence in sol-gel derived monoliths.* Chemical communications, 1999: p. 899-900.
44. Collinson, M.M., Novak B., Martin S.A., and Taussig J.S., *Electrochemiluminescence of Ruthenium(II) Tris(bipyridine) encapsulated in sol-glasses.* Analytical Chemistry, 2000. **72**(13): p. 2914-2918.
45. Collinson, M.M. and Wightman R.M., *High-frequency generation of Electrochemiluminescence at microelectrodes.* Analytical Chemistry, 1993. **65**: p. 2576-2582.

46. Collinson, M.M., Zambrano P.J., Wang H., and Taussig J.S., *Diffusion coefficients of redox probes encapsulated with sol-gel derived silica monoliths measured with ultramicroelectrodes.* Langmuir, 1999. **15**: p. 662-668.
47. Collinson, M.M., Rausch C.G., and Voigt A., *Electroactivity of redox probes encapsulated within sol-gel derived silicate films.* Langmuir, 1997. **13**: p. 7245-7251.
48. Khramov, A.N. and Collinson M.M., *Electro-generated chemiluminescence of tris(2,2'-bipyridyl)ruthenium (II) ion-exchange in nafion-silica composite films.* Analytical Chemistry, 2000. **72**: p. 2943-2948.
49. Collinson, M.M., *Sol-gel strategies for the preparation of selective materials for chemical analysis.* Critical Reviews in Analytical Chemistry, 1999. **29**(4): p. 289-311.
50. Li, J., Chia L.S., Goh N.K., Tan S.N., and Ge H., *Mediated amperometric glucose sensor modified by the sol-gel method.* Sensors and Actuators B, 1997. **40**: p. 135-141.
51. Salimi, A. and Pourbeyram A., *Renewable sol-gel carbon ceramic electrodes modified with a Ru-complex for the amperometric detection of L-cysteine and glutathione.* Talanta, 2003. **60**: p. 205-214.
52. Shankaran, D.R., Uehara N., and Kato T., *Sol-gel derived metal dispersed ceramic-graphite composite electrode for amperometric determination of dopamine.* Analytica Chimica Acta, 2003. **478**: p. 321-327.
53. Wang, H., Xu G., and Dong S., *Electrochemiluminescence sensor using tris(2,2'-bipyridyl)ruthenium (II) immobilized in Eastman-AQ55D-silica composite thin-films.* Analytica Chimica Acta, 2003. **480**: p. 285-290.
54. Shi, Y., Seliskar C.J., and Heineman W.R., *Dual-analyte spectroscopic sensing in sol-gel derived polyelectrolyte-silica composite films.* Talanta, 1998. **47**: p. 1071-1076.
55. Kanungo, M. and Collinson M.M., *Diffusion of redox probes in hydrated sol-gel-derived glasses. Effect of gel structure.* Analytical Chemistry, 2003. **75**(23): p. 6555-6559.
56. Koone, N.D. and Zerda T.W., *Diffusion of solvents and cations in porous sol-gel glass.* Journal of Sol-Gel Science and Technology, 1997. **8**(1-3): p. 883-887.
57. Kanungo, M. and Collinson M.M., *Controlling diffusion in sol-gel derived monoliths.* Langmuir, 2005. **21**(3): p. 827-829.
58. Downey, T.M. and Nieman T.A., *Chemiluminescence Detection Using Regenerable Tris(2,2'-Bipyridyl)Ruthenium(Ii) Immobilized in Nafion.* Analytical Chemistry, 1992. **64**(3): p. 261-268.
59. Bacon, J.R. and Demas J.N., *Determination of oxygen concentrations by luminescence quenching of a polymer immobilized transition-metal complex.* Analytical Chemistry, 1987. **59**(23): p. 2780-2785.
60. Bergman, I., *Rapid-response atmospheric oxygen monitor based on fluorescence quenching.* Nature, 1968. **218**: p. 396.
61. Klimant, I., Kuhl M., Glud R.N., and Holst G.G., *Optical measurement of oxygen and temperature in microscale: strategies and biological applications.* Sensors and Actuators B, 1997. **38-39**: p. 29-37.
62. Lee, S.K. and Okura I., *Photoluminescent determination of oxygen using metalloporphyrin-polymer sensing system.* Spectrochimica Acta A, 1998. **54**: p. 91-100.

63. Watkins, A.N., Wenner B.R., Jordan J.D., Xu W., Demas J.N., and Bright F., *Potable, low-cost, solid state luminescence based O_2 sensor.* Applied Spectroscopy, 1998. **52**(5): p. 750-754.
64. Xu, H., Aylott J.W., Kopelman R., Miller T.J., and Philbert M.A., *A real-time ratiometric method for the determination of molecular oxygen inside living cells using sol-gel based spherical optical nanosensors with applications to rat C6 glioma.* Analytical Chemistry, 2001. **73**(17): p. 4124-4133.
65. Wolfbeis, O.S., *Fibre-optic chemical sensors and biosensors.* Analytical Chemistry, 2000. **72**: p. 81r-89r.
66. Leiner, M.J.P., *Luminescence chemical sensors for biomedical applications: Scope and limitations.* Analytica Chimica Acta, 1991. **255**: p. 209-222.
67. Knight, A.W. and Greenway G.M., *Occurrence, mechanisms and analytical applications of electro-generated chemiluminescence.* Analyst, 1994. **119**: p. 879-890.
68. Richter, M.M., *Electrochemiluminescence (ECL).* Chemical review, 2004. **104**: p. 3003-3036.

Chapter 4 – The use of a novel electro-conducting sol-gel to develop a sensor for the detection of drugs of abuse through $Ru(bpy)_3^{2+}$ encapsulation

4.0 Aims of chapter

Given the successful encapsulation of indium tin oxide (ITO) into a sol-gel matrix, this led to the fabrication of an electro-conductive sol-gel (discussed in Chapter 2). This material was subsequently successfully applied as an electrode coating (discussed in Chapter 3), which showed an enhancement effect over bare electrodes in the ECL analysis of atropine and codeine. It therefore seemed logical to extend this work further by encapsulating tris(2,2'-bipyridyl)ruthenium(II) dichloride hexahydrate ($Ru(bpy)_3^{2+}$) within the hybrid sol-gel material. In the previous work (see Chapter 3), $Ru(bpy)_3^{2+}$ had been used in a buffer solution phase containing the analyte of interest. However by encapsulation of $Ru(bpy)_3^{2+}$ within the sol-gel matrix it would be possible to reduce reagent usage and permit the development of a field portable system. Thus allowing the detection of the reagents of interest in this work, specifically atropine and codeine, without the need to transport secondary reagents.

4.1 Encapsulation and derivatisation methodologies used with tris(2,2'-bipyridyl)ruthenium(II) dichloride hexahydrate

As discussed in Chapter 1 the inherent sensitivity and selectivity demonstrated by the chemiluminescent and electrochemiluminescent reaction of ($Ru(bpy)_3^{2+}$) has led to its widespread application for the determination of reduced species, in both static and flowing systems [1]. A major drawback of the technique however is the need to constantly supply the reagent to the site of reaction, increasing both analysis costs and waste generated.

As discussed in section 1.4, $Ru(bpy)_3^{2+}$ is oxidised, either chemically (CL) [1] or electrochemically (ECL) [2], to afford $Ru(bpy)_3^{3+}$, which when subsequently reduced by an analyte results in the emission of a photon of light. However, as $Ru(bpy)_3^{2+}$ is regenerated, the immobilisation of this reagent would not only enable the reagent to be recycled, leading to reduced analysis costs and waste generation, but would also allow the simplification of the instrumental set-up [3]. With this in mind, many groups have attempted to immobilise chemiluminescent and electrochemical reagents, using approaches such as the doping of sol-gels [3-5] fabrication of composite films [6] or more recently the preparation of solid-supported derivatives [7, 8].

In addition to $Ru(bpy)_3^{2+}$, the low temperature processing used for silicate sol-gel fabrication, facilitates the encapsulation of other modifiers such as dyes [9, 10], enzymes [11, 12] and proteins [13, 14]. However these dopant molecules are often smaller than the pores within silicate sol-gels and leaching frequently occurs; leading to irreproducible responses and a limited sensor lifetime [9]. With regards to $Ru(bpy)_3^{2+}$, many techniques have been reported within the literature to overcome leaching, including the use of sol-gel additives such as Nafion [15, 16] and titania [4] to fabricate a composite film or attaching the dopant to large anchor molecules such as dextran [17]; however few have resulted in the fabrication of stable and reproducible sensors. For example, Nafion films reportedly suffer from slow mass transfer in the films and also the problem of the $Ru(bpy)_3^{2+}$ partitioning into more hydrophobic regions within the coating [15, 18].

Other silica based composite films used to entrap $Ru(bpy)_3^{2+}$ include poly(*p*-styrenesulfonate)-silica-Triton X100 films [19, 20] and an Eastman AQ55D-silica composite [6], both of which have been applied onto glassy carbon electrodes. The $Ru(bpy)_3^{2+}$ is incorporated into these films either through initial incorporation into the precursors [19] or through an ion-exchange mechanism once the films are fabricated [20].

Organically modified silicates (ORMOSILs), are a type of hybrid sol-gel where a standard inorganic precursor such as TMOS is reacted with a organosilicon counterpart such as an organotrialkoxysilane to form an inorganic-organic sol-gel hybrid, these have also been used for the encapsulation of $Ru(bpy)_3^{2+}$ [5]. Collinson *et al.* [21, 22] believes that ORMOSILs allows improved porosity, permeability, stability and flexibility over conventional inorganic sol-gel. Although these systems may provide a more stable and rapid fabrication technique over inorganic sol-gels the author is sceptical as to whether significant improvements can be made on the determination of pore size and number due to the inherent similarities in structure.

MacCraith *et al.* [23] have reported the synthesis of a derivatised form of $Ru(bpy)_3^{2+}$, 4,4'-bis[(3-triethoxysilylpropyl)amide]-2,2'-bipyridine]bis-(2,2'-bipyridine) ruthenium(II) dichloride and demonstrated its incorporation into ORMOSIL film. This hybrid ORMOSIL film was demonstrated in the form of a fluorescent based oxygen sensor, where it was shown to possess good sensitivity. In addition, due the covalent bonding demonstrated by the $Ru(bpy)_3^{2+}$ derivative, it also did not suffer from the leaching prevalent in this type of sensor. This type of derivatisation will be discussed in greater detail in section 4.3.3.

4.2 Experimental

4.2.1 Design of instrumentation

The instrumentation used during this work is described in Chapter 3. Experimental changes that have been made will either be discussed in the relevant section or in the case of the derivatised $Ru(bpy)_3^{2+}$ work in section 4.2.4.

4.2.2 Experiment reagents

The reagents used during these experiments were all analytical grade unless otherwise stated and the water was high purity de-ionised (18 MΩ cm^{-1} resistivity) produced by an Elga Elgastat UHQ PS (High Wycombe, UK). Buffer solutions were adjusted using a Hanna instruments PHM2254 pH meter (Hanna Instruments, Kings Langley, UK) which was calibrated prior to use using pH 3, 7 and 9 pH buffer solutions provided by Aldrich (Gillingham, UK). The reagents used are as described below.

Sol-gel fabrication

As with the sol-gel coatings used in Chapter 3, the sol-gel gel solutions were prepared using an acid catalysed sol-gel route (as discussed in section 1.2.3) with tetramethoxysilane (TMOS), water and 0.1 M hydrochloric acid mixed in an 8:5:0.25 ratio. The tetramethoxysilane (99+ %) was obtained from Aldrich (Gillingham, UK), the hydrochloric acid was obtained from Fisher Chemicals (Loughborough, UK). Where appropriate, nano-particle ITO (Aldrich, Gillingham, UK) and/or $Ru(bpy)_3^{2+}$ was added to the sol-gel solution in various concentrations and mixed under stirring to allow homogeneity and sol-gel hydrolysis. This solution was then covered and stored in a fridge for at least eight hours before being used for

dip coating, were it was again stirred before use. Unless otherwise stated the following table represents the levels of reagents used in the sol-gel fabrication.

Reagent	Section 4.3.1. Sol-gel electrode coating	Section 4.3.2. Nafion/sol-gel electrode coating
TMOS	1.6ml	1.6ml
DI water	1ml	1ml
HCl (0.1M)	0.05ml	0.05ml
Nafion		1.2ml
ITO	1mg	1mg *
Ru(bpy)	$1x10^{-2}$ to $1x10^{-4}$ M	$1x10^{-3}$ M *

Table 4.1: The reagent levels used (*: unless otherwise stated) in the preparation of the sol-gel solutions; and used in the sections indicated in the fabrication of the electrode coatings.

The Nafion ((5 wt % in aliphatic alcohols and water) Aldrich, Gillingham, UK) concentration used was based on the work undertaken by Khramov and Collinson [16]; who studied the stability, electrochemical activity and ECL of $Ru(bpy)_3^{2+}$ immobilised within a sol-gel/Nafion composite film. These parameters were examined as a function of Nafion concentration where it was found that 50-70 wt % to silica was the optimum concentration. As with this study, Khramov and Collinson also used a two-step acid catalysed TMOS sol-gel, coated onto a glassy carbon electrode for the analysis of a tertiary amine containing coreactant, in this case tri-*n*-propylamine. The concentration of Nafion used within the sol-gel in this work (see Table 4.1) was chosen after consulting the literature (Khramov and Collinson [16] and Greenwood [24]).

Atropine solution

The atropine solution was prepared using the method proposed by Song *et al.* [25] using a pH 11 (0.1 M) borate buffer solution. The atropine was obtained from Aldrich (Gillingham, UK) whilst the borate buffer solution was made using boric acid and sodium hydroxide both obtained from Fisher Chemicals, Loughborough, UK. The atropine was mixed with the borate solution at the required concentration with successive serial dilutions being made where appropriate.

Codeine solution

The codeine solution was made using a pH 4 (0.05 M) acetate buffer (unless otherwise stated) as demonstrated by Greenway *et al.* [26]. The codeine was obtained from Aldrich (Gillingham, UK) and the acetate buffer solution was made using acetic acid and sodium acetate both supplied *via* Fisher Chemicals (Loughborough, UK).

4.2.3 Electrode control and potential levels

As with the work discussed in Chapter 3; the electrode potentials in this work were controlled with an Eco Chemie μAutolab II computer controlled system (discussed in section 3.2.1.). Initially the potential levels established in section 3.2.1, for both cyclic voltammetry and chrono-amperometry were also used; however these were later adapted in response to further studies, as will be discussed in section 4.3.2. Unless otherwise stated all studies used chrono-amperometry to generate the ECL signal, as this has been found to generate the best signal levels as discussed in section 3.2.1.

4.2.4 Parameters and reagents used in ruthenium derivative study

In the latter part of this study a ruthenium derivative was developed [8] capable of being covalently attached to a silica system, such as sol-gels and controlled pore glass (CPG). In this study some of the experimental parameters differed significantly from those previously discussed, and thus need describing here.

Immobilisation of ruthenium derivative onto CPG

0.05 g (0.044 mmol) of [4,4'-Bis[(3-triethoxysilylpropyl)amide]-2,2'-bipyridine] bis-(2,2'-bipyridine)ruthenium(II) dichloride was hydrolysed by heating in dilute HCl (0.1 M,10 ml) for 1 hour; prior to cooling 10.00 g of control pore glass was added and the mixture stirred overnight. The functionalised CPG was filtered under suction and washed with distilled water, acetone and DCM, to afford an orange free-flowing solid, with a Ru loading of 2.61×10^{-3} mmol g^{-1}. The CPG (120-200 mesh 500 Å pore size and 50.4 $m^2 g^{-1}$) was purchased from Sigma (Gillingham, UK)

Chemiluminescent evaluation

CL measurements were performed using an in-house fabricated borosilicate glass flow cell (2.50 mm i.d x 1.50 cm length) containing 50 mg of the functionalised CPG. The solutions were delivered using a Gilson peristaltic pump with a flow rate of 2ml min^{-1}. The CPG was retained within the flow cell through the fabrication of micro porous frits [27] at both ends of the packed bed. The cell was attached to the peristaltic pump using 1/8" Omnifit connectors (Supelco, UK). The experimental set up is illustrated in Figure 4.1

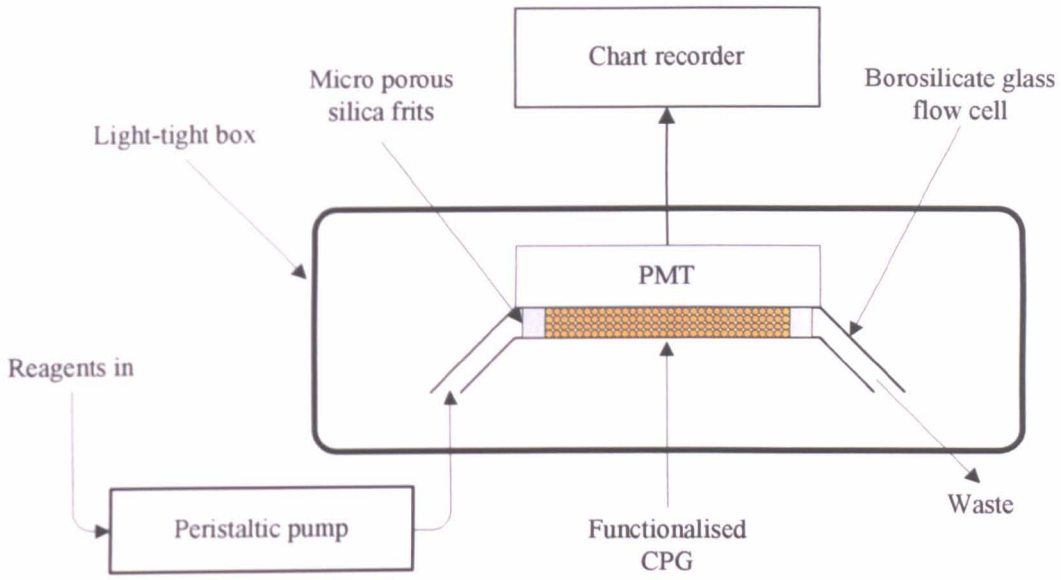

Figure 4.1: Graphical representation of the set up used for the chemiluminescent evaluation of ruthenium functionalised CPG.

Preparation of ruthenium derivative sol-gel monoliths

Hydrolysis of the ruthenium derivative (0.05g, 0.044 mmol) was achieved by heating in dilute HCl (0.1 M, 10 ml). After cooling an aliquot (100µl, 4.40 $x10^{-4}$ mmol) of the hydrolysed compound was added to 100µl of TMOS which was agitated until only a single layer was observed. After which 50 µl of NaOH (0.1 M) was added to the sol-gel solution, which resulted in the formation of an orange sol-gel monolith. The sol-gel, which formed in less than two minutes was then covered and placed in a dessicator (not under vacuum) overnight.

Preparation of sol-gel coating containing the ruthenium derivative

Again, hydrolysis of the ruthenium derivative (0.05 g, 0.044 mmol) was achieved by heating in dilute HCl (0.1 M, 10 ml). After cooling an aliquot (100 µl, $4.40x10^{-4}$ mmol) of the hydrolysed compound was added to 100 µl of TMOS which was agitated until only a single layer was observed. After which a glassy carbon electrode

(1 mm id, 2 cm length) was dipped into the solution and then slowly withdrawn in the same manner as those discussed in section 3.2.3. The sol-gel coated electrode was then placed in borate buffer (pH 8.5, 0.1 M) to induce gelation.

ECL evaluation

ECL measurements were made using the three electrode set-up as described in section 3.2.1. The electrical potential was generated using a PalmSens portable potentiostat (Palm Instrument BV, Houten, The Netherlands) which was controlled *via* a PC running the appropriate PalmSensPC software. The electrochemical programme used was cyclic voltammetry running from 0.7 to 1.3 V, with a step potential of 0.0024 V and a scan rate of 0.01 V s^{-1}, with typically five cycles. Between analyses the electrodes were stored in pH 8.5 (0.1 M) borate buffer to prevent drying and damage of the sol-gel coating.

4.3 Results and discussion

As discussed in section 4.0 the aim of the work was to encapsulate tris(2,2'-bipyridyl)ruthenium(II) dichloride hexahydrate ($Ru(bpy)_3^{2+}$) inside a sol-gel coating applied to a glassy carbon working electrode. Doing this would reduce reagent consumption and also permit the fabrication of a more field portable sensor due to the encapsulation of the sensing reagents. The following sections discuss the steps taken to produce this $Ru(bpy)_3^{2+}$ encapsulating sol-gel material and also the results obtained in terms of both encapsulation efficiency and also sensor performance with regards to analysis of tertiary amine containing drugs of abuse. These steps will be split into three sections, firstly, direct $Ru(bpy)_3^{2+}$ encapsulation within the sol-gel coating; followed by two methods for the prevention of leaching have been examined.

4.3.1 $Ru(bpy)_3^{2+}$ encapsulation within a hybrid sol-gel coating

Initial studies regarding the encapsulation of $Ru(bpy)_3^{2+}$ within the sol-gel matrix focused on the same encapsulation method used for ITO, as discussed in Chapter 3, *i.e.* through the mixing of the solid reagent into the liquid sol. It was felt that since $Ru(bpy)_3^{2+}$ is water soluble this would be the easiest method of encapsulation. This method for $Ru(bpy)_3^{2+}$ encapsulation has been employed by Collinson *et al.* [28, 29], although in that work $Ru(bpy)_3^{2+}$ was encapsulated within a sol-gel/Nafion matrix post gelation [16], *via* an ion exchange method that will be discussed in greater detail in section 4.3.2.

Initially sol-gels were developed with encapsulated $Ru(bpy)_3^{2+}$ concentrations ranging from $1x10^{-2}$ M to $1x10^{-4}$ M in order to ascertain the concentration effects of $Ru(bpy)_3^{2+}$ within the sol-gel with regards to ECL emission. These sol-gel solutions were subsequently dip coated on to glassy carbon working electrodes (see section 3.2.3 for procedure) to form the ECL sensor required for this analysis. Using a preconfigured chrono-amperometric method, ECL analysis was carried out for each sol-gel coated electrode using a $1x10^{-3}$ M atropine solution in pH 11 (0.1 M) borate buffer the results of which are shown in Figure 4.2.

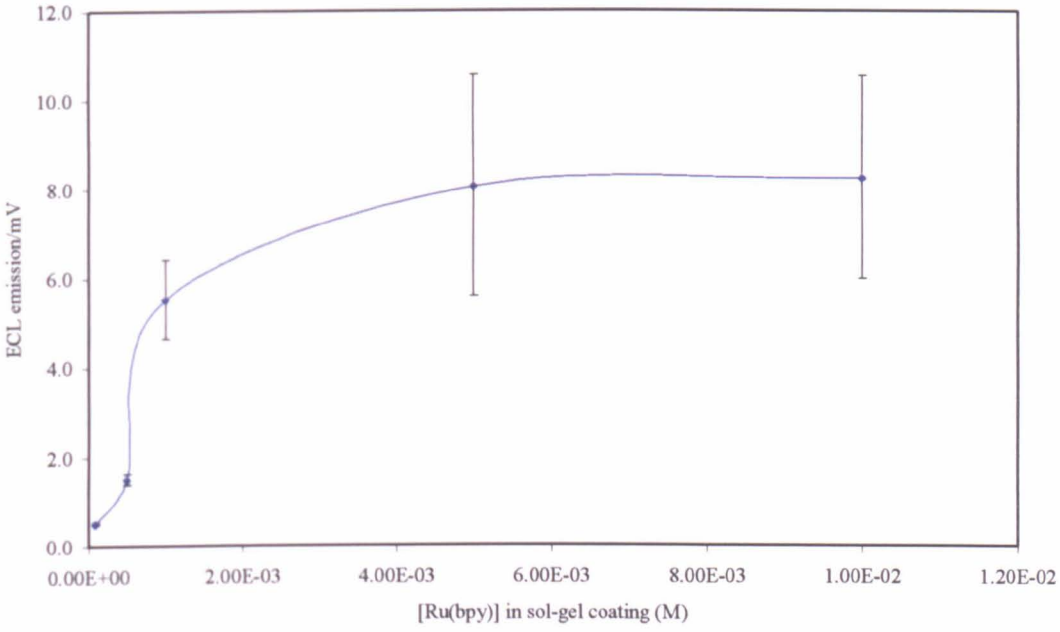

Figure 4.2: Quantitative and qualitative analysis of sol-gel encapsulated $Ru(bpy)_3^{2+}$ coated onto a glassy carbon working electrode using a $Ru(bpy)_3^{2+}$/atropine reaction; chrono-amperometry (CA) used to generate ECL signal see Table 3.2.

As already stated $Ru(bpy)_3^{2+}$ is water soluble; an advantage that allowed its easy encapsulation within the sol-gel matrix. However this solubility in aqueous solutions also caused issues upon gelation. As shown in Figure 4.2, each electrode (*i.e.*

$Ru(bpy)_3^{2+}$ concentration) included the standard deviation for its ECL emission; this standard deviation was found to increase with $Ru(bpy)_3^{2+}$ concentration. Figure 4.3 helps to demonstrates the issue by plotting the ECL signal attained per run for each $Ru(bpy)_3^{2+}$ concentration shown in Figure 4.2.

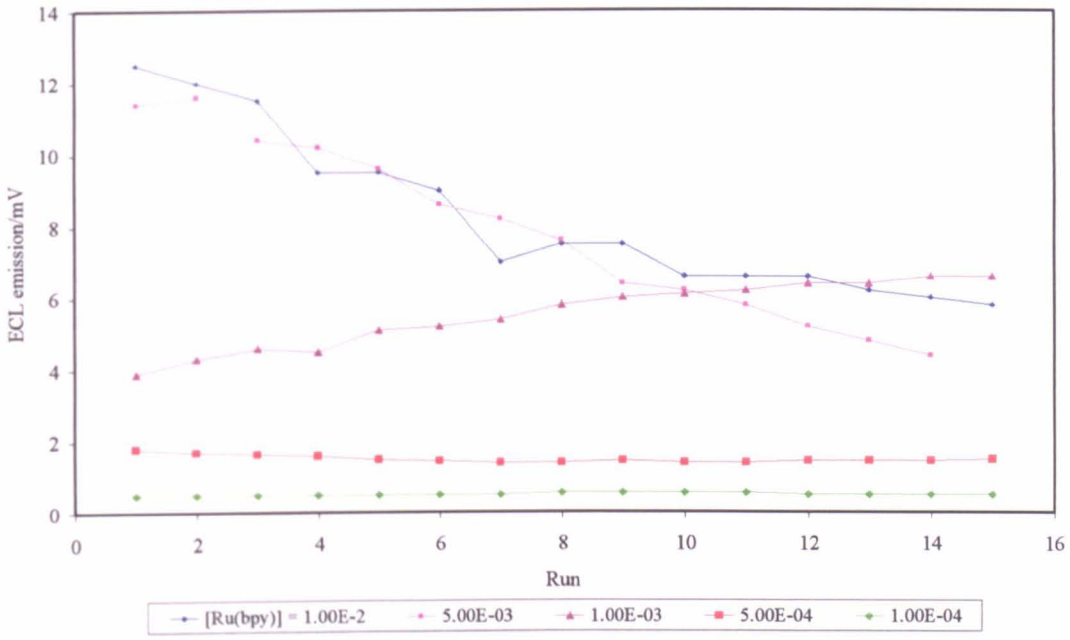

Figure 4.3: Extension of the results shown in Figure 4.2, demonstrating the loss of ECL signal occurring over a range of $Ru(bpy)_3^{2+}$ concentrations during the analysis of sol-gel encapsulated $Ru(bpy)_3^{2+}$ using a $Ru(bpy)_3^{2+}$/Atroipine ($1x10^{-3}$ M) system.

As can be seen, sixteen runs were performed for each $Ru(bpy)_3^{2+}$ concentration, and with the exception of the $Ru(bpy)_3^{2+}$ concentration at $1x10^{-3}$ M, a drop in signal is experienced for each. The most dramatic drop occurs within the two sol-gel coatings with the highest $Ru(bpy)_3^{2+}$ concentration; at these concentrations the ECL emission on the sixteenth run is less than half that attained on the first run. Although some signal loss has been encountered previously when using solution based $Ru(bpy)_3^{2+}$ with sol-gel electrodes (see Figure 4.4), the drop encountered under those

circumstance was much less and was thought to be due to deterioration of the sol-gel matrix in the alkali buffer solution.

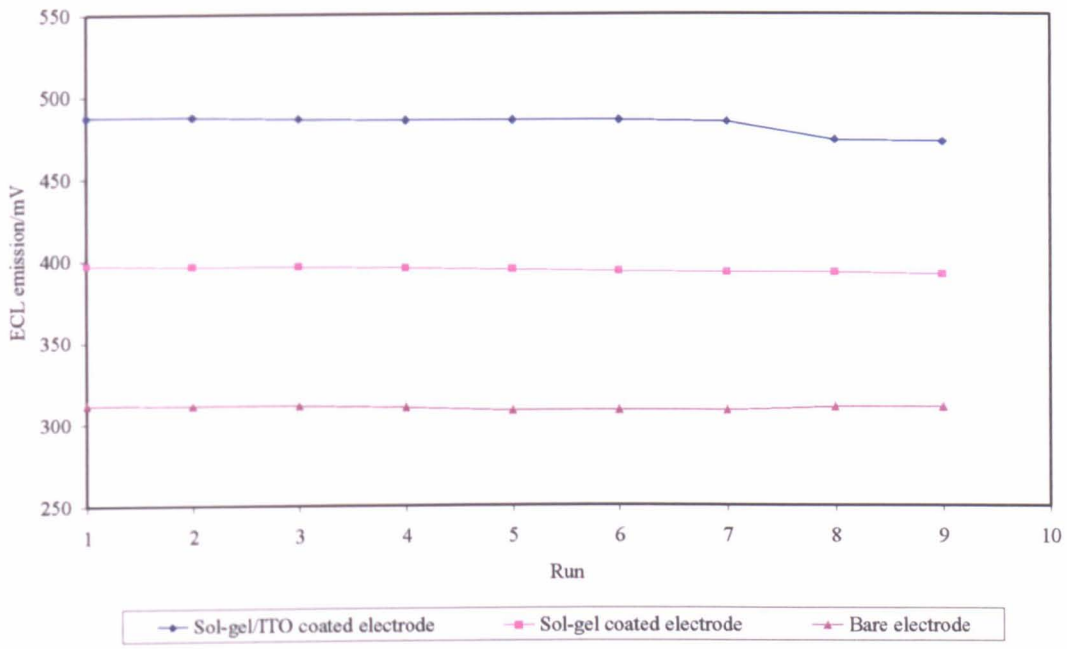

Figure 4.4: Demonstrating the slight loss of ECL signal (in comparison to Figure 4.3) found using a solution based $Ru(bpy)_3^{2+}$/atropine system (both $1x10^{-3}M$) with bare, sol-gel and sol-gel ITO coated electrodes (see Table 3.2 for CA parameters).

This large drop in signal seen in Figure 4.3 is more likely to be due to leaching. As already stated $Ru(bpy)_3^{2+}$ is highly soluble in water and therefore it is probably leaching out of the sol-gel matrix into the surrounding aqueous medium. This problem was exacerbated by the fact that each sol-gel coated electrode was stored in an aqueous based buffer solution overnight before use. Later studies using methods to prevent leaching (see section 4.3.2) further support this hypothesis. Further work such as changing the pH still gave unacceptable variation in results. It therefore became clear that another approach was needed to overcome this problem and exploit the excellent properties of the sol-gel/ITO hybrid material.

4.3.2 $Ru(bpy)_3^{2+}$ encapsulation within a hybrid sol-gel coating using Nafion ion exchange resin to prevent regent leaching

As discussed in section 4.3.1, the initial methods used for the encapsulation of $Ru(bpy)_3^{2+}$ within a sol-gel matrix were met with limited success due to reagent leaching. Other methods were needed to immobilise $Ru(bpy)_3^{2+}$ within the sol-gel matrix without or with reduced reagent loss.

Methods that have previously been exploited (section 4.3.1) include the attachment of large anchor molecules such as dextran [17], the use of organically modified sol-gels to either make the sol-gel hydrophobic [30, 31] (for example through the introduction of methyltrimethoxysilane), or by restricting its pore size [32], thereby preventing reagent loss. These approaches present issues with regards to the procedures in this work, as immediately after the sol-gel coating is applied to the electrodes it is placed in an aqueous buffer to continue the condensation and ageing process (see section 1.2.3). Under these conditions, although condensation occurs, the associated sol-gel shrinking caused by capillary forces acting within the sol-gel pores is limited due to the absence of solvent evaporation. This capillary force normally collapses/compresses the sol-gel network resulting in smaller pores; however the absence of this force means the pores would remain large reducing the efficiency of large anchor molecules. If sol-gels are allowed to undergo condensation and curing under atmospheric conditions they will shrink and pore size will be reduced and Kistler [33] noted that when they were then immersed in water this type of sol-gel frequently cracked due to capillary forces acting on the matrix structure of the sol-gels. Methods have been developed to overcome this, such as supercritical

drying and sintering, however these are not suitable for this work as the sol-gels are required to have some porosity to operate.

Having considered literature studies into the reduction of $Ru(bpy)_3^{2+}$ leaching within the sol-gel matrix two methods were considered; the first, described in this section is the introduction of a Nafion ion exchange resin within the sol-gel which may bind the $Ru(bpy)_3^{2+}$ within the sol-gel. The second, to be discussed in the section 4.3.3 is the covalent bonding of the $Ru(bpy)_3^{2+}$ to the sol-gel matrix. This section will discuss the effects of the Nafion resin on the sol-gel matrix and the encapsulated $Ru(bpy)_3^{2+}$, specifically with respect to leaching, response times and stability.

Nafion (Figure 4.5) is a sulfonated tetrafluorethylene copolymer developed by DuPont in the 1960s. It is a derivative of Teflon (tetrafluorethylene), but differs due to the incorporation of sulfonic acid groups within Teflon's polymer matrix. These sulfonic acid groups provide Nafion with its ionic properties which have allowed it to be used as an ion exchange membrane.

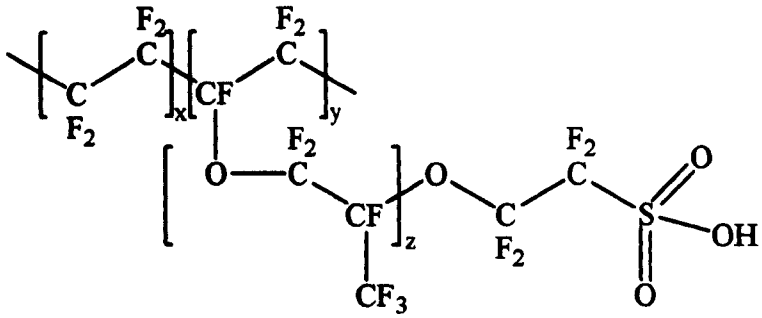

Figure 4.5: Chemical structure of Nafion.

These ion exchange properties have resulted in Nafion becoming the standard electrolyte membrane in Polymer Electrolyte Membrane Fuel Cells (PEMFCs) [34,

35]. Other examples of Nafion applications include its use as an acid catalyst [36, 37], an electrode coating (typically for electro catalytic or amperometric sensor applications) [15, 38] and an ion exchange compound for sensors, including optical sensors for the determination of metal ions such as copper, selenium and nickel [39, 40] and for the determination of glucose [41]. Different approaches have been investigated for the encapsulation of $Ru(bpy)_3^{2+}$ within Nafion, such as Nafion/sol-gel composites films [16], Nafion-stabilized magnetic nanoparticles (Nafion/Fe_3O_4) [42] and thin films [43].

4.3.2.1 Calibration studies for the optimisation of entrapped $Ru(bpy)_3^{2+}$ within a sol-gel coating

As with the previous studies, initial investigations were concerned with the effect of physical entrapment of $Ru(bpy)_3^{2+}$ and ITO within the sol gel. For comparison with the previous studies the effects of buffer pH and concentration were initially investigated. In this study the buffer contained atropine, at a concentration of $1x10^{-3}$ M, as the $Ru(bpy)_3^{2+}$ was entrapped within the sol-gel coating. As with the previous studies (see Figures 3.11 to 3.13), the highest ECL signal was recorded at high pH values (Figure 4.6), *i.e.* pH 10 and 11.

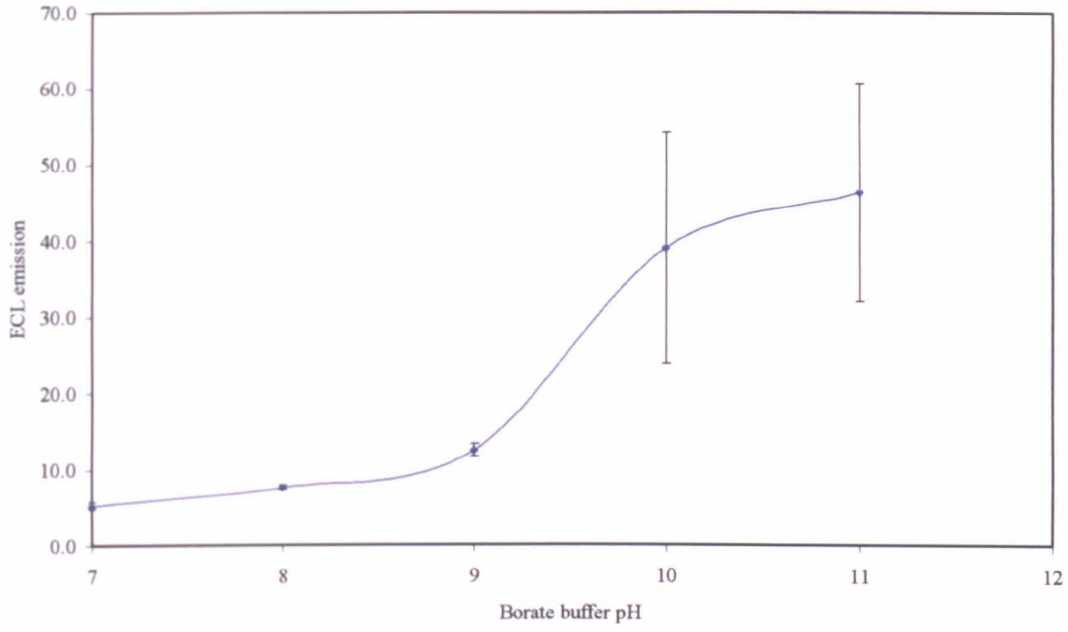

Figure 4.6: Effect of borate buffer pH on the ECL emission of a $Ru(bpy)_3^{2+}$/atropine ($1x10^{-3}$ M) system generated through chrono-amperometry with buffers maintaining a of 0.1 M. concentration (n = 3); see Table 4.1 for sol-gel parameters.

These results were expected given the previous studies discussed in section 3.3.2 and the results obtained by Song *et al.* [25]. The rapid drop in signal seen at the higher pHs was however unexpected and explanations were sort to clarify this loss, although it can be seen that this drop in signal also corresponds to the highest initial ECL signals. Before attempting to explain this phenomenon, the effects of buffer concentration were also examined, as shown in Figures 4.7 and 4.8.

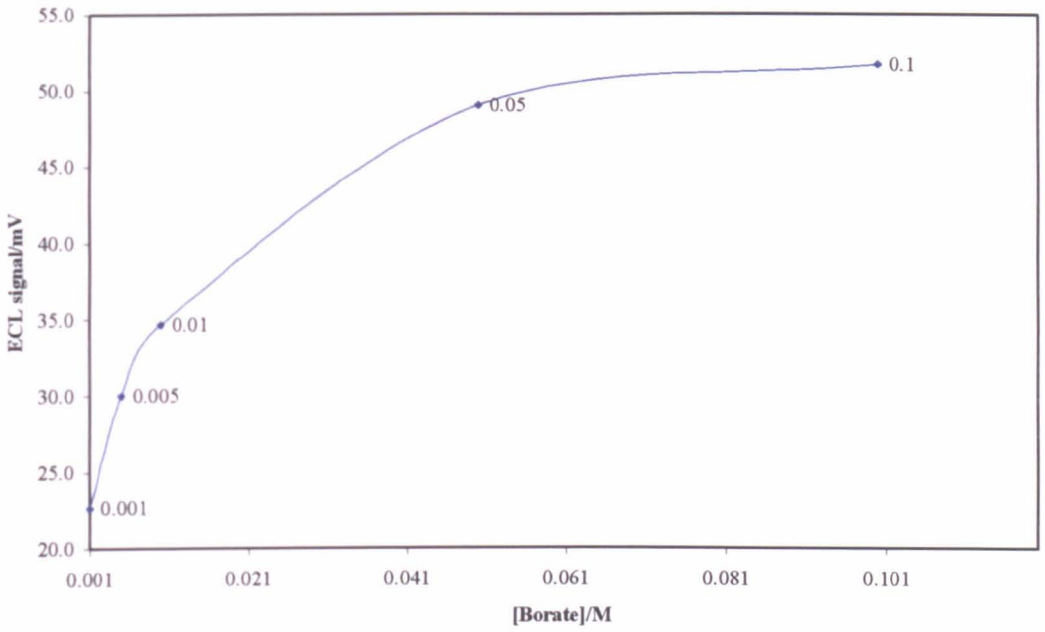

Figure 4.7: The effect of buffer concentration of the ECL emission of $Ru(bpy)_3^{2+}$ entrapped within a Nafion/sol-gel composite film (see Table 4.1); with the buffer containing atropine at a concentration of $1x10^{-3}$ M.

As with previous studies (see section 3.3.2) the buffer concentration giving the highest ECL signal was found to be 0.1 M, although 0.05 M was practically identical with a difference in average ECL emission signal of only 0.3 mV (less than 1%). Interestingly, as with the buffer pH (Figure 4.6), the ECL signal also diminished rapidly at the buffer concentration providing the highest ECL signal, *i.e.* 0.1 and 0.05 M, as shown in Figure 4.8.

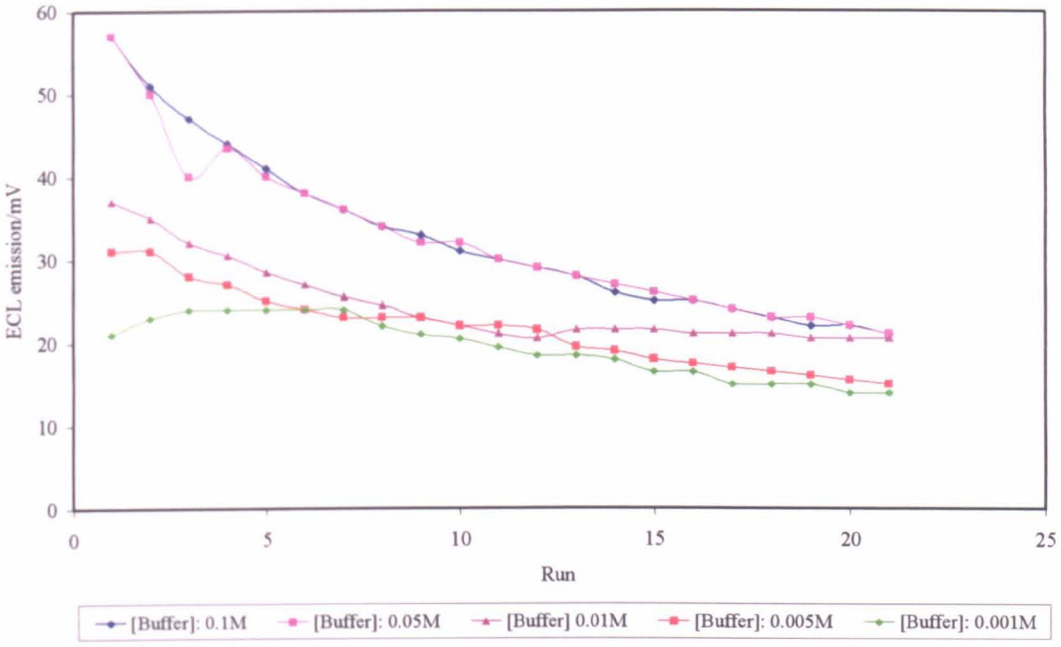

Figure 4.8: A continuation of the results shown in Figure 4.7, that demonstrate the drop in ECL signal seen at each buffer concentration for the $Ru(bpy)_3^{2+}$/Atriopin reaction over a twenty one run cycle; clearly demonstrating the lack of reproducibility with the sol-gel/Nafion system at this point in the investigation.

Given that the analysis of both buffer pH and concentration showed a lack of signal reproducibility in the areas of highest ECL signal a study was required to ascertain the reason for this loss. One possibility is that the silica coating was destroyed by the high pH of the solutions but this dramatic change had not been seen in the previous studies when the $Ru(bpy)_3^{2+}$ was in solution. It was also of interest to see if the drop in ECL signal was due to reagent leaching.

Figure 4.9 presents the findings of work undertaken to establish if a Nafion containing sol-gel coating prevented the entrapped $Ru(bpy)_3^{2+}$ from leaching into the bulk solution. In this work two $Ru(bpy)_3^{2+}$ encapsulating sol-gel coated electrodes

were immersed in 5 ml of pH 6.4 (0.1 M) phosphate buffer solutions for forty minutes, with fluorescence testing being performed on each solution at five minute intervals.

This work was performed as a comparison study between two near identical sol-gel coated electrodes, both fabricated from 1.6 ml TMOS, 1ml deionised water, 50 µl HCl (0.1 M), 1 mg ITO, and $1x10^{-3}$ M/l $Ru(bpy)_3^{2+}$. However one of the sol-gel solutions contained 1.2 ml of Nafion added to the sol-gel solution after early hydrolysis had been observed. Due to the nature of the experiment the coated electrodes were treated in the same was as those used during the normal ECL work, *i.e.* immersed in phosphate buffer prior to use to allow condensation. Therefore fluorescence data resolved in this study should be able to confirm the effectiveness of the Nafion/sol-gel coating as used in the ECL studies.

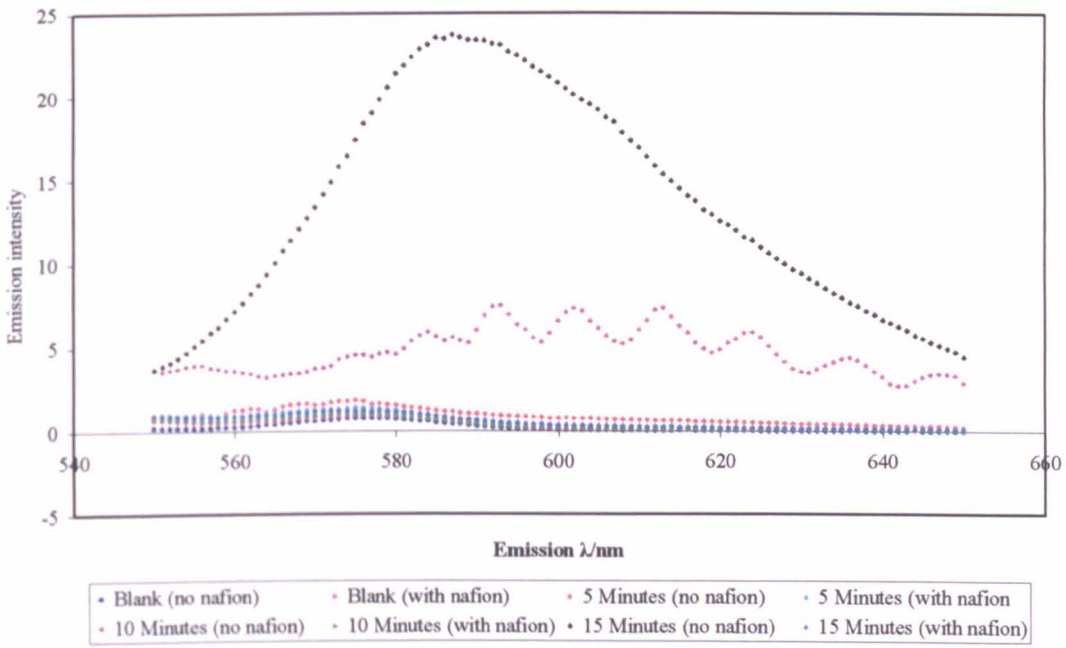

Figure 4.9: Fluorescence data obtained from the buffer solutions of two $Ru(bpy)_3^{2+}$ entrapped sol-gel coated electrodes ($1x10^{-3}$ M), differing only in that one coating

contained Nafion.. The study being performed in order to establish if Nafion prevented leaching.

Figure 4.9 clearly shows a difference in fluorescence levels between the two buffer solutions; with the solution for the Nafion free electrode providing the largest fluorescent intensity. This suggests that the $Ru(bpy)_3^{2+}$ leached into the buffer solution from the electrode; the gradual rise in luminescent intensity over time further strengthens this theory. By comparison the luminescent intensity obtained from the Nafion/sol gel coated electrode rose only slightly over the time period shown. In fact, although not demonstrated here in order to avoid graphical confusion, this study was carried out over a period of 40 minutes. Over this time period the luminescent intensity for both solutions diminished slightly, possibly due to photo bleaching; however this change was very slight in the solution for the Nafion/sol-gel electrode. Nevertheless, Figure 4.9 clearly shows a difference in luminescent intensity between the two test groups, signifying that the inclusion of Nafion within the sol-gel coating prevents or at least greatly retards the leaching of $Ru(bpy)_3^{2+}$ into the bulk solution. This theory is also is backed up through studies by Collinson *et al.* [44] and Kim *et al.* [42] amongst others, who have used Nafion to selectively entrap $Ru(bpy)_3^{2+}$ either on its own or as performed here in conjunction with a sol-gel.

Another factor that should be considered in this work is whether there is any interaction between ITO and $Ru(bpy)_3^{2+}$ when incorporating both into the sol gel. To investigate the effect of the addition of ITO into the sol-gel with entrapped $Ru(bpy)_3^{2+}$, two $Ru(bpy)_3^{2+}$ encapsulating sol-gel monoliths were fabricated with the

only variation being that one contained 1 mg of nano particle ITO within its standard sol-gel based matrix (as discussed in Chapter 2).

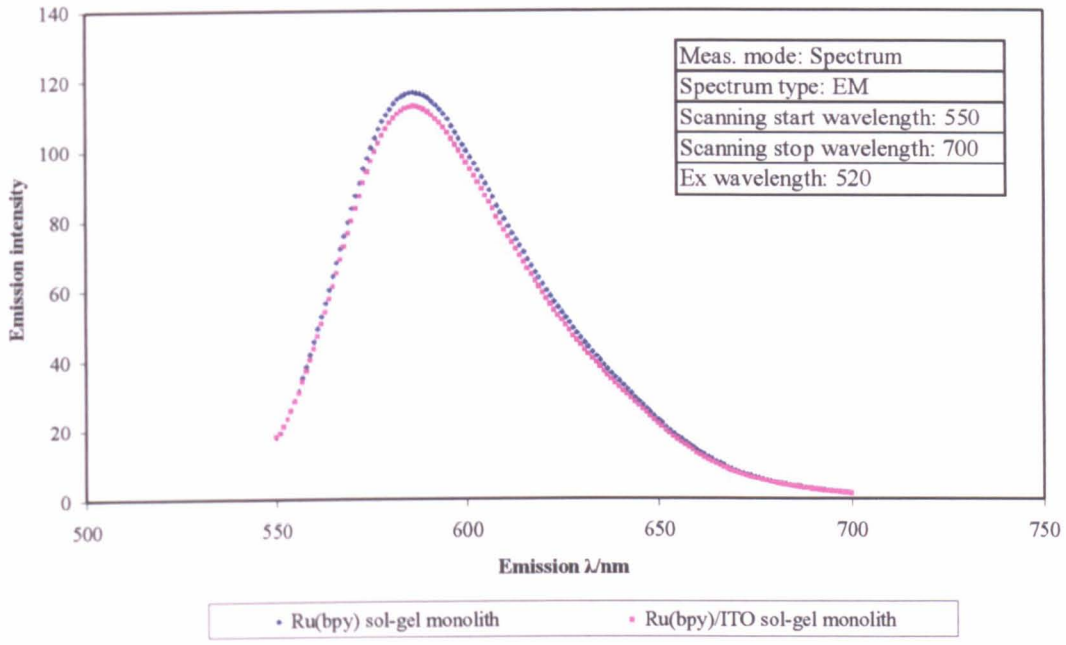

Figure 4.10: Study examining the effect of ITO on the luminescent emission of sol-gel encapsulated $Ru(bpy)_3^{2+}$ ($1x10^{-3}$ M).

Figure 4.10 demonstrated that the ITO particles had little effect on the luminescent emission wavelength or intensity obtained from the encapsulated $Ru(bpy)_3^{2+}$. In fact only a slight drop in intensity was found, which can be readily accountable to light scattering caused by the ITO, a phenomenon previously witnessed in earlier studies and discussed in section 2.3.6.

Returning to the issue of the rapid decrease in the ECL signal as it has been proved that it is not a leaching effect or due to the sol gel film being destroyed by the high pH (as this would happen more slowly) another explanation is required. Studies by

other groups, Collinson and Bard for example [44, 45], have shown that Nafion can slow diffusion of analytes within the film and may also form hydrophobic partitions due to the preferential incorporation of hydrophobic organic cations [38] as discussed later. This is another possible explanation for the drops in signal that have been reported in this section, although the effect of pH cannot be ignored.

If it is accepted that the Nafion produces a sluggish diffusion of analyte through the Nafion film, then the findings shown in Figures 4.6 to 4.8 are logical as the analyte would be used up more quickly in the more efficient ECL regimes, thus putting more demands on any diffusing analyte. This would be difficult to prove as it is affected by other factors such as the ITO and $Ru(bpy)_3^{2+}$ concentration; for example ITO could affect the porosity of the sol-gel matrix which may also limit the analyte diffusion. Therefore in order to demonstrate the problem of reagent diffusion it was decided to initially try to establish the optimum levels for $Ru(bpy)_3^{2+}$ and ITO within the sol-gel. As diffusion effects were being considered then it was also necessary to include a resting time in between ECL cycles, therefore a 60 second gap was introduced based on previous results.

Figure 4.11 shows the effect of ITO concentration on the ECL emission using a $Ru(bpy)_3^{2+}$ encapsulating sol-gel/Nafion electrode coating. This study had a dual purpose; firstly it reaffirmed the beneficial effects of introducing ITO on electro-conductance of the sol-gel matrix but it also provided a means to calibrate the optimum level of ITO within the sol-gel with regards to ECL emission.

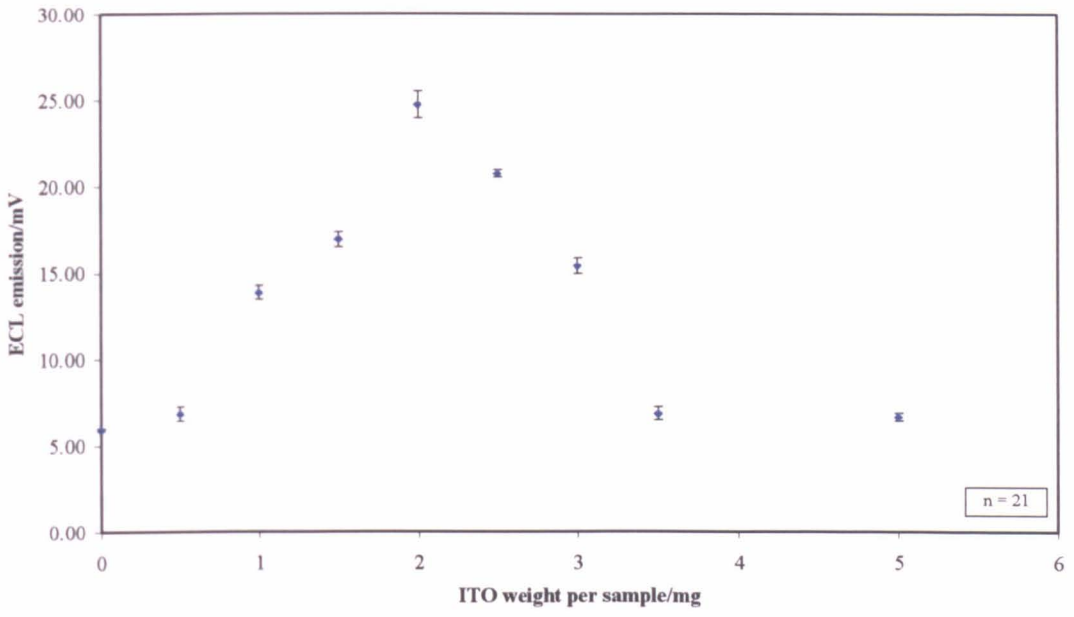

Figure 4.11: The effect of ITO concentration on the ECL emission of a $Ru(bpy)_3^{2+}$ encapsulating sol-gel/Nafion electrode coating using an atropine (borate buffer) based system with a concentration of $1x10^{-3}$ M.

Figure 4.11 shows the optimum level of ITO within the sol-gel coating; although it should be noted that this is with reference to the amount of ITO added to the initial sol-gel solution, which had a sample volume of 3.85 ml. Obviously it would be practically impossible to ascertain the level of ITO on the electrode given the low levels of ITO used in the solution and the miniscule amount of solution used for the coating. However the optimum level of ITO in solution that provided the highest ECL emission was found to be 2 mg (approx $1.8x10^{-8}$ M), beyond this level the signal dropped. It is felt that beyond the level of 2 mg the scattering caused by the ITO was greater than any possible improvements to the electro-conductance of the sol-gel, and ultimately ECL emission. This study emphasised the beneficial effects of the hybrid ITO/sol-gel especially as the sol-gel coating would also help to prevent

electrode fouling, an important aspect in the development of electro-analytical sensors.

Having ascertained the optimum level of ITO concentration, the effect of $Ru(bpy)_3^{2+}$ concentration was investigated. In this study a number of sol-gels were fabricated with concentrations of encapsulated $Ru(bpy)_3^{2+}$ ranging from 1×10^{-4} to 5×10^{-3} M Each sol-gel also contained the optimum ITO concentration as previously established (Figure 4.11). As with the ITO study discussed previously, a resting time of 60 seconds was also applied between pulses in an attempt to allow analyte diffusion within the electrode coating. As can be seen in Figure 4.12 the optimum concentration of $Ru(bpy)_3^{2+}$ within the sol-gel coating was found to be 2.5×10^{-3} M. Beyond this level the ECL signal diminished, which is almost certainly due to quenching occurring within the coating due to the emitted light being reabsorbed by $Ru(bpy)_3^{2+}$. This quenching should occur at all $Ru(bpy)_3^{2+}$ concentrations, however beyond 2.5×10^{-3} M any gains in possible generated ECL signal are offset with an increased incidence of quenching, therefore reducing the observed ECL.

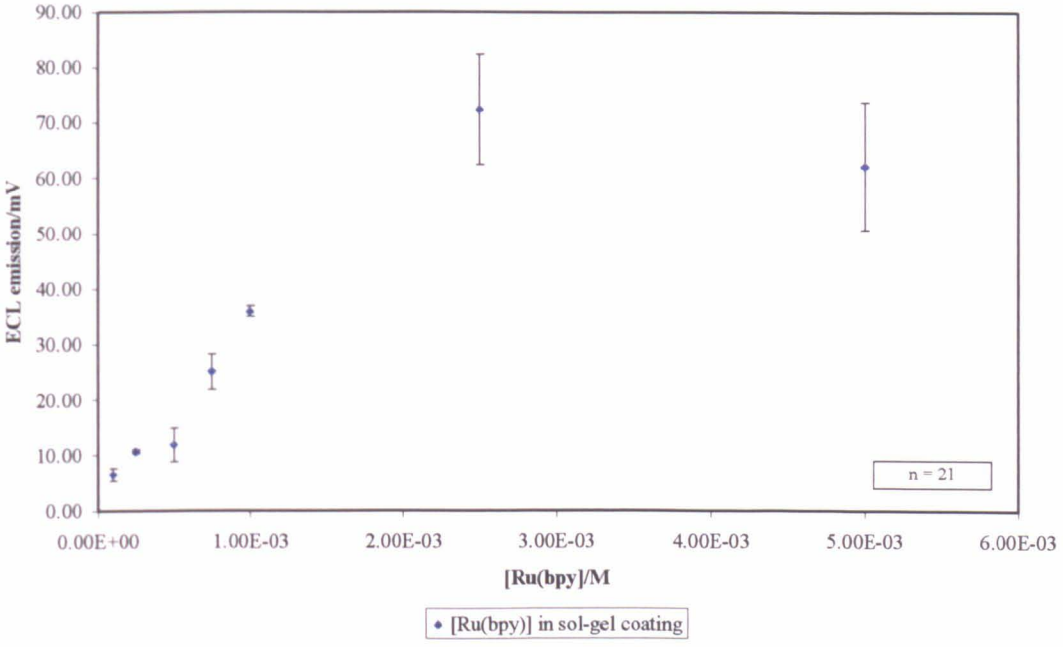

Figure 4.12: The effects of sol-gel encapsulated $Ru(bpy)_3^{2+}$ concentration on the CA derived ECL emission using a borate buffer based atropine solution; with the borate buffer composition being pH 11 (0.1 m) with an atropine concentration of $1x10^{-3}$ M

Another point of interest in Figure 4.12 is that the standard deviation for the ECL emission is greater at the higher $Ru(bpy)_3^{2+}$ concentrations (*i.e.* $2.5x10^{-3}$ and $5x10^{-3}$ M). As shown previously this standard deviation is actually caused by a steady drop in the ECL signal. Figure 4.13; further reinforcing the theory that the drop in ECL signal is due to reduced analyte diffusion by showing the full data for each $Ru(bpy)_3^{2+}$ concentration, where a greater drop in signal at the higher $Ru(bpy)_3^{2+}$ concentration is observed. This is expected given that the higher ECL emission would place an elevated demand on the analyte which in turn would create a greater demand for analyte replacement. From the two studies it is clear the optimum concentrations for $Ru(bpy)_3^{2+}$ and ITO within the sol-gel coating are $2.5x10^{-3}$ M and 2mg respectively; therefore unless otherwise stated, all further studies will use these concentrations for the sol-gel coating

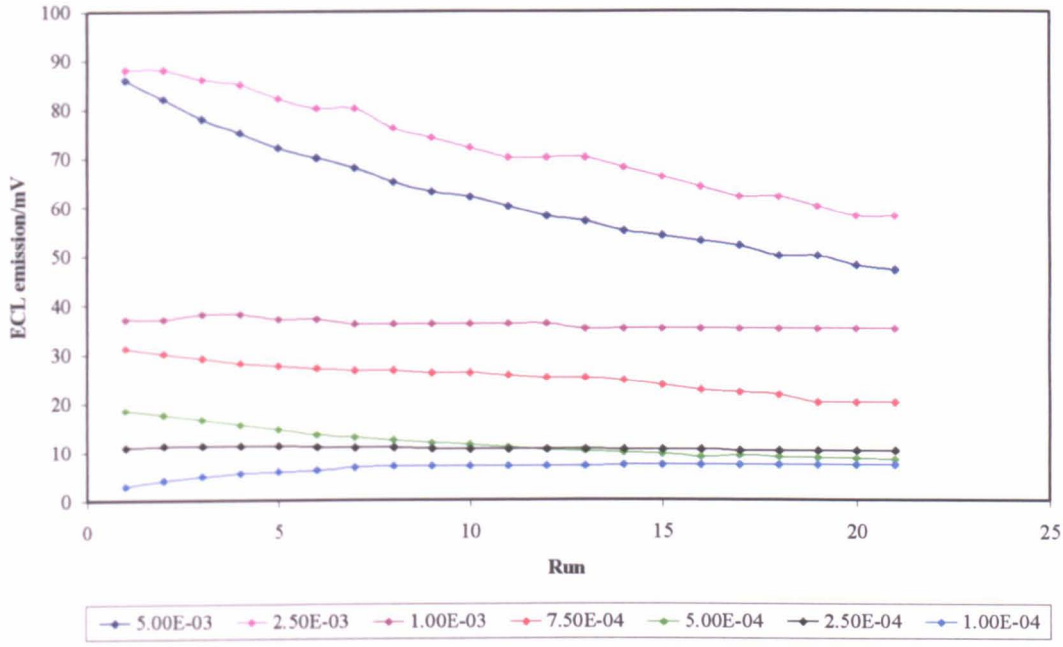

Figure 4.13: A continuation of Figure 4.12, showing the ECL emission for each $Ru(bpy)_3^{2+}$ concentration over a 21 run cycle; please note that at the higher ECL signals generated at the elevated $Ru(bpy)_3^{2+}$ concentrations lack signal stability.

Once the optimum concentrations for $Ru(bpy)_3^{2+}$ and ITO had been obtained, the electrode resting time could be studied in more depth. In the chronoamperometric method used to make the measurements (Chapter 3) a step-wise instruction set is used to guide electrical potential levels, the duration of these applied potentials and also their relative time in comparison to the other steps. It is therefore possible to change the resting time (duration between the applications of the electrical potential) to investigate the electrode process further. In section 3.3.1; a sixty second rest time was selected between applied electrical pulses when using solution based $Ru(bpy)_3^{2+}$ for the analysis of atropine. Figure 4.12 clearly demonstrates that this in not sufficient when using the $Ru(bpy)_3^{2+}$/Nafion encapsulation method, given the drop in the ECL signal. The effect of changes to the resting time were therefore investigated as shown in Figure 4.14, using the parameters set out in Table 4.2.

Step	Potential/V	Time/s
1	0	1.5
2	1.15	1
3	-1	2.5
4	0	Variable
5	1.15	1
6	-1	2.5
7	0	Variable
8	1.15	1
9	-1	2.5
10	0	10

Table 4.2: Experimental parameters for the chrono-amperometric application of electrical potential used to ascertain the effects of resting time on the stability of ECL emission signal generated from the $Ru(bpy)_3^{2+}$ encapsulating sol-gel/Nafion electrode coating.

The effects of changing the resting time between the chrono-amperometric pulses are shown in Figure 4.14. Although extending the time between pulses appears to stabilise the ECL emission, a clear downward trend in ECL emission is still seen. With regards to resting time it was felt that the optimum time between pulses was 150 seconds; beyond this the improvement in ECL signal was small and required the electrode to be immersed in the borate solution longer.

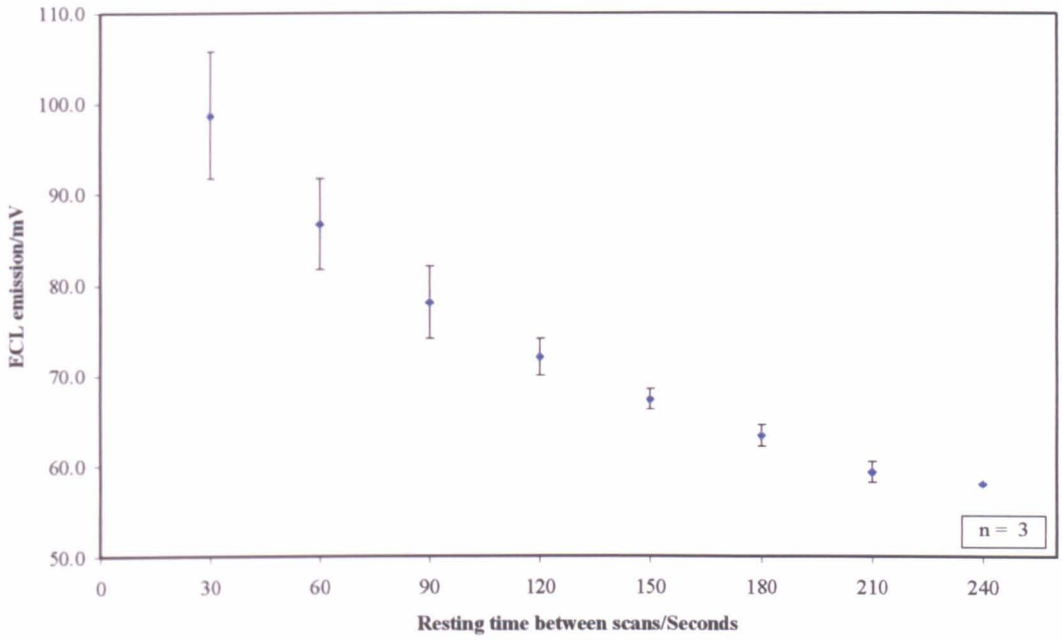

Figure 4.14: The effects of changing the resting time between the chrono-amperometric pulses on the stability of the ECL signal in the $Ru(bpy)_3^{2+}$/atropine reaction ($2.5x10^{-3}$ M and $1x10^{-3}$ M respectively); refer to Table 4.2 for CA set-up.

Finally to end this study Figure 4.15 shows the results of a further stability test with $1x10^{-3}$ M of $Ru(bpy)_3^{2+}$ using the same parameters as shown in Table 2 but incorporating a 240 second resting time. In this study the sol-gel coating contained the same concentration of $Ru(bpy)_3^{2+}$ as used in the leaching studies (Figure 4.9) that was shown to successfully prevent leaching. It can be seen in Figure 4.15 that small but steady drop in ECL signal is observed, comparable to that shown in Figure 4.13. Although this is not conclusive, in conjunction with the leaching studies performed previously it suggests that leaching is an unlikely cause of the drop in signal when using a $Ru(bpy)_3^{2+}$ encapsulating sol-gel/Nafion coating.

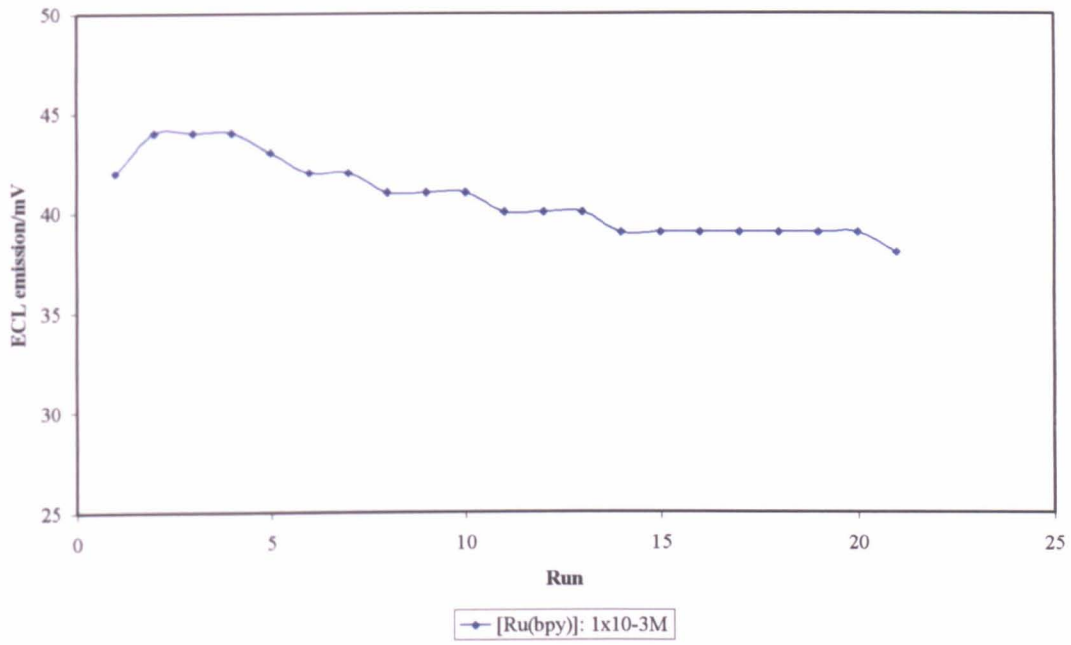

Figure 4.15: Further stability study using the $Ru(bpy)_3^{2+}$/atropine system (both reagents $1x10^{-3}$ M), with the $Ru(bpy)_3^{2+}$ encapsulated within the sol-gel coating, please note that as with Figure 4.14 a gradual drop in ECL signal is observed, even though 240 seconds of resting time are used.

4.3.2.2 Discussion and conclusion to study incorporating Nafion into matrix

This study appears to demonstrate that the Nafion does prevent leaching; however there is still a drop in ECL signal which is difficult to explain. As the drop in signal occurs at high pH values an obvious explanation could be deterioration of the sol-gel coating. These sol-gel coatings are generally regarded to be essential inert and highly chemically resistant [21, 46]. However they can be damaged mechanically and also by highly alkaline solutions (Figure 4.16), which act upon the sol-gel *via* hydrolysis or alcoholysis reactions to break it down to its original subunits (see section 1.2.3 for a more in depth explanation). However observations with sol-gel coated glass vials,

suggested that this breakdown was difficult to achieve because the buffer solutions are too weak with regards to both pH and concentration. It was found when immersing the sol-gel coated vials in 2 M sodium hydroxide that it still took many hours for the sol-gel to be destroyed. When considering this, it would seem unlikely that the analyte (buffer) solution used in this work, which has both a lower pH and concentration, would have such a rapid effect on the sol-gel coating as to account for the loss in ECL signal. In addition, the same borate buffer solution was used for the analysis of atropine in the solution based $Ru(bpy)_3^{2+}$ studies discussed in section 3.3.2; however the studies in section 3.3.2 did not suffer from the adverse effects discussed here. A further possibility is that the sol-gel is being stripped or falling from the electrode surface due to an adhesion problem, however again this situation was not noted in section 3.3.2 with near identical experimental parameters. Of course the addition of the $Ru(bpy)_3^{2+}$ and Nafion to the sol-gel may affect its mechanical stability.

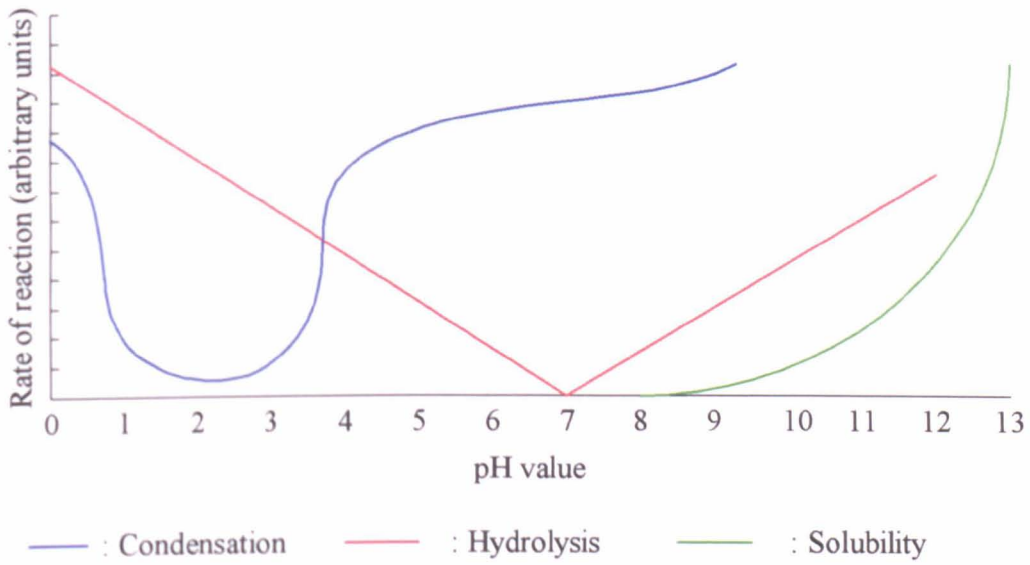

Figure 4.16: pH dependence on the solubility of silica and the reaction rates for hydrolysis and condensation.

Another possible explanation for this drop in signal is due to the previously established problem of Nafion forming hydrophobic partitions within the sol-gel matrix which may prevent analyte interaction; as suggested by Szentirmay and Martin [38]. The strong hydrophobic reaction is due to an interaction between bipyridyl ligands and the polytetrafluoroethylene backbone of the Nafion resin (see Figure 4.5) [47]. If hydrophobic partitioning is the reason for this drop in ECL signal, then any additional variation in resting time will have no effect in preventing this signal reduction.

The result determined in this section, and those established in the previous Chapters have helped to ascertain the optimum parameters for the development of the ITO/$Ru(bpy)_3^{2+}$ encapsulating sol-gel coating and also generation of the ECL signal. Using these settings, *i.e.* a sol-gel coating entrapping with 1.2 ml Nafion, 2 mg ITO and $2.5x10^{-3}$ M $Ru(bpy)_3^{2+}$ with a pulse resting time of 150 seconds, it was possible to establish a concentration calibration for atropine. Figure 4.17 demonstrates this calibration which clearly has two portions, a separate insert that demonstrates excellent sensitivity and linearity at the lower atropine concentrations. The reason for the poor sensitivity at higher concentrations is not clear. However this lack of calibration linearity could suggest that an insufficient number of $Ru(bpy)_3^{2+}$ sites are available for reaction at higher analyte concentrations.

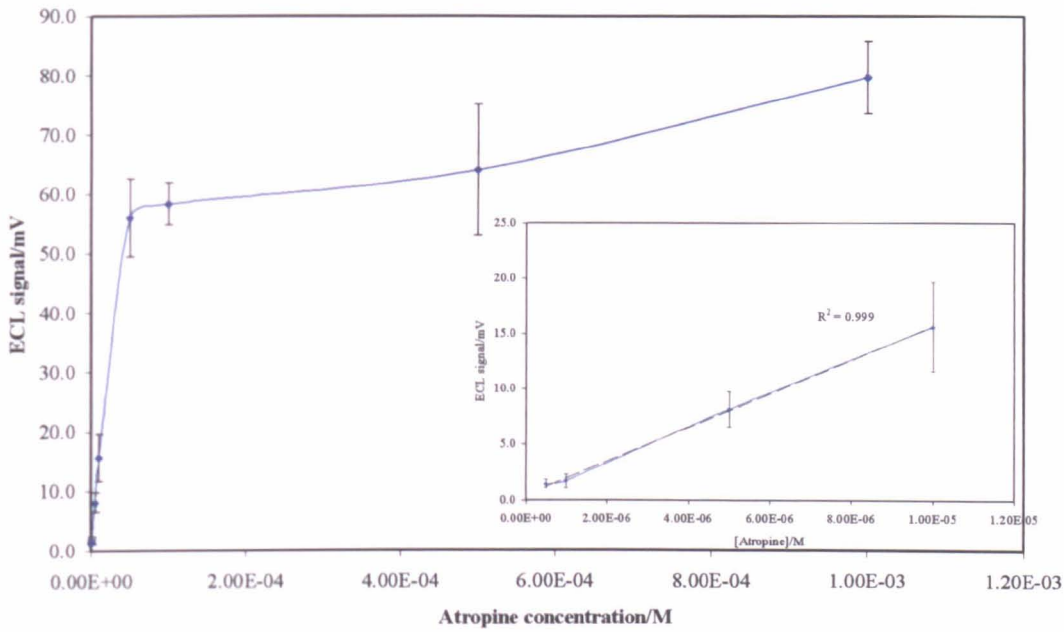

Figure 4.17: Calibration graph for atropine concentration using the optimum settings previously established. **Insert**: The results from the lower atropine concentrations showing a linear rise in ECL signal.

As can be seen from the error bars the drop in ECL signal is greatly reduced over that seen in previous studies, such as the resting time analysis (Figure 4.14) and the study to evaluate the effects of $Ru(bpy)_3^{2+}$ and ITO concentration (Figures 4.11 & 4.12). However a slight drop in signal is still apparent, which is believed to be due to a Nafion effect, either through the formation of a hydrophobic region(s) within the sol-gel or through some other effect which is stopping or reducing the efficiency of the ECL reaction.

To conclude this section it seems clear from the result shown (specifically Figure 4.11), that the hybrid ITO/sol-gel material discussed in section 3.3.4 and used here in an adapted form enhances the ECL emission of the sol-gel entrapped $Ru(bpy)_3^{2+}$. The calibration shown in Figure 4.11 noticeably demonstrates an improvement in ECL

signal in line with an increase in ITO concentration within the sol-gel coating. In conjunction with the excellent results discussed in Chapter 3, this work strengthens the case of using this materiel as an electrode coating, the Nafion issue withstanding.

4.3.3 The covalent attachment of a tris (2,2'-bipyridyl) ruthenium derivative to a tetramethoxysilane based sol-gel coating

Given the success of the hybrid ITO/sol-gel material a method was sort to overcome the issues presented by the use of Nafion. As mentioned previously, the hydrophobic partitioning is a known and inherent effect of Nafion [38]; therefore methods of replacing Nafion were investigated. Other methods reported for trapping $Ru(bpy)_3^{2+}$ include the use of organically modified silicates (ORMOSILs) [5], and covalently bonded anchor molecules such as dextran [17] (section 4,1).

It was therefore decided to investigate covalently bonding $Ru(bpy)_3^{2+}$ to the sol-gel matrix which would prevent reagent leaching and also allow the removal of Nafion from the sol-gel matrix.

In a collaboration with Dr C. Wiles (University of Hull), a $Ru(bpy)_3^{2+}$ derivative was synthesised containing hydrolysable linkers that allowed the covalent attachment of the $Ru(bpy)_3^{2+}$ derivative to a sol-gel matrix. In addition to this preventing leaching, it was envisaged that this derivative, 4,4'-bis[(3-triethoxysilylpropyl)amide]-2,2'-bipyridine]bis(2,2'-bipyridine)ruthenium(II) dichloride (Figure 4.18) would also be able to bond with other silica systems. Such as glass coils, micro channels and

optical fibres; that could be used for both chemiluminescent (CL) and electro-generated chemiluminescent techniques.

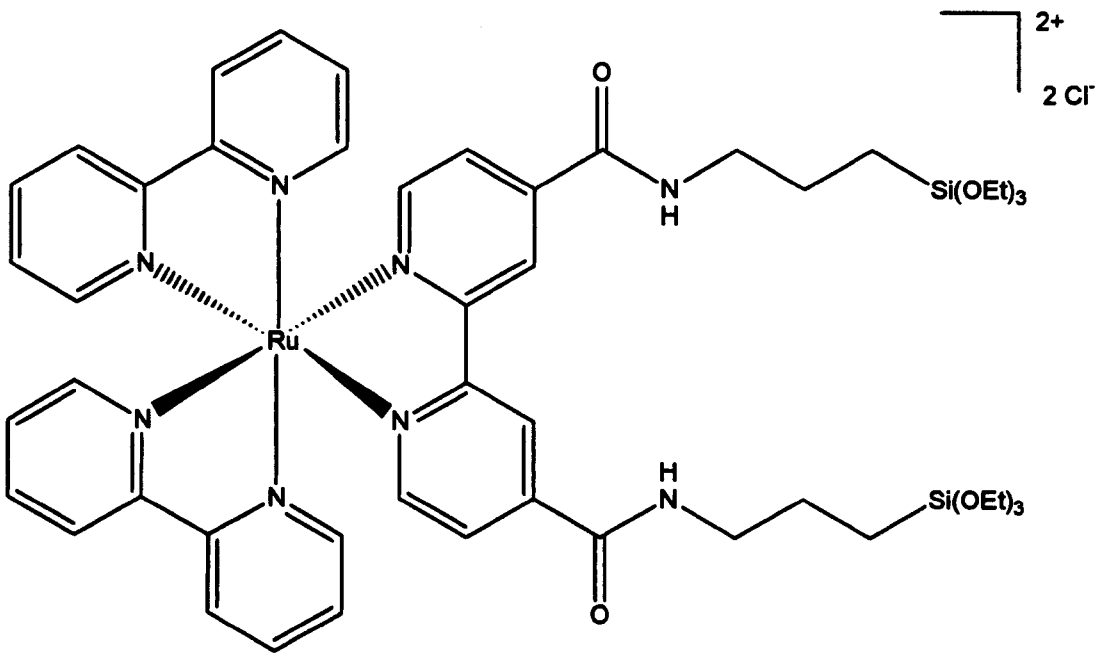

Figure 4.18: The chemical structure of 4,4'-bis[(3-triethoxysilylpropyl)amide]-2,2'-bipyridine]bis(2,2'-bipyridine)ruthenium(II) dichloride, the $Ru(bpy)_3^{2+}$ derivative synthesised for this work.

The $Ru(bpy)_3^{2+}$ derivative shown in Figure 4.18 could be covalently bonded to silica through the hydrolysis of the triethoxysilane moieties shown on the two extending ligands. The following sections discuss the evaluation of this ruthenium derivative by analysis its chemiluminescent, binding and electro-generated chemiluminescent properties.

The ruthenium derivative was initially investigated through chemiluminescent studies whilst covalently bonded to control pore glass (CPG), as described in section 4.2.4 (Figure 4.19).

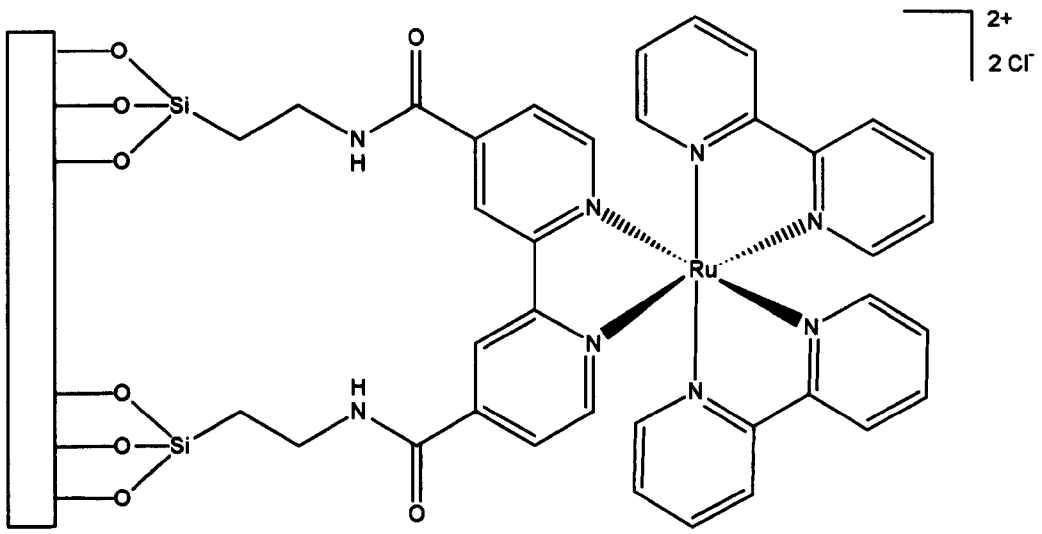

Figure 4.19: Schematic illustrating the covalent immobilisation of a tris(2,2'-bipyridyl)ruthenium(II) complex onto a silica surface.

The functionalised CPG (0.050 g, 1.305 x 10^{-3} mmol Ru) was packed into a flow cell (Figure 4.1) and its response to codeine (1 x 10^{-3} mmol) evaluated using sequential injection analysis (SIA) (Table 4.3).

Reagent	Plug volume/ml*
Cerium (VI) sulfate in H_2SO_4 (pH 1, 0.1 M)	0.40 (10)
Air gap	0.20 (5)
Codeine in deionised water (1 x 10^{-3} M)	0.40 (10)
Air gap	0.20 (5)
Deionesed water	1.00 (25)
Air gap	0.20 (5)
* Time intervals (sec) employed to obtain desired plug volume	

Table 4.3: SIA parameters employed for the CL evaluation of functionalised CPG.

Using cerium (VI) sulfate (0.1 M in 1.0 M sulfuric acid) as the oxidising agent, it was possible to confirm the successful immobilisation of a CL reagent to CPG and its application to the detection of codeine, whereby an average signal of 35.5 mV

was obtained (RSD = 2.98 %). In addition no reagent leaching was apparent from the CPG, a point that is backed-up with the reproducibility of the chemiluminescent results.

Having successfully demonstrated the covalent immobilisation of the tris(2,2'-bipyridyl)ruthenium(II) derivative to CPG and its chemiluminescent ability, the investigation was extended to evaluate its incorporation into a silicate sol-gel, which if successful would enable the fabrication of a regenerable ECL sensor. The sol-gels were prepared *via* the acid catalysed hydrolysis reaction of TMOS and the ruthenium derivative followed by base catalysed gelation, as discussed in section 4.2.4. With respect to monolith fabrication, gelation was induced by the addition of aq. NaOH with the resulting sol-gel cured in a dessicator for 24 hrs, to afford an orange translucent glassy material. In order to confirm the covalent attachment of the tris(2,2'-bipyridyl)ruthenium(II) dichloride hexahydrate derivative in to the sol-gel matrix, monoliths were prepared and stored in a range of commonly used solvent systems The solvents investigated were borate buffer (pH 8.5), phosphate buffer (pH 7.0), aq. sulfuric acid (0.01 M) and acetonitrile; in all cases no leaching has been observed over a period of a year.

In comparison, coated electrodes were prepared by dipping glassy carbon electrodes into the hydrolysed solution and withdrawing slowly, to leave a thin film; gelation was subsequently induced by placing the electrode in borate buffer for a period of 24 hrs in order to age the film, as discussed in section 4.2.4. Results were obtained using the experimental set-up as discussed in section 4.2.4, in conjunction with the following operating conditions; sample volume 5 ml, 1 x 10^{-3} M codeine in deionised

water, voltage range 0.7 to 1.3 V, step potential 0.0024 V and a scan rate of 0.01 V s-1 (5 cycles). Under these conditions an ECL signal was observed; but as with previous studies a drop in ECL signal was seen between scans due to the scan speed being quicker that the atropine diffusion. A chrono-amperometric setting was not available on the equipment used in this work and it was decided to evaluate this reproducibility of the coating using cyclic voltammetry in single scan mode with a long resting time between scans (9 minutes).

When employing $Ru(bpy)_3^{2+}$ doped silicate sol-gel films (both with and without Nafion), irreproducible ECL signals were obtained; demonstrating an overall trend of decreasing signal with time. This observation was attributed to leaching of the CL reagent and specific Nafion effects (see sections 4.3.1 & 4.3.2) However, by covalently immobilising the derivatised $Ru(bpy)_3^{2+}$ reagent within a silicate sol-gel, reproducible ECL signals of 7.7 mV (SD = 0.09mV, % RSD = 1.12, n = 22) were obtained (as shown in Figure 4.21). Although the ECL signals obtained are relatively small compared to those reported for both the functionalised CPG and also the Nafion encapsulated $Ru(bpy)_3^{2+}$, by incorporating a greater proportion of ruthenium derivative into the silicate sol-gels, larger signals would be attainable and possibly lower limits of detection.

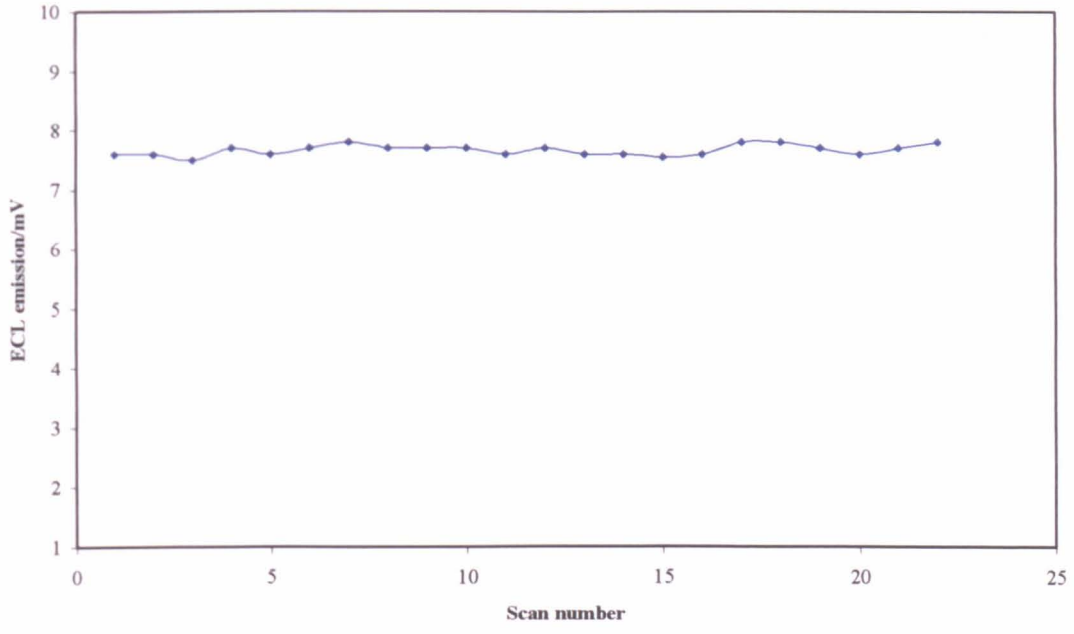

Figure 4.21: Graph showing the analysis of codeine using sol-gel electrode functionalised with $Ru(bpy)_3^{2+}$ derivative.

In summary, compared to the physical entrapment of CL reagents in silicate sol-gels, covalent immobilisation is advantageous as it ensures homogeneous distribution of the reagent within the matrix and improves reproducibility and extends sensor lifetime; whilst preventing reagent leaching and reduced analysis costs. Further investigations were not possible in the time scale of this PhD.

4.4 Conclusions

Previous chapters have discussed the fabrication and attributes of novel conducting sol-gels, both monolithic and also thin film varieties; as both a stand alone conducting material and also as an electrode coating. In conclusion in this work the sol-gel coating was further developed through the entrapment of tris(2,2'-bipyridyl)ruthenium(II) dichloride hexahydrate within the sol-gel matrix in order to allow the development of an ECL sensor for tertiary amine containing drugs of abuse.

Initially this entrapment was attempted through the direct mixing of $Ru(bpy)_3^{2+}$ within the sol-gel solution; however this was found to be unacceptable as the sol-gel coating was not able to prevent the $Ru(bpy)_3^{2+}$ from leaching from within. This was demonstrated through both a steady reduction in ECL signal and also spectrofluorimetric analysis of the bulk analyte solutions. It was therefore concluded that the sol-gel coating on its own was unable to entrap $Ru(bpy)_3^{2+}$ within its matrix and that further methods were needed. The methods studied were the encapsulation of a Nafion ion exchange resin within the sol-gel matrix and the development of a $Ru(bpy)_3^{2+}$ derivative capable of covalently bonding to the sol-gel matrix.

With regards to Nafion it was found that although it prevented the problem of $Ru(bpy)_3^{2+}$ from leaching out of the sol-gel coating it also had an effect of reducing ECL signal over time. This reduction in signal is most likely due to hydrophobic partitioning, a previously established Nafion effect [38], which would reduce the diffusion efficiency of the aqueous based analyte. In addition, extended resting times were required between each electrochemical experiment compared to those

performed in Chapter 3; again this is believed to be due to the reduced diffusion efficiency. Through adaptation of the experimental set-up it was possible to establish concentration calibrations for both atropine and codeine. The effect of ITO concentration within the sol-gel coating was also investigated and this clearly demonstrated that its incorporation increased ECL emission. Once again this established the advantageous nature of this novel coating and builds on the excellent results discussed in the previous chapters.

This final investigation in this work involved the covalent attachment of a $Ru(bpy)_3^{2+}$ derivative to the sol-gel matrix. Due to the intrinsic time constraints in this PhD, this work was limited; however it demonstrated the derivatives excellent bonding capabilities and stability in a range of commonly used solvents. In contrast to the other entrapment techniques, no leaching or signal degradation was observed with covalent immobilisation, an advantage that would allow an increase in reproducibility and sensor lifetime. In addition this derivative was also successfully employed in both CL and ECL systems. Although the ECL signal was small compared to the previous studies, by incorporating a greater proportion of the derivative within the sol-gels, larger signals and hence lower limits of detection would be attainable. Additionally, this derivative could also be employed for the functionalisation of other silica substrates such as glass coils, micro channels and optical fibres, these investigations are currently underway within the University laboratories as a continuation of this study.

4.5 References

1. Gerardi, R.D., Barnett N.W., and Lewis S.W., *Analytical applications of tris(2,2'-bipyridyl)ruthenium (II) as a chemiluminescent reagent.* Analytica Chimica Acta, 1999. **378**: p. 1-41.
2. Richter, M.M., *Electrochemiluminescence (ECL).* Chemical review, 2004. **104**: p. 3003-3036.
3. Collinson, M.M. and Novak B., *Diffusion and reactivity of ruthenium (II) tris(bipyridine) and cobalt (II) tris(bipyridine) in organically modified silicates.* Journal of Sol-Gel Science and Technology, 2002. **23**(3): p. 215-220.
4. Choi, H.N., Cho S.H., Park Y.J., Lee D.W., and Lee W.Y., *Sol-gel-immobilized Tris(2,2 '-bipyridyl)ruthenium(II) electro-generated chemiluminescence sensor for high-performance liquid chromatography.* Analytica Chimica Acta, 2005. **541**(1-2): p. 49-56.
5. Yi, C.Q., Tao Y., Wang B., and Chen X., *Electrochemiluminescent determination of methamphetamine based on tris(2,2 '-bipyridine)ruthenium(II) ion-association in organically modified silicate films.* Analytica Chimica Acta, 2005. **541**(1-2): p. 75-83.
6. Wang, H., Xu G., and Dong S., *Electrochemiluminescence sensor using tris(2,2'-bipyridyl)ruthenium (II) immobilized in Eastman-AQ55D-silica composite thin-films.* Analytica Chimica Acta, 2003. **480**: p. 285-290.
7. Barnett, N.W., Bos R., Brand H., Jones P., Lim K.F., Purcell S.D., and Russell R.A., *Synthesis and preliminary analytical evaluation of the chemiluminescence from (4-[4-dichloromethylsilanyl)-butyl]--4'-methyl-2,2'-bipyridyl)ruthenium (II) covalently bonded to silica particles.* Analyst, 2002. **127**: p. 455-458.
8. Greenway, G.M., Greenwood A., Watts P., and Wiles C., *Solid-supported chemiluminescence and electro-generated chemiluminescence based on a tris(2,2 '-bipyridyl)ruthenium(II) derivative.* Chemical Communications, 2006(1): p. 85-87.
9. Butler, T.M., MacCraith B.D., and McDonagh C., *Leaching in sol-gel derived silica films for optical pH sensing.* Journal of Non-crystalline solids, 1998. **22**: p. 249-258.
10. Grattan, K.T.V., Badini G.E., Palmer A.W., and Tseung A.C.C., *Use of sol-gel techniques for fibre-optic sensor applications.* Sensors and Actuators A, 1991. **25-27**: p. 483-487.
11. Reetz, M.T., Zonta A., Simpelkamp J., and Konen W., *In-situ fixation of lipase-containing hydrophobic sol-gel materials on sintered glass - highly efficient heterogeneous biocatalysts.* Chemical communications, 1996: p. 1397.
12. Katz, E., Buckmann A.F., and Willner I., *Self-Powered enzyme-based biosensors.* Journal of the American Chemical Society, 2001. **123**: p. 10752-10753.
13. Avnir, D., *Organic chemistry within ceramic matrices: Doped sol-gel materials.* Acc. Chemical Res., 1995. **28**: p. 328-334.
14. Lan, E.H., Dave B.C., Fukuto J.M., Dunn B., Zink J.I., and Valentine J.S., *Synthesis of sol-gel encapsulated heme proteins with chemical sensing properties.* Journal of Materials Chemistry, 1999. **9**: p. 45-53.

15. Downey, T.M. and Nieman T.A., *Chemiluminescence Detection Using Regenerable Tris(2,2'-Bipyridyl)Ruthenium(Ii) Immobilized in Nafion.* Analytical Chemistry, 1992. **64**(3): p. 261-268.
16. Khramov, A.N. and Collinson M.M., *Electro-generated chemiluminescence of tris(2,2'-bipyridyl)ruthenium (II) ion-exchange in nafion-silica composite films.* Analytical Chemistry, 2000. **72**: p. 2943-2948.
17. Plaschke, M., Czolk R., Reichert J., and Ache H., *Stability improvement of optochemical sol-gel film sensors by immobilisation of dye labelled dextrans.* Thin solid films, 1996. **279**: p. 233-235.
18. Shultz, L.L., Stoyanoff J.S., and Nieman T.A., *Temporal and spatial analysis of electro-generated Ru(bpy)(3)(3+) chemiluminescent reactions in flowing streams.* Analytical Chemistry, 1996. **68**(2): p. 349-354.
19. Wang, H.Y., Xu G.B., and Dong S.J., *Electrochemiluminescence of tris(2,2 '-bipyridine)ruthenium(II) immobilized in poly(p-styrenesulfonate)-silica-Triton X-100 composite thin-films.* Analyst, 2001. **126**(7): p. 1095-1099.
20. Wang, H.Y., Xu G.B., and Dong S.J., *Electrochemiluminescence of tris(2,2 '-bipyridyl)ruthenium (II) ion-exchanged in polyelectrolyte-silica composite thin-films.* Electroanalysis, 2002. **14**(12): p. 853-857.
21. Collinson, M.M. and Howells A.R., *Sol-gels and Electrochemistry.* Analytical Chemistry, 2000: p. 702a-709a.
22. Collinson, M.M., *Recent trends in analytical applications of organically modified silicate materials.* Trends in Analytical Chemistry, 2002. **21**: p. 30-38.
23. Malins, C., Fanni S., Glever H.G., Vos J.G., and MacCraith B.D., *The preparation of a sol-gel glass oxygen sensor incorporating a covalently bound fluorescent dye.* Analytical Communications, 1999. **36**(1): p. 3-4.
24. Greenwood, P.A., *Chemiluminescence as a detection tool for miniaturised analytical systems.* 2003, University of Hull: Hull.
25. Song, Q., Greenway G.M., and McCreedy T., *Tris(2,2'-bipyridine)ruthenium(II) electro-generated chemiluminescence of alkaloid type drugs with solid phase extraction sample preparation.* Analyst, 2001. **126**: p. 37-40.
26. Greenway, G.M., Knight A.W., and Knight P.J., *Electro-generated chemiluminescent determination of codeine and related alkaloids and pharmaceuticals with tris(2,2'-bipyridine)ruthenium (II).* Analyst, 1995. **120**: p. 2549-2552.
27. Christensen, P.D., Johnson S.W.P., McCreedy T., Skelton V., and Wilson N.G., *The fabrication of micro-porous silica structures for micro-reactor technology.* Analytical Communications, 1998. **35**(10): p. 341-343.
28. Collinson, M.M. and Martin S.A., *Solid state electro-generated chemiluminescence in sol-gel derived monoliths.* Chemical communications, 1999: p. 899-900.
29. Collinson, M.M., Rausch C.G., and Voigt A., *Electroactivity of redox probes encapsulated within sol-gel derived silicate films.* Langmuir, 1997. **13**: p. 7245-7251.
30. McKenzie, K.J., Niedziolka J., Paddon C.A., Marken F., Rozniecka E., and Opallo M., *Hydrophobic silica sol-gel films for biphasic electrodes and porotrodes.* Analyst, 2004. **129**(12): p. 1181-1185.
31. Zhang, R., Li W., Liang X.Y., Wu G.P., Lu Y.G., Zhan L., Lu C.X., and Ling L.C., *Effect of hydrophobic group in polymer matrix on porosity of organic*

and carbon aerogels from sol-gel polymerization of phenolic resole and methylolated melamine. Microporous and Mesoporous Materials, 2003. **62**(1-2): p. 17-27.

32. Harreld, J.H., Ebina T., Tsubo N., and Stucky G., *Manipulation of pore size distributions in silica and ormosil gels dried under ambient pressure conditions.* Journal of Non-Crystalline Solids, 2002. **298**(2-3): p. 241-251.
33. Kistler, S.S., *Coherent Expanded-Aerogels.* Journal of Physical Chemistry, 1932. **36**(1): p. 52-64.
34. Smitha, B., Sridhar S., and Khan A.A., *Solid polymer electrolyte membranes for fuel cell applications - a review.* Journal of Membrane Science, 2005. **259**(1-2): p. 10-26.
35. Jannasch, P., *Recent developments in high-temperature proton conducting polymer electrolyte membranes.* Current Opinion in Colloid & Interface Science, 2003. **8**(1): p. 96-102.
36. Corma, A., *Solid acid catalysts.* Current Opinion in Solid State & Materials Science, 1997. **2**(1): p. 63-75.
37. Li, Y.Z., Li Z.M., Li F., Wang Q.R., and Tao F.G., *Preparation of a Nafion-Teflon bimembrane-supported palladium catalyst and its use in the Heck reaction.* Tetrahedron Letters, 2005. **46**(36): p. 6159-6162.
38. Szentirmay, M.N. and Martin C.R., *Ion-exchange selectivity of nafion films on electrode surfaces.* Analytical Chemistry, 1984. **56**: p. 1898-1902.
39. Coo, L.D. and Martinez I.S., *Nafion-based optical sensor for the determination of selenium in water samples.* Talanta, 2004. **64**(5): p. 1317-1322.
40. Amini, M.K., Momeni-Isfahani T., Khorasani J.H., and Pourhossein M., *Development of an optical chemical sensor based on 2-(5-bromo-2-pyridylazo)-5-(diethylamino)phenol in Nafion for determination of nickel ion.* Talanta, 2004. **63**(3): p. 713-720.
41. Liu, H.Y. and Deng J.Q., *Amperometric Glucose Sensor Using Tetrathiafulvalene in Nafion Gel as Electron Shuttle.* Analytica Chimica Acta, 1995. **300**(1-3): p. 65-70.
42. Kim, D.J., Lyu Y.K., Choi H.N., Min I.H., and Lee W.Y., *Nafion-stabilized magnetic nanoparticles (Fe3O4) for [Ru(bpy)(3)](2+) (bpy = bipyridine) electro-generated chemiluminescence sensor.* Chemical Communications, 2005. **23**: p. 2966-2968.
43. Ishiji, T., Kudo K., and Kaneko M., *Microenvironmental Studies of an Ru(Bpy)(3)(2+) Luminescent Probe Incorporated into Nafion Film and Its Application to an Oxygen Sensor.* Sensors and Actuators B-Chemical, 1994. **22**(3): p. 205-210.
44. Hsueh, C.C. and Collinson M.M., *Permselectivities and ion-exchange properties of organically modified sol-gel electrodes.* Journal of Electroanalytical Chemistry, 1997. **420**(1-2): p. 243-249.
45. Martin, C.R., Rubinstein I., and Bard A.J., *Polymer-Films on Electrodes .9. Electron and Mass-Transfer in Nafion Films Containing Ru(Bpy)32+.* Journal of the American Chemical Society, 1982. **104**(18): p. 4817-4824.
46. Brinker, C.J. and Scherer G.W., *Sol-gel science - The physics and chemistry of sol-gel processing.* 1990: Academic press.
47. HeitnerWirguin, C., *Recent advances in perfluorinated ionomer membranes: Structure, properties and applications.* Journal of Membrane Science, 1996. **120**(1): p. 1-33.

Chapter 5: Conclusions

5.0 Conclusions

This thesis describes the development of novel electro-conductive sol-gel materials through from its beginning as a conducting sol-gel monolith, to the development of a sensor suitable for *insitu* monitoring , *via* the immobilisation of $Ru(bpy)_3^{2+}$ within the matrix of a sol-gel electrode coating. Initial studies concentrated on developing a suitable methodology for the fabrication of sol-gel monoliths, by investigating precursor types, reaction routes, configurations and substrate materials. This work was performed in order that subsequent sol-gel monoliths would be transparent, robust and could be easily tested for both electrical conductance and optical transparency. This was successfully achieved using a tetramethoxysilane (TMOS) based two step acid/base catalysed route, with final gelation performed in a polystyrene cuvette. This system permitted the fabrication of cuboid sol-gel monoliths which allowed simple optical evaluation through normal spectrometry routes; it was also envisaged that it would allow easy conductivity measurements, however this latter proved more complex.

Having successfully developed a sol-gel fabrication protocol, work was undertaken to confer electrical conducting properties to this normally non-conducting material through the encapsulation of conducting moieties. Two type of electro-active dopants were studied, poly(3,4-ethylenedioxythiophene) (PEDOT) and indium tin oxide (ITO). PEDOT demonstrated favourable optical properties although it did not provide the required electro-conductance within the sol-gel and was subsequently abandoned. Four ITO types were investigated differing in indium to tin ratio and particle size. Issues regarding homogeneity within the sol-gel matrix coupled with the evaluation of In:Sn

ratios using ICP-MS ascertained that a commercially available nano-particle size ITO was best suited for the work undertaken. The other samples tested either fell out of the sol-gel solution (micro-particle size ITO) or demonstrated a In:Sn ratio outside the optimum range of 10 wt. % tin [1].

This knowledge together with the ability to produce cuboid sol-gels allowed the fabrication of monolithic sol-gels encapsulating varying amounts of ITO dopant. These sol-gels proved to be electro-conducting and provided good optical transparency, especially given that this material's subsequent use involved its application as a thin film electrode coating. Other benefits of this sol-gel/ITO system include its low cost of fabrication in terms of both materials and equipment, its configuration versatility (*i.e.* thin films, powders & monoliths) and ease of characterisation. In addition its mild fabrication conditions and porous nature meant that secondary sensing molecules such as electro and photo-active dyes [2, 3], proteins [4] and enzymes [5] could be added to the sol-gel matrix. The success of these results in proving that the sol-gel coat was electro conducting coupled with the optical properties permitted the development of an application for this novel electro-conducting material.

Subsequent development of this sol-gel/ITO material came in the form of an electrode coating applied to a glassy carbon working electrode through a dip coating technique; studies using platinum electrodes encountered problems with sol-gel adhesion. Blank sol-gel and sol-gel/ITO coatings were evaluated using electro-generated chemiluminescence (ECL) in a static electrochemical cell. The ECL reaction between

tris(2,2'-bipyridine)ruthenium (II) dichloride hexahydrate ($Ru(bpy)_3^{2+}$) and the tertiary amine containing drugs atropine and codeine was used to generate the ECL signal. The electrodes coated with a blank sol-gel and ITO doped sol-gels gave ECL increases of 132 % and 179 % respectively over non coated electrodes. This increase in ECL signal was thought to occur due to the formation of an advantageous conducting micro-environment within the sol-gel. It is also believed that this sol-gel coating would help to protect the electrode, helping to prevent electrode fouling; with the additional benefit that a damaged electrode coating could be easily removed and a new one reapplied. Ultimately the application of the ITO doped sol-gel coating has produced an improvement of ECL response over the bare electrode that due to the nature of the system could be utilised with other $Ru(bpy)_3^{2+}$ systems, and possibly other luminescent based systems *i.e.* CL systems.

In order to develop an *insitu* ECL sensor, the final part of this work investigated amalgamating the two previously separate systems through the immobilisation of $Ru(bpy)_3^{2+}$ within the ITO doped sol-gel matrix. Initial attempts tried to directly mix $Ru(bpy)_3^{2+}$ with the sol-gel solution; but drops in ECL signal coupled with spectrofluorimetric analysis suggested that the water soluble $Ru(bpy)_3^{2+}$ was leaching into the aqueous analyte solution. This system therefore needed to be further developed in order to prevent reagent leaching; two methods were examined, the encapsulation of a Nafion ion exchange resin within the sol-gel matrix and the development of a $Ru(bpy)_3^{2+}$ derivative capable of covalently bonding to the sol-gel matrix.

Although Nafion was found to prevent leaching it had the effects of reducing analyte diffusion within the sol-gel which extended analysis times; in addition steady reductions in ECL signal were observed throughout this work. These effects were believed to be due to the formation of hydrophobic partitions within the Nafion and hence the sol-gel matrix. This effect would reduce the diffusion efficiency of aqueous based analytes such as those used in this work. However a study into the effects of ITO on ECL emission within the sol-gel matrix clearly showed correlation between ITO concentration and ECL signal. The optimum concentration of ITO resulted in an ECL signal increase of approximately 500 %, an upper ITO concentration limit was discovered beyond which it is believed the light scattering from the ITO prevented increases in ECL signal. This clearly demonstrates the benefit of this novel electro–conducting sol-gel material for use as an electrode coating, especially given the ancillary benefits such as electrode protection. Further studies were also able to established concentration calibrations for both atropine and codeine.

The final work undertaken in this study involved the covalent immobilisation of a $Ru(bpy)_3^{2+}$ derivative, 4,4'-bis[(3-triethoxysilylpropyl)amide]-2,2'-bipyridine] bis-(2,2'-bipyridine)ruthenium(II) dichloride to two silica substrates, CPG and a silica based sol-gel. Chemiluminescent (CL) studies of this compound were carried out using the functionalised CPG packed into a flow cell and analysed using a codeine based CL system applied though sequential injection analysis. This system produced an average CL signal of 35.5 mV with a RSD = 2.98 %. For the ECL analysis a functionalised sol-gel was fabricated and coated on to a glassy carbon electrode through dip coating as with

the previous experiments. Using an aqueous based codeine solution ($1x10^{-3}M$) reproducible ECL signals of 7.7 mV (% RSD = 1.07, n = 24) were achieved, additionally, in analysis lasting over a year no leaching has been observed from functionalised sol-gel monoliths immersed in a range of commonly used solvents Although the ECL signal in this test was small it is felt that through the increased concentration of the $Ru(bpy)_3^{2+}$ derivative within the sol-gel an increased ECL signal could be developed. Compared to the other entrapment techniques examined in this work such as the use of Nafion, the lack of leaching and signal degradation observed with this technique; coupled with its ability to bond to a range of silica surfaces, would allow an increase in reproducibility, sensor lifetime and the range of suitable CL/ECL techniques.

In conclusion, this thesis has described the development of a novel electro-conductive sol-gel from its start as a conducting sol-gel monolith to its development as a sensor for *insitu* monitoring. It is hoped that the advantages of this material such as its ability to improve the ECL signal and prevent electrode fouling have been clearly defined. There was not time to complete the study and therefore some suggestions for further work are provided.

Future work would include the development of a sol-gel with both the covalently attached reagent and the ITO to improve the sensitivity. Different derivatives with more attachment points could also be investigated to optimise the loading of covalently

attached reagent in the sol-gel. Finally the new material would be utilised in a portable sensing system for a wide range of ECL applications.

5.1 References

1. Alam, M.J. and Cameron D.C., *Optical and electrical properties of transparent conductive ITO thin films deposited by sol-gel process.* Thin solid films, 2000. **00**: p. 455-459.
2. Bardo, A.M., Collinson M.M., and Higgins D.A., *Nanoscale properties and matrix-dopant interactions in dye doped organically modified silicate thin films.* Chemical materials, 2001. **13**: p. 2713-2721.
3. Avnir, D., *Organic chemistry within ceramic matrices: Doped sol-gel materials.* Acc. Chemical Res., 1995. **28**: p. 328-334.
4. Lan, E.H., Dave B.C., Fukuto J.M., Dunn B., Zink J.I., and Valentine J.S., *Synthesis of sol-gel encapsulated heme proteins with chemical sensing properties.* Journal of Materials Chemistry, 1999. **9**: p. 45-53.
5. Wolfbeis, O.S., Oehme I., Papkoskaya N., and Klimant I., *Sol-gel based glucose biosensors employing optical oxygen transducers, and a method for compensating for variable oxygen background.* Biosensors and Bioelectronics, 2000. **15**: p. 69-76.

Appendix A - Publications and presentations

Publications: -

Greenway, G.M., **Greenwood A.**, Watts P., and Wiles C., *Solid-supported chemiluminescence and electrogenerated chemiluminescence based on a tris(2,2'-bipyridyl)ruthenium(II) derivative.* Chemical Communications, 2006(1): p. 85-87.

Presentations: -

The 10th International Conference on Electroanalysis, (ESEAC 2004), June 2004, National University of Ireland, Galway, Ireland (Poster presentation).

RSC 4th Analytical Research Forum, July 2004, University of Central Lancashire, Preston, UK (Poster presentation).

RSC 3rd Analytical Research Forum, July 2003, University of Sunderland, Sunderland, UK (Poster presentation).

RSC 2nd Analytical Research Forum, July 2002, University of Kingston, Kingston upon Thames, UK (Poster presentation).